Behaviour and Design of Aluminium Alloy Structural Elements

by

SU Meini

蘇玫妮

B.Eng. *HKU, Hong Kong*

A thesis submitted in partial fulfilment of the requirements for

the Degree of Joint Doctor of Philosophy

at Imperial College London and The University of Hong Kong

June 2014

Abstract of thesis entitled

"Behaviour and Design of Aluminium Alloy Structural Elements"

Submitted by

SU MEINI

for the degree of Joint Doctor of Philosophy
at Imperial College London and The University of Hong Kong
in June 2014

Aluminium alloys are nonlinear metallic materials with continuous stress-strain curves that are not well represented by the simplified elastic, perfectly plastic material model used in most existing design specifications. The aims of this study are to develop a more efficient design method for aluminium alloy structures by rationally exploiting strain hardening. The key components of this study include laboratory testing, numerical modelling and development of design guidance for aluminium alloy structures.

As part of the present study, the experimental programme included tests on 11 stub columns, 40 simply supported beams, 46 continuous beams and corresponding tensile coupon tests. Numerical investigations of aluminium alloy simply supported beams and continuous beams were also conducted. The validated finite element models were used for extensive parametric studies, generating 96 results for beams under three-point bending, 96 under four-point bending and 210 for continuous beams. The experiments and numerical simulations have shown the following key features of the inelastic behaviour of aluminium alloy structural elements: (1) the significance of strain hardening, indicated by the ultimate stress over the yield stress, could be up to 50%; (2) non-slender section capacities could be generally up to 40% higher than the yield limits in compression, and 50%

greater than the plastic moments in bending; (3) the experimental and numerical ultimate loads of continuous beams on non-slender sections go beyond the calculated loads corresponding to the occurrence of the first hinge by more than 10%.

Previous experimental data on aluminium alloy stub columns and simply supported beams were also collected. These collected test data were used together with the newly generated experimental and numerical results obtained from this study, totalling about 900 data, to assess the design predictions of the American, Australian/New Zealand and European specifications. On average, the existing design methods under-estimated the capacity of aluminium alloy stub columns by around 15%~22%, simply supported beams by around 18%~40% and continuous beams by around 27% ~ 50%. Existing section classification limits in Eurocode 9 (2007) were also assessed, and while they were found to be safe, some improved limits were proposed.
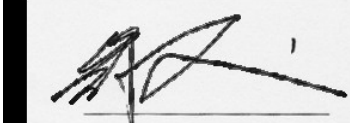
The combined experimental and numerical results were used to develop and calibrate a new design method, termed the continuous strength method (CSM). Two key components of the CSM – a base curve and a bi-linear material model for aluminium alloys have been proposed in this study. Global plastic analysis allowing for moment redistribution has also been adopted in the CSM. Unlike current practices, the CSM has the merits of adopting the continuous treatment for the cross-section deformation response, rationally exploiting the available capacity beyond the yield limit and reasonably allowing for redistributing the internal forces.

The capacity predictions of aluminium alloy structural members have been improved by more than 30% using the CSM. Reliability analyses have also been performed to assess the reliability level of different design methods according to

the American Institute of Steel Construction (2010) and European Standard EN1990 (2002) approaches. The CSM has been shown to be safe, efficient and consistent for aluminium alloy structural members.

DECLARATION

I declare that this thesis represents my own work, except where due acknowledgements are made, and that it has not been previously included in a thesis, dissertation or report submitted to this University or to any other institution for a degree, diploma or other qualification.

SU Meini

ACKNOWLEDGEMENTS

The encouragement and support from Mr Collins Xian throughout the course of my studies is also gratefully acknowledged. Last but not least, I would like to express my heartfelt thankfulness to my parents for their continuous support and unconditional love. This thesis is dedicated to them with all my love.

TABLE OF CONTENTS

LIST OF FIGURES

LIST OF TABLES

LIST OF SYMBOLS

All symbols are defined where they first appear in the text. In most cases only one meaning has been assigned to each symbol, but where this is not the case, the interpretation will be evident from the text. The symbols are listed as follows:

Latin letters

A	Cross-section area
A_{cf}	Area of compression element (flange part)
A_{cw}	Area of compression element (web part)
A_{eff}	Cross-section effective area
B	Section width
b	Flat width of flange; The "Least Squares" best-fit to the curve
C	Constant coefficients in EC9 (2007)
c_{cf}	Distance from the centreline of the compression flange to the cross-section's neutral axis
c_{cw}	Distance from the web group's extreme compression fibre to the cross-section's neutral axis
c_{tf}	Distance from the extreme tension fibre to the cross-section's neutral axis
c_{tw}	Distance from the web group's extreme tension fibre to the cross-section's neutral axis
C_p	Correction factor
COV	Coefficient of variation
E	Young's modulus
E_{sh}	Strain hardening modulus
f_b	Local buckling stress of the flat elements in flexure (AA, 2010)
f_{bc}	Weighted average factored limit state compressive stress in accordance with the ratio of the area of each element (AS/NZS,

	1997)
f_{bt}	Weighted average factored limit state tensile stress in accordance with the ratio of the area of each element (AS/NZS, 1997)
f_c	Local buckling stress of the flat elements in uniform compression (AA, 2010)
f_{csm}	CSM limiting stress
f_d	Design stress
f_f	Design stress for the flanges
f_t	Tensile stress corresponding to the flexural tensile strength (AA, 2010)
f_u	Ultimate tensile stress
f_w	Design stress for the webs
f_y	Yield strength, taken as the 0.2% proof strength
F_{AA}	Ultimate load of continuous beams predicted by the AA (2010)
$F_{AS/NZS}$	Ultimate load of continuous beams predicted by the AS/NZS (1997)
F_{coll}	Ultimate load level at which the plastic collapse mechanism forms (with cross-sectional capacity at the hinge equal to $W_{pl}f_y$)
F_{csm}	Ultimate load of continuous beams predicted by the CSM
F_{design}	Design Strength for continuous beams
F_{EC9}	Ultimate load of continuous beams predicted by EC9 (2007)
F_{EC9-H}	Ultimate load of continuous beams predicted by the plastic hinge method in Annex H of EC9 (2007)
F_{exp}	Experimental ultimate load of continuous beams
F_{FE}	Numerical ultimate load of continuous beams
F_{h1}	Ultimate load level at which the first hinge forms (with cross-sectional capacity at the hinge equal to $W_{pl}f_y$)
F_m	Mean value of fabrication variables
F_{pl}	Ultimate load predicted by the traditional plastic design method
F_u	Experimental or numerical ultimate load of continuous beams

H	Section depth
h	Flat depth of web
I_f	Second moment of inertial for flanges
I_w	Second moment of inertial for webs
k	Buckling coefficient allowing for different loading and boundary conditions
k_c	A reduction coefficient for compression members at yielding (AS/NZS, 1997)
k_n	Fractile factor for n number of tests
L	Member length
M_{AA}	Ultimate moment capacity of simply supported beams predicted by the AA (2010)
$M_{AS/NZS}$	Ultimate moment capacity of simply supported beams predicted by the AS/NZS (1997)
M_{csm}	Ultimate moment capacity of simply supported beams predicted by the CSM
M_{design}	Design Strength for simply supported beams
M_{EC9}	Ultimate moment capacity of simply supported beams predicted by EC9 (2007)
M_{EC9-F}	Ultimate moment capacity of simply supported beams predicted by Annex F of EC9 (2007)
M_{el}	$W_{el}f_y$ is the elastic moment capacity
M_{exp}	Experimental ultimate moment
M_{FE}	Ultimate moment capacities of simulated models of simply supported beams
M_m	Mean value of material factor
M_{nc}	Nominal strength moment for compression
M_{nt}	Nominal strength moment for tension
M_{pl}	$W_{pl}f_y$ is the plastic moment capacity

M_u	Experimental or numerical ultimate moment capacities of simply supported beams
n	Exponent in the Ramberg-Osgood expression; number of samples
p	Probability
P_{AA}	Collapse load of stub columns predicted by the AA (2010)
$P_{AS/NZS}$	Collapse load of stub columns predicted by the AS/NZS (1997)
P_{csm}	Collapse load of stub columns predicted by the CSM
P_{design}	Design Strength for stub columns
P_{EC9}	Collapse load of stub columns predicted by EC9 (2007)
P_{EC9-F}	Collapse load of stub columns predicted by Annex F of EC9 (2007)
P_{exp}	Test ultimate load of stub columns
P_f	Failure probability
P_m	Mean value of test and numerical-to-predicted load ratios
P_s	Survival probability
P_u	Experimental or numerical ultimate load of stub columns
P_y	Af_y, the yield load
Q	Nominal load effect
Q_m	Mean value of load effect
r_d	Design resistance
r_e	Experimental values
r_m	Mean value of resistance
r_n	Nominal resistance
r_t	Theoretical resistance
R	Rotation capacity
R_m	Mean value of resistance
R_n	Nominal resistance
S	Slenderness limits in AA (2010) and AS/NZS (1997)
t	Wall thickness
t_{eff}	Wall effective thickness

V_F	Coefficient of variation of fabrication factor
V_M	Coefficient of variation of material factor
V_P	Coefficient of variation of test and numerical-to-predicted load ratios
V_r	Coefficient of variation of the resistance
V_{rt}	Coefficient of variation of all the basic variables
V_R	Coefficient of variation of the resistance
V_x	Coefficient of variation of the basic variables
V_d	Coefficient of variation of the errors in the design model
V_Q	Coefficient of variation of the total load effect
W_{eff}	Elastic modulus of effective section
W_{el}	Elastic section modulus
W_{pl}	Plastic section modulus
x	Proportion of ultimate strain
x_p	Fractile value for a probability p
y	Distance to the neutral axis
y_{max}	Distance between extreme compression fibre and the neutral axis

Greek letters

α	Hinge demand; Weighting factor
α_ξ	Shape factor depending on the alloy ductility features as required in Annex G (EC9, 2007)
α_R	Weighting factor of the resistance
α_Q	Weighting factor of the action
β	Reliability index
β/ε	Slenderness parameter codified in EC9
Δd	Differences in stress
δ	Deflection at the hinge point; The error term
δ_u	End shortening at ultimate load

ε	Engineering strain
ε_{csm}	CSM limiting strain
ε_{lb}	Local buckling strain, equal to stub column end shortening divided by stub column length at ultimate load
ε_f	Material fracture strain
ε_{true}^{pl}	True plastic strain
ε_u	Strain at ultimate tensile stress
$\varepsilon_{u,\,test}$	Strain at ultimate tensile stress obtained from tensile coupon tests
$\varepsilon_{u,\,pred}$	Predicted strain at ultimate tensile stress
ε_y	Yield strain (f_y/E)
ϕ	Resistance factor
γ	Load factor
$\gamma_{M0}{'}$	Partial safety factor based on the mean curve
γ_{M0}	Partial safety factor according to EN1990 (2002); Partial safety factor based on the best fit model
η	Correction factor
κ	Curvature
κ_{el}	Elastic curvature corresponding to the elastic moment M_{el}
κ_{pl}	Elastic curvature corresponding to the plastic moment M_{pl}
κ_{rot}	Curvature at the point where the moment resistance drops back below
κ_u	Curvature at ultimate load
$\bar{\lambda}_p$	Cross-section; plate slenderness
μ	Mean value of the population
v	Poisson's Ratio
θ	Rotation at hinge point
θ_{pl}	Plastic rotation corresponding to the plastic moment M_{pl}
θ_{rot}	Rotation at the point where the moment resistance drops below M_{pl}
ρ_c	Local buckling factor

σ	Engineering stress; standard deviation of the population
σ_{cr}	Elastic buckling stress
σ_{trure}	True stress
σ_R	Standard deviation of resistance
σ_Q	Standard deviation of action

CHAPTER 1

INTRODUCTION

1.1 Background

The commercial birth of aluminium is generally attributed to a Frenchman, Paul Louis Touissant Heroult and an American, Charles M. Hall, simultaneously in 1886 (Mazzolani, 1995). However, pure aluminium itself is a metal with relatively low strength; thus aluminium alloys have been developed with a small amount of additional elements to enhance its engineering properties. The earliest examples of the use of aluminium alloys in building structures date back to the 1950s. A thorough account of the initiation and growth of aluminium alloys production is given by Mazzolani (1995).

In the last twenty years, aluminium alloy structural members have been used increasingly in various engineering applications. The global aluminium demand has steadily increased from 34.50 million metric tonnes in 2006 to 45.15 million metric tonnes in 2012, and the main suppliers include China, Russia, US, Japan, Canada and Australian. The price of aluminium alloys is generally half of stainless steel materials by weight. Aluminium alloys have a range of advantageous characteristics such as high strength to weight ratio, good corrosion resistance, ease of fabrication into different cross-section shapes, aesthetic appearance and a recycling rate of more than 90%. As a result of their corrosion resistance, aluminium alloys often need no protective coatings against corrosion, bringing improved economy. Another advantage of aluminium alloys over steel is the ease of fabrication, when employing the extrusion process. Despite the aforementioned advantages, there are also drawbacks to using aluminium alloys for structural applications. It can be seen in Fig. 1.1 that the modulus of elasticity

of aluminium (E = 70 GPa) is only about one third of carbon steel (E = 210 GPa) and the yield strength of aluminium alloy is typically only around 200 MPa, though this can vary between alloys.

Similar to stainless steel, the aluminium alloy material stress-strain behaviour is a continuous curve without a clear yielding point. This nonlinear curve exhibits significant strain hardening and reasonable ductility. Strain hardening refers to the increase in strength of metallic materials beyond the yield limit as a result of plastic deformation, as shown in Fig. 1.2. The occurrence of strain hardening may significantly influence the capacities of non-slender cross-sections.

As for aluminium alloy structural design, most previous studies have been focused on simple members, i.e. determinate structures, while indeterminate structures involving moment redistribution still need further investigation. Statically indeterminate structures may be able to redistribute the loads when the first plastic hinge is formed and finally fail at the formation of a plastic collapse mechanism. In this case, plastic design may be adopted for members of stocky sections with sufficient rotation capacity. The use of continuity in a structural system brings several benefits, such as increased load-carrying capacity and reduced deflections (Nethercot et al., 1995).

For the design of aluminium alloy structural members, there are a number of established international design specifications, such as the Aluminum Design Manual (AA, 2010), the Australian/New Zealand Standard (AS/NZS, 1997) and Eurocode 9 (EC9, 2007). These design specifications were mainly developed based on the design rules of steel structures and limited investigation on aluminium alloys. The conservatism in the current design specifications has been demonstrated by recent studies, while the reasons might be largely attributed to the ignorance or inappropriate exploitation of strain hardening and moment

2

redistribution. Key to expanding the usage of aluminium alloys further is to have efficient structural design rules, underpinned by sound research. Hence, a new plastic design method is proposed for both determinate and indeterminate aluminium alloy members in the present study.
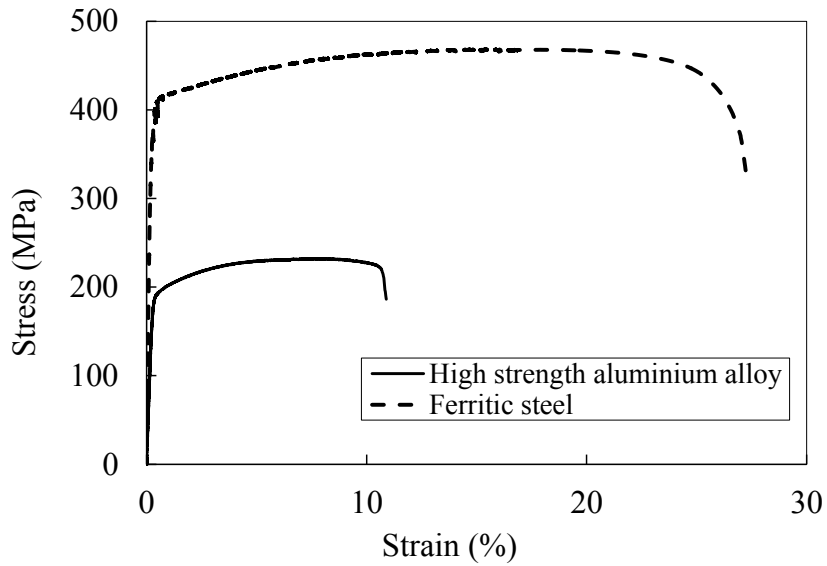
Fig. 1.1   Comparison of stress-strain curves for ferritic steel and high strength aluminium alloy
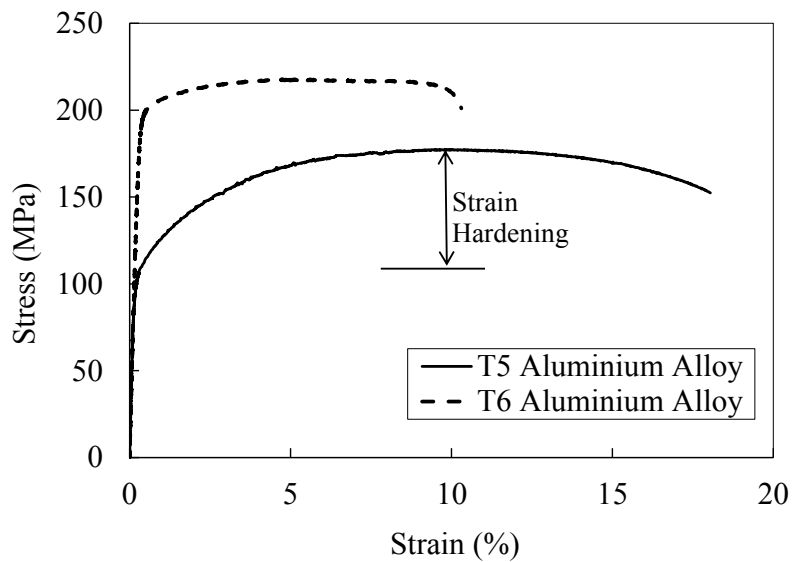
Fig. 1.2   Static stress-strain curves for T5 (normal-strength) and T6 (high-strength) aluminium alloys

3

1.2 Objectives

Four key objectives of this research have been identified, as shown below. The overall research methodology used in this study included a literature review, laboratory tests, numerical simulations, data analysis and reliability analysis. A literature review of the relevant research was firstly performed to get an initial understanding of the research field and find out the research gap. The experiments of aluminium alloy structural members were rationally designed and carried out. The tests were replicated by finite element (FE) modelling using the FE package ABAQUS, followed by parametric studies to generate more numerical results to supplement the test data. Two cross-sections types - square and rectangular hollow sections (SHS/RHS) and SHS/RHS with internal cross stiffeners as well as different normal and high strength aluminium alloy tempers are used in the study. A large data pool comprising all the available data was built and acted as a basis to calibrate new design methods. To validate the newly proposed design rules, result comparisons between the experimental and numerical strengths and the predicted values were performed, followed by the statistical analysis to validate the reliability level.

Following this general methodology, some specific tasks and research activities for each key objective are explained and justified:

(1) To study the strain hardening nature of aluminium alloys at the cross-sectional level

Experiments and a numerical study on aluminium alloy stub columns and simply supported beams were carried out. Meanwhile, relevant data were collected from the literature. Cross-sections of the specimens were mostly non-slender sections, in order to study the cross-section behaviour under the strain hardening effect. The cross-section capacities from tests and numerical simulations were compared

with the theoretical yield limits (for stub columns) as well as the theoretical elastic and plastic moment capacities (for simply supported beams). Therefore, the extra capacities of experimental and numerical results beyond the theoretical fully yielding limits can indicate the influence of strain hardening. Meanwhile, the stress and strain distributions in the cross-section profile, during the loading process, obtained from the numerical study were also evidence for the existence of strain hardening.

(2) *To investigate the significance of moment redistribution of indeterminate structures at the global system level*

Five-point bending tests were designed and conducted to investigate the feasibility of global plastic design for indeterminate aluminium alloy structures. A numerical study was also carried out to change the load levels between the first hinge and the collapse mechanism as well as the rotational demands on the plastic hinges. Cross-sections of specimens were mostly non-slender sections with high rotation capacity. Comparisons between the ultimate capacities with the calculated loads corresponding to the formation of the first hinge and the collapse mechanism could validate the behaviour of moment redistribution, while the numerical models can illustrate the internal force transferring mechanism.

(3) To develop a deformation-based design method to exploit the effects of strain hardening and moment redistribution

The proposed design approach is referred as the continuous strength method (CSM), which has been safely applied to carbon steel and stainless steel materials (Gardner, 2008; Gardner et al., 2011; Afshan and Gardner, 2013). The combined large data pool in this study was used to calibrate the CSM approach specifically for aluminium alloy determinate and indeterminate structural members. Result comparisons and reliability analysis were performed for the proposed CSM

approach and other existing design methods, in order to validate the accuracy, consistency and reliability of the proposed CSM approach.

(4) *To propose a new section classification framework using the CSM slenderness parameter*

Upon validation of the numerical models against tests, a parametric study was conducted to expand the available cross-section capacities over a wider range of cross-section slenderness. The compressive and flexural capacities of aluminium alloy cross-sections were used to revisit the existing section classification framework in Eurocode 9 (2007) and also propose a new classification framework using the CSM slenderness parameter and corresponding limits. The improvement of the new framework can be shown in the result comparisons and reliability analysis.

1.3   Applications in construction industry

In the years after 1886 when aluminium became an industry material, it was employed in the sheet metal roofing of the dome of the church of San Gioacchina in Rome in 1897 (Dwight, 1999). However, the earliest application of aluminium alloys was found in Europe in the 1950s (Mazzolani, 1995). Since then, especially in the past 20 years, aluminium alloy structural members are becoming widely used in a range of engineering applications such as building facades, roof systems, moving bridges and structures situated in humid environments. Examples of all these applications are spread all over the world, such as the first aluminium alloy bridge in the world – Canada Arvida Bridge (Fig. 1.3), Liverpool South Parkway in UK (Fig. 1.5), and the Tornado Tower in Qatar which used 450 tonnes of aluminium alloys and earned the "Best Tall Building" Award in the Middle East and Africa in 2009 (Fig. 1.4). Besides structural applications, aluminium alloy sections have also been increasingly used in the

aeronautical industry (Fig. 1.6), electricity systems (Fig. 1.7), the rail industry and the shipping industry. Numerous examples of applications of aluminium alloys have been given by Mazzolani (1995).

Fig. 1.3   Arvida Aluminium Bridge, Canada (Aluminum company of Canada Ltd, 1940)

Fig. 1.5   South Parkway, Liverpool (Badger, 2009)

Fig. 1.4   Tarnado Tower, Qatar (The Aluminum Association, 2008)

Fig. 1.6   Electronic Transmission Tower (EIS, 2013)

Fig. 1.7   Offshore helidecks (Mazzolani, 1995)

1.4 Outline of thesis

The research study focused on the behaviour and design of aluminium members, including compressive members and flexural members. The thesis has been structured into the following nine chapters:

This Chapter provides a brief introduction to the birth of aluminium alloys, the material properties, existing design rules, engineering applications of aluminium alloys, the research objectives and an outline of the thesis.

Chapter 2 contains a review of the literature that is relevant to this research project. The review is intended to give an overview of important topics such as material properties, existing tests and numerical modelling of aluminium alloy structures, with the majority of the literature being introduced.

Chapter 3 reports the material properties of the test specimens by means of longitudinal tensile coupon tests and Webster hardness tests. The measurement of initial local geometric imperfections was also conducted. An extensive laboratory testing programme including stub column tests, simply supported bending tests and continuous bending tests is also described in this chapter.

Chapter 4 describes a numerical modelling programme that was run in parallel with the tests. The validated models were used in the parametric studies to investigate the effect of variation in key individual parameters and to generate further results in the areas unexplored experimentally.

Chapter 5 illustrates the development of a more rational and efficient method for the structural design of aluminium alloys – the continuous strength method (CSM).

Two key components - the continuous base curve and the CSM bi-linear material model – are explained in detail. The continuous strength method for both determinate and indeterminate structures is proposed.

Chapter 6 compares the test and numerical results with the predicted capacities from international design specifications including the Aluminum Design Manual (2010), the Australian/New Zealand Standard (1997) and Eurocode 9 (2007), as well as the traditional plastic design and the CSM approaches. Existing section classification for internal elements is also reviewed, while a new section classification framework is proposed.

Chapter 7 undertakes the statistical analyses for the design provisions in the AA (2010), AS/NZS (1997), EC9 (2007) and the CSM approaches to assess the reliability level. Two analysis procedures codified in the AISC (2010) and EN1990 (2002) were used

Finally, a summary of the important findings of this project, conclusions and suggestions for further work are provided in Chapter 8.

CHAPTER 2
LITERATURE REVIEW

2.1 Introduction

Research on aluminium alloy structural members has been conducted since the early 1940s (Templin et al., 1938). Key relevant research findings on aluminium alloy structures are covered in this chapter. The literature is categorized into several broad subject areas and listed in chronological order in each sub-section of this chapter.

2.2 Extrusion process

To date, the manufacturing technologies of aluminium alloy members include casting, extrusion, forging and drawing (Mazzolani, 1995). Most of the aluminium alloy structural members used in building and construction industry are extruded members. The present research is focused on aluminium alloy hollow sections fabricated by the extrusion process. Hence, in order to have a better understanding of the material properties and structural behaviour of aluminium alloys, the extrusion process, referring to Mazzolani (1995) and Dwight (1999), is briefly presented herein, with the schematic illustration in Fig. 2.1.

(1) Pure aluminium is a metal with low strength; to improve its mechanical properties, a small amount of additional alloys are added into the aluminium fusion.

(2) The fused aluminium alloys are then cast into a suitable sized billet.

(3) The preheated billet is put in a heated container, and pressed to pass through a drawplate with a hole, which is called as a die. The shape of the hole in the drawplate determines the shape of the extruded section.

(4) Solution treatment (quenching) or air-quenching is needed for different alloy tempers, followed by artificially or nature ageing.

(5) Following the extrusion process, a high-tension force is applied to the tube on a straightening table.
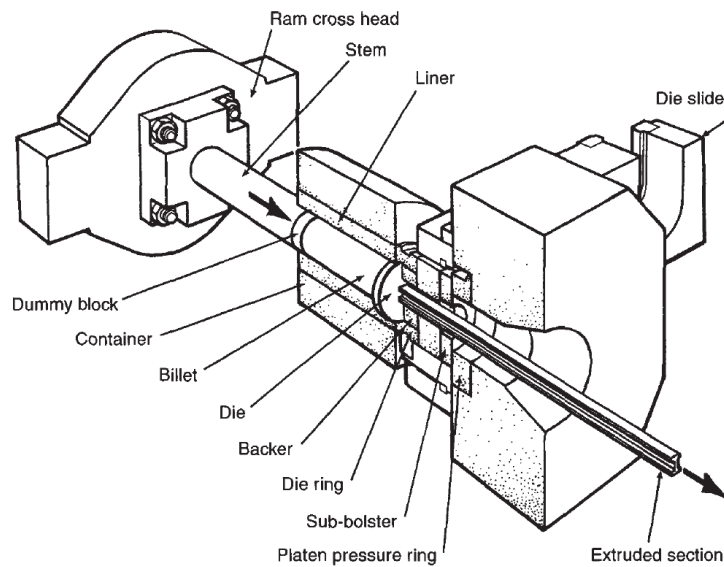
Fig. 2.1   Schematic illustration of extrusion process (Dwight, 1999)

2.3 Aluminium alloy material properties

Accurate material modelling is one of the key aspects of efficient design methods; hence, many studies on the aluminium alloy material properties have been carried out in the past few years. Relevant literature on this topic has therefore been reviewed herein.

Two general types of material model are (1) the continuous model and (2) the piecewise model. The most well-known continuous model was developed by

Ramberg and Osgood (1943) based on the form $\varepsilon = \varepsilon\,(\sigma)$, and was modified by Hill (1944), where ε is strain and σ is stress. Though the model has been widely used to describe the nonlinear stress-strain behaviour of metallic materials, it was observed that the model generally overestimates the material strength at high strains (Gardener and Nethercot, 2001). There were also some other continuous models in the form of $\sigma=\sigma\,(\varepsilon)$, such as those proposed by Baehre (1966) and Mazzolani (1972). As for the piecewise model, the stress-strain relationship may generally be represented by either a bi-linear model or tri-linear model, as presented in Annex E of EC9 (2007). Based on the treatment of the inelastic portion, these simplified piecewise models can be divided as the elastic-perfectly plastic model or the elastic-linear hardening model. The way that the existing models used to account for strain hardening is a good reference to consider strain hardening in this study.

Similar to stainless steel, aluminium alloys also exhibit rounded stress-strain behaviour with strain hardening at large plastic strain stage. Since this study is focused on plastic design, two key parameters of the material properties are explored in detail, i.e. strain hardening and ductility. In order to improve design efficiency, these two factors have to be considered carefully and incorporated into the material model.

2.3.1 Strain hardening

Recent investigations have acknowledged the attainment of strain hardening in metallic materials. Some aluminium alloys might exhibit a higher level of strain hardening than stainless steel and carbon steel. Coupon test results highlight the different mechanical properties and behaviour of different aluminium tempers. The normal strength aluminium alloys (i.e. T1, T2, T3, T4 and T5), referred to as Buckling Class B material in accordance with EC9 (2007), have lower yield

strength, considerable strain hardening and higher ductility, but the high strength aluminium alloys (i.e. T6, T7, T8 and T9), referred to as Buckling Class A material in EC9 (2007), has higher yield strength, but less pronounced strain hardening and lower ductility, as illustrated in Fig. 1.2. Previous compression test results of non-slender sections were found to exceed the theoretical yield limits (Mennink, 2002; Zhu and Young, 2006a and 2008; Ashraf and Young, 2011), while in the case of flexural members, significant increase in moment resistances beyond the fully plastic moment capacity was also observed for non-slender sections (Moen et al., 1999a; Zhu and Young, 2006b and 2009; Kim and Peköz, 2010). Similar findings were also reported by Hasan and Hancock (1988) and Kemp et al. (2002) for carbon steel and stainless steel materials. Both cases are largely attributed to the occurrence of strain hardening. This has been recognised in Annexes F and H of EC9 (2007), where alternative methods accounting for strain hardening are provided.

In material models, strain hardening has been considered in the following ways:

(1) An exponent n to characterize the shape of the rounded curve which is related to the strain hardening rate of the material in the Ramberg and Osgood (1943) expression.

(2) An exponent to define the strain hardening rate of different aluminium alloys (i.e. normal and high strength aluminium alloys) in the straight-line equations given by Hill and Clark (1955).

(3) A generalised shape factor that takes account of material strain hardening properties explained by Mazzolani (1995)

(4) A strain hardening modulus E_{sh} codified in EC9 (2007)

2.3.2 Ductility

Aluminium alloys are typically less ductile than structural steels and stainless steels, however, its structural sections may also have high rotation capacity to allow moment redistribution and to enable the application of plastic design methods. The strain at fracture ε_f of aluminium alloys is about 10% to 25%, with higher strength aluminium alloys generally having less ductility (Mazzolani, 1995).

To date, particular attention has been paid to the possibility of premature tensile failure due to reduced material ductility and some informative annexes have been included in EC9 (2007) to estimate the post-elastic behaviour of aluminium alloys. EC9-Annex E (2007) includes a method to predict the ultimate strain ε_u (i.e. the strain corresponding to the ultimate tensile stress of the material), as given in Eqs. 2.1 and 2.2. Similar to the fracture strain ε_f, the ultimate strain might also be deemed as an indicator of the ductility.

$$\varepsilon_u = 0.3 - 0.22(f_y/400) \quad \text{for} \quad f_y < 400 \text{ N/mm}^2 \tag{Eq. 2.1}$$

$$\varepsilon_u = 0.08 \quad \text{for} \quad f_y \geq 400 \text{ N/mm}^2 \tag{Eq. 2.2}$$

where f_y is the yield stress or the 0.2% proof stress.

Findings from the literature review relating to aluminium alloy properties have shown the existence of strain hardening and reasonable ductility in the material; hence, the influences of these two parameters on the cross-section capacities and the global system behaviour are investigated in the present research.

14

2.4 Laboratory testing

Central to the development of efficient design rules is high quality laboratory test data. As a relatively new material, the volume of test results for aluminium alloy structures is found to be relatively low, with some areas virtually unexplored. In this study, in order to investigate the effects of strain hardening and moment redistribution on the structural behaviour of aluminium alloy members, cross-section compressive and flexural capacities as well as indeterminate structure failure loads are required. Hence, previous studies on stub column tests, simply supported bending tests and five-point bending tests are reviewed. This section contains a brief review of relevant laboratory tests conducted on aluminium alloy structural members.

2.4.1 Stub columns

The early laboratory tests on aluminium alloy stub columns were carried out at Cornell University by Bijlaard and Fisher (1953) to investigate the compression strength of H-sections and square tubes in post-buckling range. The investigation was part of the Technical Note 2994 for National Advisory Committee for Aeronautics. Over the past few decades, a series of studies has been carried out to examine the load-bearing capacity of aluminium alloy structural members.

With an emphasis on the behaviour of cross-sections in compression, the key studies are introduced herein. Experimental investigations into the compressive capacity of aluminium alloy cross-sections have been carried out on different cross-section shapes, including square and rectangular hollow sections (SHS/RHS) (Mazzolani et al., 1996 and 1997a; Langseth and Hopperstad, 1997; Landolfo et al., 1999; Hassinen, 2000; Faella et al., 2000; Mennink, 2002; Zhu and Young, 2006a and 2008), channels (Mazzolani et al., 2001; Mennink, 2002) and angles

15

(Mazzolani et al., 2011). The experimental structural performance data generated in these studies have been supplemented by the numerical results from Mazzolani et al. (1997b), Mennink (2002) and Zhu and Young (2006b). These tests and numerical analyses were performed on specimens with a wide range of cross-section slenderness ratios. Furthermore, Mennink et al. (2002) also reported the experimental work on 39 columns of 12 different complex cross-sections. It was found that the majority of aluminium alloy stub column tests were intensively conducted in Europe by Mazzolani's research team to provide the background data for revising the latest version of Eurocode 9 (2007).

Table 2.1 gives a summary of all available compression tests conducted in previous studies, which have been reported in sufficient detail. These data are used herein to assess the exiting design guidance for aluminium alloy cross-sections under compression and to underpin the development of advanced design provisions.

Table 2.1   Previous tests conducted on aluminium alloy stub columns in the literature

Section shape	Reference resource	No. of tests
SHS/RHS	Bijlaard and Fisher (1953)	4
	Langseth and Hopperstad (1997)	7
	Faella et al. (2000)	70
	Hassinen (2000)	2
	Mennick (2002)	7
	Zhu and Young (2006)	5
Angles	Mennick (2002)	9
	Mazzolani et al. (2011)	33
Channels	Mazzolani et al. (2001)	194

2.4.2 Simply supported beams

This section reviews relevant flexural tests on aluminium alloy sections. The earliest documented tests on aluminium alloy members subjected to bending were conducted by Dumont and Hill (1940). As part of the Technical Note No. 770 from National Advisory Committee for Aeronautics, Dumont and Hill (1940) studied the lateral stability of equal-flanged I-section subjected to pure bending. Though a number of tests were conducted, these tests were not reported in sufficient detail to allow the data to be used in the validation of proposed design methods.

Experimental and numerical studies have been carried out by a few researchers since then, seeking to improve the design provisions for aluminium alloy beams. For instance, Lai and Nethercot (1992) developed finite element (FE) models, which incorporated the heat-affected zone to investigate its influence on flexural capacity. Moen et al. (1999a and 1999b) conducted an experimental programme and a numerical investigation on the strengths and rotation capacities of beams subjected to a moment gradient. De Matteis et al. (2001) carried out a numerical investigation on aluminium beams of rectangular hollow sections using ABAQUS, in order to reassess the existing classification limits in Eurocode 9. Kim and Peköz (2010) conducted tests and developed numerical models of aluminium alloy stocky section beams to determine the ultimate bending capacities with an emphasis on strain hardening and ductility effects, which were found to be even greater than the plastic moment capacities.

Table 2.2 provides a summary of the existing tests on aluminium alloy simply supported beams under in-plane bending. It aims at providing a set of available data to review the existing design rules and meanwhile to calibrate the new design method proposed in this study.

Table 2.2   Previous tests conducted on aluminium alloy simply supported
beams

Test Configuration	Section shape	Reference resource	No. of tests
3-point bending	SHS/RHS	Moen et al. (1999)	25
	I-section	Moen et al. (1999)	8
4-point bending	SHS/RHS	Lai and Nethercot (1992)	4
		Zhu and Young (2006)	4
		Zhu and Young (2009)	10

2.4.3 Continuous beams

According to Wang (2011), most of the indeterminate structural tests were carried
out in the 1950s and 1960s. To date, only a limited number of tests have been
carried out on continuous beams of nonlinear materials, including those conducted
by Panlilio (1947) on two-span systems and those of Welo (1991) on three-span
arrangements, with both studies examining the deformation and bending
capacities of aluminium alloy members. More recent experimental studies,
exploring the behaviour of cold-formed and hot-finished steel and stainless steel
elements, have also been reported (Mirambell and Real, 2000; Gardner et al., 2010;
Theofanous et al., 2014).

Unfortunately, insufficient data were reported from the aforementioned studies
on aluminium alloy structures, and hence, no previous continuous bending test
results were collected and used in this research. Hence, there is a need to conduct
continuous bending tests in this study to observe the load transfer and moment
redistributing behaviour within indeterminate structures.

2.5 Numerical models

With the development of sophisticated finite element (FE) software packages, numerical modelling has now become a key tool in research to supplement laboratory testing. Numerical models of aluminium alloy structural members have been successfully developed in many studies. Literature review was carried out to carefully analyse the key input parameters and boundary constraints. It should be noted that the general purpose FE software ABAQUS 6.10-1 (2010) was employed in this study, so that a general review of relevant studies of aluminium alloy numerical modelling is given below.

There have been a number of numerical studies on the structural behaviour of determinate aluminium alloy elements, such as plates (Moen et al. 1998; Xiao and Menzemer, 2003), columns (Lai and Nethercot, 1992; Mazzolani et al., 1997b; Hassinen, 2000; Zhu and Young, 2006b), and beams under three-point bending (Moen et al., 1999b; De Matteis et al., 2001, 2004) and four-point bending (Opheim, 1996; Wang et al., 2007; Kim and Peköz, 2010), but simulations of indeterminate aluminium alloy structures are far fewer.

With respect to indeterminate structures, Manganiello et al. (2006) developed FE models of indeterminate aluminium alloy structures and validated the FE models against the five-point bending test results of Welo (1991). Following validation, FE models were used to generate data on the structural performance of beams with fixed-ended boundary condition, continuous beams and portal frames.

2.5.1 Element type

The reduced integration four-noded doubly curved shell element S4R has been employed in numerous previous studies. This S4R general purpose shell element

has six degrees of freedom per node and has provided accurate solutions to problems of similar nature addressed in this study (Ellobody and Young, 2005). Generally, the element type of S4R and a uniform mesh size of 10 mm × 10 mm have been shown to perform well for the modelling of aluminium alloy members (Zhou and Young, 2008; Zhu and Young, 2006b and 2009).

2.5.2 Material modelling

The measured stress–strain curves obtained from the tensile coupon tests on material cut from the flat portions of the test specimens were used in the analyses. In the material models, the finite element software ABAQUS treats the stress-strain curve as two parts. The first elastic part behaves linearly, and hence, only the Young's modulus and the yield stress are required as input parameters. In the second part of the stress-strain curve, the material nonlinearity was included in the FE models by specifying sets of values of true stress and plastic strain to define a piecewise linear response. This model transfers the engineering stress-strain curve to the true stress-strain curve, in order to include the effect of cross-section large deformation under tension or compression. The relationship between the true stress σ_{true} and the engineering stress σ, as well as the true plastic strain ε_{true}^{pl} and the engineering strain ε are given in Eqs. 2.3 and 2.4, respectively (ABAQUS, 2010).

$$\sigma_{true} = \sigma(1+\varepsilon) \qquad \text{(Eq. 2.3)}$$

$$\varepsilon_{true}^{pl} = ln(1+\varepsilon) - \sigma_{true} / E \qquad \text{(Eq. 2.4)}$$

where E is the Young's modulus.

2.5.3 Geometric imperfections

Initial geometric imperfections (both local and global) are introduced into structural members during production, fabrication, handling and construction, and can significantly influence the structural behaviour of any structural component prone to instability (Law, 2010). Since this study is focused on the cross-section capacities of aluminium alloys, therefore, only initial local geometric imperfections were incorporated in the in-plane bending models in the form of the lowest regular elastic buckling mode shape. Hence, a linear eigenvalue buckling analysis was initially performed (Dawson and Walker, 1972; Ashraf et al., 2006; Zhu and Young, 2006b; Theofanous and Gardner, 2010). It was found that sensitivity of the simulated results to imperfections was generally relatively low (Moen et al., 1999b).

2.5.4 Residual stresses

Residual stresses of the test specimens were not measured and not explicitly modelled in the FE analyses for two reasons: (1) the presence of bending residual stress in cross-sections is, to a significant extent, implicitly reflected in the material properties obtained from the tensile coupon tests (Rasmussen and Hancock, 1993; Jandera et al., 2008); (2) residual stresses have only a very small effect on the load-bearing capacity of extruded aluminium alloy members (Mazzolani, 1995; Zhu and Young, 2009). Similar findings were also reported for stainless steel and carbon steel materials (Ashraf et al., 2006; Law, 2010).

2.5.5 Analysis technique

In FE modelling, the load was applied by imposing vertical displacement to the solid bearing plates (Zhu and Young, 2006b and 2009), which was identical to

that used in the tests. The Riks procedure with automatic increment size described in ABAQUS 6.10-1 (2010) was adopted, in order to allow tracing the post-ultimate path for the modelled specimens (Zhu and Young, 2006b; Theofanous and Gardner, 2010).

From the literature review, it can be found that finite element modelling has become a commonly used tool to supplement laboratory tests and has been maturely used to model aluminium alloy structural members. Hence, based on the findings and conclusions from previous studies, appropriate finite element models can be developed in this study for aluminium alloy structural members, with reference to the relevant literatures.

2.6   Design guidelines

Due to the early commercial development and the wide applications of aluminium alloys, design rules for aluminium alloy structures have been put forward. Historically aluminium alloy design rules were based on assumed analogies with carbon steel behaviour, with modifications made where necessary to fit in with aluminium alloy test results.

2.6.1 International specifications

There are a number of established international aluminium alloy structural design specifications currently available. These specifications provide design rules for a range of structural components and applications though, in some areas, design provisions are overly conservative.

The earliest dedicated design rules for aluminium structures were developed at Aluminum Company of America (Alcoa) beginning around 1930 (Kissell and Ferry, 1995). In 1952, the American Society of Civil Engineers (ASCE) published several research reports on aluminium alloy structural design. Meanwhile, some major producers of aluminium alloys also developed some design handbooks for their products. The nationally recognized design specification was firstly published by the Aluminium Association, and was entitled '*Aluminum Design Manual*'. The current version of the manual was published in 2010 (AA, 2010).

In 1967 aluminium alloys were studied for the first time by a specific board of the European Convention for Constructional Steelwork (ECCS). In 1992, a sub-committee in CEN Technical Committee, led by F.M. Mazzolani, was formed and worked on aluminium alloy structures. The current European design specification for aluminium alloy structures, Eurocode 9 (EC9, 2007), was published in 2007. EC9 is the first design specification that allows for a complete inelastic analysis for aluminium alloy structures (De Matteis et al., 2001). Background information of EC9 was documented in *Aluminium Alloy Structures* (Mazzolani, 1995).

The joint standard of Australia and New Zealand *AS/NZS 1664.1:1997* for aluminium alloy structural design was prepared by the Joint Standards Australian/New Zealand Committee. The originated version of the code was published in 1975, which was then superseded by a later version in the year of 1979, while now the latest version was published in 1997.

Other international design specifications have also been established in different countries all over the world. The most well-known specifications included the *Structural use of aluminium: Part 1- code of practice for design BS8118* (1991)

in UK and the *Strength Design in Aluminum CSA-S157* (2005) drafted by the Canadian Standards Association.

2.6.2 Other design approaches

In order to improve design efficiency and spread the use of aluminium alloys in industry, a number of research programmes have been investigated into the design methods. Findings from these research programmes have enabled the development and publication of design guidance.

In order to calculate the design strengths of aluminium alloy columns, Hill and Clark (1955) modified some buckling constants in the straight-line equations which were originally proposed by Templin et al. (1938). The modified equations have shown satisfactory for different tempers of aluminium alloys. Later on, these modified buckling constants were generally codified in the Aluminum Design Manual (AA, 2010).

In 1968, Jombock and Clark proposed the weighted average method to calculate the crippling strength of formed sheet sections. This weighted average method has been adopted by the AA (2010) and AS/NZS (1997) to evaluate section capacity. It should be noted that the compression section capacity is weighted averaged according to each element area, while the weighted average design moment is according to the elastic section modulus of each element.

As reported by Frey and Mazzolani (1977), buckling curves for axially loaded aluminium alloy non-welded columns were established by the European Convention for Constructional Steelwork committee (ECCS). These curves have taken into account the variations in material tempers, cross-section slenderness as well as effects of initial curvature.

Recently, the direct strength method (DSM), initially proposed by Schafer and Peköz (1998) for the design of cold-formed steel structural members, was extended to aluminium alloy thin-walled sections, and verified against a series of beam tests conducted by Zhu and Young (2009). The DSM has been included in the North American Specification (AISI, 2007 and 2012) and the Australian/New Zealand Standard (AS/NZS, 2005) for the design of cold-formed steel structural members.

Most recently, a deformation-based design approach, the continuous strength method (CSM), was proposed for stainless steel structural members (Gardner and Ashraf, 2006; Gardner, 2008; Gardner and Theofanous, 2008; Gardner et al., 2011; Afshan and Gardner, 2013). The CSM approach has been included in the AISC design guideline for structural stainless steel design in the year of 2013. At the cross-sectional level, the CSM involves determining deformation capacity of cross-section from slenderness and cross-section load-carrying capacities based on a strain hardening material model; at the global system level, the CSM allows for global plastic design with reference to the rotation demands on the plastic hinges. Due to the similarity between steel materials and aluminium alloys, the existing CSM approach is modified and calibrated specifically against the available data pool for aluminium alloys in this study.

2.7   Summary

In general, investigations into aluminium alloy structures have been found to be relatively limited compared to other metallic materials, such as carbon steel and stainless steel. Meanwhile, the literature is mainly focused on elastic design, while the consideration of strain hardening, material ductility and global plastic analysis might need further study. By means of assuming analogies of material properties and structural behaviours with carbon steel and stainless steel,

sufficient progress has been made to permit the development of design guidelines.

The purpose of this chapter is to provide an overview of previous researches on aluminium alloy structural design. The literature review has laid the foundation for the present study, and it leads to the plan and the formulation of the methodology of the present study. More literature will be introduced and examined in the following appropriate chapters.

CHAPTER 3

EXPERIMENTAL INVESTIGATIONS

3.1 Introduction

The experimental programme in this study consists of tensile coupon tests, stub column tests, simply supported bending tests (three-point and four-point bending) and continuous bending tests (three loading configurations). The compression capacities, moment capacities, rotation capacities and collapse loads were obtained in this study. All experiments were carried out at the Structures Laboratory of the Department of the Civil and Environmental Engineering in The University of Hong Kong.

3.2 Specimen preparation

In this study, the cross-sections of specimens under investigation are aluminium alloy square and rectangular hollow sections (SHS/RHS) with or without internal cross stiffeners (Fig. 3.1).

(a)   (b)
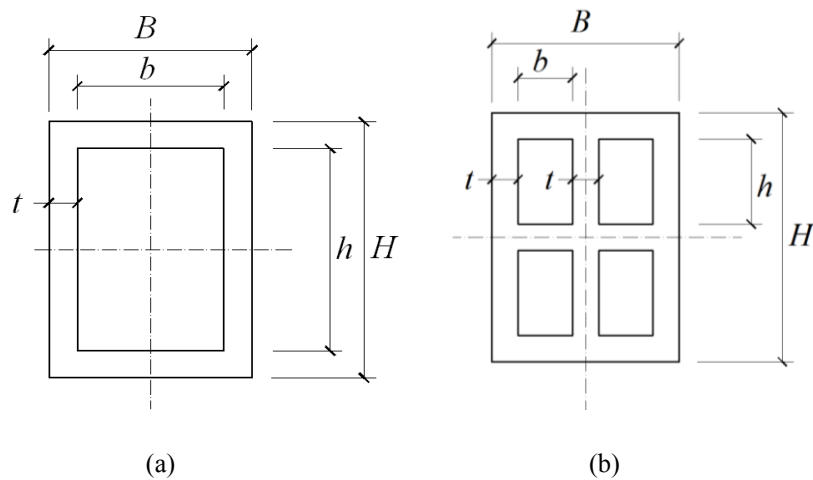
Fig. 3.1   Definition of symbols for (a) SHS/ RHS and (b) SHS/RHS with

internal cross stiffeners with all elements of thickness t

The test specimens in this study were labelled according to the material strength, cross-section dimensions and test configuration, as shown in Fig. 3.2. For example, the label "H70×55×4.2C-R" defines the following specimen.

- The first letter indicates the material of the specimen, where "H" refers to high strength aluminium alloy 6061-T6, while "N" refers to normal strength aluminium alloy 6063-T5;

- The second part of the label indicates the cross-section dimensions. In this label, it refers to a rectangular hollow section with dimensions of width (70 mm) × height (55 mm) × thickness (4.2 mm) (see Fig. 3.1(a)). If there is a "+" in front of the label (such as "+H95×95×4.3C"), it means the hollow section has internal cross stiffeners of the same thickness as the outer walls of the section (see Fig 3.1(b)). The arrangement of the cross-sectional dimensions also indicates the bending axis. For example, the specimen H70×55×4.2B3-R was bent about the minor axis;

- The symbol "C" following the dimensions means a column compression test. As for a simply supported beams, the symbol "B3" refers to the three-point loading configuration, whereas "B4" signifies the four-point loading configuration. In terms of continuous beams, three different loading configurations were employed and are indicated in the labels. (Table 3.1);

- Finally, if the test was repeated, a letter "R" is included in the end of the label.
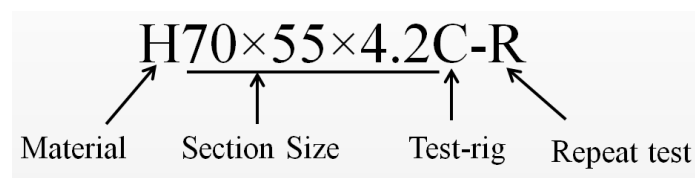
Fig. 3.2   Explanation of the components in a specimen label

Table 3.1   Labels for corresponding test configurations.

Test Configuration	Stub Columns	Simply Supported Beams		Five-point Bending Beams		
		Three-point bending	Four-point bending	Set-up I	Set-up II	Set-up III
Label	C	B3	B4	B5I	B5II	B5III

3.3 Material properties

The non-welded material properties of each specimen were determined by means of longitudinal tensile coupon tests in conjunction with Webster hardness tests. Initial geometric local imperfections were measured on some selected test specimens.

3.3.1 Webster hardness tests

Surface hardness of the material is one of the material properties that help to identify different metallic materials such as brass, copper, mild steel and even different tempers of aluminium alloys. Webster hardness measurements were conducted in accordance with the *Standard Test Method for Indentation Hardness of Aluminium Alloys by Means of a Webster Hardness Gage* (2010). By comparing the value obtained from the Webster hardness gage with the criteria in the standard, the temper of the specimen can be identified (see Fig. 3.3). Generally, high strength aluminium alloys have greater hardness values of 13-15, and normal strength aluminium alloys have smaller values of 10-12.

Fig. 3.3   Surface hardness measurements by Webster Hardness Gage

3.3.2 Tensile coupon tests

The material properties of each specimen were determined by means of longitudinal tensile coupon tests. The tested coupon specimens were cut from the flat portion in the longitudinal direction from the tubes. The coupon specimens were machined from the flat faces of structural sections with a 50 mm gauge length. The coupons were tested in a 250 kN capacity MTS displacement controlled testing machine using friction grips (Fig. 3.4). Two strain gauges and an extensometer of 50 mm gauge length were used to measure the longitudinal strains (Fig. 3.5). The static curves were achieved by pausing the applied strain for 1.5 minutes near the 0.2% proof stress and the ultimate tensile stress. Coupon tests all conformed to the *Australian standard AS 1391* (AS, 2007) and the *ASTM standard* (ASTM, 1997).

Fig. 3.4   Tensile coupon test set-up

Fig. 3.5   Tensile coupon test with two strain gauges and an extensometer to

measure strain

The coupon specimens had necking in the middle range and followed by rapture, as shown in Fig. 3.6. A pair of typical dynamic and static stress-strain curves obtained from tensile coupon test is plotted in Fig. 3.7. The coupon test results for

each specimen are shown in Table 3.2 to Table 3.4 and Table 3.6 to Table 3.7. The results highlight the different mechanical properties and behaviour of the two tempers. The T5 temper has lower yield strength, considerable strain hardening, lower hardness values but high ductility, whereas the T6 temper has higher yield strength, less pronounced strain hardening, higher hardness values and lower ductility, as illustrated in Fig. 1.2.
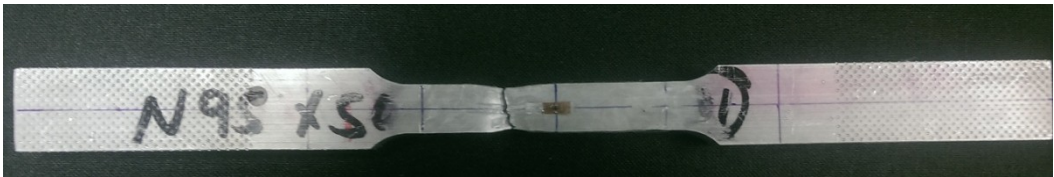
Fig. 3.6   A tested coupon failed by rupture within the gauge length range
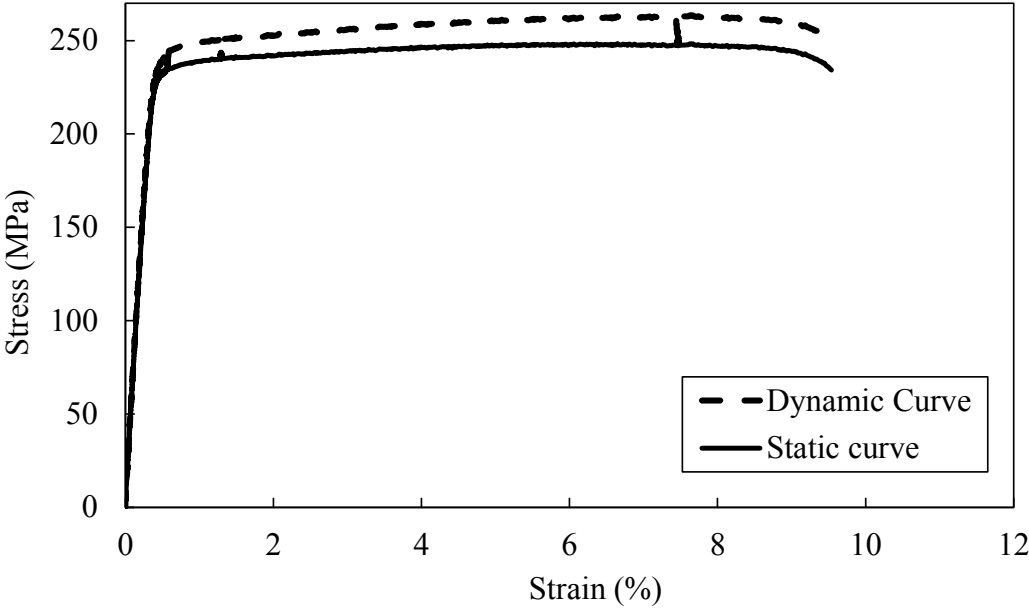
Fig. 3.7   A pair of typical dynamic and static stress-strain curves for the section $H64 \times 64 \times 3.0$

3.3.3 Initial local geometric imperfections

Initial local geometric imperfections were measured to aid the explanation of structural performance and to include in numerical models. Prior to testing, initial local geometric imperfections were measured at mid-height around the four faces of four selected stub columns - H64$\times$64$\times$3.0C, H95$\times$50$\times$10.5C, +H95$\times$95$\times$4.3C-R and +N95$\times$50$\times$10.5C. The specimens were mounted on the bed of a milling machine, and measurements were taken by means of a Mitutoyo Co-ordinate Measuring Machine with an accuracy of 0.001 mm, as shown in Fig. 3.8. Imperfections were recorded at 2 mm intervals; a typical measured imperfection profile is shown in Fig. 3.9. The negative values of local imperfection measurements indicated concave profiles and the positive values indicated convex profiles.

The maximum measured local imperfection amplitude of the test specimens was approximately 0.2 mm. Since the specimens were cut from the same batch of tubes, this initial local imperfection amplitude of 0.2 mm was applied to all other specimens in the numerical analyses.
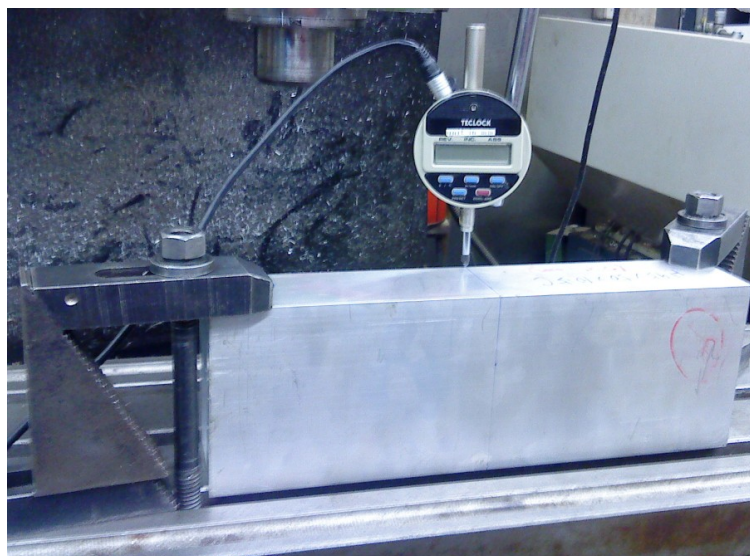
Fig. 3.8   Measurement of initial local geometric imperfections
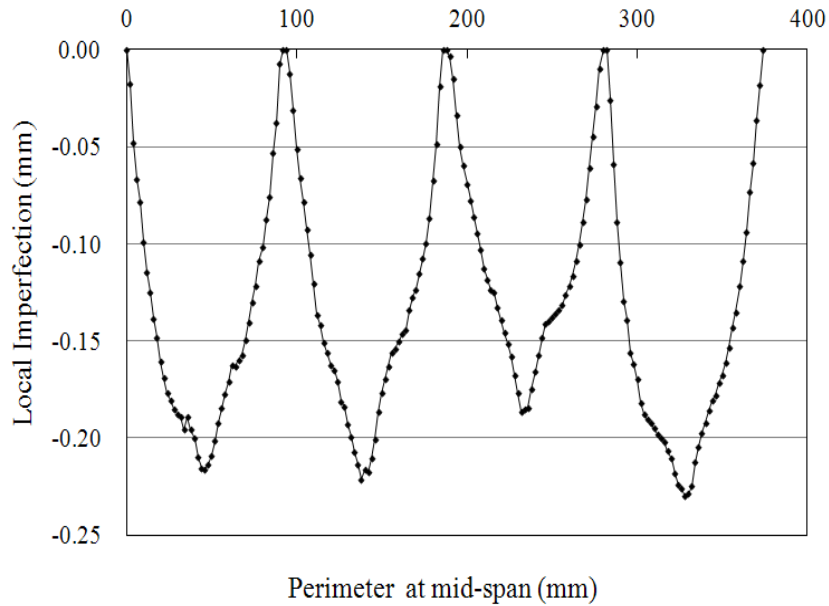
Fig. 3.9   Initial local geometric imperfection profile around mid-span

perimeter of specimen +H95×95×4.3C-R

3.4   Stub column tests

A series of 15 stub column tests on a range of aluminium alloy cross-sections were performed. Among the 15 specimens, 10 were SHS/RHS and 5 were SHS/RHS with internal cross stiffeners. The nominal lengths of the stub columns were selected as three times the larger cross-sectional dimension.

3.4.1 Test specimens

The test specimens were manufactured by extrusion of grades 6063-T5 and 6061-T6 heat-treated aluminium alloys, with 4 being normal strength temper (6063-T5) and 11 being high strength temper alloy (6061-T6). The average measured cross-sectional dimensions and tensile material properties are shown in Table 3.2 for each test specimen. The symbols are defined, with reference to Fig. 3.1, as follows: L is the stub column length, E is the Young's modulus, f_y is the

material yield stress (taken as the 0.2% proof stress), f_u is the material ultimate tensile stress, ε_u is the strain corresponding to the ultimate tensile stress of the material, ε_f is the strain corresponding to the material fracture and n is the exponent of the Ramberg-Osgood expression (Ramberg and Osgood, 1943). The nominal length of the stub columns complied with the guidelines provided by the Structural Stability Research Council (Ziemian, 2010), to ensure failure occurs at the cross-section instead of overall buckling. After initial cutting, the ends of the specimens were milled flat to ensure a uniform distribution of applied loads.

Table 3.2   Measured stub column dimensions and material properties from the tensile coupon tests

Specimen	B (mm)	H (mm)	t (mm)	L (mm)	E (GPa)	f_y (MPa)	f_u (MPa)	ε_u (%)	ε_f (%)	n	Webster hardness
H64×64×3.0C	63.9	63.9	2.85	191.5	66	234	248	6.7	9.5	12	13
H64×64×3.0C-R	63.9	63.9	2.85	191.5	66	234	248	6.7	9.5	12	13
H70×55×4.2C	69.9	54.9	4.08	209.8	65	193	207	5.1	9.8	22	12
H70×55×4.2C-R	69.9	54.9	4.09	209.9	65	193	207	5.1	9.8	22	12
H95×50×10.5C	94.8	49.7	10.36	284.9	71	229	242	5.4	8.4	11	12
H120×70×10.5C	119.9	69.9	10.39	360.0	69	226	238	7.9	10.2	10	12
H120×120×9.0C	120.0	120.0	8.91	360.2	65	225	234	6.3	8.0	13	12
N95×50×10.5C	94.9	49.7	10.37	285.2	69	179	220	8.1	14.1	10	11
N120×70×10.5C	119.9	69.8	10.45	360.9	71	139	194	6.6	14.1	9	11
N120×120×9.0C	120.0	120.0	8.92	361.3	69	181	228	8.9	14.5	9	11
+H95×95×4.3C	95.4	95.3	4.17	284.8	67	228	240	6.0	6.4	12	12
+H95×95×4.3C-R	95.4	95.3	4.17	284.8	67	228	240	6.0	6.4	12	12
+H120×70×10.5C	120.1	69.9	10.27	360.0	69	215	229	7.5	10.7	8	10
+H120×70×10.5C-R	120.0	69.9	10.26	360.0	69	215	229	7.5	10.7	8	10
+N95×50×10.5C	94.6	49.7	10.03	284.4	72	151	181	9.6	14.7	11	8

3.4.2 Test rig and procedure

A servo controlled hydraulic testing machine was used to apply compressive force by displacement control to the specimens at a constant rate of 0.4 mm/min. The tests were generally completed approximately by one hour. An initial load of 2 kN

was applied to the specimens to ensure full contact between the specimen and the upper and lower end plates. During testing, the machine was paused for 1.5 minutes prior to reaching the ultimate load, at the ultimate load and before the end of the test. The purpose of the pause is to obtain the static curve. The columns were compressed between fixed ends, restrained against rotations, twisting and warping. The test configuration for specimen $H70 \times 55 \times 4.2C$ is shown in Fig. 3.10. Three 25 mm-range LVDTs were used to measure the vertical deformation of the specimens. These were located between the upper and lower end plates. Strain gauges were attached at 10 mm intervals in the axial direction at mid-height of selected stub columns to determine the axial strain and to monitor local buckling. Since all sections are doubly symmetric, strain gauges were only adhered to one-quarter of the section perimeter. The applied load and readings from the LVDTs and strain gauges were recorded by a data logger at one second intervals during the tests.

Fig. 3.10   Stub column test configuration for specimen $H70 \times 55 \times 4.2C$

3.4.3 Results and failure modes

Compression tests on stub columns revealed the compression response of the cross-sections. The load-deformation curves for all tested stub columns are shown in Fig. 3.11. The values of experimental ultimate loads P_{exp} are given in Table 6.1 of Chapter 6, where comparisons with the nominal compressive design strengths predicted by the Aluminum Design Manual (AA, 2010), the Australian/New Zealand Standard (AS/NZS, 1997), Eurocode 9 (EC9, 2007) and the modified continuous strength method (CSM) are also given. It should be noted that four repeated tests have been conducted, and differences between the first test result and the repeated test result are within 1%, which can fully indicate the reliability of the stub column tests.
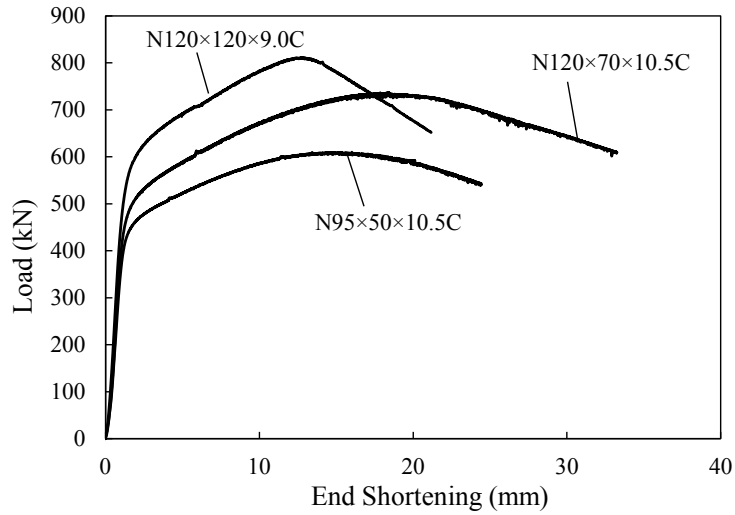
(a) SHS/RHS of normal strength aluminium alloys
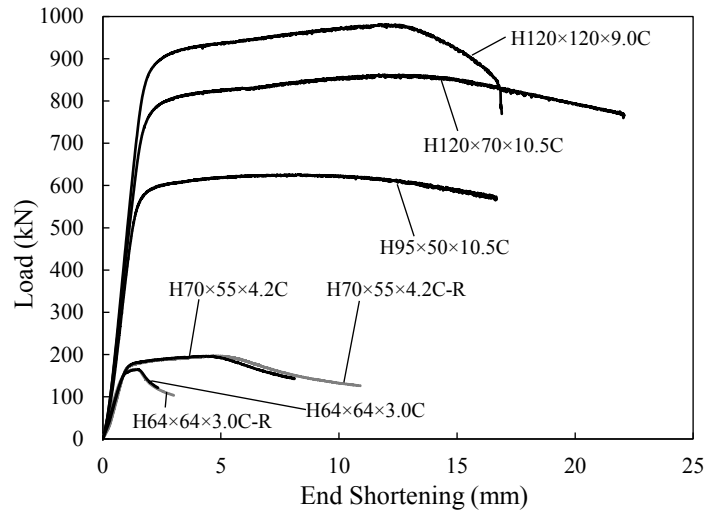
(b) SHS/RHS of high strength aluminium alloys
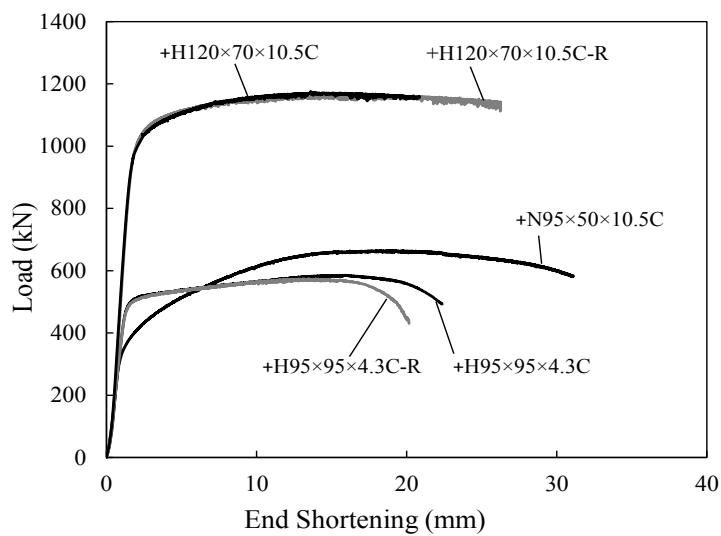
(c) SHS/RHS with internal cross stiffeners

Fig. 3.11   Load-end shortening curves from stub column tests

All specimens failed by a combination of material yielding and inelastic local buckling, as shown in Fig. 3.12, though for some test specimens, evidence of global buckling was observed around the ultimate load level. Local buckling was more pronounced in the more slender sections, as indicated by the non-uniform axial strain distributions shown for specimen $H64 \times 64 \times 3.0C$ in Fig. 3.13(a), compared to the more uniform distribution observed in the cross-stiffened specimen $+H95 \times 95 \times 4.3C$, shown in Fig. 3.13(b). The delay of local buckling in more stocky sections enabled deformation into the strain hardening range and, the attainment of ultimate loads significantly greater than the yield load Af_y, where A is the cross-section area. It should be noted that in some cases, ultimate capacities greater than Af_u were observed, which are achieved due to the increased cross-sectional areas arising from the Poisson's effect in the compressed sections.

| (a) | (b) | (c) |
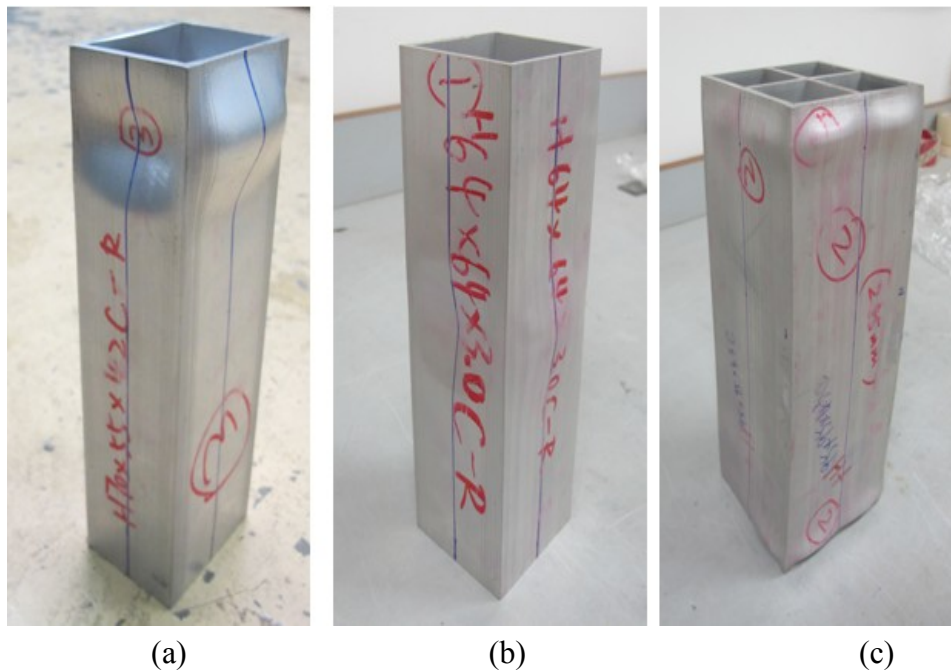
Fig. 3.12   Stub column failure modes for specimens (a) $H70 \times 55 \times 4.2C$-R, (b) $H64 \times 64 \times 3.0C$-R and (c) $+H95 \times 95 \times 4.3C$
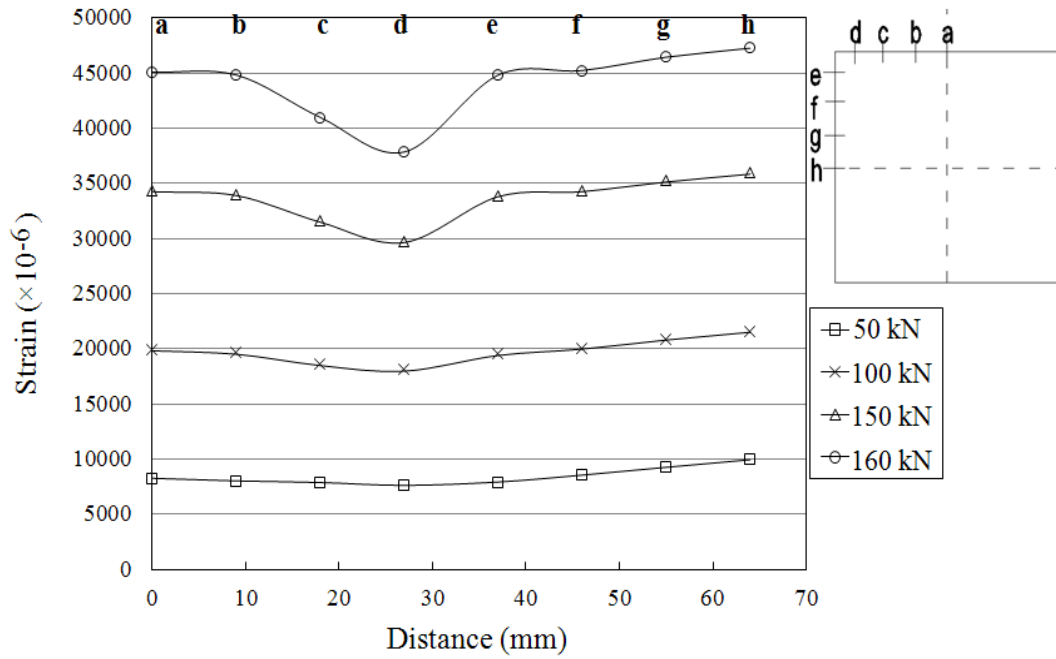
(a) H64×64×3.0C
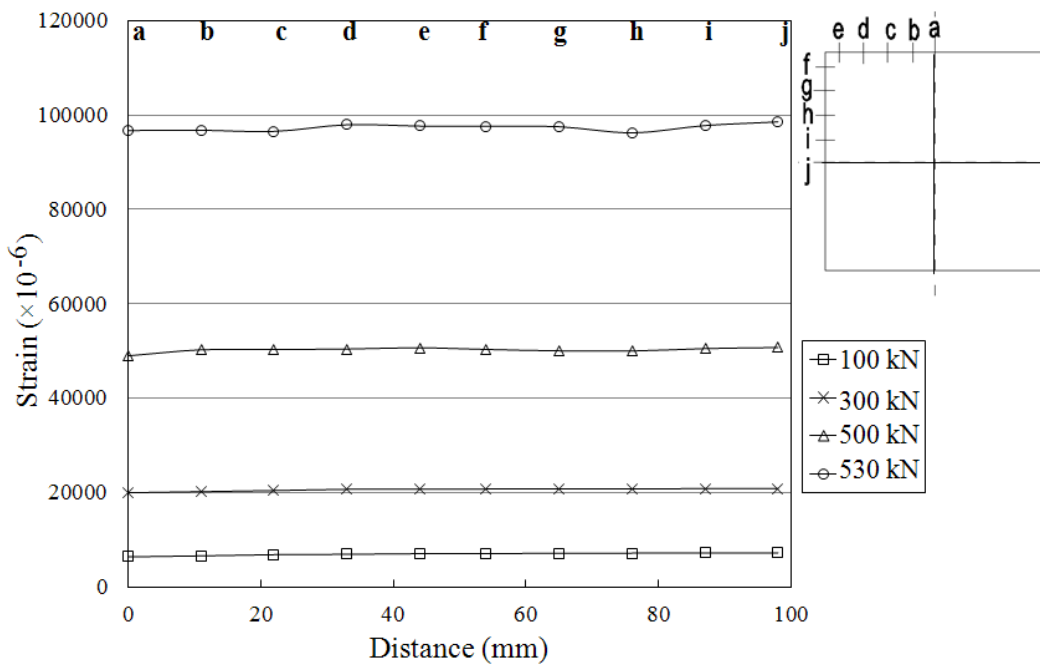
(b) +H95×95×4.3C

Fig. 3.13   Strain distribution around one quarter of the cross-section at

various load levels

40

3.5 Simply supported beam tests

Two series of simply supported bending tests, with 20 under three-point bending and 20 under four-point bending, have been carried out. The bending tests were conducted to assess moment capacities, rotation capacities and the significance of strain hardening.

3.5.1 Test specimens

The test specimens were fabricated by extrusion of grades 6063-T5 and 6061-T6 heat-treated aluminium alloys. The width-to-thickness ratios for box sections ranged from 2.8 to 20.5, while the ratios became 0.4 to 3.2 for box sections with internal cross stiffeners. The flexural specimens were defined by the symbols illustrated in Fig. 3.1. The cross-sectional dimensions and tensile material properties shown in Table 3.3 and Table 3.4 are the average measured values for each test specimen. The lengths of the beams were designed as 600 mm for three-point bending and 900 mm for four-point bending, but extension of 45 mm beyond each support was needed to ensure sufficient movement and rotation.

Table 3.3   Measured three-point bending specimen dimensions and material

properties from the tensile coupon tests

Specimen	B (mm)	H (mm)	t (mm)	L (mm)	E (GPa)	f_y (MPa)	f_u (MPa)	ε_u (%)	ε_f (%)	n	Webster hardness
H70×55×4.2B3	69.8	55.2	4.09	694.8	67	207	222	6.8	11.8	16	13
H55×70×4.2B3	54.7	69.8	4.09	693.4	67	207	222	6.8	11.8	16	13
H95×50×10.5B3	94.7	49.6	10.34	695.0	68	229	242	5.4	8.4	11	12
H50×95×10.5B3	49.5	94.6	10.34	693.0	68	229	242	5.4	8.5	11	12
H64×64×3.0B3	63.9	63.8	2.89	692.7	67	232	245	6.8	10.1	10	12
H120×120×9.0B3	120.0	119.9	8.90	691.4	65	225	234	6.3	8.0	13	12
H120×70×10.5B3	119.8	69.8	10.28	691.4	68	226	238	7.9	10.1	10	12
H70×120×10.5B3	69.8	119.8	10.26	691.8	68	226	238	7.9	10.1	10	12
H70×55×4.2B3-R	69.8	54.8	4.07	694.1	65	193	207	5.1	9.8	22	12
H50×95×10.5B3-R	49.5	94.7	10.33	692.8	68	229	242	5.4	8.4	11	11
H64×64×3.0B3-R	63.9	63.9	2.83	696.3	67	232	245	6.8	10.1	10	12
N120×70×10.5B3	120.0	69.9	10.4	689.1	71	139	194	6.6	14.1	9	10
N70×120×10.5B3	69.9	119.9	10.4	688.1	71	139	194	6.6	14.1	9	10
N120×120×9.0B3	119.9	119.9	8.9	692.8	69	181	228	8.9	14.5	9	11
+H50×95×10.5B3	49.7	94.7	10.35	693.6	70	199	218	4.7	11.0	8	11
+H95×50×10.5B3	94.6	49.8	10.30	695.8	70	199	218	4.7	11.0	8	11
+H70×120×10.5B3	69.8	119.9	10.28	689.4	70	192	222	8.5	11.2	14	12
+H120×70×10.5B3	119.9	69.8	10.32	692.4	70	192	222	8.5	11.2	14	12
+H95×95×4.3B3	95.2	95.1	4.13	690.6	67	228	240	6.0	6.4	12	12
+H95×95×4.3B3-R	95.2	95.3	4.17	693.9	67	228	240	6.0	6.4	12	12

Table 3.4   Measured four-point bending specimen dimensions and material properties from the tensile coupon tests

Specimen	B (mm)	H (mm)	t (mm)	L (mm)	E (GPa)	f_y (MPa)	f_u (MPa)	ε_u (%)	ε_f (%)	n	Webster hardness
H70×55×4.2B4	69.9	54.9	4.09	990.0	67	207	222	6.8	11.8	16	14
H55×70×4.2B4	54.9	69.9	4.10	993.1	67	207	222	6.8	11.8	16	14
H95×50×10.5B4	94.7	49.6	10.35	993.8	68	229	242	5.4	8.4	11	12
H50×95×10.5B4	49.6	94.7	10.37	988.3	68	229	242	5.4	8.4	11	12
H64×64×3.0B4	63.9	63.9	2.86	991.2	67	232	245	6.8	10.1	10	12
H120×120×9.0B4	120.0	112.0	8.92	995.8	65	225	234	6.3	8.0	13	12
H120×70×10.5B4	119.8	69.8	10.40	993.6	68	226	238	7.9	10.1	10	12
H70×120×10.5B4	69.9	119.8	10.30	996.5	68	226	238	7.9	10.1	10	12
H64×64×3.0B4-R	63.8	63.9	2.87	993.4	67	232	245	6.8	10.1	10	12
H70×55×4.2B4-R	70.0	54.9	4.08	989.5	67	207	222	6.8	11.8	16	14
H55×70×4.2B4-R	54.9	70.0	4.09	989.5	67	207	222	6.8	11.8	16	14
N50×95×10.5B4	49.7	94.8	10.36	995.3	69	164	211	7.3	13.7	10	11
N120×70×10.5B4	119.8	69.9	10.42	989.1	71	139	194	6.6	14.1	9	10
N70×120×10.5B4	69.9	119.8	10.42	996.3	71	139	194	6.6	14.1	9	10
N120×120×9.0B4	119.9	119.9	8.91	993.2	69	181	228	8.9	14.5	9	11
+H70×120×10.5B4	69.9	119.9	10.30	991.0	70	192	222	8.5	11.2	14	12
+H120×70×10.5B4	120.0	69.9	10.31	971.9	69	210	238	4.6	6.5	13	11
+H95×95×4.3B4	95.3	95.2	4.16	994.6	66	228	236	6.0	7.7	19	12
+N50×95×10.5B4	49.7	94.6	10.13	998.8	72	122	186	9.9	17.0	9	8
+N95×50×10.5B4	94.6	49.7	10.08	1000.5	72	122	186	9.9	17.0	9	8

3.5.2 Test rig and procedure

The bending tests were conducted by bending about the major and minor axis. A servo-controlled hydraulic testing machine was used to apply compressive force by displacement control to the solid bearing plates at a constant rate of 0.8 mm/min. The applied loads, as well as the readings from the LVDTs and strain gauges, were recorded by a data logger at one second intervals during the tests. Each test was generally completed within 90 minutes.

Hinges and pins were simulated by half rounds and rollers, respectively. The distance between the loading point and the supports was 300 mm. Stiffening steel plates of 100 mm width and 10 mm thickness, as well as wooden blocks within the tubes, were used at the loading points and the supports to prevent web crippling due to high load concentrations. Furthermore, steel bearing plates were placed between the specimens and rollers/half rounds for the purpose of spreading the concentrated loads.

In the three-point bending tests, the simply supported specimens were loaded at the mid-span, as shown in Fig. 3.14 and Fig. 3.15. One 100 mm LVDT was used to measure the vertical deflection at the mid-span. Two 25 mm LVDTs were placed at each end of the specimens to measure the end rotations. For the relatively slender sections (H70×55×4.2B3, H55×70×4.2B3 and H64×64×3.0B3), three strain gauges were adhered to the compression flange at a distance of 5 mm from the loading point, with two gauges near the flange-web junctions and one in the middle of the flange, to monitor possible local buckling (see Fig. 3.16).

In the four-point bending tests, the specimens were loaded symmetrically at two points through a spreader beam, as shown in Fig. 3.17 and Fig. 3.18. One 100 mm LVDT and two 50 mm LVDTs were used to measure the vertical deflection at the mid-span and at the loading points, respectively, in order to obtain the mid-span deflection and curvature in the constant moment region. Two 25 mm LVDTs were placed at each end of the beams to measure the end rotations.

Fig. 3.14   Schematic illustration of three-point bending test configuration

(dimensions in mm)

Fig. 3.15   Experimental setup for three-point bending tests

Fig. 3.16   Strain gauges attached on the compression flange

Fig. 3.17   Schematic illustration of four-point bending test configuration
(dimensions in mm)
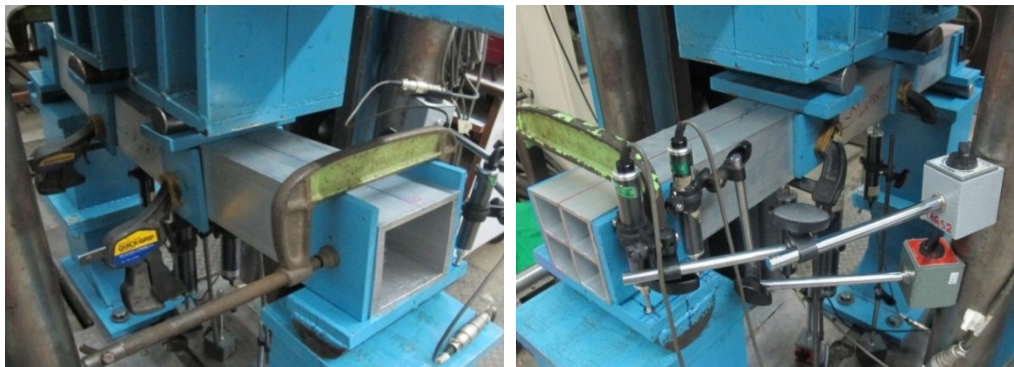
Fig. 3.18   Experimental setup for four-point bending tests

3.5.3 Results and failure modes

The moment–end rotation curves obtained from the three-point tests and the moment–curvature curves obtained from the four-point bending tests are presented in Fig. 3.19 and Fig. 3.20, respectively. The specimens generally failed by spread of plasticity (see Fig. 3.21(a)), except for beams H50×95×10.5B3 and H70×120×10.5B3 which failed by tensile material fracture at the mid-span. A

distinct sound was heard when the material split on the tension flange at failure, as seen in Fig. 3.21(b). As for some relatively stocky sections, local buckling were not observed during the tests, while for the relatively slender sections, inelastic local buckling occurred after significant plastic deformation.

The test results are presented in Table 6.3 and Table 6.4 for three-point bending and four-point bending tests, respectively. The end rotations reported in Table 6.3 for the three-point bending tests were calculated by the two LVDTs at each end of the beam (see Fig. 3.14). The curvatures reported in Table 6.4 for the four-point bending tests were derived though the deflection differences measured by the three LVDTs at the mid-span range (see Fig. 3.17). It should be noted that four repeated tests have been conducted for three-point bending tests and three repeated tests for four-point bending tests, and differences between the first test result and the repeated test result are generally within 5%, which can fully indicate the reliability of the simply supported bending tests.
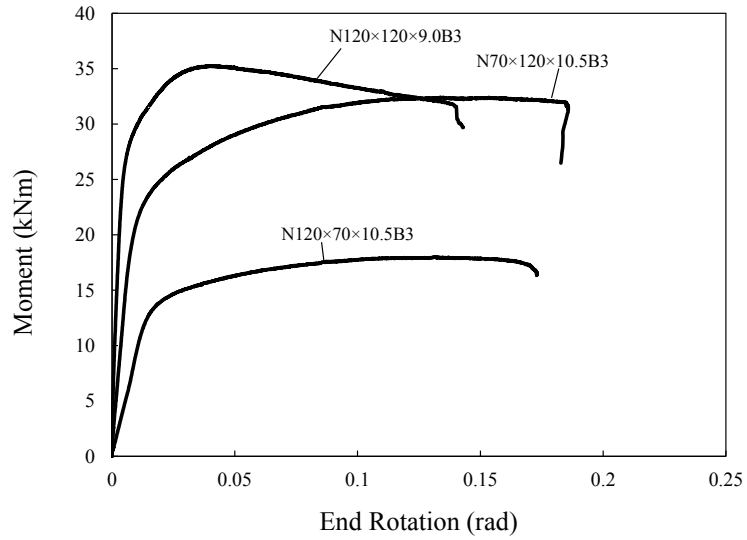
(a) SHS/RHS of normal strength aluminium alloy
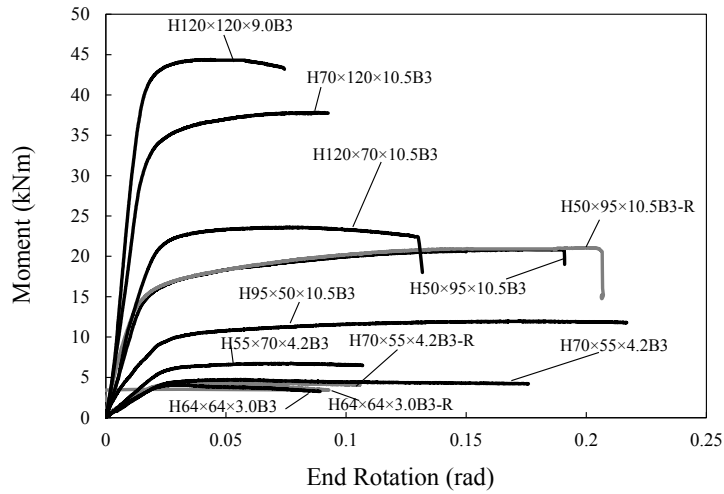
(b) SHS/RHS of high strength aluminium alloy
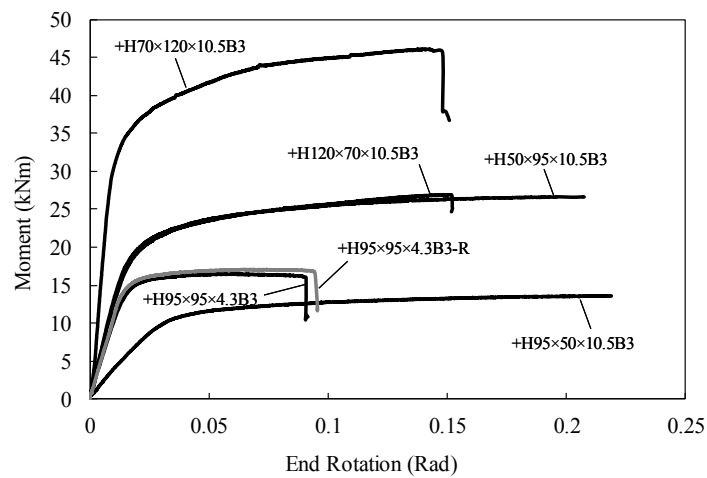
(c) SHS/RHS with internal cross stiffeners

Fig. 3.19   Moment–end rotation curves from three-point bending tests
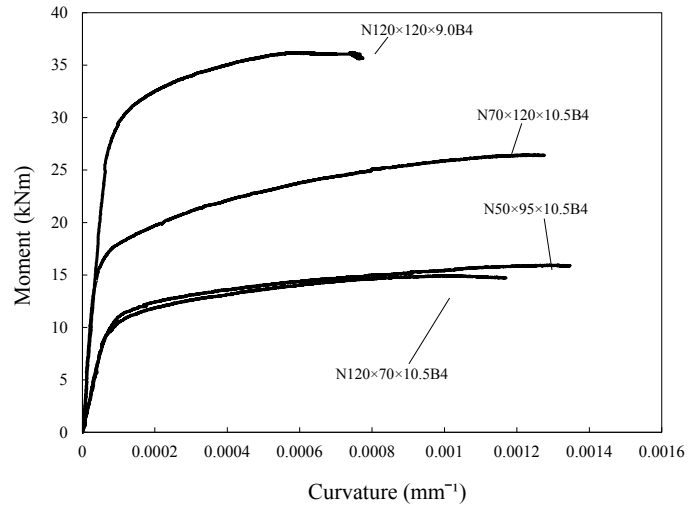
48

(a) SHS/RHS of normal strength aluminium alloy
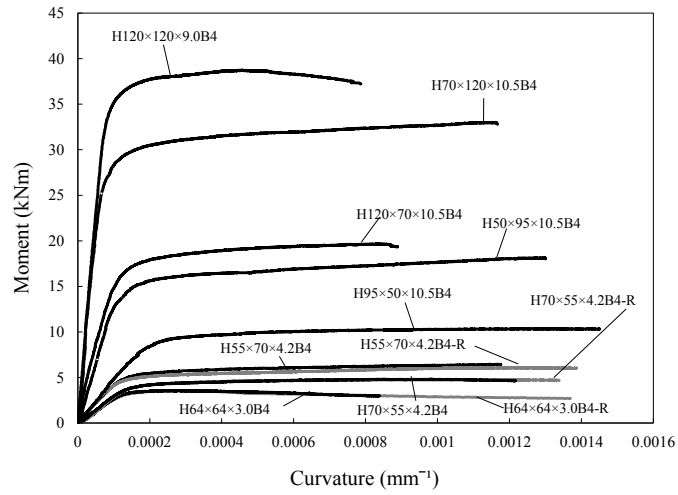
(b) SHS/RHS of high strength aluminium alloy
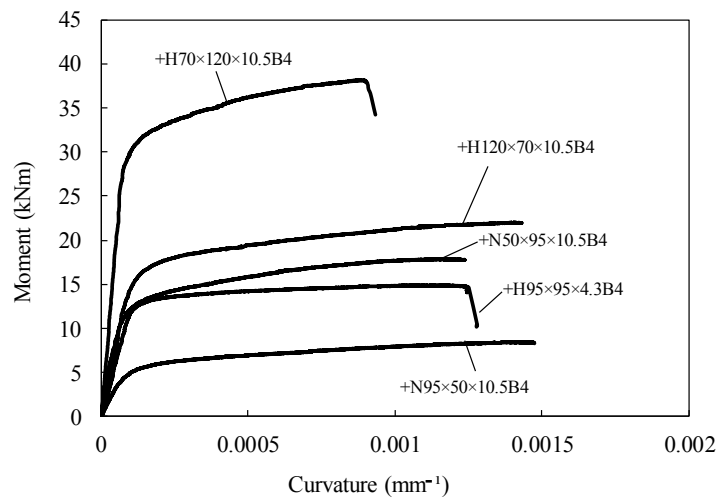
(c) SHS/RHS with internal cross stiffeners

Fig. 3.20   Moment–curvature curves from four-point bending tests

49

(a)
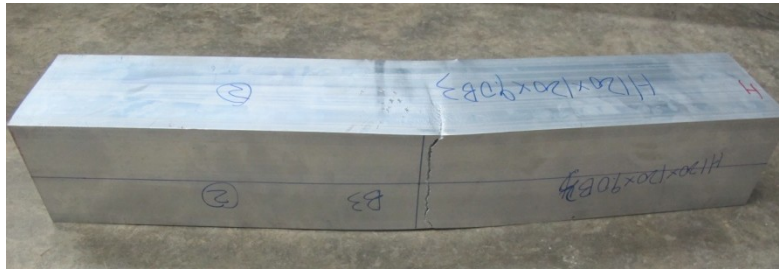
(b)

Fig. 3.21   Tested specimens failed by: (a) plasticity and inelastic local buckling, as well as (b) material fracture on the tension flange

3.5.4 Comparisons between three-point and four-point bending tests

Each cross-section in the present study was tested in two loading configurations, namely the three-point bending and four-point bending. In the former case, the members experience a moment gradient with coexistent shear while in the latter case, the members are subjected to a central region of constant moment and zero shear. Typical failed specimens from the three-point and four-point bending tests are presented in Fig. 3.22(a) and (b), respectively. The moment resistances and rotation capacities, as well as the comparisons between the test results for the two loading configurations, are shown in Table 3.5. Note that an LVDT error occurred during the testing of specimen H120×120×9.0B4, thus end rotation of this specimen could not be obtained.
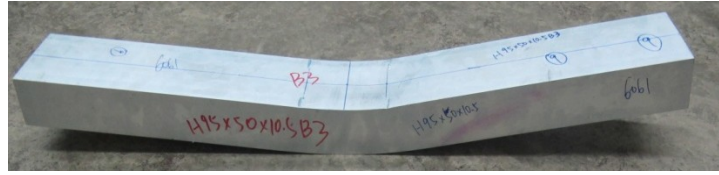
(a)

(b)

Fig. 3.22　　　Typical failed specimens from the (a) three-point and (b)

four-point bending tests

It should be noted that the definition of the rotation capacity R related to rotation θ_{rot} at the theoretical plastic hinge location for the three-point bending tests (Eq. 3.1) or to constant curvature κ_{rot} developed in the uniform moment region for the four-point bending tests (Eq. 3.2).

$$R = \frac{\theta_{rot}}{\theta_{pl}} - 1 \qquad\qquad\qquad\qquad (Eq. 3.1)$$

$$R = \frac{\kappa_{rot}}{\kappa_{pl}} - 1 \qquad\qquad\qquad\qquad (Eq. 3.2)$$

where θ_{pl} and κ_{pl} are the elastic rotation and curvature corresponding to the plastic moment $M_{pl} = W_{pl}f_y$, where W_{pl} is the plastic section modulus, θ_{rot} and κ_{rot} are the rotation and curvature at the point where the moment resistance drops back below M_{pl}. The definitions of rotation capacity based on the moment-rotation and the moment-curvature relationships have been explained and employed by Chan and Gardner (2008).

It can be seen from Table 3.5 that the ultimate moment capacities obtained from the three-point bending tests M_{exp}(B3) are consistently higher than those obtained

51

from the four-point bending tests M_{exp}(B4). For the normal strength aluminium (6063-T5) specimens, the ratio of M_{exp}(B3)/M_{exp}(B4) ranged between 1.12 and 1.41, while for the high strength (6061-T6) material, this ratio varied between 1.01 and 1.20. The presented comparative results obtained in this section coincide with the findings of others (Lay and Galambos, 1965, 1967; Kuhlmann, 1989; Chan and Gardner, 2008; Theofanous et al., 2009). This behaviour could be explained by the fact that local buckling is delayed in the presence of a moment gradient due to the restraint that the most heavily loaded cross-section experiences from the adjacent material which is at a lower stress level. Meanwhile, similar conclusions are also reached for rotation capacities by Theofanous et al. (2009), who found that both the ultimate moment capacity and rotation capacity are improved in the presence of a moment gradient, as compared to uniform bending. However, most of the moments obtained from the tests in this study did not drop back below M_{pl} due to large deformations and premature fracture, which hampered meaningful comparisons of rotation capacity.

Table 3.5   Comparison of moment and rotation capacity between the three-point and four-point bending tests.

Specimen	Three-point bending		Four-point bending		$\dfrac{M_{exp}(B3)}{M_{exp}(B4)}$
	M_{exp}(B3) (kNm)	Rotation capacity R (B3)	M_{exp}(B4) (kNm)	Rotation capacity R (B4)	
H70×55×4.2B3/B4	4.75	7.04	4.72	6.97	1.01
H55×70×4.2B3 /B4	6.76	9.00	6.49	7.70	1.04
H95×50×10.5B3/B4	12.09	6.02	10.35	7.25	1.17
H50×95×10.5B3/B4	21.09	10.76	18.04	12.75	1.17
H64×64×3.0B3 /B4	4.10	2.71[*]	3.59	0	1.14
H120×120×9.0B3/B4	44.42	5.75	38.75	---	1.15
H120×70×10.5B3/B4	23.59	6.58	19.66	6.12	1.20
H70×120×10.5B3 /B4	37.86	8.30	33.00	14.76	1.15
N120×70×10.5B3/B4	20.73	11.44	14.97	17.29	1.38
N70×120×10.5B3 /B4	37.30	31.50	26.45	29.31	1.41
N120×120×9.0B3/B4	40.53	25.48	36.22	12.46	1.12
Mean					1.18

Note: test moments did not drop back below M_{pl} except specimen H64×64×3.0B3

3.6   Continuous beam tests

In this section, experimental data on indeterminate aluminium alloy structures are presented. Two span bending tests (i.e. continuous beams over three supports) were employed. The experimental programme comprised 46 five-point bending tests of three different loading configurations. The bending tests were conducted to assess the flexural resistances and rotation capacities of aluminium alloy beams, as well as the significance of strain hardening and moment redistribution.

3.6.1 Test specimens

The test specimens were manufactured by extrusion, where 32 of them of grade 6061-T6 and 14 of grade 6063-T5 heat-treated aluminium alloy. The cross-sections of specimens and labelling systems are illustrated in Fig. 3.1; meanwhile, cross-sectional dimensions and material properties are given in Table 3.6 and Table 3.7 for SHS/RHS and SHS/RHS with internal cross stiffeners, respectively. Three loading configurations were examined for each cross-section. The nominal length was designed as 1600 mm, plus 90 mm extensions at the end supports.

Table 3.6   Measured five-point bending specimen dimensions and material properties from the tensile coupon tests (SHS/RHS)

Specimen	B (mm)	H (mm)	t (mm)	L (mm)	E (GPa)	f_y (MPa)	f_u (MPa)	ε_u (%)	ε_f (%)	n	Webster hardness
H55×70×4.2B5I	54.9	70.0	4.09	1695	70	261	282	6.0	6.5	16	14
H55×70´4.2B5I-R	54.9	69.9	4.08	1649	70	261	282	6.0	6.5	16	14
H70×55×4.2B5I	70.0	54.9	4.10	1702	70	261	282	6.0	6.5	16	14
H50×95×10.5B5I	49.7	94.7	10.34	1646	70	179	220	8.1	14.1	8	13
H95×50×10.5B5I	94.8	49.8	10.38	1696	70	179	220	8.1	14.1	8	12
H64×64×3.0B5I	63.9	63.9	2.86	1693	66	234	248	6.7	9.5	12	12
N50×95×10.5B5I	49.8	94.8	10.38	1696	69	164	211	7.3	13.7	10	11
N70×120×10.5B5I	70.0	119.9	10.42	1690	71	139	194	6.6	14.1	9	11
N120×70×10.5B5I	119.9	69.9	10.27	1652	71	139	194	6.6	14.1	9	11
N120×120×9.0B5I	120.0	120.0	8.89	1700	71	183	225	9.7	14.3	10	11
H55×70×4.2B5II	54.9	69.9	4.09	1652	70	261	282	6.0	6.5	16	14
H55×70×4.2B5II-R	54.9	69.9	4.07	1699	70	261	282	6.0	6.5	16	14
H70×55×4.2B5II	69.9	54.9	4.10	1695	70	261	282	6.0	6.5	16	14
H50×95×10.5B5II	49.7	94.8	10.39	1669	70	192	232	7.2	10.0	13	11
H95×50×10.5B5II	94.7	49.6	10.33	1694	70	179	220	8.1	14.1	8	11
H64×64×3.0B5II	63.9	63.9	2.85	1698	67	232	245	6.8	10.1	12	12
N70×120×10.5B5II	69.9	119.7	10.27	1694	71	139	194	6.6	14.1	9	11
N120×70×10.5B5II	119.8	69.9	10.26	1649	71	139	194	6.6	14.1	9	11
N120×120×9.0B5II	119.9	119.9	8.90	1696	69	188	229	9.1	13.2	11	11
H55×70×4.2B5III	54.9	69.9	4.08	1692	67	207	222	6.8	11.8	16	13
H55×70×4.2B5III-R	54.9	69.9	4.10	1694	70	261	282	6.3	6.5	16	14
H70×55×4.2B5III	69.9	54.9	4.11	1693	65	193	207	5.1	9.8	23	12
H50×95×10.5B5III	49.7	94.8	10.36	1643	70	192	232	7.2	10.0	13	12
H95×50×10.5B5III	94.8	49.7	10.34	1655	70	192	232	7.2	10.0	13	12
H64×64×3.0B5III	63.9	63.9	2.85	1696	66	234	248	6.7	9.6	12	12
N70×120×10.5B5III	69.9	119.8	10.27	1654	71	139	194	6.6	14.4	9	11
N120×70×10.5B5III	119.9	69.9	10.33	1644	71	139	194	6.6	14.1	9	11

Table 3.7   Measured specimen dimensions and material properties from the tensile coupon tests (SHS/RHS with internal cross stiffeners)

Specimen	B (mm)	H (mm)	t (mm)	L (mm)	E (GPa)	f_y (MPa)	f_u (MPa)	ε_u (%)	ε_f (%)	n	Webster hardness
+H50×95×10.5B5I	49.9	94.7	10.33	1660	70	199	218	4.7	11.0	8	11
+H95×50×10.5B5I	94.8	49.9	10.35	1646	70	199	218	4.7	11.0	8	11
+H70×120×10.5B5I	69.9	120.0	10.30	1699	70	192	222	8.5	11.2	13	12
+H120×70×10.5B5I	120.0	70.0	10.30	1652	70	192	222	8.5	11.2	13	12
+H95×95×4.3B5I	95.3	95.2	4.17	1648	66	228	236	6.0	7.7	19	12
+H95×95×4.3B5I-R	95.2	95.2	4.14	1652	67	228	240	6.0	6.4	12	12
+N50×95×10.5B5I	49.7	94.6	10.28	1649	68	151	182	9.6	14.7	14	6
+N95×50×10.5B5I	94.7	49.7	10.27	1644	68	151	182	9.6	14.7	14	6
+H50×95×10.5B5II	49.7	94.6	10.26	1643	70	199	218	4.7	11.0	8	11
+H70×120×10.5B5II	69.9	120.0	10.26	1656	70	192	222	8.5	11.2	13	12
+H120×70×10.5B5II	120.0	69.9	10.33	1695	70	192	222	8.5	11.2	13	12
+H95×95×4.3B5II	95.3	95.2	4.17	1693	67	228	240	6.0	6.4	12	12
+H95×95×4.3B5II-R	95.2	95.2	4.15	1695	66	228	236	6.0	7.7	19	12
+N95×50×10.5B5II	94.6	49.7	10.31	1656	68	151	181	9.6	14.7	9	6
+H50×95×10.5B5III	49.76	94.7	10.29	1698	70	199	218	4.7	11.0	8	11
+H70×120×10.5B5III	69.94	120.0	10.25	1699	69	210	238	4.6	6.5	13	11
+H120×70×10.5B5III	120.1	69.9	10.35	1690	69	215	229	7.5	10.7	9	10
+H95×95×4.3B5III	95.27	95.2	4.15	1606	69	208	238	7.0	9.5	15	13
+H95×95×4.3B5III-R	95.14	95.3	4.16	1696	67	228	240	6.0	6.4	12	12

3.6.2 Test rig and procedure

Three symmetric five-point bending configurations were employed herein, as shown in Fig. 3.23. The symbol "B5I" following the dimension refers to the first five-point loading configuration I where $L_1=L_2=400$ mm, while the other two configurations are denoted as B5II where $L_2=266.7$ mm (i.e. the loads are at one third of the span from the central support) and B5III where $L_2=533.3$ mm (i.e. the loads are at two thirds of the span from the central support).The purpose of adopting different test configurations was to vary the ratio of load levels between the formation of the first hinge and the final collapse mechanism, thus placing different rotation demands on the first-forming plastic hinge (Wang, 2011).

Similar to the simply supported bending tests, the loads were applied at two points through a spreader beam, as shown in Fig. 3.23. A 1000 kN capacity servo-controlled hydraulic testing machine was used to apply compressive force by displacement control at a constant rate of 0.8 mm/min for all tests. Steel rollers and a half round were employed to achieve rotationally free conditions at the beams ends, central support and loading points; longitudinal translation was restrained at the central support. Steel stiffening plates of 100 mm width and 10 mm thickness, as well as wooden blocks within the tubes were used at the loading points and the mid-span support to prevent web crippling due to high load concentrations. Furthermore, steel bearing plates were placed between the specimen and rollers or a half round for the purpose of spreading the concentrated loads. Two 100 mm LVDTs were used to measure the vertical deflection at the loading points. Two 50 mm LVDTs were placed 150 mm either side of the mid-span, in order to estimate the mid-span rotation. Two further LVDTs were placed at each end of the beams to measure the end rotations (see Fig. 3.24).
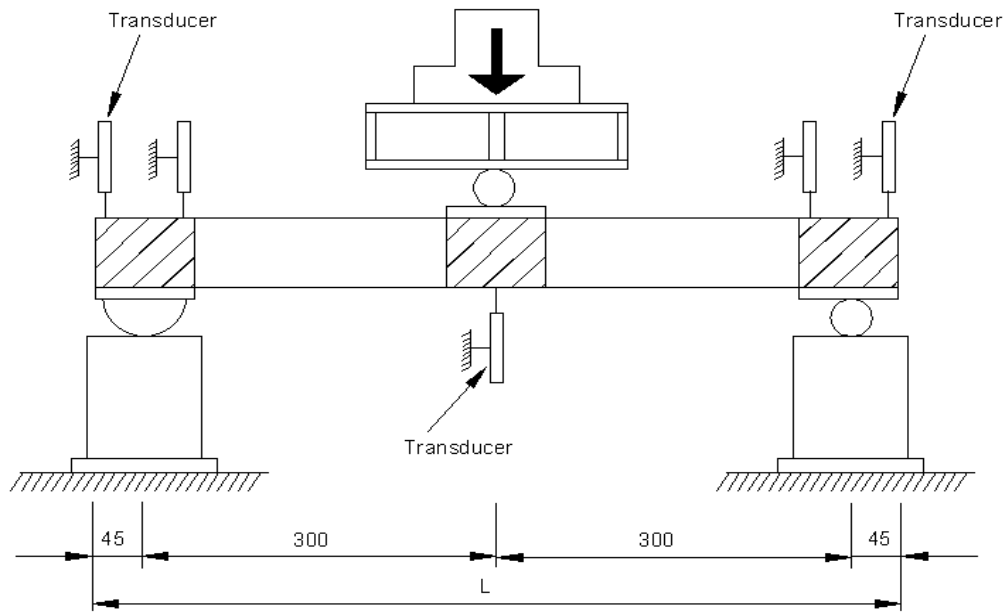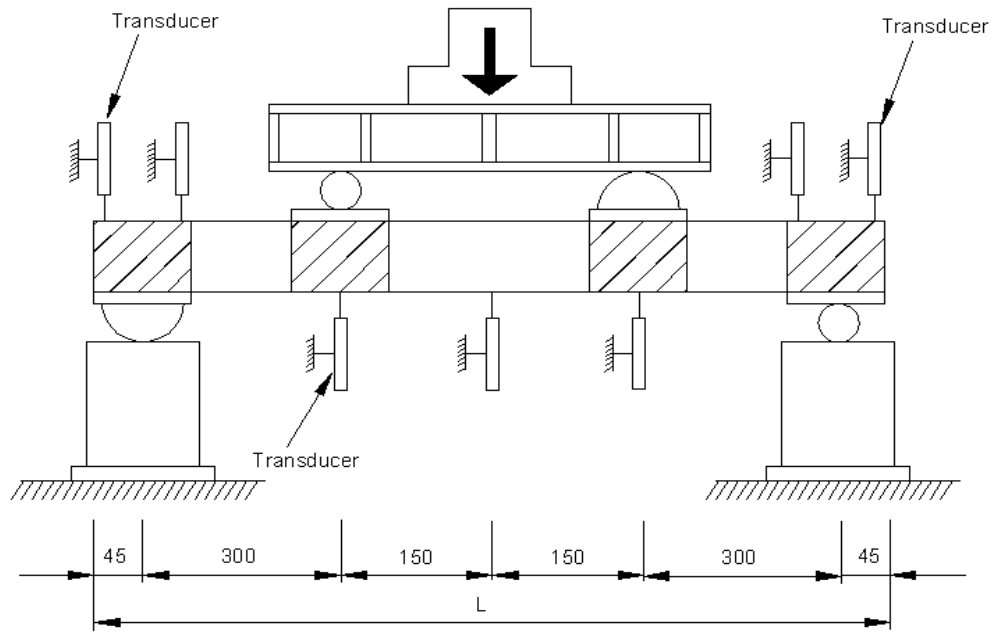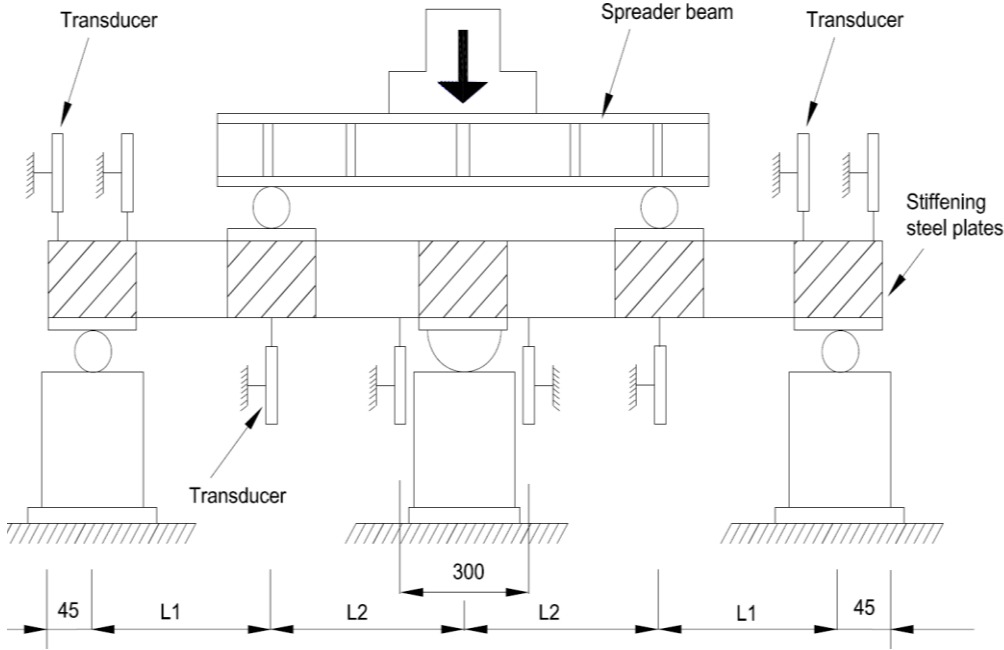

Fig. 3.23   Schematic illustration of five-point bending configuration

(dimensions in mm)

Fig. 3.24   Experimental setup for five-point bending tests

3.6.3 Results and failure modes

The specimens failed by material yielding and the formation of a collapse mechanism comprising three plastic hinges. For the loading configurations I and II, the first hinge formed at the central support while the latter two hinges formed at the loading points. In the loading configuration III, the plastic hinges formed in the reverse sequence. Significant local buckling was not visible in the test specimens before the first hinge formed, but could be observed on the relatively slender sections after significant plastic deformation. Three deformed specimens (i.e. N50×95×10.5B5I, N120×70×10.5B5II, H95×50×10.5B5III) exhibiting three distinct plastic hinges are shown in Fig. 3.25.

Fig. 3.25   Location of plastic hinges in deformed continuous beams
(N50×95×10.5B5I, N120×70×10.5B5II and H95×50×10.5B5III)

The five-point bending test results are presented in Table 6.8 to Table 6.10 for three different loading configurations, respectively. It should be noted that two repeated tests have been conducted for each loading configuration; similarly, good agreement between the first test result and the repeated test result were observed.

The load-deflection curves for the 46 continuous bending tests are shown in Fig. 3.26 and Fig. 3.27. In all cases, the ultimate loads attained in the tests were found to be beyond the theoretical loads corresponding to the occurrence of the first hinge (F_{h1}), as well as the calculated loads corresponding to the formation of the plastic collapse mechanism (F_{coll}), which is discussed in more detail in Chapter 6.
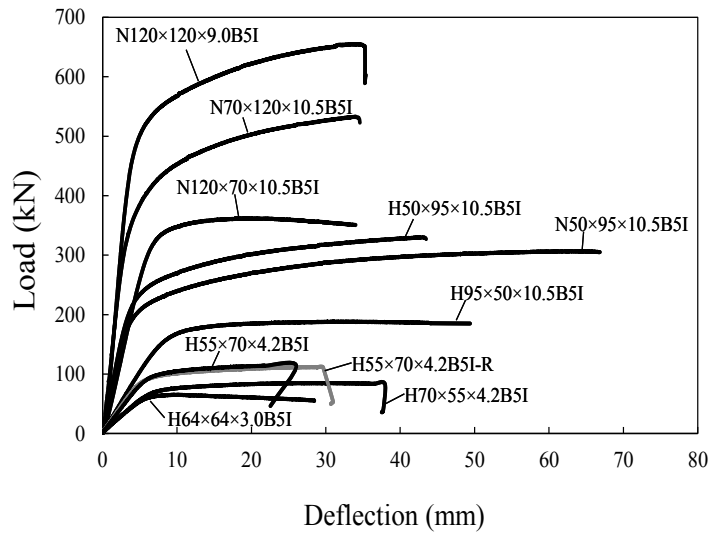
(a) Configuration I
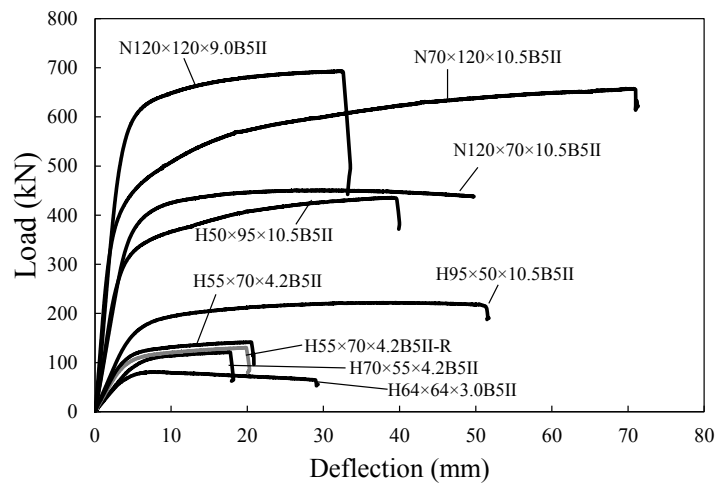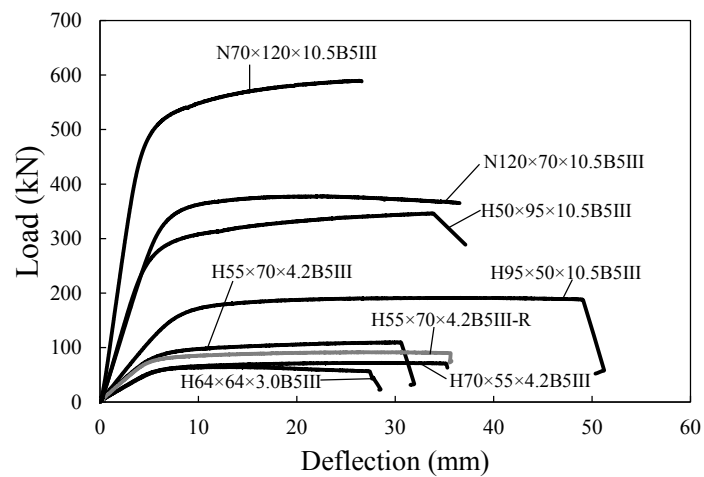
(b) Configuration II

(c) Configuration III

Fig. 3.26   Load versus mid-span deflection curves from five-point bending
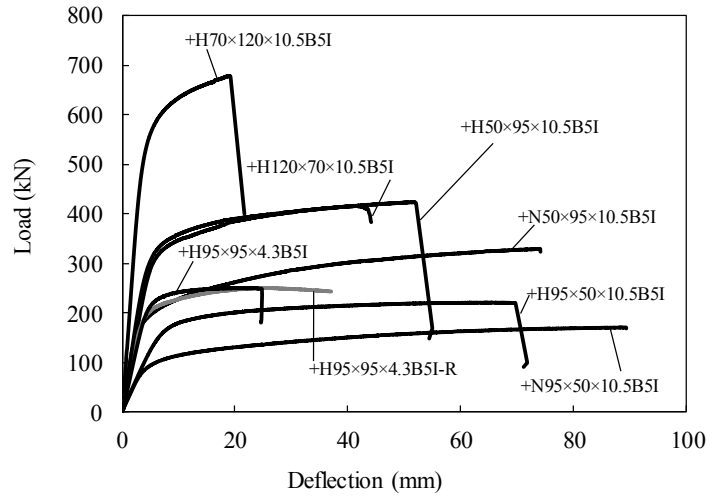
tests on SHS/RHS

(a) Configuration I
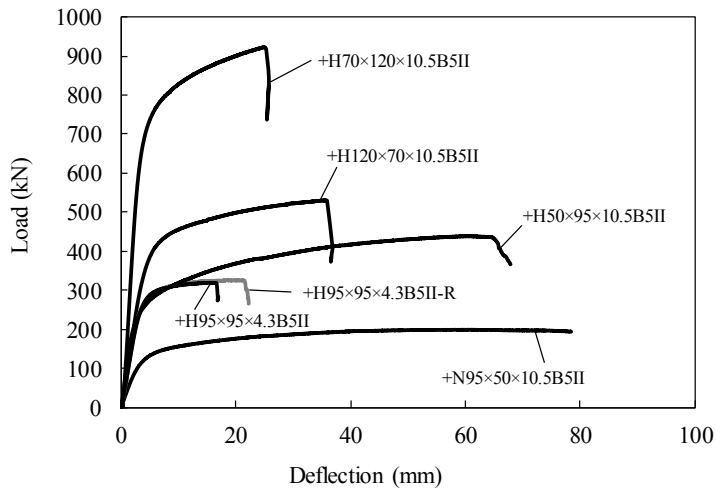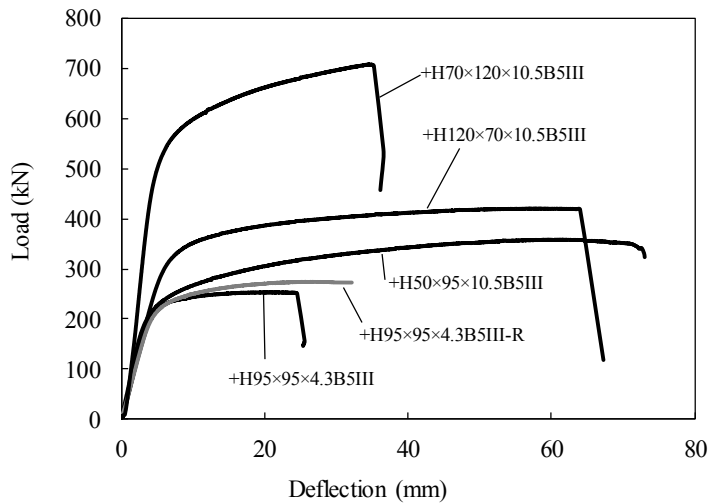
(b) Configuration II

(c) Configuration III

Fig. 3.27   Load – mid-span deflection curves from five-point bending tests

on SHS/RHS with internal cross stiffeners

3.7 Summary

A total of 11 stub column tests, 40 simply supported beam tests, 46 continuous beam tests and a number of tensile coupon tests have been conducted. The numerical parametric studies are presented in Chapter 4 to generate additional numerical results. The combined experimental and numerical results are used in Chapter 6 (in conjunction with all available test results in the literature) for comparisons with design predictions of the proposed CSM approach as well as the existing Aluminum Design Manual (AA, 2010), the Australian/New Zealand Standard (AS/NZS, 1997) and Eurocode 9 (EC9, 2007).

CHAPTER 4
NUMERICAL STUDIES

4.1 Introduction

Owing to the cost and time taken to generate extensive test data on aluminium alloy structures, numerical studies were undertaken in parallel to supplement the experimental investigations. The nonlinear finite element (FE) analysis package *ABAQUS 6.10-1* (2010) was employed in this research to simulate the bending experiments and, once validated, to conduct parametric investigations. This chapter describes the development of the FE models, the validation of the models against existing test data presented in the previous chapter, and the parametric studies to generate further results.

4.2 Numerical simulations and validation

4.2.1 General

To ensure the accuracy of simulated models, the measured geometry, initial local geometric imperfections and material properties of the test specimens were included in the finite element (FE) models. The models were built based on the centreline dimensions of cross-sections.

Contact simulation was employed to model the relation between the solid plates (master surface) and the beam surfaces (slave surface): hard contact in the normal direction and friction penalty contact (with the friction coefficient = 0.1) in the tangential direction. Penetration of the contact pairs was prevented.

Residual stresses of the test specimens were not measured in the experimental work and not explicitly introduced into the FE models, but their influence was inherently presented in the coupon test results and thus already included in the material modelling.

Initial geometric imperfections exist in all structural members and influence their structural responses, and hence they were included in this numerical study. For convenience in numerical analyses, the initial local geometric imperfections were incorporated in the form of the lowest regular local buckling mode shape (See Fig. 4.1 for continuous beams), as obtained from linear eigenvalue buckling analysis (Dawson and Walker, 1972). The amplitude was defined as 0.2 mm, as recommended in Chapter 3. It was found that sensitivity of the simulated results to imperfections was generally relatively low.
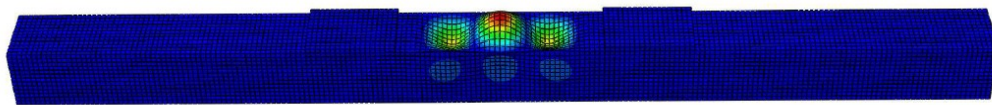
Fig. 4.1   Initial local geometric imperfections incorporated in FE models (i.e. the lowest appropriate buckling mode) for specimen $H64 \times 64 \times 3.0B4$

Even though specimens displayed symmetry in geometry and loading configurations, the authors still opted for modelling the full specimen length and full cross-sections. This was done to ensure that possible anti-symmetric local buckling modes were not suppressed, which, in some cases, had marginally lower corresponding eigenvalues than their symmetric counterparts (Theofanous et al., 2014).

Boundary conditions were carefully modelled in accordance with the tests conducted at the laboratory. Line loads were applied through bearing plates, to

avoid high load concentrations. Appropriate degrees of freedom were restrained at the bottom flange of the specimens to simulate simple support conditions. The beams were restrained longitudinally at the mid-span only.

Displacement-controlled nonlinear numerical analyses were performed by employing the Riks programme (ABAQUS, 2010) to allow the post ultimate path of the modelled specimens to be captured. The loading control employed in the FE analyses was identical to that used in the tests, by means of imposing vertical displacement to the solid bearing plates. The applied loads, the resistances, the mid-span deflection as well as the end rotations were obtained from the numerical analyses.

4.2.2 Type of element and mesh

The reduced integration four-nodded doubly curved shell element S4R has been employed in the present study to model the aluminium alloy members. This S4R general purpose shell element has six degrees of freedom per node. The steel loading plates utilised in the tests were modelled using 10 mm thick solid extruded plates that were free to rotate in-plane. A uniform optimum mesh size of 10 mm × 10 mm was chosen for the FE models to achieve accurate results within reasonable computational time.

Shell element is a combination of the two-dimensional plate bending element and membrane element. Shell element is applicable for thin-walled structures, and has been well employed in thin-walled structure problems. Furthermore, shell element is easier to mesh and needs less computational time comparing to other types of elements.

4.2.3 Material properties

As one of the most important aspects of FE simulations, the accuracy of material modelling significantly affects the performance of the FE models. In the linear analyses stage, the material properties were defined by the Young's modulus, the Poisson's ratio and the yield stress (0.2% proof stress). In the nonlinear stage, the material nonlinearity was included in the FE models by specifying sets of values of true stress and plastic strain to define a piecewise linear response. The relationship between true stress σ_{true} and engineering stress σ, as well as true plastic strain ε_{true}^{pl} and engineering strain ε have been given in Eqs. 2.3 and 2.4, respectively, as explained in Chapter 2.5.2 and specified in *ABAQUS 10-1* (2010). The true stress-strain curve was discretised and represented by approximately 20 points in the FE models.

4.2.4   Validation of simply supported beam model

4.2.4.1   Comparison of failure modes

In general, the initial stiffness, failure modes (Fig. 4.2 and Fig. 4.3) and the general shape of the moment-curvature curves (Fig. 4.4) of the FE models followed those obtained from the experiments closely. Fig. 4.2 and Fig. 4.3 show that elastic local buckling was not observed in both tests and FE models, while both test specimens and FE models failed by material yielding.
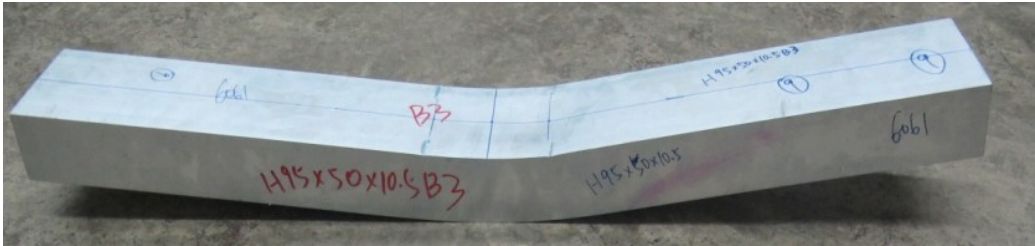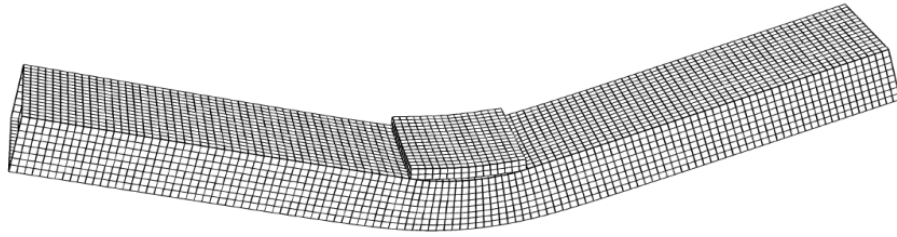
Fig. 4.2   Comparison between the three-point bending experimental and

numerical specimen (H95×50×9.0B3)
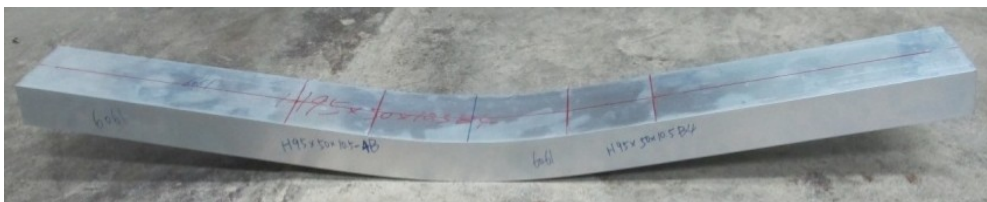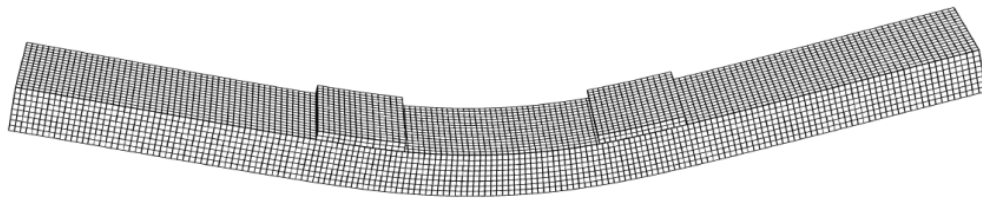
Fig. 4.3   Comparison between the four-point bending experimental and

numerical specimen (H95×50×9.0B4)

A typical comparison of the moment-curvature curves (for specimen H120×120×9.0B4) is depicted in Fig. 4.4, indicating good agreement between the experimental and numerical behaviour of a typical simple beam, while the comparisons for other specimens are presented in Appendices C and D. Fig. 4.5 shows stress and strain distribution profiles of the mid-span cross-section at the elastic, plastic and ultimate bending moments, corresponding to Fig. 4.4. It can be observed that at the elastic moment capacity level (see Fig. 4.5 (a) and (b)), the stress of the profile was varying linearly; at the plastic moment capacity level (see Fig. 4.5 (c) and (d)), the section was almost fully yielding with the external fibre reached the ultimate stress of the material; at the ultimate load level (see Fig. 4.5 (e) and (f)), the cross-section is fully yielded and the ultimate stress was reached.
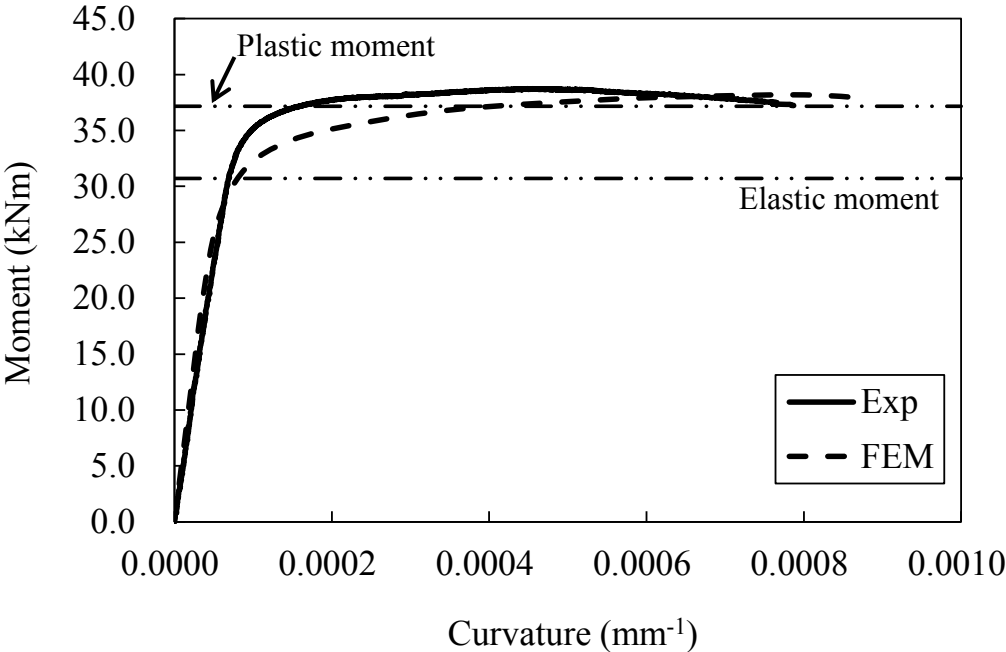
Fig. 4.4   Experimental and numerical moment-curvature curves for specimen H120×120×9.0B4

67
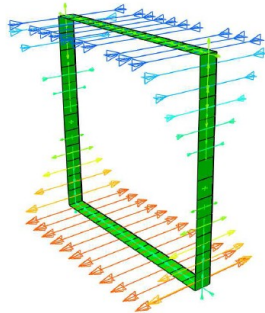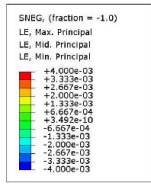
(a) Strain distribution at elastic moment   (b) Stress distribution at elastic moment
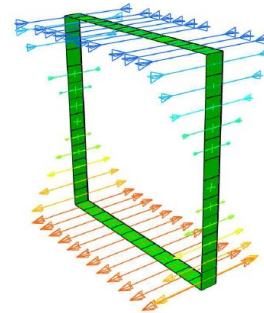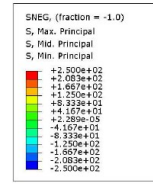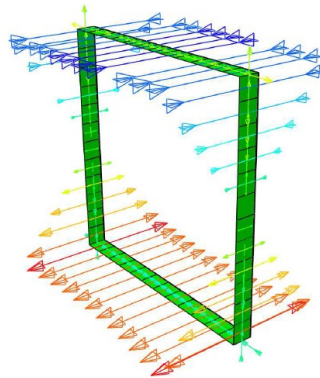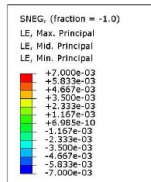
(c) Strain distribution at plastic moment   (d) Stress distribution at plastic moment
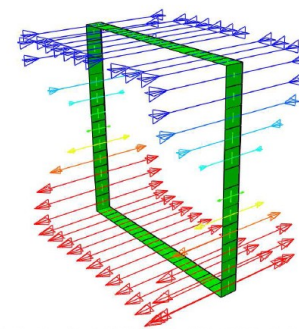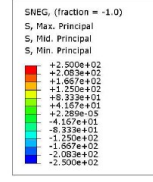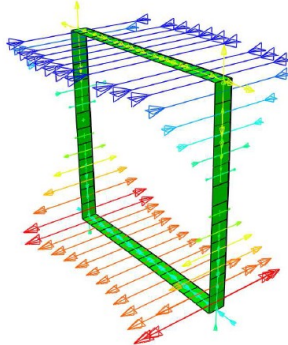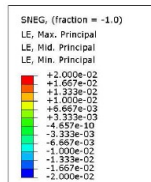
(e) Strain distribution at ultimate moment   (f) Stress distribution at ultimate moment
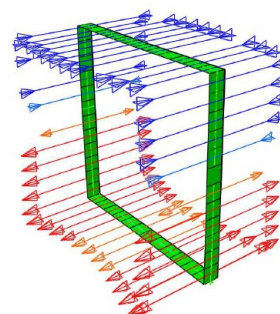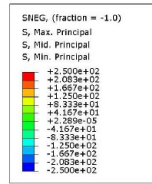
Fig. 4.5   Stress and strain distributions at the mid-span cross-section of specimen H120×120×9.0B4

4.2.4.2 Comparison with test results

The accuracy of the numerical simulations was assessed by comparing the ultimate moments achieved in the FE models (M_{FE}) with the experimental values (M_{exp}), as illustrated in Table 4.1. The results were seen to be in good overall agreement, leading to 1% - 2% over-prediction in general for both three-point and four-point beams and a small scatter (coefficient of variation = 0.059 for three-point bending and 0.076 for four-point bending), which indicates that the FE models are capable of replicating the experimentally observed structural response of the specimens accurately.

Table 4.1   Comparison between experimental and numerical results

Specimen	M_{exp} (kNm)	M_{FE} (kNm)	$\dfrac{M_{exp}}{M_{FE}}$	Specimen	M_{exp} (kNm)	M_{FE} (kNm)	$\dfrac{M_{exp}}{M_{FE}}$
H70×55×4.2B3	4.8	5.0	0.96	H70×55×4.2B4	4.7	4.3	1.09
H70×55×4.2B3-R	4.4	4.6	0.95	H70×55×4.2B4-R	4.8	4.3	1.11
H55×70×4.2B3	6.8	6.2	1.09	H55×70×4.2B4	6.5	6.8	0.96
H95×50×10.5B3	12.1	11.9	1.02	H55×70×4.2B4-R	6.1	6.8	0.90
H50×95×10.5B3	21.1	22.0	0.96	H95×50×10.5B4	10.4	10.5	0.99
H50×95×10.5B3-R	20.8	21.4	0.97	H50×95×10.5B4	18.0	19.1	0.94
H64×64×3.0B3	4.1	4.3	0.95	H64×64×3.0B4	3.6	3.8	0.95
H64×64×3.0B3-R	4.3	4.4	0.98	H64×64×3.0B4-R	3.6	3.8	0.95
H120×120×9.0B3	44.4	44.4	1.00	H120×120×9.0B4	38.8	38.4	1.01
H120×70×10.5B3	23.6	25.4	0.93	H120×70×10.5B4	19.5	17.4	1.12
H70×120×10.5B3	37.9	40.8	0.93	H70×120×10.5B4	33.0	35.5	0.93
N120×70×10.5B3	18.0	20.0	0.90	N50×95×10.5B4	16.0	18.3	0.87
N70×120×10.5B3	32.4	33.4	0.97	N120×70×10.5B4	15.0	17.2	0.87
N120×120×9.0B3	234.1	275.4	0.85	N70×120×10.5B4	26.5	28.2	0.94
+H50×95×10.5B3	26.7	24.7	1.08	N120×120×9.0B4	36.2	35.5	1.02
+H95×50×10.5B3	13.6	13.5	1.01	+N50×95×10.5B4	17.6	18.7	0.94
+H70×120×10.5B3	45.7	43.1	1.06	+N95×50×10.5B4	8.4	7.8	1.08
+H120×70×10.5B3	26.9	26.7	1.00	+H70×120×10.5B4	38.2	37.8	1.01
+H95×95×4.3B3	16.5	16.4	1.00	+H120×70×10.5B4	22.0	21.4	1.03
+H95×95×4.3B3-R	17.1	16.8	1.02	+H95×95×4.3B4	14.9	14.3	1.04
		Mean	0.98			Mean	0.99
		COV	0.059			COV	0.076

4.2.5 Validation of continuous beam models

4.2.5.1 Comparison of failure modes

Observed failure modes in the tests included material yielding with the formation of a collapse mechanism and tensile material fracture. Inelastic local buckling occurred on the compression flanges of the relatively slender sections after significant plastic deformation, whereas the formation of a collapse mechanism comprising three plastic hinges was clearly observed in all simulated specimens. A comparison of the typical failure modes between tested and simulated specimens is depicted in Fig. 4.6. Full load-deflection responses obtained from all tests and simulations were compared (see Appendix E); a typical example is shown in Fig. 4.7. In general, the initial stiffness and the general shape of the numerical load-deflection curves closely matched those obtained from experiments.

In the experimental programme, some specimens failed by material fracture at the tension flanges, due to exceedance of the material fracture strain ε_f. This failure mode was accounted for in the FE models by monitoring the tensile strains and identifying when the tensile fracture strain ε_f as obtained from the tensile coupon tests, was reached. This is shown in Fig. 4.7, where a typical load-deformation response is given. In the graph, the solid dot signifies the point where the strain at the tension flange of the simulated specimen reaches the material fracture strain ε_f, hence signifying tensile failure.

70

Fig. 4.6   Experimental and numerical failure modes for specimen
H95×50×10.5B5I
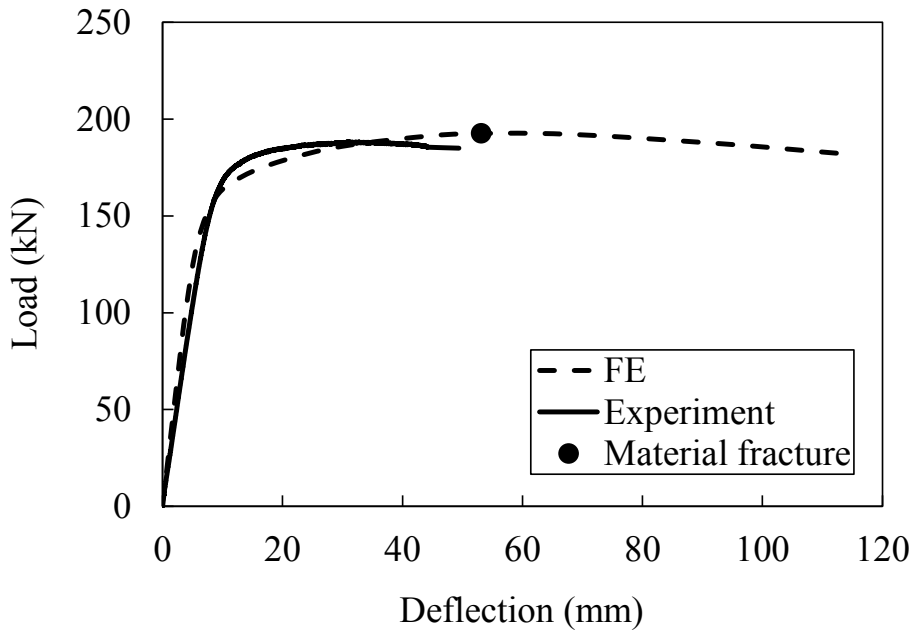
Fig. 4.7   Experimental and numerical load-deflection curves for specimen
H95×50×10.5B5I

A pair of typical curves for loading configuration II (from specimen
H64×64×3.0B5II) is shown in Fig. 4.8. Key observations from Fig. 4.8 include: (1)
Initially, the moment at the support was approximately twice that in the span, as
predicted by elastic bending theory; (2) the support moment therefore reached its
ultimate capacity earlier than the span moment, after which the support moment

decreased slightly while, at the same time, the span moment kept increasing until reaching its cross-section moment capacity; (3) the applied load continued to increase after the support moment had reached its maximum value, and only dropped when the degree of reduction in the support moment outweighed the increase in the span moment; (4) both the support moment and the span moment achieved capacities greater than the plastic moment M_{pl}, owning to the effect of strain hardening. The stress distribution profile of the cross-section at the mid-span (i.e. the location of the first hinge location) and the loading points (i.e. the location of the second hinges) are presented in Fig. 4.9, while the Fig. 4.9 (a) and (b) correspond to the formation of the first hinge, and Fig. 4.9 (c) and (d) indicate the stress distributions at the experimental ultimate load level. It is found that after the formation of the first hinge, the cross-section bending moment of the first hinge beyond the plastic moment capacity, while the cross-section bending moment at the location of the second hinges keep increasing until the whole system reached the ultimate load level.
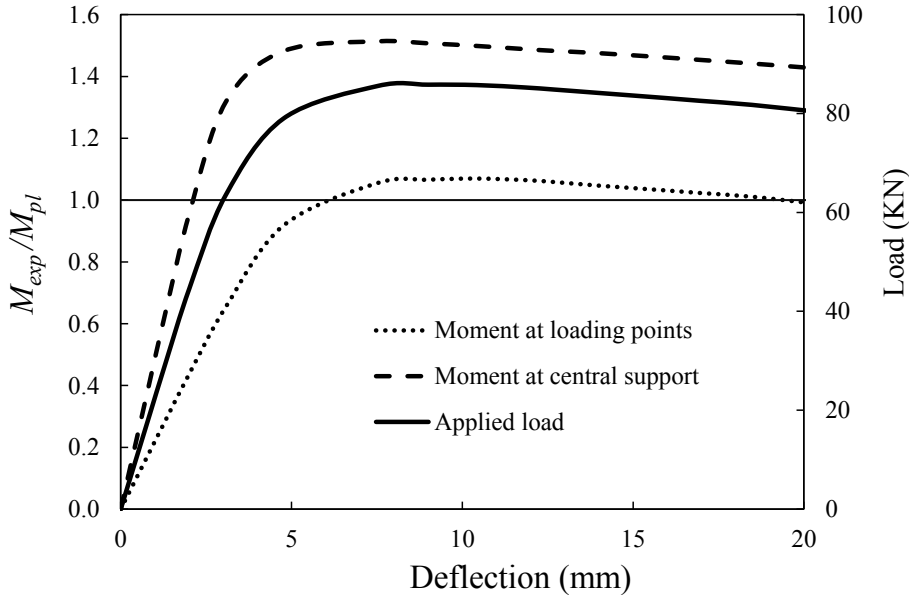
Fig. 4.8   Applied load and moment displacement curves for specimen H64×64×3.0B5II obtained from finite element analyses

72

(a) Stress distribution of the mid-span
cross-section at the formation of the first hinge

(b) Stress distribution of cross-section at the
loading points at the formation of the first hinge

(c) Stress distribution of the mid-span
cross-section at the ultimate load level

(d) Stress distribution of cross-section at the
loading points at the ultimate load level
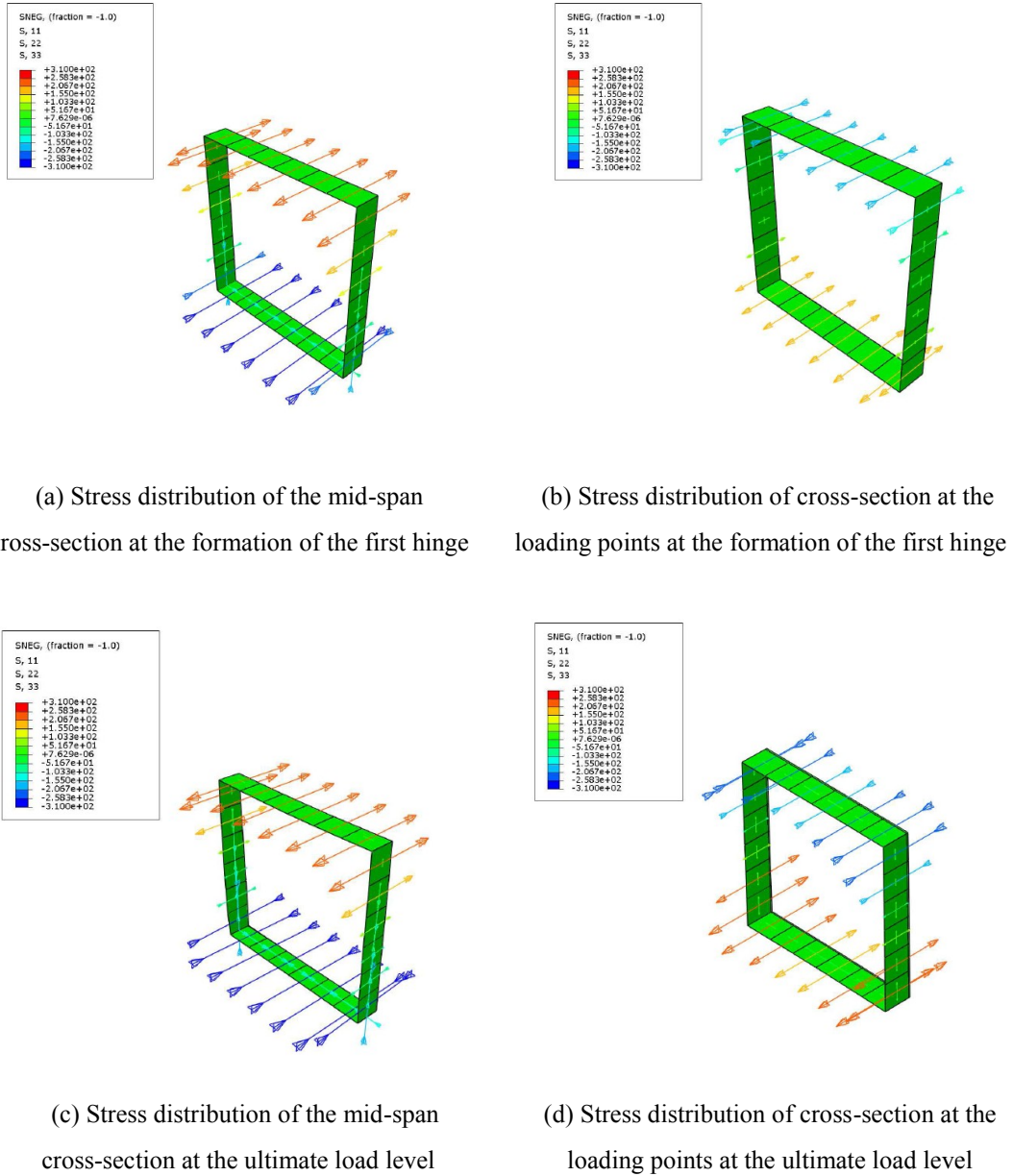
Fig. 4.9   Stress distributions of the cross-sections at mid-span (the location

of the first hinge) and loading points (the location of the second hinges) for

specimen H64×64×3.0B5II

4.2.5.2 Comparison with test results

The FE models developed in this study were initially validated against a total of 46

test results from the three different bending configurations (Table 4.2). Overall,

good agreement between the experimental (F_{exp}) and numerical results (F_{FE}) was observed, though for some cases, the predicted capacities deviated to some extent from the experimental results. On average, ultimate loads were predicted 100% accurate to tests (the ratio F_{exp}/F_{FE} = 1.00) with a low coefficient of variation (COV = 0.062) (Table 4.2). Therefore, it can be concluded that the FE models developed herein are able to simulate the structural behaviour of members and to capture strain hardening and the spread of plasticity in the aluminium alloy continuous beams.

Table 4.2   Comparison of ultimate loads between experimental and numerical results

Specimen	F_{exp} (kN)	F_{FE} (kN)	$\dfrac{F_{exp}}{F_{FE}}$
H55×70×4.2B5I	114.1	115.	0.99
H55×70×4.2B5I-R	112.3	120.	0.93
H70×55×4.2B5I	84.9	77.3	1.10
H50×95×10.5B5I	329.9	358.	0.92
H95×50×10.5B5I	188.2	192.	0.98
H64×64×3.0B5I	65.3	68.5	0.95
N50×95×10.5B5I	306.7	332.	0.92
N70×120×10.5B5I	532.9	506.	1.05
N120×70×10.5B5I	362.0	401.	0.90
N120×120×9.0B5I	655.2	665.	0.99
H55×70×4.2B5II	141.5	124.	1.14
H55×70×4.2B5II-R	130.6	124.	1.05
H70×55×4.2B5II	120.2	124.	0.96
H50×95×10.5B5II	436.0	473.	0.92
H95×50×10.5B5II	222.1	242.	0.92
H64×64×3.0B5II	80.8	85.8	0.94
N70×120×10.5B5II	693.9	693.	1.00
N120×70×10.5B5II	450.8	462.	0.98
N120×120×9.0B5II	657.8	665.	0.99
H55×70×4.2B5III	91.6	90.2	1.02
H55×70×4.2B5III-R	109.6	117.	0.93
H70×55×4.2B5III	72.1	68.1	1.06
H50×95×10.5B5III	346.2	357.	0.97
H95×50×10.5B5III	191.4	199.	0.96
H64×64×3.0B5III	64.3	64.9	0.99
N70×120×10.5B5III	589.7	646.	0.91
N120×70×10.5B5III	377.7	382.	0.99

Table 4.2   (cont'd)

Specimen	F_{exp} (kN)	F_{FE} (kN)	$\dfrac{F_{\text{exp}}}{F_{FE}}$
+H50×95×10.5B5I	423.8	377.8	1.12
+H95×50×10.5B5I	220.9	212.1	1.04
+H70×120×10.5B5I	678.4	680.4	1.00
+H120×70×10.5B5I	416.3	415.0	1.00
+H95×95×4.3B5I	250.4	239.1	1.05
+H95×95×4.3B5I-R	250.6	244.9	1.02
+N50×95×10.5B5I	329.6	328.7	1.00
+N95×50×10.5B5I	171.1	178.4	0.96
+H50×95×10.5B5II	438.9	431.5	1.02
+H70×120×10.5B5II	922.7	871.5	1.05
+H120×70×10.5B5II	530.4	535.3	1.00
+H95×95×4.3B5II	319.4	326.7	0.98
+H95×95×4.3B5II-R	326.0	310.1	1.05
+N95×50×10.5B5II	199.1	218.1	0.91
+H50×95×10.5B5III	358.4	317.3	1.13
+H70×120×10.5B5III	708.2	655.7	1.08
+H120×70×10.5B5III	420.2	402.0	1.04
+H95×95×4.3B5III	274.3	253.3	1.08
+H95×95×4.3B5III-R	253.4	232.5	1.09
		Mean	1.00
		COV	0.062

4.3 Parametric studies

Having validated the numerical models against the experimental results, these models were used to carry out extensive parametric studies to assess the bending behaviour of aluminium alloy beams over a wider range of cross-section slenderness. Meanwhile, the parametric studies were also performed to assess the effect of key parameters, such as cross-section slenderness, cross-section aspect ratio and moment gradient on the strength, strain hardening and moment distribution behaviour of aluminium alloy members.

The parametric studies were performed on simply supported and continuous beams subjected to major and minor axes bending. Local geometric imperfections were assumed to be in the pattern of the lowest regular elastic buckling mode shape with an amplitude of 0.2 mm, as measured in the experimental program. The material properties of a typical high strength aluminium alloy specimen H64×64×3.0B3 and a typical normal strength aluminium alloy specimen +N95×50×10.5B5III were employed in the parametric studies to define the material properties for normal strength and high strength aluminium alloys, respectively. The size of the element mesh was chosen as 10 mm × 10 mm for all models.

4.3.1 Simply supported beams

An extensive parametric study was carried out to generate 192 additional numerical results for simply supported beams, where 132 are SHS/RHS and 60 are SHS/RHS with internal stiffeners, respectively (see Appendix F). Half of the results were from three-point bending tests and half from four-point bending. A wide range of both b/h ratios (0.30 - 3.35) and b/t ratios (2.76 - 55.14) were considered in the numerical parametric study for SHS/RHS, while b/h ratios became 0.28 - 3.62 and b/t ratios ranged from 0.88 to 27.07 for stiffened SHS/RHS. Outer section dimensions and thickness up to 180 mm and 12.0 mm were modelled respectively. For each cross-section, three-point and four-point bending configurations as well as high strength and normal strength aluminium alloys were modelled. The distance between supports and loading points varied from 400 mm to 900 mm depending on the section size, so that the overall length was ranged from 890 mm (the shortest three-point beams) to 3690 mm (the longest four-point beams).

76

In the parametric study, it was found that when the cross-sections became more slender, local buckling was more prone to occur before the cross-sections yielding. Meanwhile, stress concentration near the loading points was also more prominent on relatively slender sections.

4.3.2 Continuous beams

The validated FE models are used to conduct a parametric study aiming to develop a better understanding of the inelastic behaviour of indeterminate aluminium alloy structures. Similar to the simply supported beams, the parametric study was carried out to expand the available data over a wider cross-section slenderness range. A total of 20 different cross-sections were considered. Cross-sections with outer wall dimensions up to 180 mm and the thickness varying between 2.5 mm to 12.0 mm were modelled. The considered cross-sections involved the four different classes (EC9, 2007). The overall beam lengths were 1690 mm, 2490 mm and 3690 mm for small (width 50 mm × height 130 mm, width 130 mm × height 50 mm), medium (width 140 mm × height 100 mm) and large (width 180 mm × height 180 mm, width 160 mm × height 200 mm) cross-sections, respectively.

A total of 120 numerical results for continuous beams of SHS/RHS, and 90 for stiffened SHS/RHS beams have been generated herein. The FE models also enable careful examination of the inelastic behaviour and moment distribution in the considered indeterminate structural systems. The newly generated numerical results are presented in Appendix F. In the numerical models, the failure was defined as either when a plastic collapse mechanism was formed or the material fracture strain ε_f was reached on the tension flange, whichever occurred first.

Similar to simply supported beams, local buckling was also observed in the five point bending beams before or during the formation of the first hinge, when the cross-sections were getting slender. Meanwhile, stress concentration near the loading points was more prominent.

4.4 Summary

This chapter has described the FE modelling of aluminium alloy SHS/RHS and stiffened SHS/RHS subjected to bending. Key parameters and constraints have been chosen through carefully examination of experimental data to achieve a consistent approach. Parametric studies have been conducted to generate additional data. A summary of the findings are listed below:

- For all simulated specimens (simply supported beams and continuous beams), the numerical predictions have been demonstrated a high degree of accuracy: on average, ultimate loads were predicted within 2% difference compared with those test results and with low coefficients of variation (not exceed 0.080); the general form of the load-deflection response and the failure modes obtained from the tests and finite element analyses are similar.

- Upon validation, the FE models were used to conduct parametric studies, and hence to generate a large number of numerical results: 192 simply supported beams (132 being SHS/RHS and 60 being SHS/RHS with internal cross stiffeners); 210 five-point bending beams (120 being SHS/RHS and 90 being SHS/RHS with internal cross stiffeners). These numerical data are employed in the following studies to calibrate new design methods and evaluate existing methods.

CHAPTER 5

CONTINUOUS STRENGTH METHOD (CSM)

FOR ALUMINIUM ALLOYS

5.1 Introduction

Aluminium alloys exhibit nonlinear material stress-strain curves with significant strain hardening and reasonable ductility. However, current aluminium alloy specifications have adopted the elastic, perfectly plastic material model for simplicity. This chapter considers the effects of strain hardening at the cross-sectional level and moment redistribution of indeterminate structures at the global system level, and thereafter explores the way to include them in the proposed CSM approach. A detailed account of the CSM for aluminium alloys is given in this chapter.

Departing from current practices, the continuous strength method (CSM) is a recently proposed design approach for aluminium alloy structures. The CSM was initially developed for stainless steel and carbon steel materials, allowing for strain hardening and global plastic design. A series of studies (Gardner, 2002; Gardner, 2008; Gardner and Theofanous, 2008; Gardner et al., 2011) have been conducted to develop and improve the CSM in the past decade. The CSM has been recently included in the latest version of AISC stainless steel design guidelines (2013). Owing to the general similarity of structural behaviour between stainless steel, carbon steel and aluminium alloys, this chapter investigates the feasibility of applying the CSM to aluminium alloy structures.

5.2 General concepts

The continuous strength method (CSM) is a deformation-based design framework that allows for the beneficial influence of strain hardening, thus it was initially developed for fully effective (i.e. non-slender) sections which can benefit from strain hardening (Gardner, 2002; Gardner, 2008; Gardner and Theofanous, 2008; Gardner et al., 2011). However, it is found that the flexural capacity of some un-symmetric slender sections such as angles or even single symmetric slender sections such as channels (minor axis bending) and T-sections (major axis bending) can also be enhanced due to strain hardening on the tensile element components. The neutral axis of these sections are much closer to the extreme compression fibre, leading to, though, local buckling on the compression flanges at the early stage before yielding, the tension components can experience large plastic strains with strain hardening effect. Thus, the CSM has been extended to allow partial plasticity for slender sections in this study by supplementing the base curve with a second part for slender sections. That is to say, the CSM can now be applied to the full range of cross-sections without limitations.

One of the basic treatments of the CSM diverting from the traditional design methods is to assess the cross-section capacities in a continuous manner, instead of placing the cross-sections into discrete behavioural classes. The rationale behind this treatment is the continuous stress-strain material curves for stainless steel and aluminium alloys without sharply defined yield point. Hence, this method could be regarded as a continuous method for member design. While the other key difference between the CSM and the traditional methods is the treatment to the global indeterminate system. The CSM allows for global plastic design for the indeterminate structures, but assuming the cross-section capacities at different hinges correspond to the degree of rotation at each specific hinge,

which means that the resistance at different hinges are not necessary equal to the full CSM design capacity.

The two main features of the method are (1) a base curve defining the level of strain that a cross-section can tolerate as a function of cross-section slenderness and (2) a strain hardening bi-linear material model. These two components have been established for structural carbon steel and stainless steel in previous studies (Gardner, 2002; Gardner and Theofanous, 2008; Gardner et al., 2011). Building on recent design proposals, developments of a base curve, a suitable strain hardening material model and global plastic analysis for aluminium alloy structures are described in the following sections.

5.3   Base curve for metallic materials

The CSM base curve defines the level of strain that a cross-section can carry before failure. This curve provides a continuous relationship between cross-section deformation capacity and cross-section slenderness. The development of the base curve has close relationship with the plate buckling theory (Gardner, 2008). The basic philosophy of the base curve is to indicate the occurrence of local plate buckling regarding to the plate slenderness. It was developed based on both stub column test results and four-point bending test results on carbon steel, stainless steel and aluminium alloys. Different cross-section types such as SHS/RHS, stiffened SHS/RHS, I-sections, angles and channels are all involved in the analyses.

In the CSM, the cross-section slenderness $\bar{\lambda}_p$ is defined in a non-dimensional form as the square root of the ratio of the yield stress f_y to the elastic buckling stress σ_{cr} of the cross-section (Eq. 5.1). The elastic buckling stress can be determined according

to the analytical approximations of Seif and Schafer (2010) or a numerical approach, such as CUFSM (Li and Schafer, 2010). Both take into account the effects of element interaction. Alternatively, $\bar{\lambda}_p$ may be determined on an element by element basis, by taking the cross-section slenderness as that of its most slender constituent plate. In this study, the programme CUFSM (Li and Schafer, 2010) was used. Conservatively, element interaction can be ignored and cross-section slenderness is taken as that of its most slender constituent plate element. The cross-section deformation capacity $\varepsilon_{csm}/\varepsilon_y$ for non-slender sections is defined in a normalised form as the strain at ultimate load ε_{lb} minus 0.2% plastic strain, divided by the yield strain ε_y, where $\varepsilon_y=f_y/E$, E being the Young's modulus. Note that subtraction of the 0.2% plastic strain from the deformation capacity enables compatibility with the bilinear material model described in the following section. When interpreting the test data of stub columns, the deformation capacity is determined from the end shortening at the ultimate load δ_u and the stub column lengths (for sections reaching the yield load) or the ultimate load P_u (for sections failing before reaching the yield load), as given by Eqs. 5.2 and 5.3, respectively. In bending, under the assumption that plane sections remain plane and normal to the neutral axis, there is a linear relationship ($\varepsilon=\kappa y$) between strain ε and curvature κ, where y is the distance to the neutral axis. The deformation capacity of a cross-section in bending is defined in a similar way by Eqs. 5.4 and 5.5, respectively. The following symbols are used: κ_{el} = curvature at yield, κ_u = curvature at ultimate load, L = stub column length, M_u = ultimate bending capacity, $M_{el}= W_{el}f_y$, elastic moment capacity (W_{el} being the elastic section modulus), $P_y = Af_y$ is the yield limit for stub columns, P_u = ultimate stub column capacity and y_{max} = distance between extreme compression fibre and the neutral axis.

$$\bar{\lambda}_p = \sqrt{f_y / \sigma_{cr}}$$ (Eq. 5.1)

$$\frac{\varepsilon_{csm}}{\varepsilon_y} = \frac{\varepsilon_{lb} - 0.002}{\varepsilon_y} = \frac{\delta_u / L - 0.002}{\varepsilon_y} \quad \text{for } P_u \geq P_y \quad \text{and} \quad \bar{\lambda}_p \leq 0.68$$ (Eq. 5.2)

$$\frac{\varepsilon_{csm}}{\varepsilon_y} = \frac{P_u}{P_y} \quad \text{for } P_u < P_y \text{ or } \bar{\lambda}_p > 0.68$$ (Eq. 5.3)

$$\frac{\varepsilon_{csm}}{\varepsilon_y} = \frac{\varepsilon_{lb} - 0.002}{\varepsilon_y} = \frac{\kappa_u y_{max} - 0.002}{\kappa_{el} y_{max}} \quad \text{for } M_u \geq M_{el} \quad \text{and} \quad \bar{\lambda}_p \leq 0.68$$ (Eq. 5.4)

$$\frac{\varepsilon_{csm}}{\varepsilon_y} = \frac{M_u}{M_{el}} \quad \text{for } M_u < M_{el} \text{ or } \bar{\lambda}_p > 0.68$$ (Eq. 5.5)

The first part of the base curve for all metallic materials of non-slender sections is given by Eq. 5.6. The two upper bounds to the CSM strain ε_{csm} are $15\varepsilon_y$ and $0.5\varepsilon_u$, which relate to limiting plastic deformations and avoiding material fracture, respectively. The experimental and numerical data points from stub column tests and four-point bending tests within the applicability limits, which failed by inelastic local buckling and material yielding, are plotted in Fig. 5.1 for deformation capacity versus cross-section slenderness, together with the base curve. The first part of the base curve, initially developed for carbon steel and stainless steel, may be seen to also provide a good prediction of deformation capacity for aluminium alloy cross-sections.

$$\frac{\varepsilon_{csm}}{\varepsilon_y} = \frac{0.25}{\bar{\lambda}_p^{3.6}} \quad \text{but} \quad \frac{\varepsilon_{csm}}{\varepsilon_y} \leq \text{lesser } (15, \frac{0.5\varepsilon_u}{\varepsilon_y}) \quad \text{for } \bar{\lambda}_p \leq 0.68$$ (Eq. 5.6)

The second part of the base curve is for slender sections, as given in Eq. 5.7. Since the strain ratios ($\varepsilon_{csm}/\varepsilon_y$) for slender sections are proportional to load ratios (P_u/P_y and M_u/M_{el}), the relationship between the cross-section deformation capacity and cross-section slenderness is actually in the same format as the direct strength method (DSM) curve. It is found that the DSM curve proposed by Schafer and

Peköz (1998) for the design of cold-formed carbon steel is able to represent the structural behaviour of aluminium alloy slender sections accurately. For compatibility with the first part of the CSM base curve, the curve for slender sections should also pass through the point $\overline{\lambda}_p = 0.68$ and $\varepsilon_{csm}/\varepsilon_y = 1$). Thus, the second part of the CSM base curve is derived by modifying one of the coefficients, but still keeps the same format as the DSM curve and the Winter's curve.

$$\frac{\varepsilon_{csm}}{\varepsilon_y} = (1 - \frac{0.195}{\overline{\lambda}_p^{0.8}}) \frac{1}{\overline{\lambda}_p^{0.8}} \qquad \text{for } \overline{\lambda}_p > 0.68 \qquad \text{(Eq. 5.7)}$$
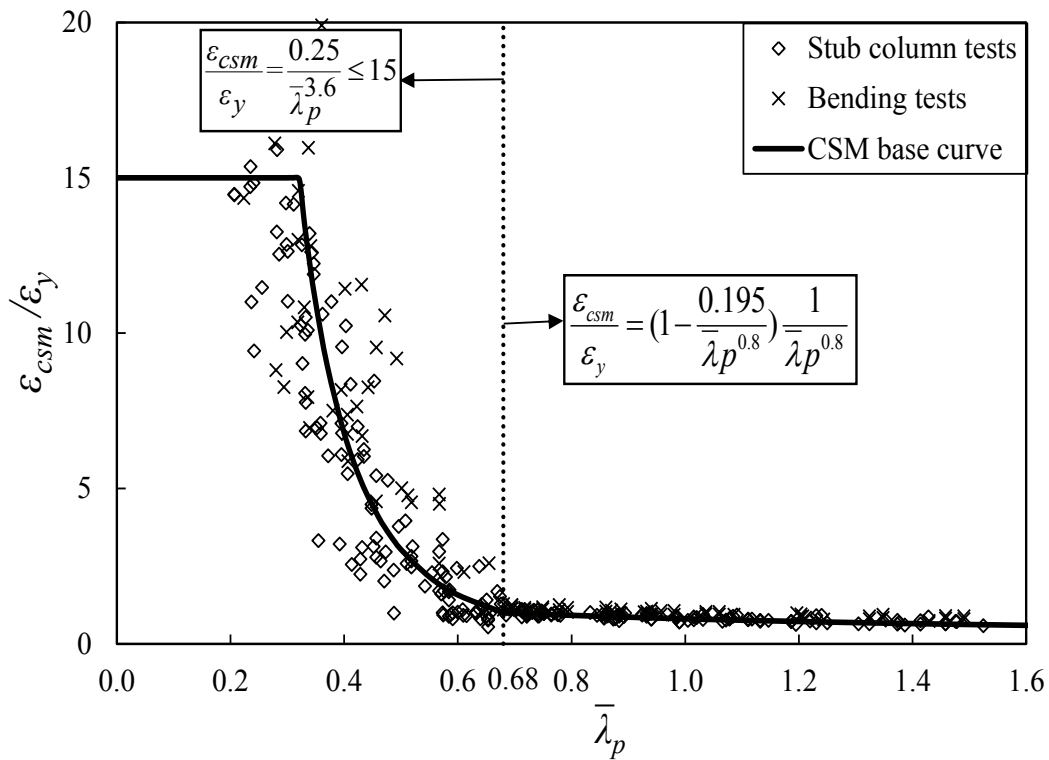
Fig. 5.1   Base curve – relationship between strain ratio and plate slenderness

84

5.4 Material model

The CSM employs an elastic, linear hardening material model, with the strain hardening modulus varying with material grades. The slope of the linear hardening region is defined on the basis of passing through two fixed points, and the first point is the 0.2% proof stress f_y where the corresponding strain at $\varepsilon_y + 0.002$ and the second pint is the ultimate tensile stress f_u at 0.5 of the ultimate strain plus 0.2% strain $(0.5\varepsilon_u + 0.002, f_u)$. The addition of the 0.2% strain to the second point during the derivation of the model allows curve shift left by 0.2% strain, with no change in the slope, such that the final model passes through the points (ε_y, f_y) and $(0.5\varepsilon_u, f_u)$. The development of this material model and the choice of parameters are described in the following sections.

5.4.1 Ultimate strain prediction

The strain at the ultimate tensile stress ε_u is a key factor in the material model, particularly in determining the slope of the strain hardening region. However, in most cases, this value is not reported by manufacturers and thus it is not readily available to designers. EC9 (2007) provides formulas to predict the ultimate material strain ε_u, as given in Eqs. 5.8 and 5.9. A comparison between EC9 (2007) predictive model and experimental data for ε_u (Langseth and Hopperstad, 1997; Moen et al., 1999a; Zhu and Young, 2006a) is shown in Fig. 5.2. The experimental values of ultimate strain $\varepsilon_{u,test}$ may be seen to be generally lower than the predicted values $\varepsilon_{u,\,pred}$, from EC9 (2007), and with large scatter. In this study, a new expression (Eq. 5.10) is proposed for the prediction of ultimate strain. It follows a similar format to the ultimate strain prediction equation for stainless steel in EN1993-1-4 (2006); the model coefficients were calibrated based on the tensile coupon test results by means of least square regression. Note that no data with $f_u/f_y \leq 1.01$ was used in the development of Eq. 5.10; therefore this may be considered

as the limit of applicability to Eq. 5.10. The predictions improved significantly for the ultimate strain as shown in Fig. 5.2.

$$\varepsilon_u = 0.3 \text{-} 0.22(f_y/400) \qquad \text{for} \quad f_y < 400 \text{ N/mm}^2 \qquad \text{(Eq. 5.8)}$$

$$\varepsilon_u = 0.08 \qquad \text{for} \quad f_y \geq 400 \text{ N/mm}^2 \qquad \text{(Eq. 5.9)}$$

$$\varepsilon_u = 0.13(1 \text{-} f_y/f_u) + 0.059 \qquad \text{(Eq. 5.10)}$$
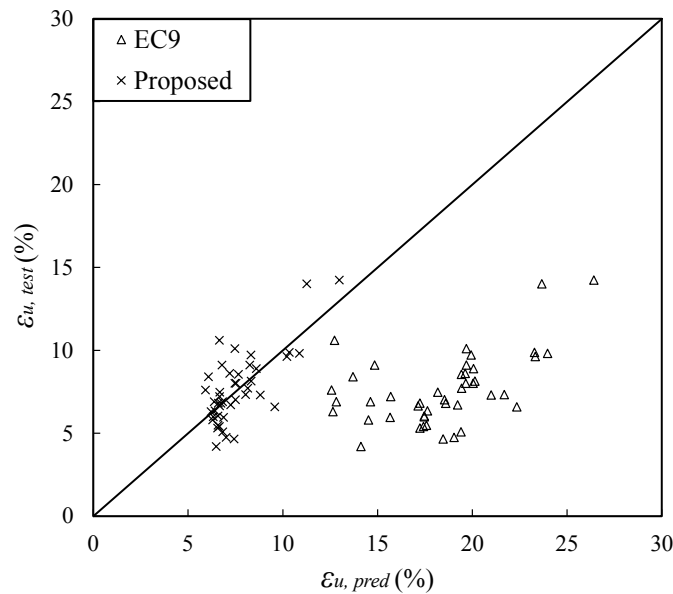
Fig. 5.2   Test versus predicted ultimate strain

5.4.2 Strain hardening slope

The CSM bi-linear material model contains two parts: the initial elastic part and the linear hardening part (Fig. 5.3). The elastic part is defined by the Young's Modulus of the material. The strain hardening region has a strain hardening slope E_{sh}, defined, for aluminium alloys, by Eq. 5.11. A suitable expression for defining E_{sh} was initially explored by considering two end points at $(\varepsilon_y + 0.002, f_y)$ and $(x\varepsilon_u + 0.002, f_u)$, where x is the proportion of ultimate strain. The 0.2% plastic strain

deduced from end points, and resulting the material model passes through the points (ε_y, f_y) and $(x\varepsilon_u, f_u)$. The value of x was determined from experimental data (Zhu and Young, 2006a) with two considerations. The first consideration was to obtain an accurate fit to measured σ-ε curves; this was achieved through least square regression. The second was to ensure that the simplified model did not over-predict any experimental σ-ε curves to a significant degree. A value of $x = 0.5$ was found to satisfy both considerations, with a maximum over-prediction in stress Δd of less than 5% when compared to the collected set of 33 measured σ-ε curves. Note that lower values of x provided an improved least square fit to the collected test data but higher maximum over-predictions, while the opposite was found for higher values of x. In addition to providing a suitably accurate representation of experimental data, the value of $x = 0.5$ also matches that given in Annex E of EC9 (2007). A typical comparison between a measured σ-ε curve and the CSM material model is shown in Fig. 5.3.

$$E_{sh} = \frac{f_u - f_y}{0.5\varepsilon_u - \varepsilon_y} \qquad \text{(Eq. 5.11)}$$
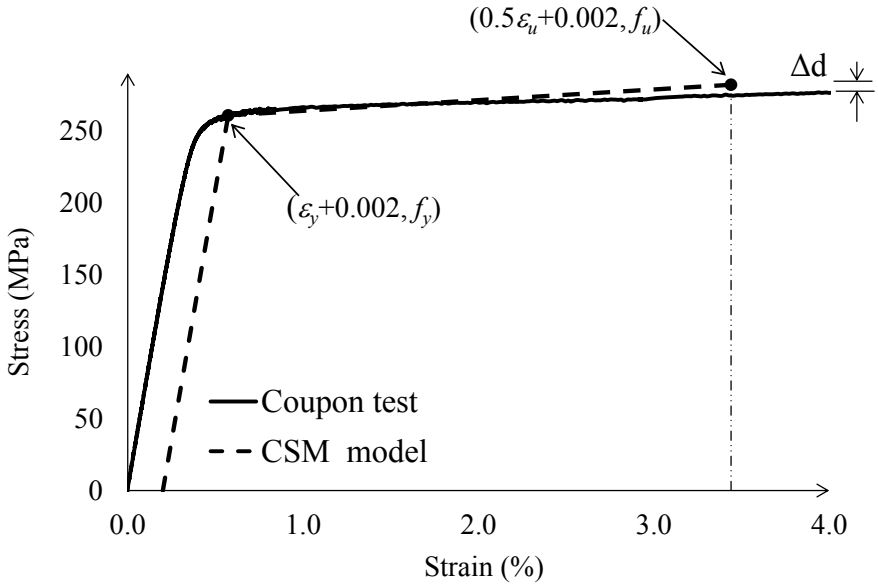
Fig. 5.3   Measured stress-strain curve and the CSM bi-linear material model for a typical section.

5.5 Design procedures and worked examples

The design procedure of the CSM has been reported at various stages of advancement. The applicability of the strain hardening slope in the CSM is limited to stub columns and symmetric bending beams of cross-section with $\bar{\lambda}_p \leq 0.68$. This limit indicates the transition between slender sections (i.e. those failed below the yield limit) and non-slender sections (i.e. those failed beyond the yield limit), and is shown in Fig. 5.4 and Fig. 5.5. Further investigation is needed for unsymmetric bending beams.

Fig. 5.4 shows the results of stub column tests on SHS/RHS, SHS/RHS with internal stiffeners, channels and angles, where the test ultimate loads are normalised by the yield limit Af_y. Fig. 5.5 shows the results of simply supported bending tests on SHS/RHS, SHS/RHS with internal stiffeners and I-sections, where the ultimate moments are normalised by the plastic moment capacity $W_{pl}f_y$. Both figures reveal that non-slender sections ($\bar{\lambda}_p \leq 0.68$) can achieve capacities beyond the fully yielded limit due to strain hardening.
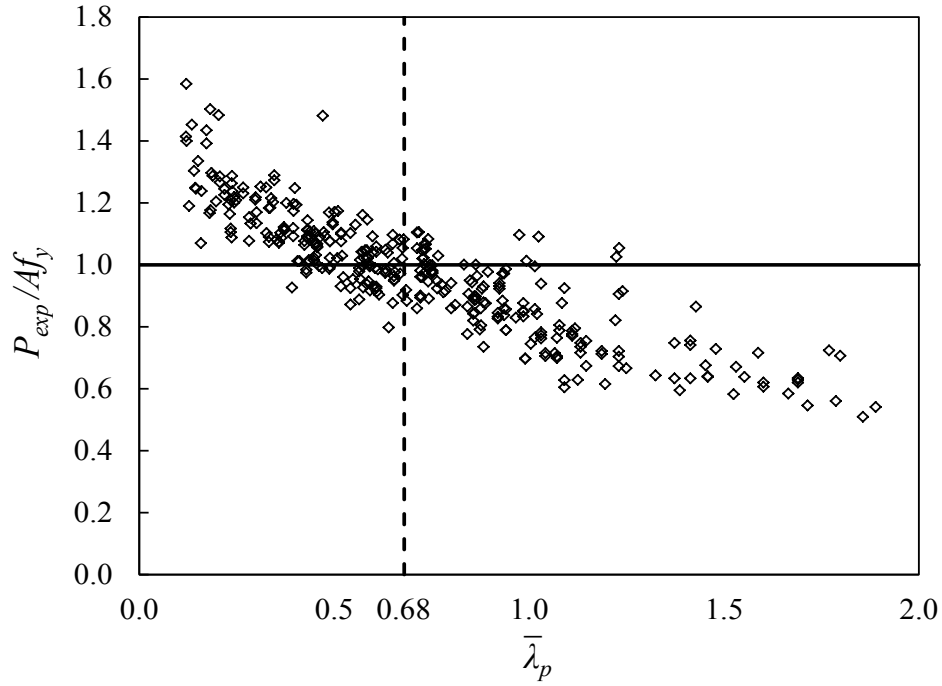
Fig. 5.4   Comparison of 348 stub column test results with yield limit.
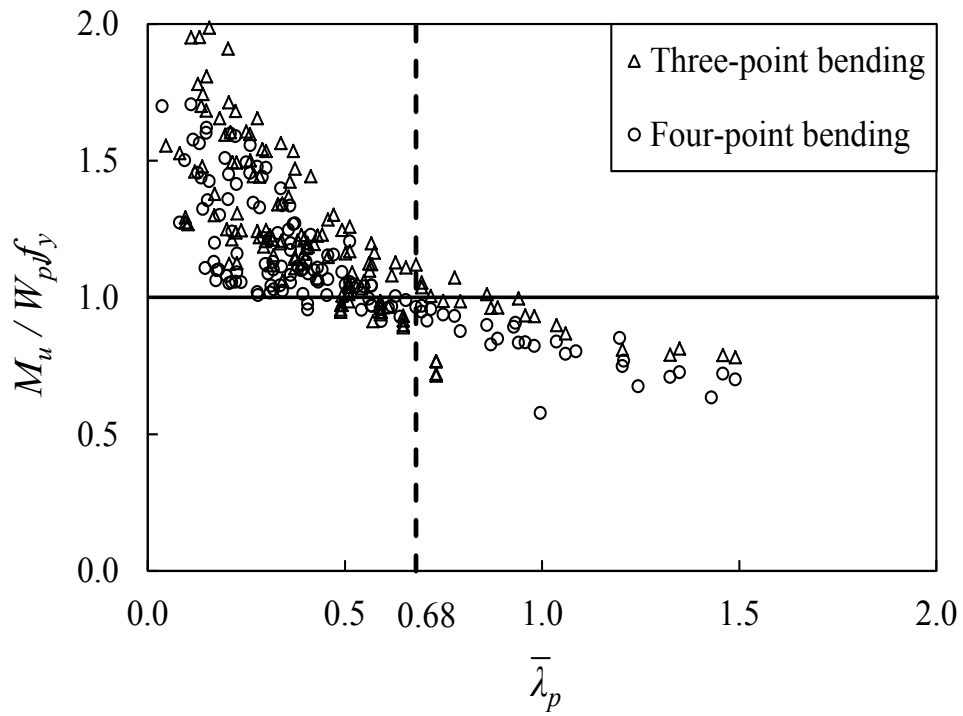
Fig. 5.5   Comparison of 275 simply supported bending experimental and

numerical results with plastic limit.

In the case of indeterminate structures, such as five-point bending beams, the experimental and numerical ultimate loads F_u are normalized by the theoretical plastic loads F_{coll}, as plotted in Fig. 5.6. The failure loads for plastic analyses (F_{coll}) are the theoretical loading level required to form a plastic collapse mechanism. It is based on the formation and subsequent rotation of plastic hinges at their plastic moment capacities $W_{pl}f_y$. A number of specimens with semi-compact or even slender sections can also achieve higher ultimate loads than the theoretical plastic loads F_{coll}, while all the plastic and compact sections have greater ultimate loads than the theoretical plastic loads.
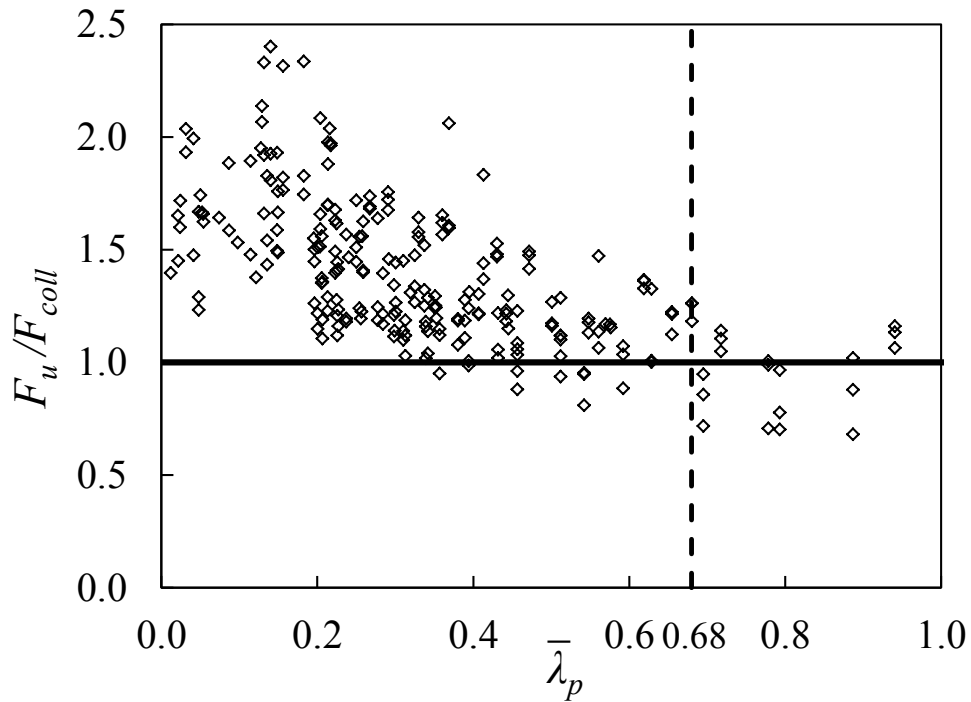
Fig. 5.6   Comparison of 256 five-point bending experimental and numerical results with theoretical collapse loads

5.5.1 Stub columns

The resulting CSM design procedure for determining the compressive strength of aluminium alloy cross-sections may be summarized in the following steps. A worked example for a RHS stub column is illustrated below.

(1) Calculate the cross-section slenderness $\bar{\lambda}_p$

$$\bar{\lambda}_p = \sqrt{f_y/\sigma_{cr}}$$

If $\bar{\lambda}_p \leq 0.68$:
non-slender section

If $\bar{\lambda}_p > 0.68$:
slender section

(2) Determine the level of strain that the cross-section can endure ε_{csm} from the base curve:

$$\frac{\varepsilon_{csm}}{\varepsilon_y} = \frac{0.25}{\bar{\lambda}_p^{3.6}} \quad \text{but} \quad \frac{\varepsilon_{csm}}{\varepsilon_y} \leq \text{lesser} (15, \; \frac{0.5\varepsilon_u}{\varepsilon_y})$$

(2) Determine the level of strain that the cross-section can endure ε_{csm} from the base curve:

$$\frac{\varepsilon_{csm}}{\varepsilon_y} = (1 - \frac{0.195}{\bar{\lambda}_p^{0.8}}) \frac{1}{\bar{\lambda}_p^{0.8}}$$

(3) The corresponding limiting stress f_{csm} can be found from:

$$f_{csm} = f_y + E_{sh} (\varepsilon_{csm} - \varepsilon_y)$$

(3) The cross-section compression strength P_{csm} can be found from:

$$P_{csm} = \frac{\varepsilon_{csm}}{\varepsilon_y} P_y$$

(4) The cross-section compression strength P_{csm} could be obtained from:

$$P_{csm} = A f_{csm}$$

Worked example - Stub column capacity:

The CSM predicted capacity of a stub column on RHS H70×55×4.2C, and the test reported in this study, is determined as follows:

Cross-section dimensions and material properties:

$H = 69.9$ mm	$B = 54.9$ mm	$t = 4.08$ mm	$A = 951.9$ mm^2
E=65 GPa	$f_y = 193$ MPa	$f_u = 207$ MPa	
$\varepsilon_u = 0.13(1- 193 / 207) + 0.059 = 0.068$		$\varepsilon_y = 193/65000 = 0.003$	

Step 1: Determine cross-section slenderness

$\bar{\lambda}_p \; (=\sqrt{f_y /\sigma_{cr}}) = 0.36$ (The value of $\bar{\lambda}_p$ is determined by the programme CUFSM (Li and Schafer, 2010))

Step 2: Determine the cross-section deformation capacity

$$\frac{\varepsilon_{csm}}{\varepsilon_y} = \frac{0.25}{\bar{\lambda}_p^{3.6}} = \frac{0.25}{0.36^{3.6}} = 10.28 \, (\leq \text{lesser } (15, \; \frac{0.5\varepsilon_u}{\varepsilon_y} = 11.67))$$

Step 3: Determine strain hardening slope

$$E_{sh} = \frac{f_u\text{-}f_y}{0.5\varepsilon_u\text{-}\varepsilon_y} = \frac{207 - 193}{0.5\times 0.068 - 0.003} = 437.5 \text{ MPa}$$

Step 4: Determine the stress and capacity

$f_{csm} = f_y + E_{sh} \, (\varepsilon_{csm}\text{-}\varepsilon_y) = 193 + 437.5 \times (10.28 \text{-} 1) \times 0.003 = 205.18 \text{MPa}$

$P_{csm} = Af_{csm} = 951.9 \times 205.18 = 195.31\text{kN}$

(Tested ultimate load = 196.2 kN)

5.5.2 Simply supported beams

In-plane bending resistance may be calculated on a similar basis to compression resistance. A detail account of the design model for flexural cross-sections is given by Gardner et al. (2010). The same design model is adopted for aluminium alloys in this research to consider three different stages: elastic stage, elastic-plastic stage and strain hardening stage. The design procedures for aluminium alloy simply supported beams are summarised as follows:

(1) Calculate the cross-section slenderness $\bar{\lambda}_p$

$$\bar{\lambda}_p = \sqrt{f_y / \sigma_{cr}}$$

If $\bar{\lambda}_p \leq 0.68$:
non-slender section

If $\bar{\lambda}_p > 0.68$:
slender section

(2) Determine the level of strain that the cross-section can endure ε_{csm} from the base curve:

$$\frac{\varepsilon_{csm}}{\varepsilon_y} = \frac{0.25}{\bar{\lambda}_p^{3.6}} \quad \text{but} \quad \frac{\varepsilon_{csm}}{\varepsilon_y} \leq \text{lesser}(15, \frac{0.5\varepsilon_u}{\varepsilon_y})$$

(2) Determine the level of strain that the cross-section can endure ε_{csm} from the base

curve: $\dfrac{\varepsilon_{csm}}{\varepsilon_y} = (1 - \dfrac{0.195}{\bar{\lambda}_p^{0.8}})\dfrac{1}{\bar{\lambda}_p^{0.8}}$

(3) The corresponding limiting stress M_{csm} can be found from:

$$M_{csm} = W_{pl}f_y[1 + \frac{E_{sh}}{E}\frac{W_{el}}{W_{pl}}(\frac{\varepsilon_{csm}}{\varepsilon_y} - 1) - (1 - \frac{W_{el}}{W_{pl}})/(\frac{\varepsilon_{csm}}{\varepsilon_y})^2]$$

(3) The cross-section compression strength M_{csm} can be found from:

$$M_{csm} = \frac{\varepsilon_{csm}}{\varepsilon_y} M_{el}$$

Worked example - Simply supported beam capacity:

The CSM predicted capacity of a three-point bending beam on SHS N120×120×9.0B3, and the test reported in this study, is determined as follows:

Cross-section dimensions and material properties:

$H = 119.9$ mm	$B = 119.9$ mm	$t = 8.89$ mm	$A = 3947.9$ mm^2
$W_{el} = 136141$ mm^3	$W_{pl} = 164727$ mm^3	$E = 69$ GPa	$f_y = 181$ MPa
$f_u = 228$ MPa	$M_{pl} = 29.750$ kNm		
$\varepsilon_u = 0.13(1 - 181 / 228) + 0.059 = 0.086$		$\varepsilon_y = 181/69000 = 0.003$	

Step 1: Determine cross-section slenderness

$\bar{\lambda}_p \ (= \sqrt{f_y / \sigma_{cr}}) = 0.29$ (The value of $\bar{\lambda}_p$ is determined by the programme CUFSM, (Li and Schafer, 2010))

Step 2: Determine the cross-section deformation capacity

$$\frac{\varepsilon_{csm}}{\varepsilon_y} = \frac{0.25}{\bar{\lambda}_p^{3.6}} = \frac{0.25}{0.29^{3.6}} = 21.54 \ (> \text{lesser} \ (15, \ \frac{0.5\varepsilon_u}{\varepsilon_y} = 15.3))$$

$$\therefore \ \frac{\varepsilon_{csm}}{\varepsilon_y} = 15$$

Step 3: Determine strain hardening slope

$$E_{sh} = \frac{f_u - f_y}{0.5\varepsilon_u - \varepsilon_y} = \frac{228 - 181}{0.5 \times 0.086 - 0.003} = 1175 \ \text{MPa}$$

Step 4: Determine the cross-section capacity at each hinge

$$\frac{M_{csm}}{M_{pl}} = 1 + \frac{E_{sh}}{E} \frac{W_{el}}{W_{pl}} (\frac{\varepsilon_{csm}}{\varepsilon_y} - 1) - (1 - \frac{W_{el}}{W_{pl}})(\frac{\varepsilon_{csm}}{\varepsilon_y})^{-2}$$

$$= 1 + \frac{1175}{69000} \frac{136141}{164727} (15 - 1) - (1 - \frac{136141}{164727})(15)^{-2}$$

$$= 1.20$$

$M_{csm} = 1.20 \times 29.750 = 35.7$ kNm

(Tested ultimate load = 35.3 kNm)

5.5.3 Continuous beams

The CSM for indeterminate structures is an extension of the CSM for determinate structures, and provides allowance for plastic moment redistribution. In addition to considering material characteristics at the cross-sectional level, the CSM for indeterminate structures employs concepts from traditional plastic design – global plastic analysis – for non-slender sections. However, the CSM considers the degree of rotation at each plastic hinge (see Fig. 5.7), leading to different cross-section capacities at different hinges (Fig. 5.8), which is the key diversion from the traditional plastic design. The moment resisted by each cross-section is proportional to the required hinge rotation, as indicated in Fig. 5.8. The critical plastic hinge is first identified as the one with the highest hinge rotation demand, and this hinge is assigned a full CSM cross-section moment capacity. The moments at subsequent hinges are determined by reducing the full CSM moment proportionally to the hinge rotational demand ratios (Gardner et al., 2011). Based on the resulting deformations, the corresponding bending moment diagram at collapse is determined. Satisfaction of the three conditions of equilibrium, compatibility and plasticity remains a strict requirement in defining the unique plastic collapse load of a structure in the continuous strength method (Gardner et al., 2011).
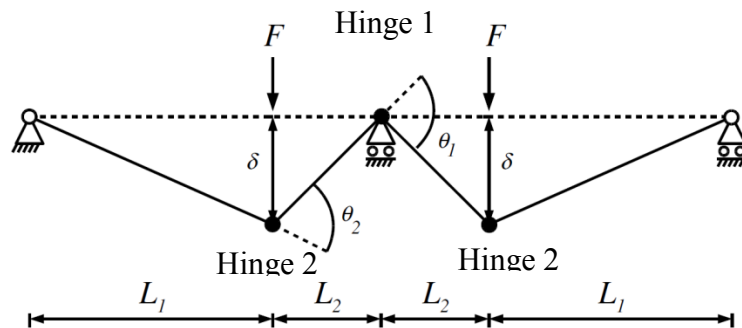
Fig. 5.7   Plastic collapse mechanism for five point bending beam (Gardner et al., 2011)

95
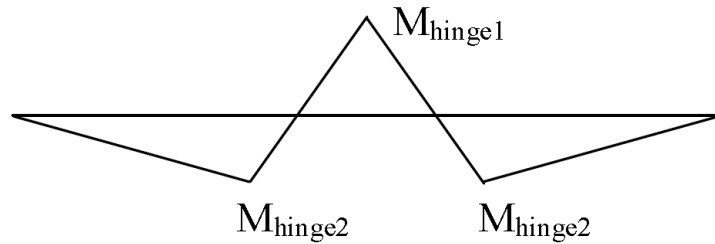
Fig. 5.8   Bending moment diagram to form a collapse mechanism based on the CSM (Gardner et al., 2011)

The resulting CSM design procedure for determining the design strengths of indeterminate aluminium alloy structures is summarized in the following seven steps. It basically comprises of two parts: first, to determine the cross-section resisting moment; second, to derive the resisting load. Note that if $(\varepsilon_{csm}/\varepsilon_y)_{max}$ derived from step (4) is less than 3.6 for SHS/RHS, global plastic analysis is not recommended (Gardner et al., 2011) and elastic global analysis should be used; $\varepsilon_{csm}/\varepsilon_y = 3.6$ corresponds to the Class 2 limit according to the classification system of EC9 (2007). This results in a step in resistance at the boundary between Classes 2 and 3 cross-sections, as shown in Fig. 6.20.

(1)　　Identify the location of the plastic hinges in a manner similar to traditional plastic design and determine the hinge rotation θ_i.

(In the case of five-point bending beams, $\theta_1 = 2\delta/L_2$ and $\theta_2 = \delta/L_1 + \delta/L_2$ are derived, as illustrated in Fig. 6.7).

(2)　　Calculate the cross-section slenderness

$$\bar{\lambda}_p = \sqrt{f_y / \sigma_{cr}}$$

If $\bar{\lambda}_p \leq 0.68$: non-slender section

If $\bar{\lambda}_p > 0.68$: slender section

(3)　　Determine the level of strain that the cross-section can endure ε_{csm} from the base curve:

$$\frac{\varepsilon_{csm}}{\varepsilon_y} = \frac{0.25}{\bar{\lambda}_p^{3.6}} \quad \text{but} \quad \frac{\varepsilon_{csm}}{\varepsilon_y} \leq \text{lesser} \left(15, \frac{0.5\varepsilon_u}{\varepsilon_y}\right)$$

(3)　　Determine the level of strain that the cross-section can endure ε_{csm} from the base curve: $\dfrac{\varepsilon_{csm}}{\varepsilon_y} = \left(1 - \dfrac{0.195}{\bar{\lambda}_p^{0.8}}\right)\dfrac{1}{\bar{\lambda}_p^{0.8}}$

If $\dfrac{\varepsilon_{csm}}{\varepsilon_y} \geq 3.6$ (for box section)

If $\dfrac{\varepsilon_{csm}}{\varepsilon_y} < 3.6$ (for box section)

(4)　　The cross-section compression strength M_{csm} can be found from:

$$M_{csm} = \frac{\varepsilon_{csm}}{\varepsilon_y} M_{el}$$

(4)　　Given the hinge rotation θ_i, section height h_i and strain ratio $(\varepsilon_{csm}/\varepsilon_y)_i$, calculate the corresponding hinge demands α_i:

$$\alpha_i = \frac{\theta_i h_i}{(\varepsilon_{csm}/\varepsilon_y)_i}$$

The critical hinge is identified as the one with the highest hinge demand $\alpha_{max} = max\{\alpha_i\}$, with the strain ratio at the critical hinge now labelled $(\varepsilon_{csm}/\varepsilon_y)_{max}$.

(5)　　Global elastic analysis: the failure load is determined when the first hinge forms at M_{csm}.

(5)　　The theoretical strain ratio at the hinges $(\varepsilon_{csm}/\varepsilon_y)_{hinge,i}$ are reduced proportionally to the hinge rotation ratios:

$$\left(\frac{\varepsilon_{csm}}{\varepsilon_y}\right)_{hinge,i} = \frac{\alpha_i}{\alpha_{max}}\left(\frac{\varepsilon_{csm}}{\varepsilon_y}\right)_{max} \quad \text{but} \quad \left(\frac{\varepsilon_{csm}}{\varepsilon_y}\right)_{hinge,i} \leq \left(\frac{\varepsilon_{csm}}{\varepsilon_y}\right)_i$$

(6)　　Calculate the corresponding cross-section bending moment capacity M_i at each plastic hinge based on $(\varepsilon_{csm}/\varepsilon_y)_{hinge,i}$:

$$\left(\frac{M_{csm}}{M_{pl}}\right)_i = \left(1 + \frac{E_{sh}}{E}\frac{W_{el}}{W_{pl}}\left(\frac{\varepsilon_{csm}}{\varepsilon_y} - 1\right) - \left(1 - \frac{W_{el}}{W_{pl}}\right)/\left(\frac{\varepsilon_{csm}}{\varepsilon_y}\right)^2\right)_i$$

(7)　　Derive the total applied load by formulate the expression balancing external work done by the applied loads F_j acting through virtual displacements δ_j, to that of the internal work resulting from the hinge rotations θ_i.

$$\sum_j F_j \delta_j = \sum_i M_i \theta_i$$

Worked example-Continuous beam capacity:

The CSM predicted capacity of a five-point bending beam of SHS N120×120×9.0B5II, and the test reported in this study, is determined as follows:

Cross-section dimensions and material properties:

H = 119.9 mm	B = 119.9 mm	t = 8.90 mm

W_{el} = 136086 mm^3 W_{pl} = 164668 mm^3 E=69 GPa f_y = 188 MPa

f_u = 229 MPa M_{pl}=30.875 kNm

ε_u = 0.13(1- 188 / 229) + 0.059 = 0.082 ε_y = 188/69000 = 0.003

Loading configuration II with L_1=535 mm and L_2=268 mm

Step 1: Identify the location of the plastic hinges, of number i, in a manner similar to traditional plastic design and determine respective hinge rotations θ_i refered to Fig. 5.7.

L_1=2L_2

θ_1= 2δ/L_2= 4δ/L_1

θ_2= δ/L_1+δ/L_2=3δ/L_1

Step 2: Determine cross-section slenderness

$\bar{\lambda}_p$ $(=\sqrt{f_y/\sigma_{cr}})$ = 0.30 (The value of $\bar{\lambda}_p$ is determined by the programme CUFSM (Li and Schafer, 2010))

Step 3: Determine the cross-section deformation capacity

$$\frac{\varepsilon_{csm}}{\varepsilon_y} = \frac{0.25}{\bar{\lambda}_p^{3.6}} = \frac{0.25}{0.30^{3.6}} = 19.07 \; (> \text{lesser} \; (15, \; \frac{0.5\varepsilon_u}{\varepsilon_y}=15.3))$$

$$\therefore \; \frac{\varepsilon_{csm}}{\varepsilon_y} = 15$$

Step 4: Determine strain hardening slope

$$E_{sh} = \frac{f_u\text{-}f_y}{0.5\varepsilon_u\text{-}\varepsilon_y} = \frac{229-188}{0.5\times0.082-0.003} = 1078.9 \; \text{MPa}$$

Step 5: Determine the corresponding hinge demands

∵ The beam is homogeneous

$$\alpha_1 = \frac{\theta_1 h_1}{(\varepsilon_{csm}/\varepsilon_y)_1} = \frac{\theta_1 h}{\varepsilon_{csm}/\varepsilon_y}$$

$$\alpha_2 = \frac{\theta_2 h_2}{(\varepsilon_{csm}/\varepsilon_y)_2} = \frac{\theta_2 h}{\varepsilon_{csm}/\varepsilon_y} = \frac{3}{4}\frac{\theta_1 h}{\varepsilon_{csm}/\varepsilon_y}$$

$$\alpha_{max} = \alpha_1$$

$$\left(\frac{\varepsilon_{csm}}{\varepsilon_y}\right)_{max} = \frac{\varepsilon_{csm}}{\varepsilon_y}$$

∴ Hinge 1 is the critical hinge.

Step 6: Determine the cross-section deformation capacity at each hinge location

$$\left(\frac{\varepsilon_{csm}}{\varepsilon_y}\right)_{hinge,1} = \frac{\alpha_1}{\alpha_{max}}\left(\frac{\varepsilon_{csm}}{\varepsilon_y}\right)_{max} = \frac{\varepsilon_{csm}}{\varepsilon_y} = 15$$

$$\left(\frac{\varepsilon_{csm}}{\varepsilon_y}\right)_{hinge,2} = \frac{\alpha_2}{\alpha_{max}}\left(\frac{\varepsilon_{csm}}{\varepsilon_y}\right)_{max} = \frac{3}{4}\frac{\varepsilon_{csm}}{\varepsilon_y} = 11.25$$

Step 7: Determine the cross-section capacity at each hinge location

$$\left(\frac{M_{csm}}{M_{pl}}\right)_1 = \left(1 + \frac{E_{sh}}{E}\frac{W_{el}}{W_{pl}}(\frac{\varepsilon_{csm}}{\varepsilon_y}-1) - (1-\frac{W_{el}}{W_{pl}})/(\frac{\varepsilon_{csm}}{\varepsilon_y})^2\right)_1$$

$$= 1 + \frac{1078.9}{69000}\frac{136086}{164668}(15-1) - (1-\frac{136086}{164668})(15)^{-2}$$

$$= 1.18$$

$(M_{csm})_1 = 1.18 \times 30.875 = 36.432$ kNm

$$\left(\frac{M_{csm}}{M_{pl}}\right)_2 = \left(1 + \frac{E_{sh}}{E}\frac{W_{el}}{W_{pl}}(\frac{\varepsilon_{csm}}{\varepsilon_y}-1) - (1-\frac{W_{el}}{W_{pl}})/(\frac{\varepsilon_{csm}}{\varepsilon_y})^2\right)_1$$

$$= 1 + \frac{1078.9}{69000}\frac{136086}{164668}(11.25-1) - (1-\frac{136086}{164668})(11.25)^{-2}$$

$$= 1.13$$

$(M_{csm})_2 = 1.13 \times 30.875 = 34889$ kNm

Step 8: Determine total applied load

$$2F\delta = M_1\theta_1 + 2M_2\theta_2$$
$$\quad = 4M_1\delta / L_1 + 6M_2\delta / L_1$$

$$2F = 4M_1 / L_1 + 6M_1 / L_1$$
$$\quad = 4\times 36.432 / 535 + 6\times 34.889 / 535$$
$$\quad = 663.67\text{kN}$$

(Tested ultimate load = 657.8 kN)

5.6 Summary

Aluminium alloys are nonlinear metallic materials with continuous stress-strain curves that cannot be well represented by the simplified elastic, perfectly plastic material model used in most of existing design specifications. Departing from current practices, the continuous strength method (CSM) is a recently proposed design approach for aluminium alloy structures with consideration of strain hardening for non-slender sections. The CSM is a deformation-based method and employs a base curve to define the continuous function of cross-section slenderness and deformation capacity. This chapter has explained the background and the two key components of the CSM - (1) the base curve and (2) the strain hardening material model. Calculation procedures and worked examples of the CSM for aluminium stub columns, simply supported beams and continuous beams have been illustrated. In the following chapters, the predictions of CSM are compared with approximately 900 experimental and numerical results.

The CSM overwhelms the existing design approaches in several aspects:

(1) The CSM has taken advantages of strain hardening nature of aluminium alloys in the elastic, strain hardening material model, proposed in this study

specifically for aluminium alloys. Hence, the extra capacities beyond the theoretical yield limit can be utilised by the CSM.

(2) The continuous nature of stress-strain material curve has been considered in the CSM by the base curve, which defines the continuous relationship between the cross-section plate slenderness and the cross-section deformation capacity. Classification of cross-sections into discrete behavioural classes is no longer needed in the CSM. As mentioned earlier, the first part of the base curve for non-slender sections has been validated against carbon steel and stainless steel data; and in this present study, the base curve is examined against aluminium alloy data. Furthermore, a second part of the base curve for slender sections has been proposed in this study and extends the original curve to cover the full slenderness range.

(3) The interaction effect between adjacent elements has been taken into account in the cross-section plate slenderness by using the analytical approximations (Seif and Schafer, 2010) or a numerical approach, such as CUFSM (Li and Schafer, 2010), as recommended in this study. The accuracy of both estimation approaches have been validated herein.

(4) The global plastic analysis in the CSM diverts from the traditional global plastic design. The CSM considers the degree of rotation at each plastic hinge, leading to different cross-section capacities at different hinges, which is more rational. However, the internal force and moment redistributing mechanism within indeterminate structures still needs further investigation on other structural configurations.

CHAPTER 6
DESIGN STRENGTHS AND COMPARISON

6.1 Introduction

The key objective in this study is to propose a safe and efficient design approach for aluminium alloy structures, while the common way to validate a design method is by comparing the predicted design strengths with test results. This chapter presents an overview of the existing and newly proposed design methods, and describes how test and FE results have been used for the development, calibration and validation of the CSM.

Results from other laboratory testing programmes (see Appendix G) are collected and analysed in conjunction with those generated as part of the current study (described in Chapter 3). In addition, numerical results generated from parametric studies in this study are also employed. The data pool includes data of aluminium alloy stub columns, simply supported beams and continuous beams. Cross-section shapes considered in the study comprise: SHS/RHS, SHS/RHS with internal cross stiffeners, I-sections, angles and channels. Different aluminium alloy tempers from T4 to T7 are covered.

In this chapter, the experimental and numerical resistances, i.e. P_u for stub columns, M_u for simply supported beams and F_u for continuous beams, are compared with the nominal flexural design strengths predicted by the American (P_{AA}, M_{AA} or F_{AA}), Australian/New Zealand ($P_{AS/NZS}$, $M_{AS/NZS}$ or $F_{AS/NZS}$) and European (P_{EC9}, M_{EC9} or F_{EC9} and P_{EC9-F}, M_{EC9-F} or F_{EC9-H}) specifications for aluminium alloy structures, In addition, the capacities calculated based on the CSM (P_{csm}, M_{csm} or F_{csm}) and traditional plastic design method (F_{pl}) are also evaluated against the experimental

and numerical results, where applicable. The comparisons were performed using the measured material properties and geometries of the sections, with all safety factors set equal to unity.

6.2 Stub columns

6.2.1 Data pool

Test data of aluminium alloy stub columns from the literature (Bijlaard and Fisher, 1953; Langseth and Hopperstad, 1997; Mazzolani et al., 1996, 1997a and 1997b; Landolfo et al., 1999; Hassinen, 2000; Mennick, 2002; Zhu and Young, 2006a, 2008; Mazzolani et al., 2011) have been combined with those newly generated in the present study and used to evaluate the design predictions of cross-sectional compressive capacities. A total of 346 experiments have been considered, with both closed and open section types: 110 SHS/RHSs, 203 plain channel sections and 33 angle sections. The average measured cross-sectional dimensions and material properties are given in Appendix G.

6.2.2 Aluminum Design Manual (AA, 2010)

The design rules in Aluminum Design Manual (AA, 2010) for aluminium alloy stub columns is defined as the design stress f_d multiplied by the gross cross-sectional area A (see Eq. 6.1). Since local buckling is the only possible failure mode for stub columns, the design stress should be only determined based on the cross-section components.

Design local buckling stress for compressive components are expressed using buckling constants and classified into three categories base on limit states: material yielding, inelastic buckling and post-buckling, which are detailed in Clause B.5.4

(AA, 2010). Expressions for local buckling stress varied according to the boundary conditions of each element such as flat elements supported on one edge or two edges. Local buckling stress for the gross section can be chosen as the most conservative element strength, or either determined by the weighted average local buckling strength, illustrated in Clause E.4.1 (AA, 2010). The latter approach is used herein, in which the limit state compressive stress for the section as a whole is the weighted average limit state stress for each element. The limit state stress of the section is the weighted average value in accordance with the ratio of the area of the element to the total area of the section (see Eq. 6.2).

To conclude, the design resistance of stocky sections is defined as the yield stress f_y multiplied by the gross cross-sectional area A, while a reduced stress is used for slender sections.

$$P = f_d A$$

(Eq. 6.1)

$$f_d = \frac{\sum_{i=1}^{n} f_{ci} A_i + f_y \left(A - \sum_{i=1}^{n} A_i \right)}{A}$$

(Eq. 6.2)

where f_{ci} is the local buckling stress of element i component with area of A_i.

Calculation procedure is listed as below:

```
┌─────────────────────────────────────────────┐
│ (1)Calculate Slenderness limits S₁, S₂        │
└─────────────────────────────────────────────┘
```

$$\text{(1)Calculate Slenderness limits } S_1, S_2$$

$$\text{If } b/t \le S_1:\text{ Yielding}$$

$$\text{If } S_1 < b/t \le S_2:\text{ Inelastic yielding}$$

$$\text{If } b/t > S_2:\text{ Post-buckling}$$

$$\text{(2) Determine design strength for each elements } f_{ci}$$

(3) Determine the section design strength for the cross-section as a whole

$$f_d = \frac{\sum_{i=1}^{n} f_{ci} A_i + f_y \left(A - \sum_{i=1}^{n} A_i\right)}{A}$$

(4) Calculate the compression capacity of stub columns

$$P = f_d A$$
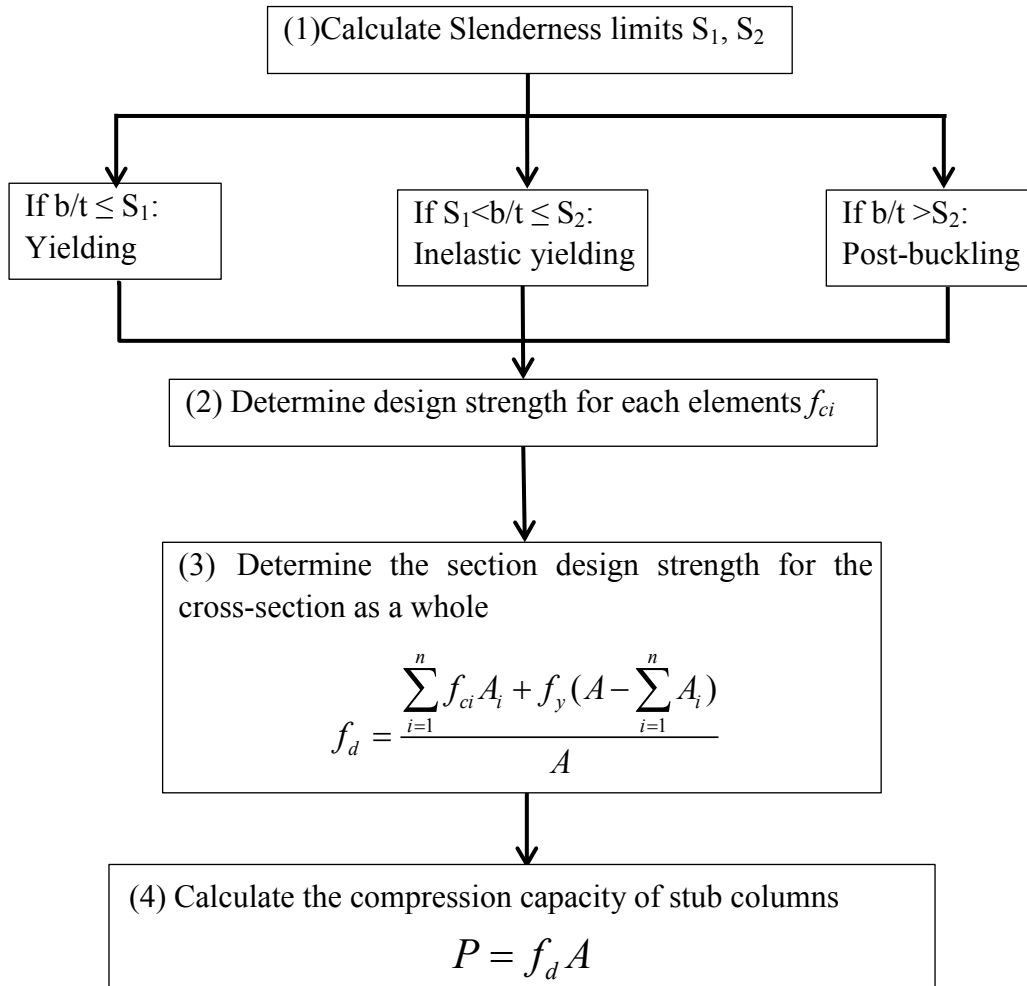
The mean ratio of experimental to predicted ultimate loads for the AA Standard (P_u/P_{AA}) was 1.19 with the corresponding coefficient of variation (COV) of 0.251 (see Fig. 6.1 as well as Table 6.1 and Table 6.2).

Fig. 6.1   Comparison between experimental results and design strengths predicted by the Aluminum Design Manual (AA, 2010)

6.2.3 Australian/New Zealand Standard (AS/NZS, 1997)

The AS/NZS (1997) provisions for calculating the design strengths of aluminium alloy stub columns are generally the same as the AA (2010), except with a reduction coefficient k_c for compression members in the yielding limit state, as codified in Clause 3.4.10 (AS/NZS, 1997). Thus, the predictions for stocky sections of the AS/NZS (1997) are more conservative than those from the AA (2010).

The mean value of experimental-to-predicted ultimate loads for the AS/NZS Standard ($P_u/P_{AS/NZS}$) is 1.28 with COV of 0.250. The AS/NZS (1997) provided the most conservative design strengths, as shown in Fig. 6.2.
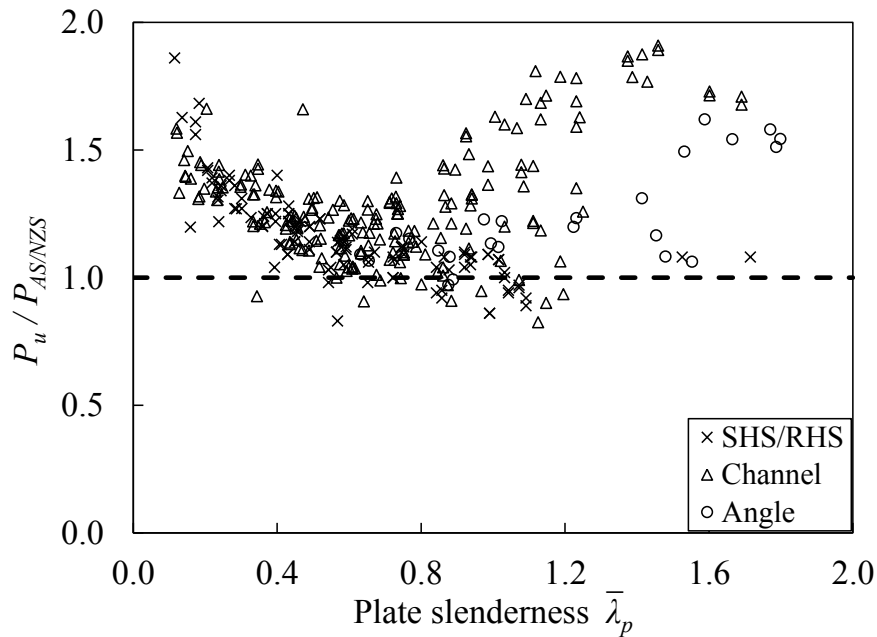
Fig. 6.2　　　Comparison between experimental results and design strengths

predicted by the Australia/New Zealand Standard (AS/NZS, 1997)

6.2.4 Eurocode 9 (EC9, 2007)

6.2.4.1 Traditional method in main content

Eurocode 9 (EC9, 2007) provides design rules for cross-section compressive capacity in Clause 6.2.4, which limit the resistance of non-slender sections to the yield load (Af_y) and employs an effective thickness concept for slender sections ($A_{eff}f_y$). Unlike the AA and AS/NZS specifications, the yield stress f_y is used for all sections in EC9, but the local buckling is taken into consideration by reducing the thickness of elements. It is necessary to classify a cross-section into four classes based on the slenderness of the most slender component. Classes 1, 2 and 3 sections derive the cross-section capacities according to Eq. 6.3, while design for Class 4 sections refers to Eq. 6.4.

$$P = f_y A \qquad \text{(Eq. 6.3)}$$

$$P = f_y A_{eff} \qquad \text{(Eq. 6.4)}$$

The effective section area A_{eff} is based on the reduced thickness t_{eff}, which is defined by Eq. 6.5. The calculation procedure for the local buckling factor ρ_c is specified in Clause 6.1.5 of EC9 (2007), which is applied to any uniform thickness Class 4 components that is wholly or partly in compression.

$$t_{eff} = t \rho_c \qquad \text{(Eq. 6.5)}$$

The calculation procedure is summarized as below:

```
                    ┌──────────────────────────────┐
                    │  (1) Classify cross-sections  │
                    └──────────────────────────────┘
     Classes 1, 2 and 3 sections          Class 4 sections
```

(2) Determine cross-section capacity for Classes 1, 2 and 3 sections: $P = f_y A$	(2) Determine local buckling factor ρ_c for each Class 4 element $\rho_c = \dfrac{C_1}{(\beta / \varepsilon)} - \dfrac{C_2}{(\beta / \varepsilon)^2}$

(3) Calculate effective thickness for each Class 4 element $t_{eff} = t \rho_c$

(4) Determine the effective section area A_{eff} based on the effective thickness t_{eff}

(5) Calculate the compression capacity of stub columns

$$P = f_y A_{eff}$$

The comparisons of EC9 (2007) predictions with the test results gave a mean value of P_{exp}/P_{EC9} of 1.18 and a corresponding COV of 0.168. Relevant data are plotted in Fig. 6.3.
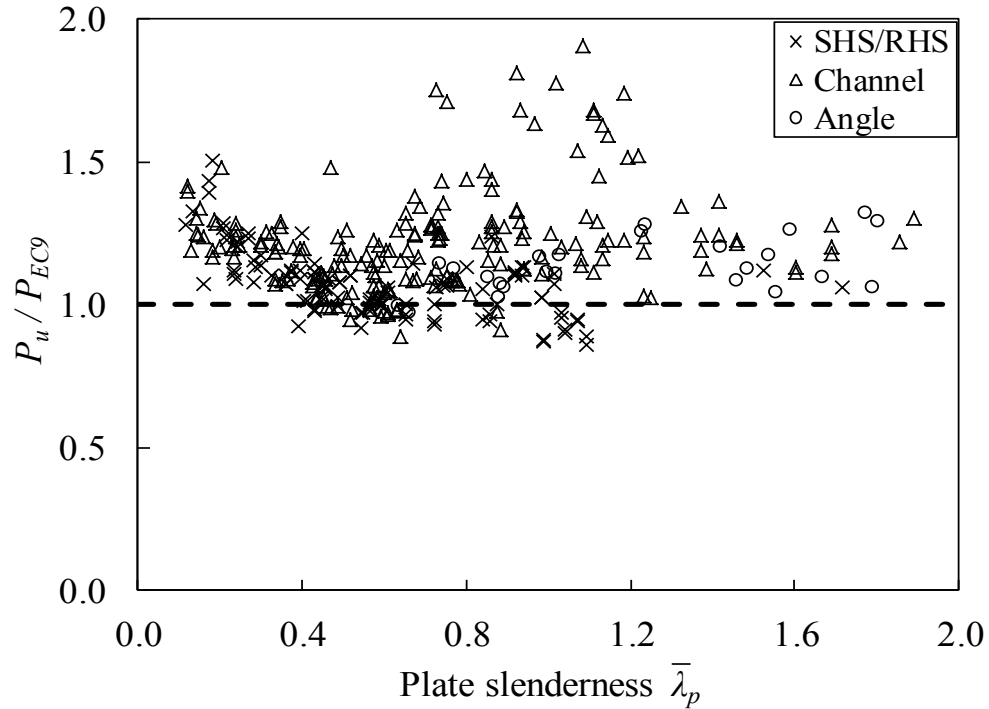
Fig. 6.3   Comparison between experimental results and design strengths predicted by Eurocode 9 (EC9, 2007)

6.2.4.2 Method in Annex F

To recognise the effect of strain hardening on cross-section capacity, EC9 (2007) provides an alternative approach in Annex F to utilizes the ultimate stress f_u for Class 1 sections. However, the enhancement has been limited to Class 1 sections that might experience large strains.

The comparisons of EC9-Annex F (2007) predictions with the test results gave a mean value of P_{exp}/P_{EC9-F} of 1.17 and a corresponding COV of 0.169 (see Table 6.1 and Table 6.2 as well as Fig. 6.4). Overall, among the existing design standards,

Annex F in EC9 (2007) provided the most accurate predictions of stub column compression capacity.
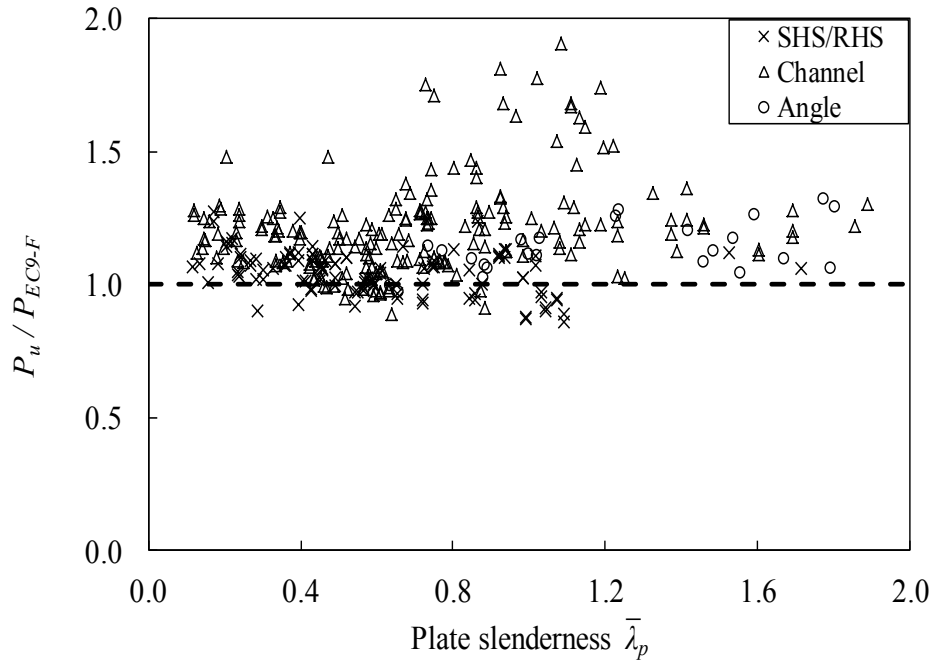
Fig. 6.4   Comparison between experimental results and design strengths predicted by Annex F of Eurocode 9 (EC9, 2007)

6.2.5 Continuous strength method (CSM)

The calculation procedure of the CSM for stub columns has been demonstrated in Chapter 5. The comparisons are presented in Fig. 6.5 and Table 6.1 - Table 6.2. Overall, a mean value prediction P_{exp}/P_{csm} of 1.04 with a COV of 0.090 are achieved, which represents improved accuracy and reduced scatter in comparison with other approaches considered in this study.
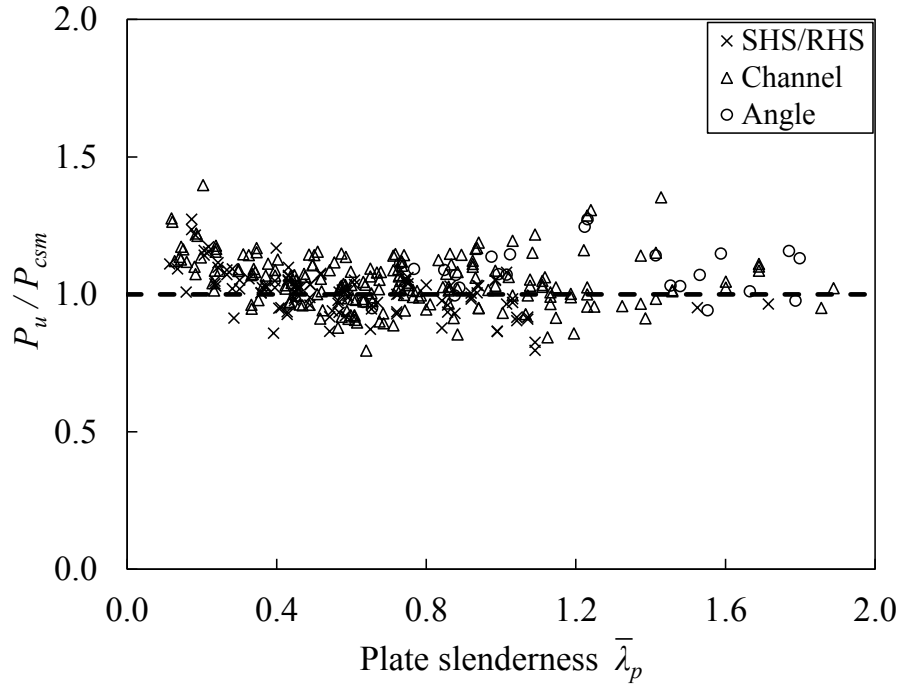
Fig. 6.5   Comparison between experimental and numerical results with design strengths predicted by the proposed CSM

6.2.6 Summary

A comparison of the test results with the design strengths of the American, Australian/New Zealand and European specifications, as well as the continuous strength method (CSM) for aluminium alloy stub columns, has been performed. Table 6.1 only presents the comparisons with the experimental data (P_{exp}) that newly generated in this study, while the comparisons of all data (P_u) are summarised in Table 6.2. The treatments of different design methods are illustrated in Fig. 6.6.

It was found that the design predictions of the three design specifications are more conservative for stocky cross-sections. The conservatism was attributed primarily to the ability of the cross-sections to achieve capacities greater than the yield load as a result of strain hardening. The failure modes predicted by the three specifications are all material yielding (with allowance for strain hardening in the

case of Annex F of EC9), which coincided with the observed failure modes. The design strengths predicted by the CSM, with systematic exploitation of strain hardening, were found to be more accurate and more consistent.
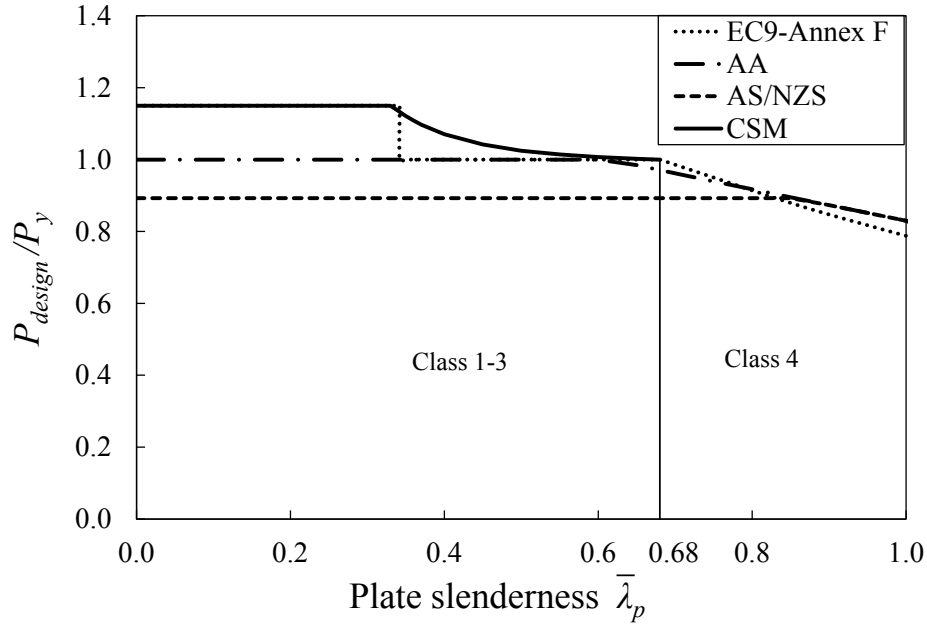
Fig. 6.6   Curves indicating design capacities of different design approaches for stub columns

Table 6.1 Comparisons of stub column test results with different design methods

Specimen	$\bar{\lambda}_p$	P_{exp} (kN)	$\dfrac{P_{exp}}{P_{AA}}$	$\dfrac{P_{exp}}{P_{AS/NZS}}$	$\dfrac{P_{exp}}{P_{EC9}}$	$\dfrac{P_{exp}}{P_{EC9-F}}$	$\dfrac{P_{exp}}{P_{csm}}$
H64×64×3.0C	0.58	164.2	1.02	1.15	1.02	1.02	1.02
H64×64×3.0C-R	0.57	165.4	1.02	1.14	1.02	1.02	1.01
H70×55×4.2C	0.36	196.2	1.07	1.20	1.07	1.07	1.00
H70×55×4.2C-R	0.36	196.9	1.02	1.20	1.07	1.02	1.01
H95×50×10.5C	0.16	626.2	1.07	1.20	1.07	1.01	1.01
H120×70×10.5C	0.24	862.5	1.09	1.22	1.09	1.03	1.03
H120×120×9.0C	0.33	981.5	1.10	1.23	1.10	1.06	1.06
N95×50×10.5C	0.14	609.8	1.45	1.63	1.33	1.15	1.09
N120×70×10.5C	0.18	736.9	1.50	1.68	1.50	1.10	1.22
N120×120×9.0C	0.29	811.1	1.13	1.27	1.13	0.92	0.91
+H95×95×4.3C	0.28	585.6	1.21	1.36	1.15	1.10	1.09
+H95×95×4.3C-R	0.28	574.2	1.19	1.33	1.13	1.07	1.07
+H120×70×10.5C	0.24	1164.3	1.16	1.30	1.11	1.05	1.04
+H120×70×10.5C-R	0.24	1174.4	1.17	1.32	1.12	1.06	1.05
+N95×50×10.5C	0.13	664.8	1.66	1.86	1.28	1.37	1.11

112

Table 6.2   Summary of comparisons between experimental results with

design strengths (for stub columns)

	$\dfrac{P_u}{P_{AA}}$	$\dfrac{P_u}{P_{AS/NZS}}$	$\dfrac{P_u}{P_{EC9}}$	$\dfrac{P_u}{P_{EC9-F}}$	$\dfrac{P_u}{P_{csm}}$
Mean, P_m	1.19	1.28	1.18	1.17	1.04
COV, V_p	0.251	0.250	0.168	0.169	0.090

6.3 Simply supported beams

6.3.1 Data pool

Previous studies conducted by Moen et al. (1999), Lai and Nethercot (1992) and
Zhu and Young (2009) together with the data obtained from the current study have
provided some relevant experimental results, including 45 obtained from
three-point bending tests of SHS/RHS with/without internal stiffeners and
I-sections as well as 38 from four-point bending tests of SHS/RHS with/without
internal stiffeners. Numerical models were also developed, after which the
validated models were used to carry out extensive parametric studies. A total of
192 numerical results were generated to supplement the experimental data, with
half being three-point bending and half being four-point bending. A wide range of
both b/h ratios (0.29 - 3.35) and b/t ratios (4.25 - 55.14) were considered in the
numerical parametric study for SHS/RHS, while b/h ratios became 0.28 - 3.62
and b/t ratios ranged from 3.40 to 26.50 for stiffened SHS/RHS. Outer section
dimensions and thickness were up to 180 mm and 12 mm in the FE models,
respectively.

6.3.2 Aluminum Design Manual (AA, 2010)

The AA (2010) standard provides design rules for aluminium alloy simply supported beams in Clause F.8.3 of Part I, where only elastic analysis is allowed. Since the study focuses on cross-section capacity and the available bending results have been subjected to in-plane bending, the lateral torsional buckling checking can be exempted, and only components at the cross-sectional level are examined.

The cross-section moment capacity is equal to the product of the elastic section modulus and the design stress. Similar to compressive section design, the flexural design strength for cross-sections can be taken as either the least of the design stress for the flanges (f_f) and webs (f_w) multiplying the elastic section modulus or the nominal weighted average design moment. The nominal weighted average design moment is the sum of elastic section modulus of each element multiplied by its individual flexural stress (see Eq. 6.6), which is adopted throughout this study. Although both weighted average compressive and tensile flexural strengths should be considered, the weighted average compressive flexural strength is the critical strength in this study, so the tensile flexural strength is not considered herein. The flow chat for the calculation procedure is shown below.

$$M = \frac{f_f I_f}{c_{cf}} + \frac{f_w I_w}{c_{cw}} \qquad \text{(Eq. 6.6)}$$

where I_f *and* I_w *are* the second moment of inertial for flanges and webs, c_{cf} is the distance from the centreline of the compression flange to the neutral axis of the cross-section, c_{cw} is the distance from the centreline of the web group's extreme compressive fiber to the neutral axis of the cross-section.

Calculation procedure is illustrated as below:

```
                    ┌──────────────────────────────────────────┐
                    │ (1) Calculate Slenderness limits S₁, S₂   │
                    └──────────────────────────────────────────┘
```

(1) Calculate Slenderness limits S_1, S_2

If $b/t \leq S_1$:
Yielding

If $S_1 < b/t \leq S_2$:
Inelastic yielding

If $b/t > S_2$:
Post-buckling

(2) Determine the local buckling stress of flanges f_f and webs f_w

(3) Determine the section design strength for the cross-section

$$M = \frac{f_f I_f}{c_{cf}} + \frac{f_w I_w}{c_{cw}}$$
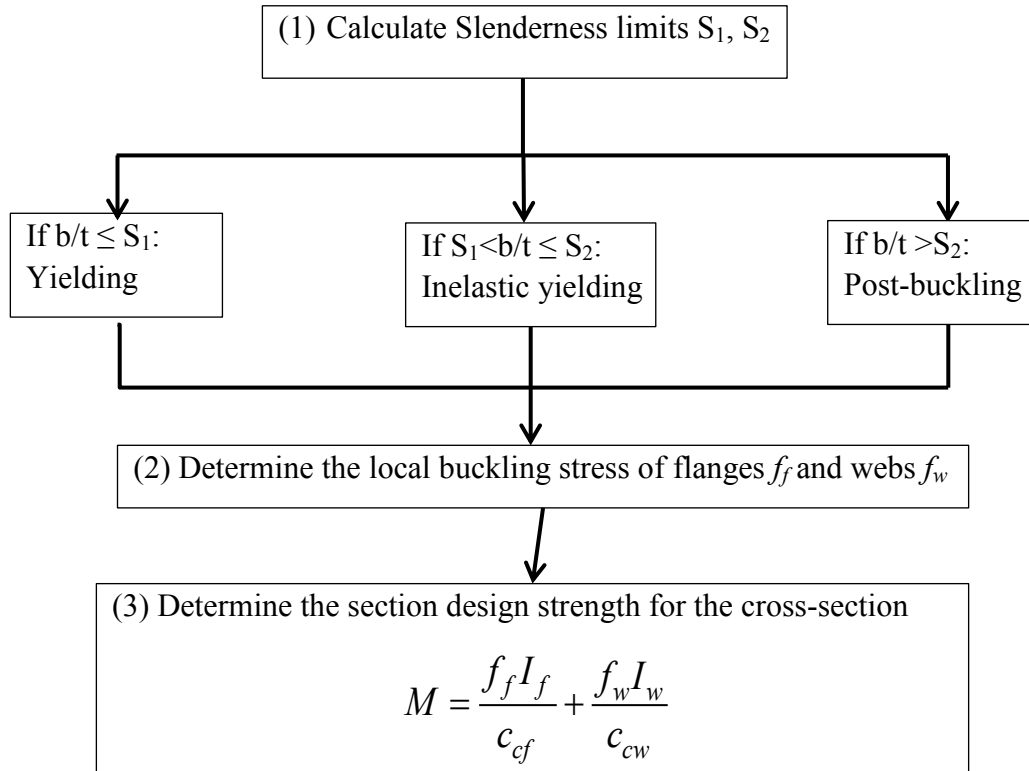
In the case of simply supported beams, the predictions of the AA (2010) was found to be conservative, which have the great mean values of 1.27 and 1.40 with the corresponding COV of 0.187 and 0.207 for the moment ratio M_u/M_{AA} of SHS/RHS and stiffened SHS/RHS, respectively. Table 6.3 and Table 6.4 present comparisons of three-point and four-point bending test results, respectively. Comparisons of all the experimental and numerical data (M_u) with the AA predictive values (M_{AA}) are shown in Fig. 6.7 and Table 6.5 - Table 6.6.
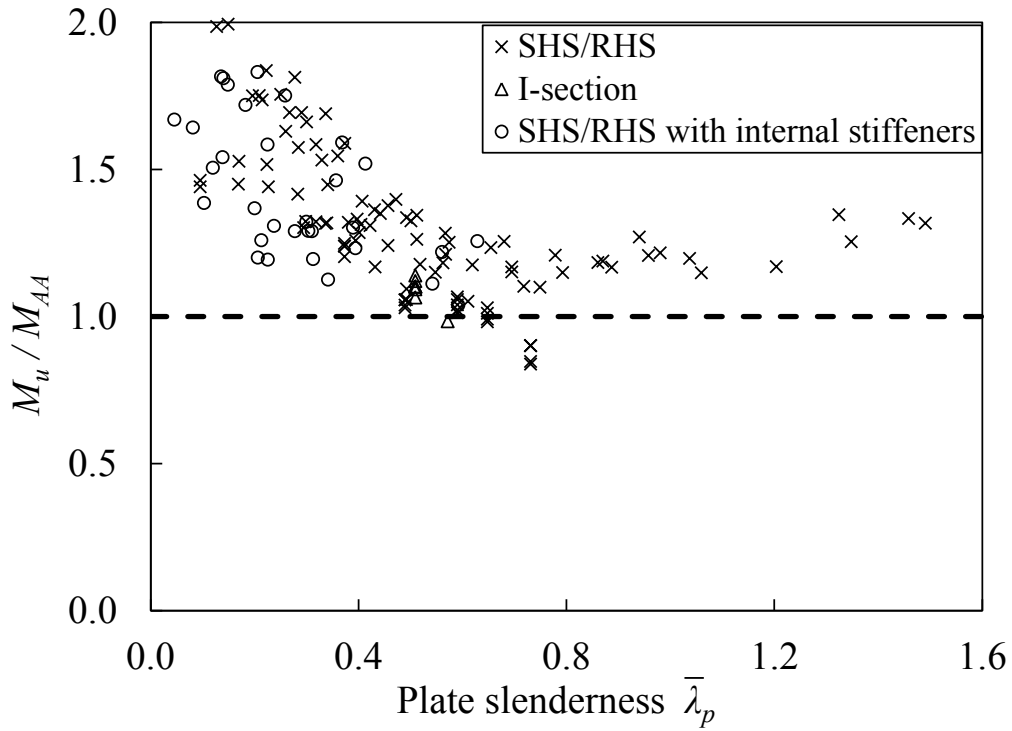
(a) Three-point bending
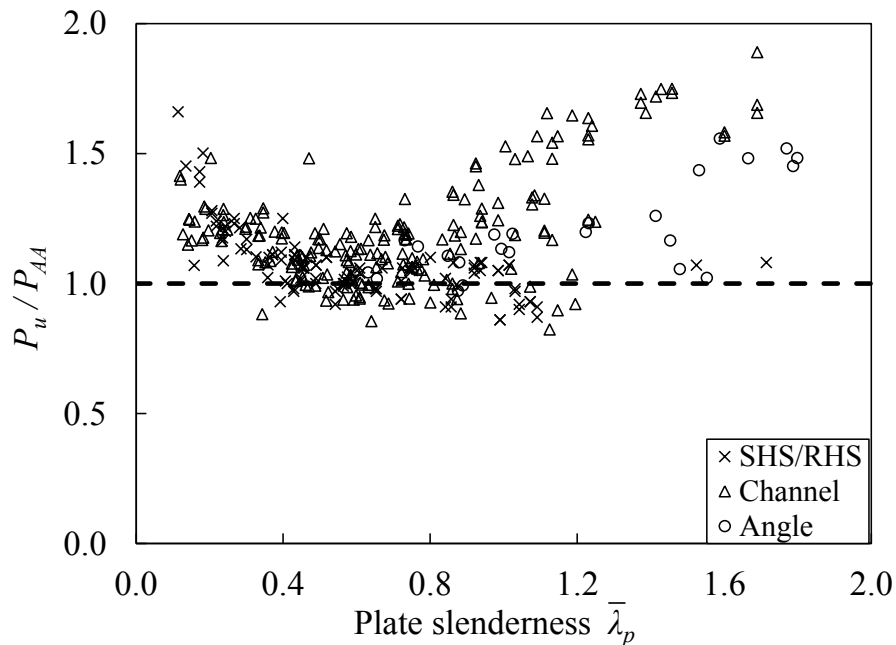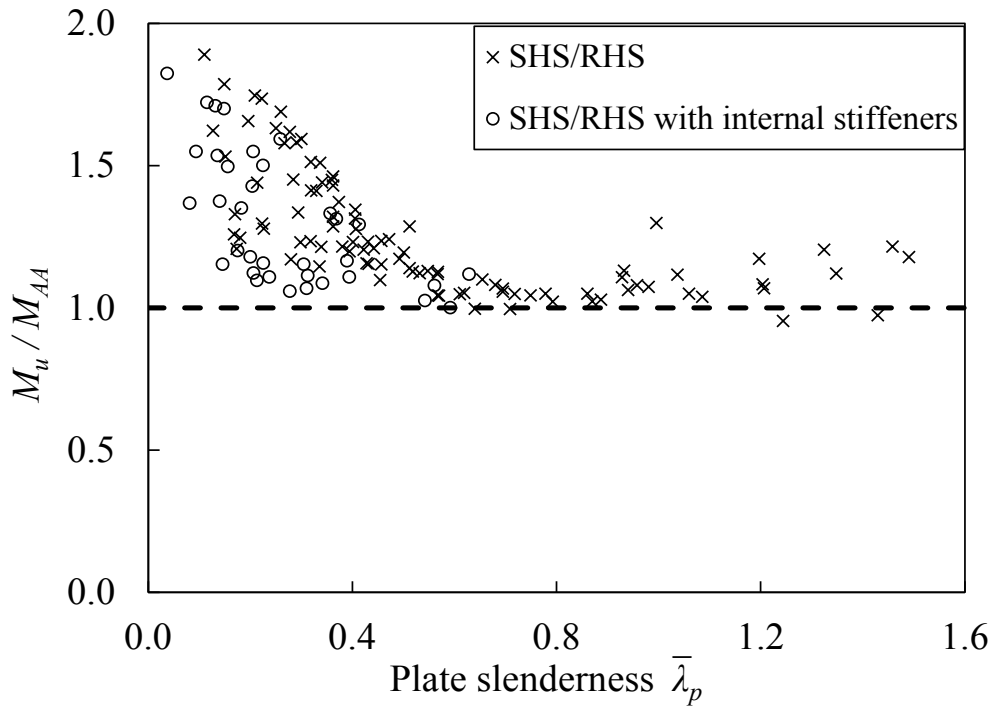

(b) Four-point bending

Fig. 6.7   Comparisons between experimental and numerical results of with

design strengths predicted by the Aluminum Design Manual (AA, 2010)

6.3.3 Australian/New Zealand Standard (AS/NZS, 1997)

The design rules for cross-sectional component elements in the AS/NZS (1997) provision are similar to those in the AA (2010). The design details can be referred to Clause 3.4 (AS/NZS, 1997). However, after obtaining the limit state stress for each element, the AS/NZS employs the weighted average compressive or tensile stress as the limit state stress for the section as a whole, whichever is more critical. In all cases considered in this study, the limit state compressive stress was found to be the critical stress. As stated in Clause 4.7.2 of the AS/NZS (1997), the limit state compressive stress for the section as a whole (f_d) takes weighted average of the limit state stress of compressive flange (f_f) and webs (f_w) in accordance to the ratio of the area of each element (A_{cf} and A_{cw}) to the area of the compression part, where A_{cf} is the area of the flange in compression and A_{cw} is the area of the webs in compression. The design rules given in the AS/NZS (1997) provisions are using the elastic modulus of the cross-section and multiply by the weighted average compressive stress (f_d). The significant diversion between the AA (2010) and the AS/NZS (1997) is the way to calculate the design stress for the cross-section, where section modulus was used in the AA (2010), and area was used in the AS/NZS (1997).

Calculation procedure is illustrated as below:

(1) Calculate Slenderness limits S_1, S_2

| If $b/t \leq S_1$: Yielding | If $S_1 < b/t \leq S_2$: Inelastic yielding | If $b/t > S_2$: Post-buckling |

(2) Determine the local buckling stress of flanges f_f and webs f_w

(3) Determine the state limit stress for the section as a whole

$$f_d = \frac{f_f A_{cf} + \dfrac{1}{3} f_w A_{cw}}{A_{cf} + \dfrac{1}{3} A_{cw}}$$

(4) Determine the moment capacity of the cross-section

$$M = W_{el} f_d$$
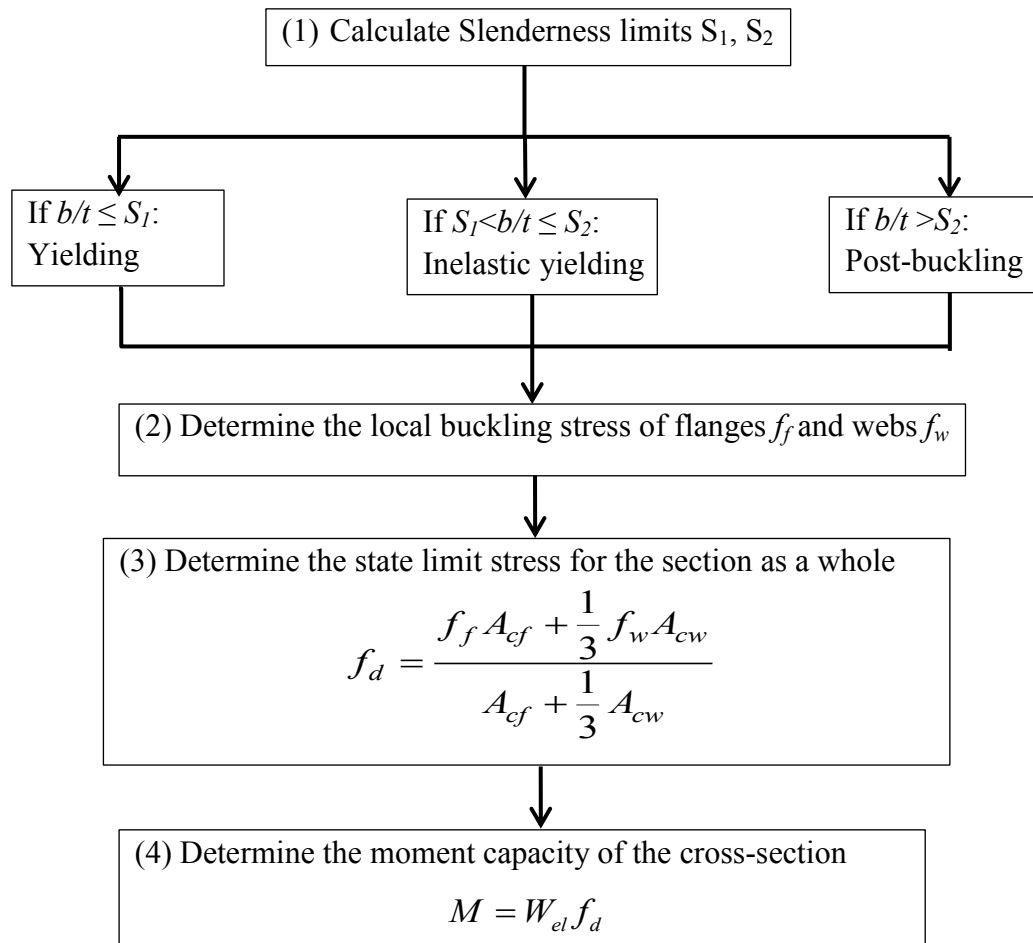
The AS/NZS Standard (1997) is conservative, which has the large mean values of 1.40 and 1.66 with COV of 0.212 and 0.233 for the moment ratio $M_u/M_{AS/NZS}$ of SHS/RHS and stiffened SHS/RHS, respectively. The AS/NZS (199) provides the most conservative predication among the three specifications. Comparisons between the experimental and numerical results with the AS/NZS predictions are shown in Fig. 6.8, while the comparison results are presented in Table 6.3 - Table 6.6.
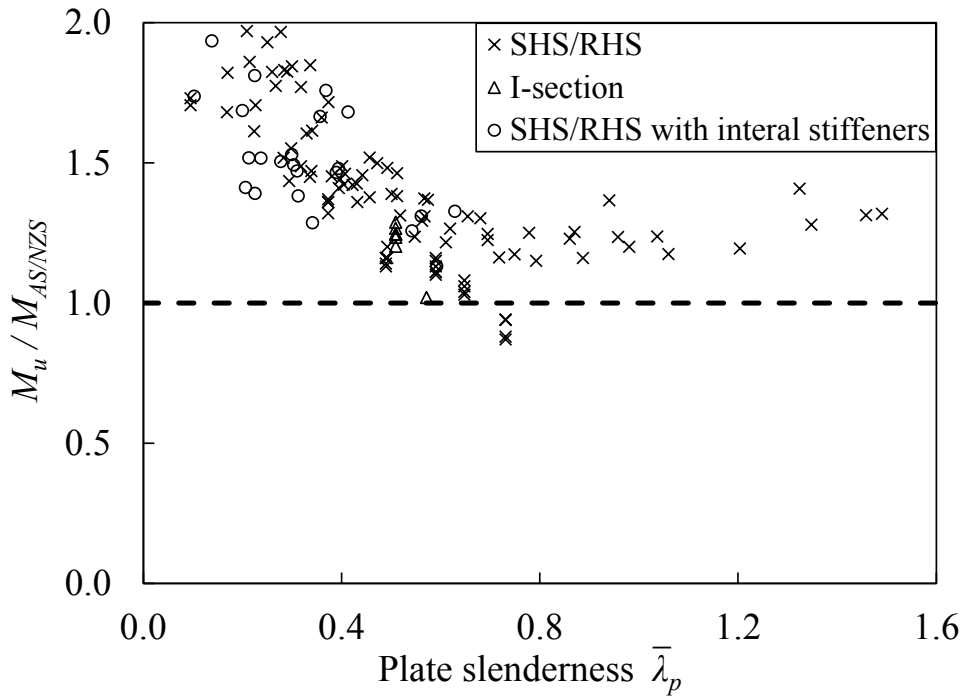
(a) Three-point bending
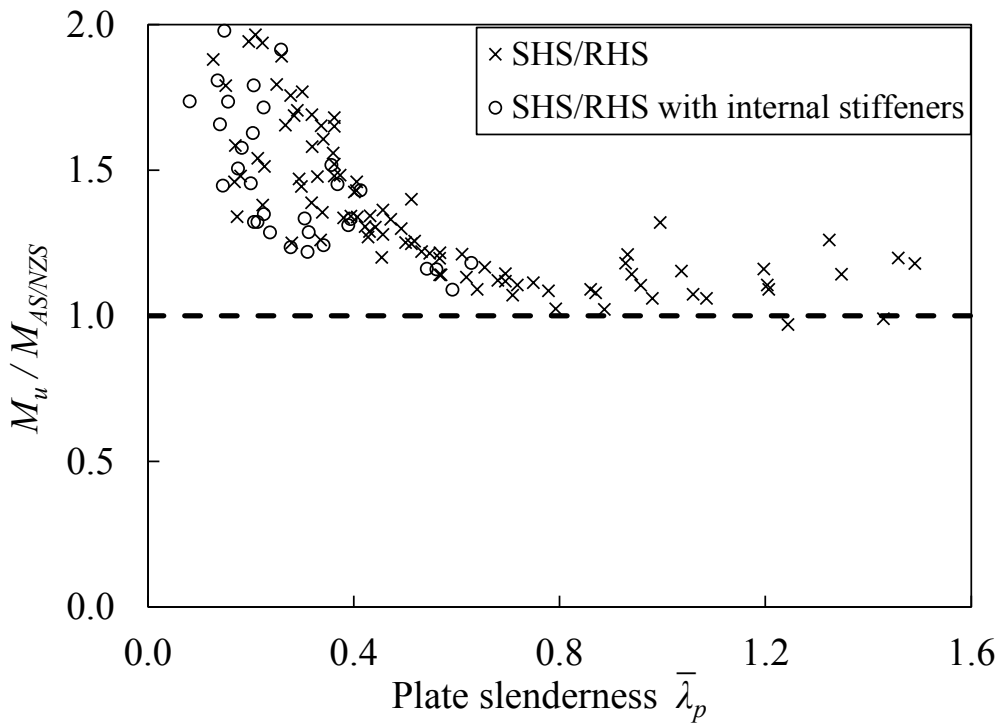
(b) Four-point bending

Fig. 6.8   Comparison between experimental and numerical results with

design strengths predicted by the Australian/New Zealand Standard (AS/NZS,

1997)

6.3.4 Eurocode 9 (EC9, 2007)

6.3.4.1 Traditional method in main content

Eurocode 9 (2007) specifies the cross-section bending moment capacity design in Clause 6.2.5 of EC9. Similar to cross-section compression design, classification is the first step to be done, where the class of the most slender element is taken as the class for the section. In EC9, resistance is defined as the yield stress multiplied by the plastic section modulus W_{pl} for Classes 1 and 2 sections, by the elastic section modulus W_{el} for Class 3 sections and by the elastic modulus of an effective section W_{eff} for Class 4 sections.

Calculation procedure is summarised as below:

```
                    ┌─────────────────────────────┐
                    │ (1) Classify cross-sections  │
                    └─────────────────────────────┘
```

Classes 1-2	Class 3 sections	Class 4 sections
(2)　Determine cross-section capacity: $M=W_{pl}f_y$	(2)　Determine cross-section capacity: $M=W_{el}f_y$	(2) Determine local buckling factor ρ_c for each Class 4 element $$\rho_c = \frac{C_1}{(\beta/\varepsilon)} - \frac{C_2}{(\beta/\varepsilon)^2}$$

(3) Calculate effective thickness for each Class 4 element

$$t_{eff} = t\rho_c$$

(4) Determine the elastic section modulus for effective section area W_{eff} based on the effective thickness t_{eff}

(5) Determine the cross-section capacity:

$$M = W_{eff} f_y$$

EC9 generally underestimated the test and numerical results by 20% and 25% for SHS/RHS and stiffened SHS/RHS, with the corresponding COV of 0.159 and 0.188 for M_u/M_{EC9} ratio, as presented in Table 6.5 and Table 6.6. Comparative results between tests (or simulations) and predictions are plotted in Fig. 6.9.
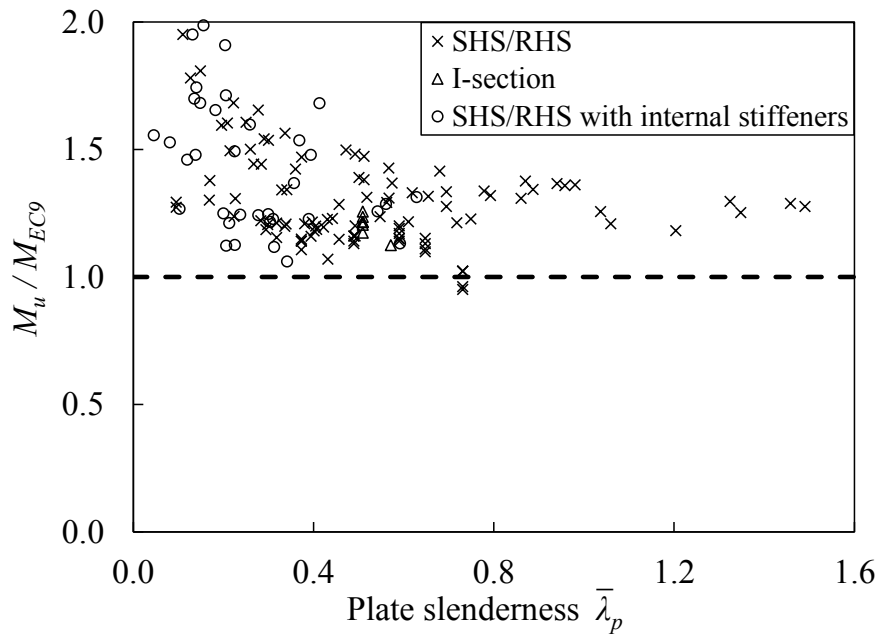
(a) Three-point bending
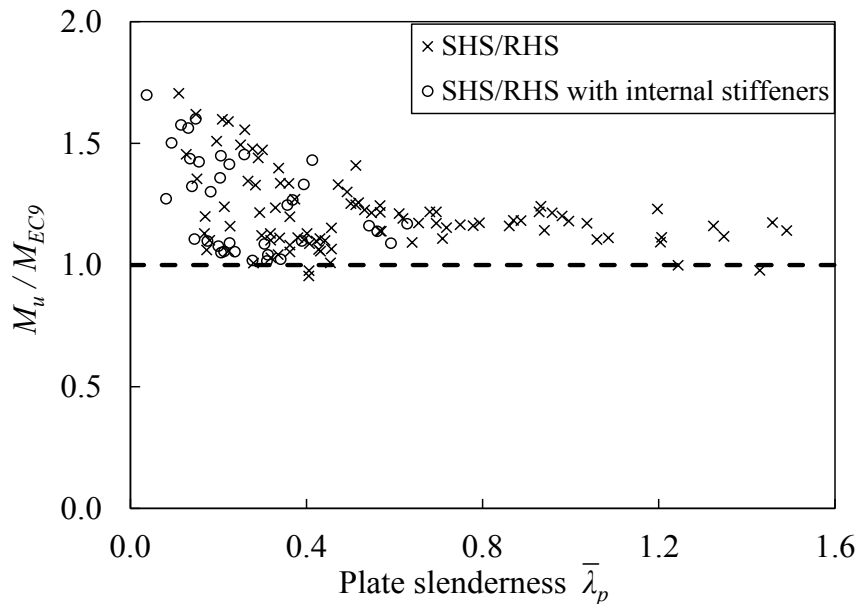
(b) Four-point bending

Fig. 6.9   Comparison between experimental and numerical results with design strengths predicted by Eurocode 9 (EC9, 2007)

121

6.3.4.2 Method in Annex F

EC9 (2007) also provides an alternative design method in Annex F to allow estimating the post-elastic behaviour of cross-sections. This alternative method enables higher capacities to be determined for Class 1 sections by taking account of strain hardening. The effect of strain hardening depends on the type of alloys. It should be noted that the upper bound of the design limit for Class 1 section has become $W_{pl}f_u$ in Annex F. It is designed based on the assumption that Class 1 sections can develop the collapse load without having local instability in the section. Thus, the design approach in Annex F only diverts from the main text of the code on the predictions of Class 1 sections.

When adopting Annex F in the design for Class 1 section, EC9 provides better predictions: the mean values of 1.21 (for SHS/RHS) and 1.27 (for SHS/RHS with internal stiffeners) with the corresponding COV of 0.109 (for SHS/RHS) and 0.150 (for SHS/RHS with internal stiffeners) for the comparative ratio M_u/M_{EC9-F}. Comparing the traditional elastic design in the main text of the code, the improvement of the alternative method in Annex F is notable, with mean value being closer to unity and less scatter (Fig. 6.10 and Table 6.3 -Table 6.6).

(a) Three-point bending

(b) Four-point bending
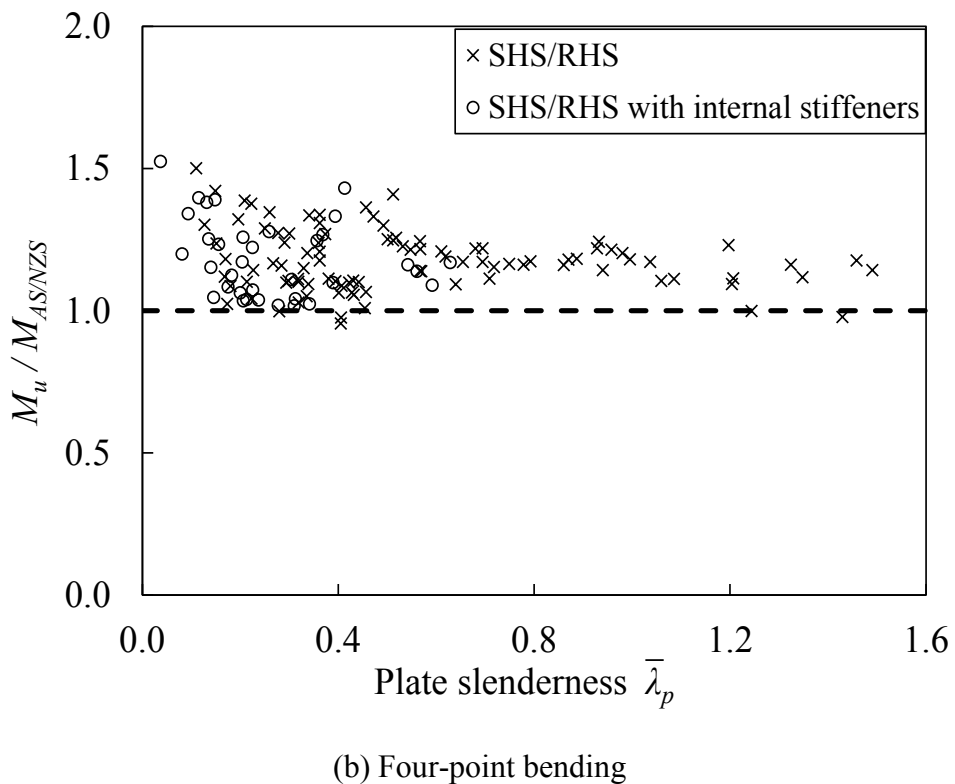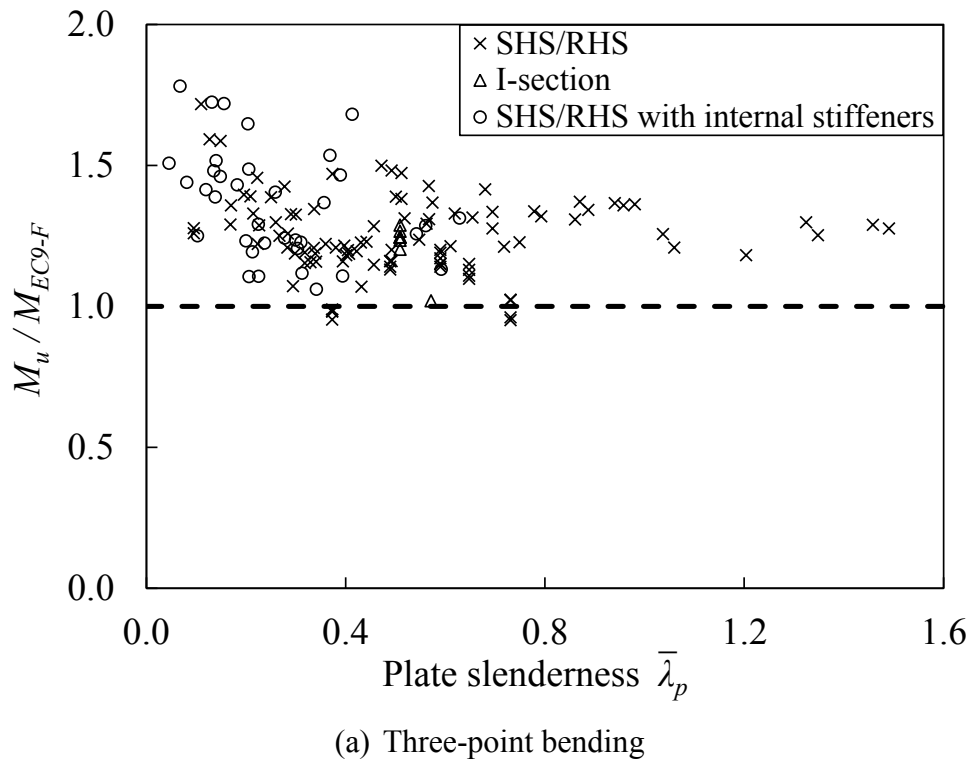
Fig. 6.10   Comparison between experimental and numerical results with

design strengths predicted by Annex F of Eurocode 9 (EC9, 2007)

6.3.5 Continuous strength method (CSM)

Design procedure for the CSM has been discussed in the previous chapter. The CSM approach (mean value of M_u/M_{csm} = 1.14 and COV = 0.114 for SHS/RHS; mean value of M_u/M_{csm} = 1.19 and COV = 0.153 for stiffened SHS/RHS) provides more accurate predictions of the bending capacity, with up to approximately 40% improvement compared to the AS/NZS predictions. Comparisons between the experimental results and the CSM predictions are shown in Table 6.3 and Table 6.4, while Table 6.5 and Table 6.6 as well as Fig. 6.11 summarise the comparisons with both experimental and numerical results.
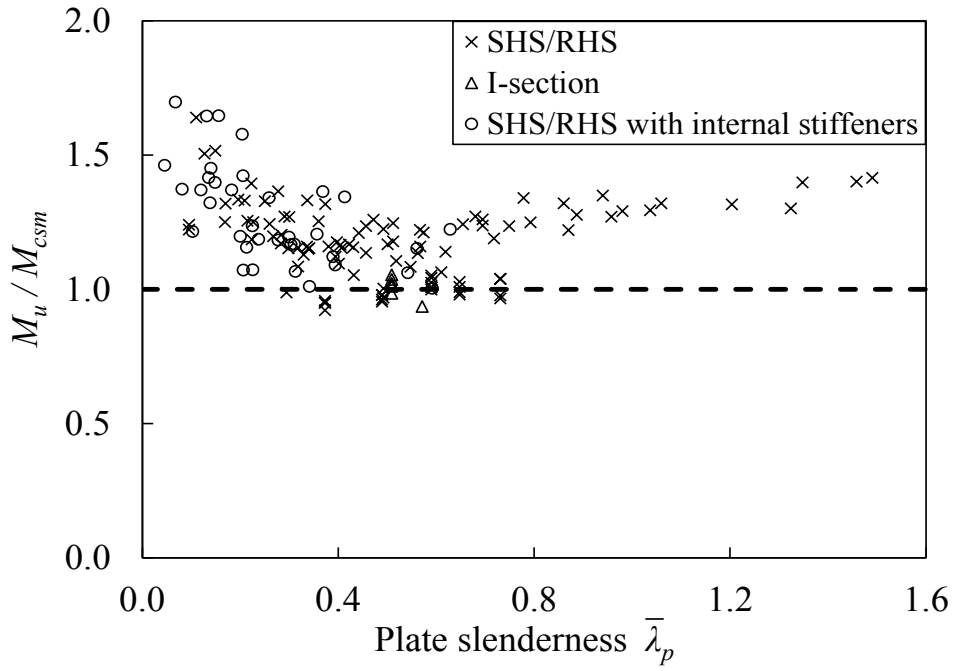
(a) Three-point bending
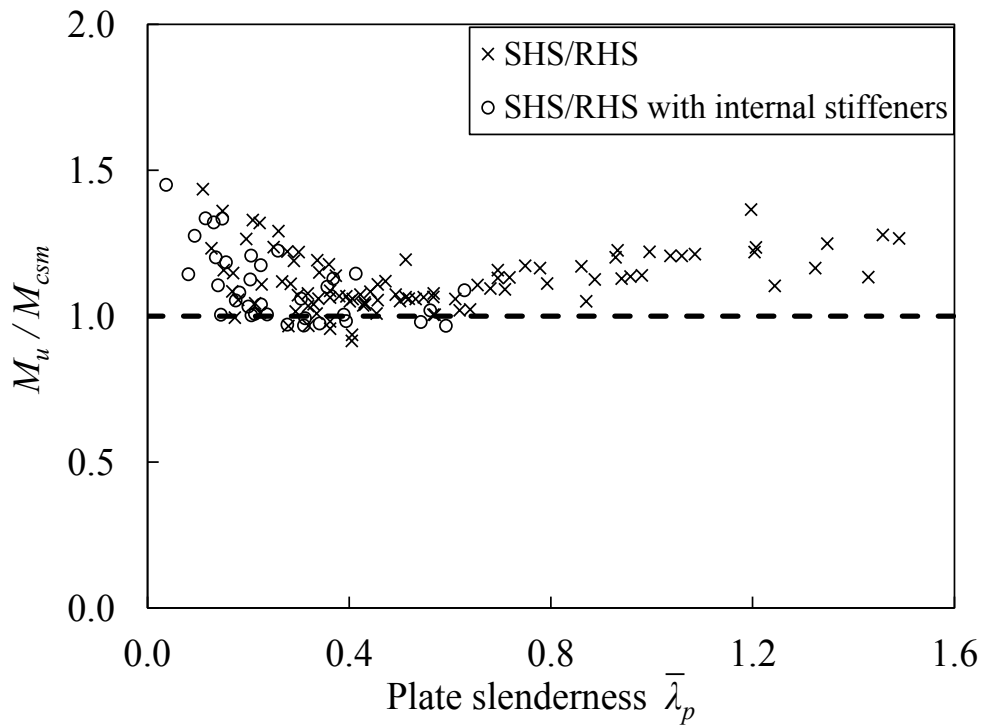
(b) Four-point bending

Fig. 6.11 Comparison between experimental and numerical results with design

strengths predicted by the proposed CSM

6.3.6 Summary

The combined data set from the tests and the numerical simulations (M_u) were used to assess the accuracy of three international design specifications (i.e. the Aluminum Design Manual (2010), the Australian/New Zealand Standard (1997) and Eurocode 9 (2007)) as well as the continuous strength method (CSM) for predicting the moment capacity of simply supported beams (see Table 6.3 - Table 6.6). The results revealed that the three design specifications generally underestimated the observed moment resistance, especially for stocky sections, where capacities well beyond the fully plastic moment resistance were typically achieved in the tests. Through a deformation-based approach that incorporated strain hardening, the continuous strength method is shown to offer improved predictions of capacity, up to 30% beyond those achieved by current specifications. The relationships between design capacities (M_{design}) and cross-section slenderness for the four design methods considered in this study are illustrated in Fig. 6.12.
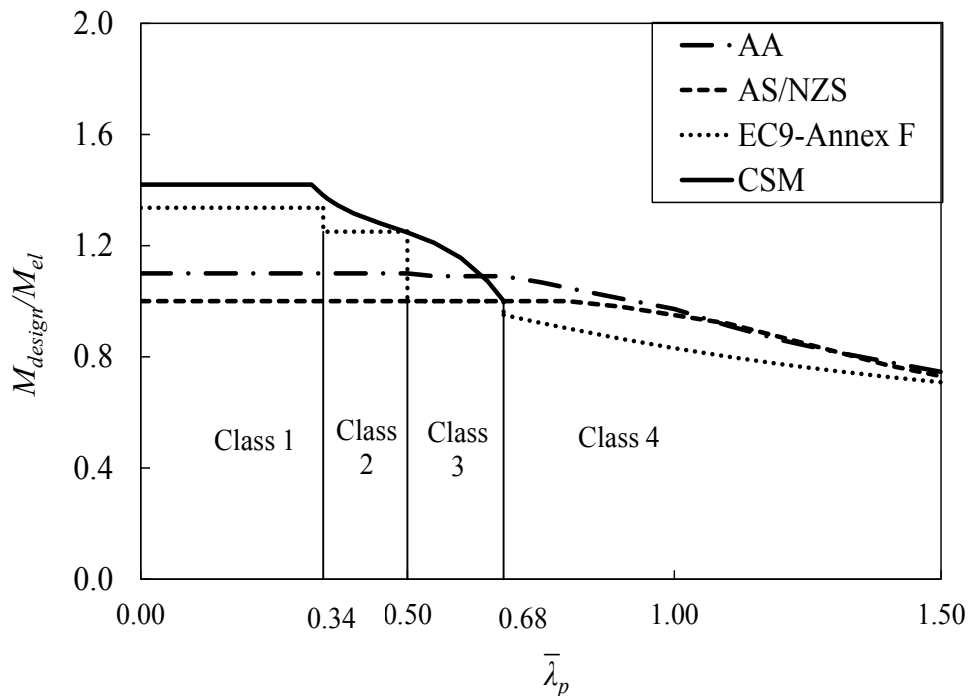
Fig. 6.12   Curves indicating design capacities from different design approaches for aluminium alloy elements in bending

Table 6.3   Summary of comparisons between three-point bending test results and design strengths

Specimen	$\bar{\lambda}_p$	M_{exp} (kNm)	$\dfrac{M_{exp}}{M_{AA}}$	$\dfrac{M_{exp}}{M_{AS/NZS}}$	$\dfrac{M_{exp}}{M_{EC9}}$	$\dfrac{M_{exp}}{M_{EC9-F}}$	$\dfrac{M_{exp}}{M_{csm}}$
H70×55×4.2B3	0.40	4.8	1.31	1.42	1.20	1.20	1.17
H70×55×4.2B3-R	0.40	4.4	1.33	1.44	1.22	1.21	1.18
H55×70×4.2B3	0.32	6.8	1.58	1.77	1.15	1.15	1.08
H95×50×10.5B3	0.22	12.1	1.52	1.61	1.24	1.22	1.19
H50×95×10.5B3	0.10	21.1	1.46	1.73	1.29	1.28	1.24
H50×95×10.5B3-R	0.10	20.8	1.44	1.70	1.27	1.26	1.22
H64×64×3.0B3	0.56	4.1	1.18	1.29	1.29	1.29	1.13
H64×64×3.0B3-R	0.57	4.3	1.25	1.37	1.37	1.37	1.21
H120×120×9.0B3	0.34	44.4	1.32	1.45	1.20	1.21	1.16
H120×70×10.5B3	0.28	23.6	1.42	1.52	1.22	1.21	1.17
H70×120×10.5B3	0.17	37.9	1.45	1.68	1.30	1.29	1.25
N120×70×10.5B3	0.21	18.0	1.74	1.86	1.49	1.33	1.26
N70×120×10.5B3	0.13	32.4	1.98	2.30	1.78	1.59	1.50
N120×120×9.0B3	0.29	35.3	1.30	1.43	1.19	1.07	0.99
+H50×95×10.5B3	0.05	26.7	1.67	2.20	1.48	1.51	1.45
+H95×50×10.5B3	0.12	13.6	1.51	2.01	1.53	1.41	1.37
+H70×120×10.5B3	0.08	45.7	1.64	2.08	1.22	1.44	1.37
+H120×70×10.5B3	0.14	26.9	1.54	1.93	1.46	1.39	1.32
+H95×95×4.3B3	0.30	16.5	1.29	1.49	1.55	1.21	1.17
+H95×95×4.3B3-R	0.30	17.1	1.32	1.53	1.25	1.23	1.19

Table 6.4   Summary of comparisons between four-point bending test results and design strengths

Specimen	$\bar{\lambda}_p$	M_{exp} (kNm)	$\dfrac{M_{exp}}{M_{AA}}$	$\dfrac{M_{exp}}{M_{AS/NZS}}$	$\dfrac{M_{exp}}{M_{EC9}}$	$\dfrac{M_{exp}}{M_{EC9-F}}$	$\dfrac{M_{exp}}{M_{csm}}$
H70×55×4.2B4	0.66	4.72	1.31	1.43	0.95	0.95	0.92
H70×55×4.2B4-R	0.34	4.83	1.35	1.46	0.98	0.98	0.94
H55×70×4.2B4	0.94	6.49	1.51	1.69	1.10	1.10	1.03
H55×70×4.2B4-R	0.51	6.07	1.41	1.58	1.03	1.03	0.97
H95×50×10.5B4	1.32	10.35	1.30	1.38	1.06	1.04	1.01
H50×95×10.5B4	0.17	18.04	1.25	1.48	1.10	1.09	1.05
H64×64×3.0B4	0.23	3.59	1.04	1.14	1.14	1.14	1.00
H64×64×3.0B4-R	0.25	3.60	1.04	1.14	1.14	1.14	1.00
H120×120×9.0B4	0.30	38.75	1.15	1.26	1.04	1.05	1.01
H120×70×10.5B4	0.43	19.66	1.17	1.25	1.01	1.00	0.97
H70×120×10.5B4	0.61	33.00	1.26	1.46	1.13	1.12	1.08
N50×95×10.5B4	0.89	15.74	1.53	1.79	1.35	1.24	1.16
N120×70×10.5B4	0.28	14.97	1.44	1.54	1.24	1.10	1.04
N70×120×10.5B4	0.37	26.45	1.62	1.88	1.45	1.30	1.23
N120×120×9.0B4	0.57	36.22	1.34	1.47	1.22	1.10	1.02
+H70×120×10.5B4	0.08	38.19	1.37	1.74	1.11	1.20	1.14
+H120×70×10.5B4	0.15	22.00	1.15	1.45	1.27	1.05	1.00
+H95×95×4.3B4	0.30	14.87	1.15	1.33	1.09	1.11	1.06
+N50×95×10.5B4	0.04	17.62	1.82	2.40	1.70	1.52	1.45
+N95×50×10.5B4	0.09	8.42	1.55	2.06	1.50	1.34	1.27

Table 6.5   Summary of comparisons between experimental and numerical results with design strengths (for simply supported beams on SHS/RHS)

	$\dfrac{M_u}{M_{AA}}$	$\dfrac{M_u}{M_{AS/NZS}}$	$\dfrac{M_u}{M_{EC9}}$	$\dfrac{M_u}{M_{EC9-F}}$	$\dfrac{M_u}{M_{csm}}$
Mean, P_m	1.27	1.40	1.26	1.21	1.14
COV, V_p	0.187	0.212	0.159	0.109	0.114

Table 6.6 Summary of comparisons between experimental and numerical results with design strengths (for simply supported beams on SHS/RHS with internal cross stiffeners)

	$\dfrac{M_u}{M_{AA}}$	$\dfrac{M_u}{M_{AS/NZS}}$	$\dfrac{M_u}{M_{EC9}}$	$\dfrac{M_u}{M_{EC9-F}}$	$\dfrac{M_u}{M_{csm}}$
Mean, P_m	1.40	1.66	1.35	1.27	1.19
COV, V_p	0.207	0.233	0.188	0.150	0.153

6.4 Continuous beams

In order to assess the accuracy of different design approaches for indeterminate structures, 46 experimental and 210 numerical results (F_u) obtained from this study are compared with the design strengths predicted by the American (F_{AA}) (AA, 2010), Australian/New Zealand ($F_{AS/NZS}$) (AS, 1997) and European (F_{EC9}) (EC9, 2007) specifications for aluminium alloy structures, as well as the capacities calculated based on the traditional plastic design method (F_{pl}), the plastic hinge method provided in Annex H of EC9 (F_{EC9-H}) and the CSM for indeterminate aluminium structures (F_{csm}). Comparisons between the calculated design values and experimental ultimate loads obtained from the continuous beam tests are shown in Table 6.8 - Table 6.10, while comparisons covering both experimental and numerical results are summarized in Table 6.11 and Table 6.12.

6.4.1 Data pool

An experimental programme comprising 27 continuous beam tests on specimens with a series of SHS/RHS and 19 of stiffened SHS/RHS was conducted in this study. The overall nominal length of the continuous beams was 1690 mm for all test specimens. Three symmetric five-point bending configurations were employed. Both normal strength (i.e. 6063-T5) and high strength (i.e. 6061-T6) aluminium alloys were considered. In addition to the test results, the numerical parametric study was conducted to expand the available data over a wider cross-section slenderness range and has generated 120 numerical results. Cross-sections with outer wall dimensions up to 180 mm and the thickness varying between 2.5 mm and 12.0 mm were modelled. Thus, aspect ratios from 0.28 to 3.62 and a wide range of plate slenderness (*b/t* ratios: 0.88-55.14), covering the four cross-section classes, were considered.

6.4.2 Traditional plastic moment

Traditional plastic design method is conventionally applied to indeterminate structures with Class 1 sections. The collapse load F_{pl} is the theoretical load causing a collapse mechanism based on the formation of plastic hinges at their full plastic moment capacities. It is determined by means of a global plastic design with the plastic moment capacity $M_{pl}=W_{pl}f_y$ at each hinge, as illustrated in Fig. 6.13, and therefore it takes consideration of moment redistribution for continuous beams with Class 1 sections. In order to calculate the ultimate loads at which a plastic collapse mechanism first forms, the critical collapse mechanism needs to be found and the locations of a series of plastic hinges are identified to satisfy three conditions: equilibrium, mechanism and plasticity. Following that, the collapse load F_{pl} can be calculated using the principle of virtual work (Bruneau et al., 1998). This method determines the plastic collapse load by equating the internal work in the plastic hinges to the external work done by the applied loads.
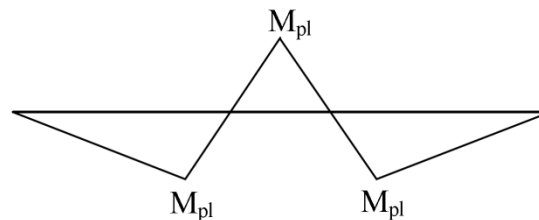
Fig. 6.13   Collapse bending moment diagram from traditional global plastic

analysis (Wang, 2011)

Continuous beams with Classes 2, 3 and 4 sections are designed excluding redistribution, and the capacity is determined when the capacity of the most heavily loaded cross-section is reached, i.e. using elastic global analysis with cross-section capacities $W_{pl}f_y$, $W_{el}f_y$ and $W_{eff}f_y$ for Classes 2, 3 and 4 sections, respectively, where W_{pl}, W_{el} and W_{eff} are the plastic section modulus, elastic section

modulus and elastic modulus of effective sections, respectively. Comparative results are all plotted in Fig. 6.14.

The mean ratio of experimental and numerical results to predicted values F_u/F_{pl} is, on average, 1.47 with a COV of 0.196 (for SHS/RHS) and 1.55 with a COV of 0.210 (for SHS/RHS with internal stiffeners). This indicates that the capacity of non-slender sections can still continue to rise significantly after the plastic hinge attains the prescribed moment capacity ($W_{pl}f_y$). The key diversion between the traditional plastic design method and the plastic hinge method (in Annex H of EC9) is the treatment of Class 1 sections, with the latter allowing for strain hardening and hence achieving more accurate predictions.
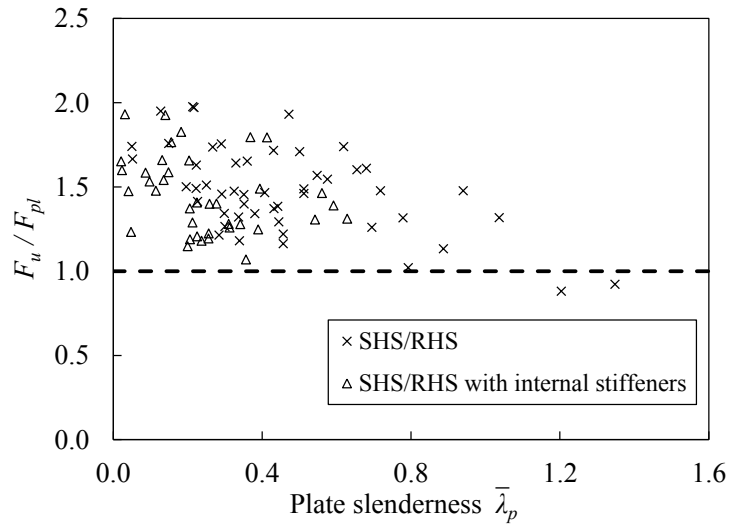
(a) Configuration I
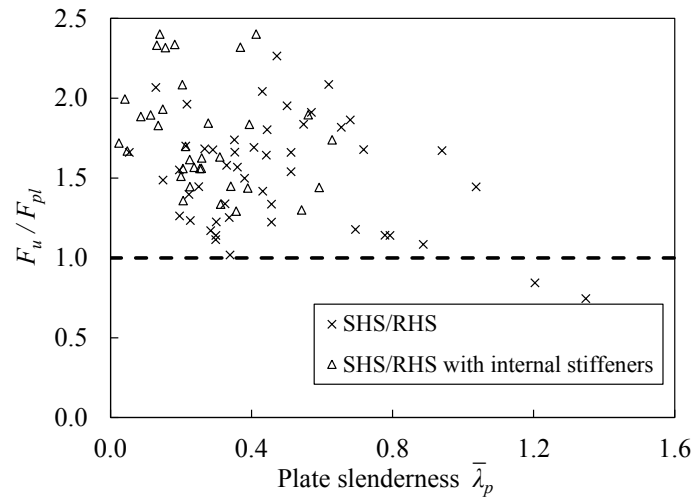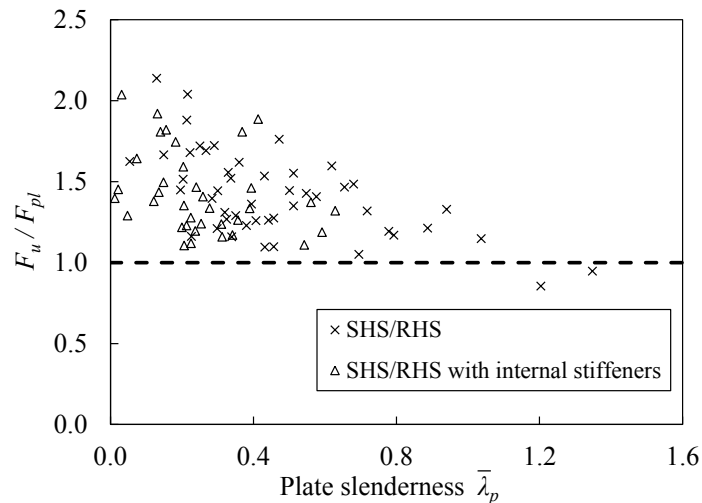
(b) Configuration II

(c) Configuration III

Fig. 6.14 Comparison between experimental and numerical results of continuous

beams with design strengths predicted by the traditional plastic design method

132

6.4.3 Aluminum Design Manual (AA, 2010)

The AA (2010) specification employs the global elastic design for indeterminate structures of all types of cross-sections. The design load is determined from global elastic analysis when the first hinge forms. The critical moment that the first hinge can resist is calculated by referring to the cross-section flexural design, which has been discussed in Chapter 6.3.2. The global elastic analysis can be adopted through hand calculations - moment distribution method and slope deflection method.

The mean values of the load ratio F_u/F_{AA} are 1.71 and 1.70 for SHS/RHS and stiffened SHS/RHS, with the corresponding coefficients of variation (COV) of 0.256 and 0.251, respectively. The predictions were seen to be rather conservative, particularly for stocky sections, as indicated in Fig. 6.15.
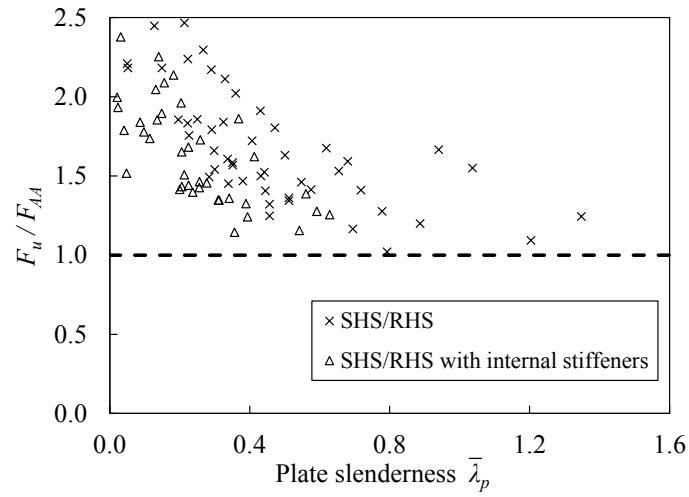
(a) Configuration I
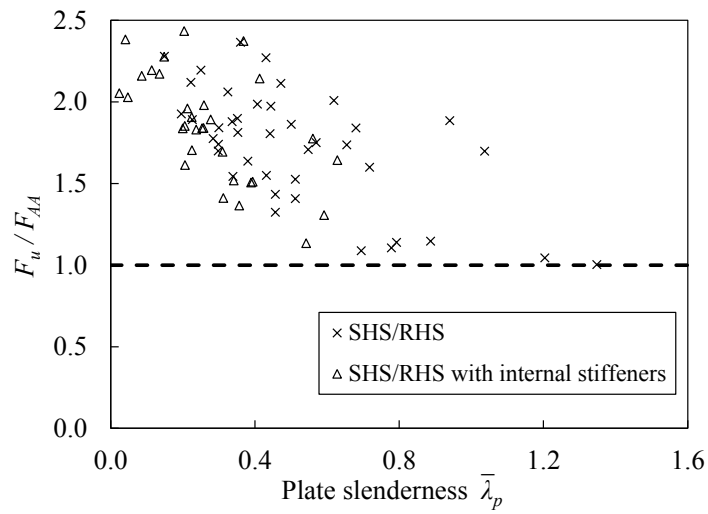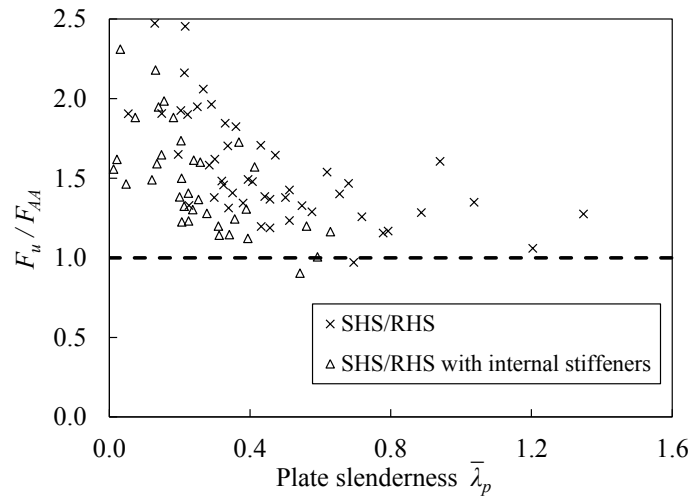
(b) Configuration II

(c) Configuration III

Fig. 6.15   Comparison between experimental and numerical results of

continuous beams with design strengths predicted by the Aluminum Design

Manual (AA, 2010)

134

6.4.4 Australian/New Zealand Standard (AS/NZS, 1997)

The AS/NZS (1997) also employs global elastic analysis for indeterminate structures. Thus, the AS/NZS (1997) and AA (2010) share similar treatments for indeterminate structures as well as determinate structures. However, different coefficients used in the cross-section capacity design might lead to variations in predictions when designing in accordance to the AA (2010) and the AS/NZS (1997).

By observing the presented comparative results in Table 6.8 - Table 6.12 and Fig. 6.16 for continuous beams of three loading configurations, the AS/NZS (1997) was found to be the most conservative design specification (mean value of $F_u/F_{AS/NZS} = 1.88$ and COV = 0.275 for SHS/RHS; mean value = 2.02 and COV = 0.276 for stiffened SHS/RHS), followed by the AA Standard. The predictions may all be seen to be rather conservative, as indicated in Fig. 6.16.
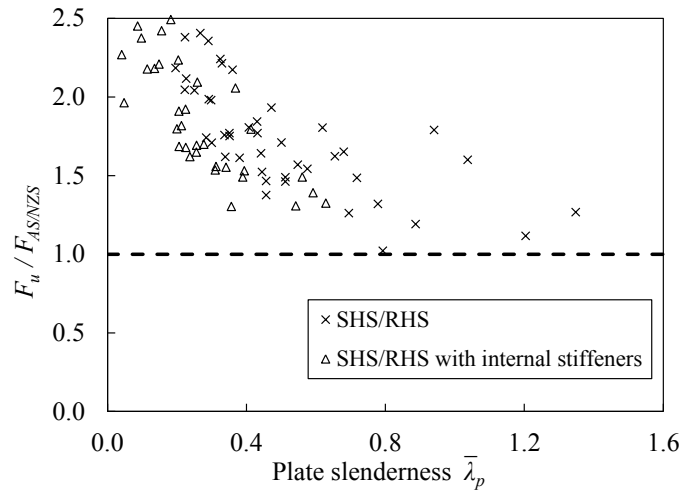
(a) Configuration I
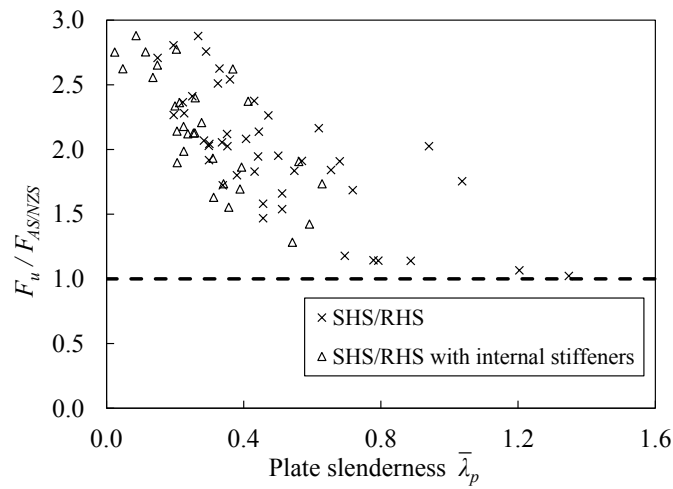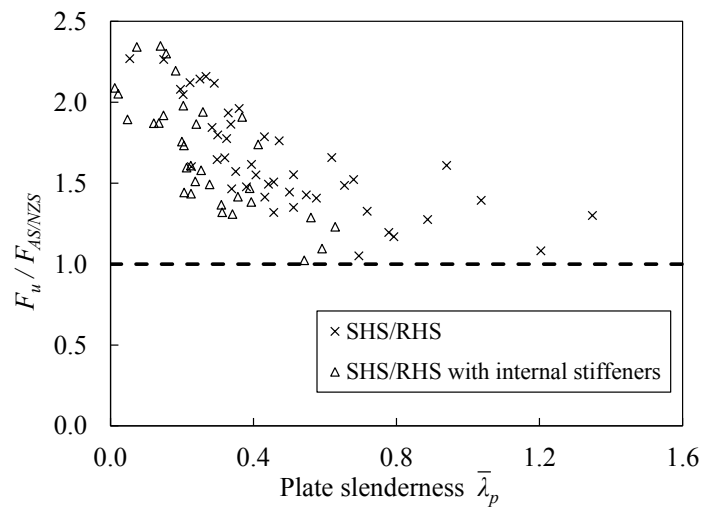
(b) Configuration II

(c) Configuration III

Fig. 6.16 Comparison between experimental and numerical results of continuous

beams with design strengths predicted by the Australian/New Zealand Standard

(AS/NZS, 1997)

136

6.4.5 Eurocode 9 (EC9, 2007)

6.4.5.1 Traditional method in main content

Similar to the AA and AS/NZS, the main content of EC9 only provides elastic design for indeterminate structures, even for Class 1 sections. Thus, after determining the flexural design capacity for the cross-section, as explained in section 7.3.4, the design ultimate loads can be derived according to the global elastic analysis.

The mean value of the load ratio F_u/F_{EC9} is 1.63 for both section shapes, while the COV are 0.212 and 0.236 for SHS/RHS and stiffened SHS/RHS, respectively. The predictions of EC9 are generally more accurate than those of the AA and AS/NZS, though the global elastic analysis is employed by all of them. The comparative results are shown in Fig. 6.17.
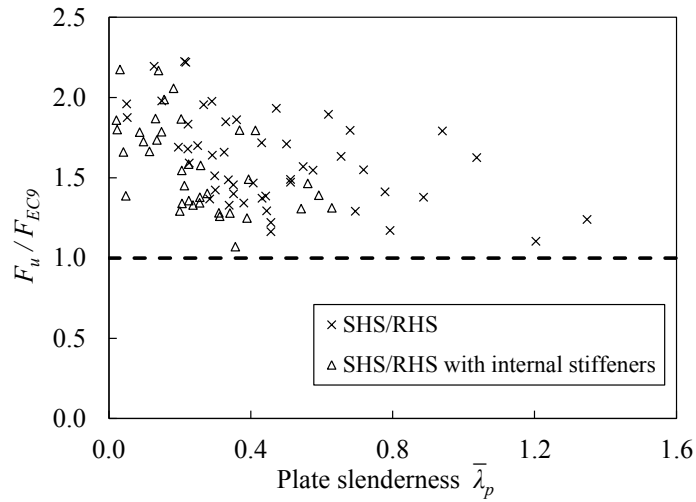
(a) Configuration I
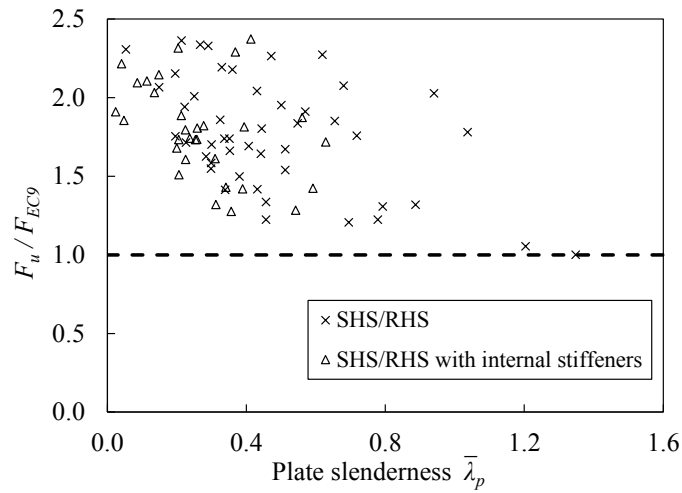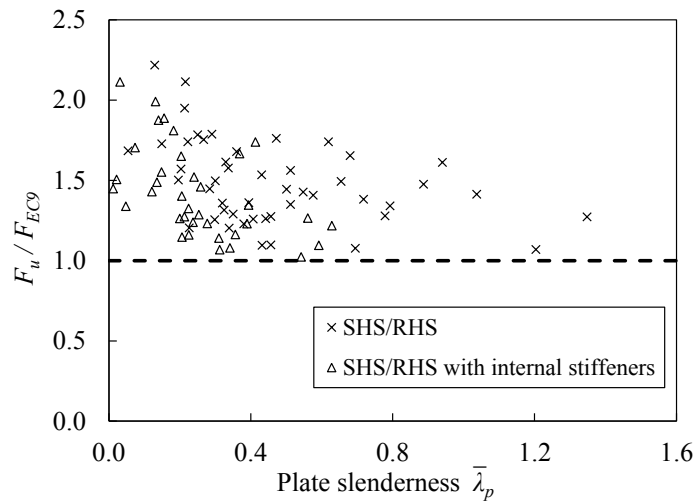
(b) Configuration II

(c) Configuration III

Fig. 6.17   Comparison between experimental and numerical results of

continuous beams with design strengths predicted by Eurocode 9 (EC9, 2007)

6.4.5.2 Plastic hinge method in Annex H (EC9, 2007)

Besides the traditional elastic approach, Eurocode 9 (2007) provides an alternative plastic design method for indeterminate structures in Annex H (EC9, 2007). This method applied principally to plastic (Class 1) sections, but it can also be used for compact (Class 2) and semi-compact (Class 3) sections, provided specific account is taken of local buckling. The plastic hinge method (F_{EC9-H}) is applied to Class 1 sections herein; that is to say, predictions of F_{EC9} and F_{EC9-H} only differ for Class 1 sections and are the same for Classes 2, 3 and 4 sections. The cross-sectional ultimate moment for plastic hinge method is defined by Eq. 6.7, where η is a correction factor to the conventional yield stress to take into consideration the available hardening behaviour of the material, α_ξ is the shape factor depending on the alloy ductility features as required in Annex G (EC9, 2007) and W_{el} is the elastic section modulus. The cross-sectional ultimate bending moment is calculated as a fully plastic moment with allowance for strain hardening. The plastic hinge method also takes benefits from global plastic analysis at the system level.

$$M_u = \eta\, \alpha_\xi f_y\, W_{el} \leq W_{pl} f_u \qquad\qquad \text{(Eq. 6.7)}$$

The predictions of the plastic hinge method are the most accurate compared to other existing international specifications (see Fig. 6.18). The ratios of experimental to predicted ultimate loads F_u/F_{EC9-H} are 1.42 for SHS/RHS and 1.37 for SHS/RHS with internal stiffeners, with COV of 0.203 for SHS/RHS and 0.178 for SHS/RHS with internal stiffeners. The comparison results indicate that the plastic hinge method has benefited from global plastic design (i.e. moment redistribution) and strain hardening.
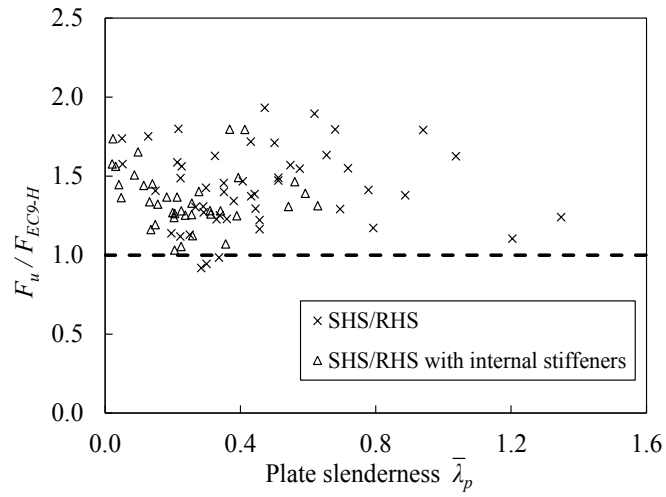
(a) Configuration I
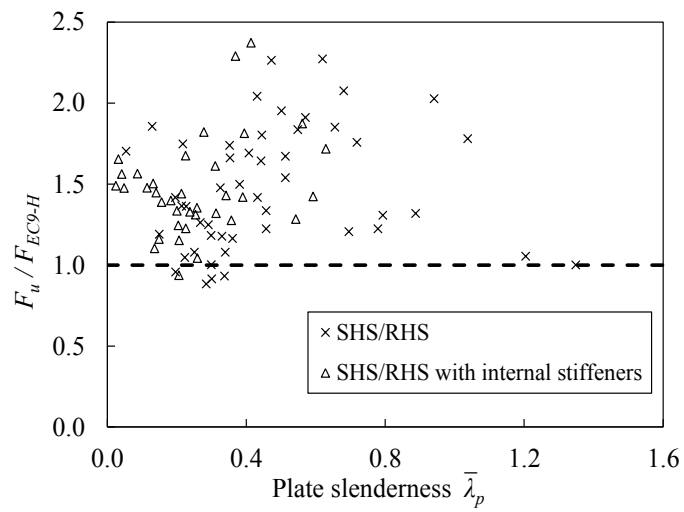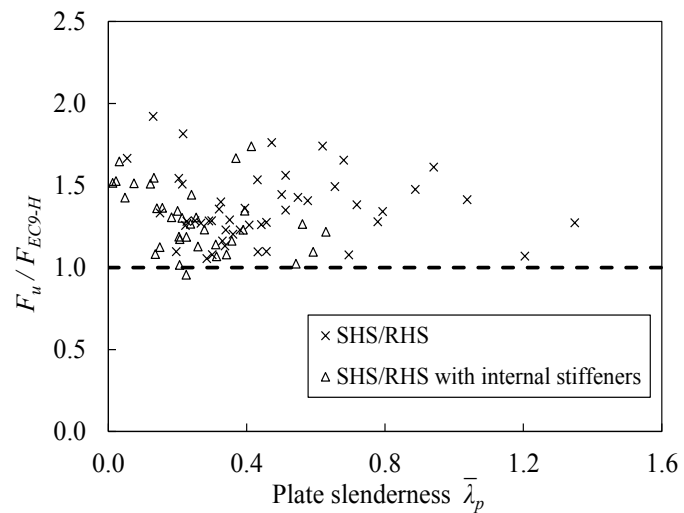
(b) Configuration II

(c) Configuration III

Fig. 6.18 Comparison between experimental and numerical results of continuous

beams with design strengths predicted by Annex H of Eurocode 9 (EC9, 2007)

6.4.6 Continuous strength method (CSM)

The CSM for indeterminate structures has been discussed in Chapter 5.5.3. The continuous strength method (CSM) for indeterminate structures combines the merits of the traditional plastic analysis, considering a plastic collapse mechanism, and an account assessment of cross-section moment capacity allowing for strain hardening.

The comparison of the test and numerical results with the CSM predictions (F_u/F_{csm}) gives a mean value of 1.34 for SHS/RHS and 1.25 for stiffened SHS/RHS with the corresponding COV of 0.161 and 0.165, respectively. The CSM for indeterminate structures provides the most precise predictions of the test and numerical results, with the mean value being closest to unity and the COV being the lowest (see Fig. 6.19).
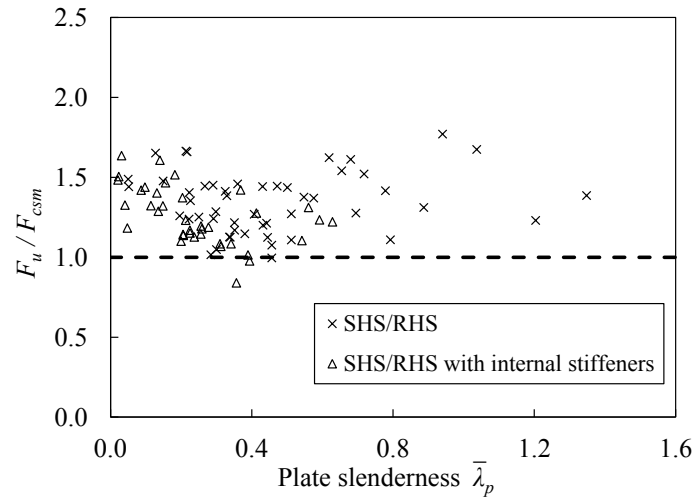
(a) Configuration I
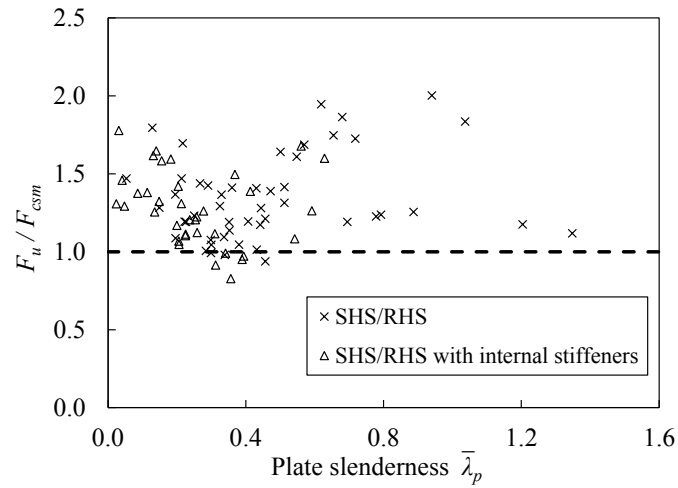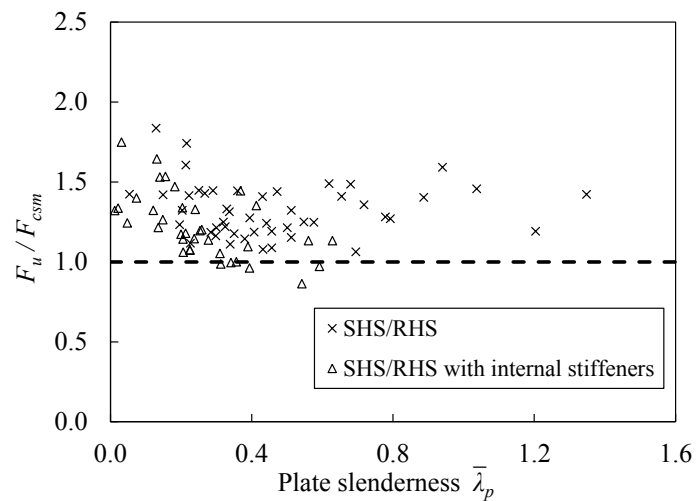
(b) Configuration II

(c) Configuration III

Fig. 6.19 Comparison between experimental and numerical results of continuous

beams with design strengths predicted by the proposed CSM

142

6.4.7 Summary

The combined 256 experimental and numerical continuous beam data included a wide range of cross-sectional slenderness, cross-sectional aspect ratio and moment gradient. The data set was used to investigate design efficiency of the American (2010), Australian/New Zealand (1997) and European (2007) provisions, as well as the traditional plastic design method, the plastic hinge method (EC9, 2007) and the continuous strength method for indeterminate aluminium alloy structures. Calculation concepts and design treatments of the aforementioned methods are presented in Table 6.7, where the following symbols are used: c_{cf} is the distance from the centreline of the compression flange to the neutral axis of the cross-section, c_{cw} is the distance from the centreline of the web group's extreme compressive fibre to the neutral axis of the cross-section, c_{tf} is the distance from the extreme tensile fibre to the neutral axis of the cross-section, c_{tw} is the distance from the web group's extreme tensile fibre to the neutral axis of the cross-section, f_c is the local buckling stress of the flat elements in uniform compression, F_t is the yield stress in tension, f_b is the stress corresponding to the strength of flat elements in flexure, f_{bc} and f_{bt} are the weighted average compressive/tensile stress in accordance with the ratio of the area of each elements, I_f and I_w are the moments of inertia of the flange/web group about the neutral axis of the cross-section, M_{nc} and M_{nt} are the nominal weighted average moment for compression/tension, W_{pl}, W_{el} and W_{eff} are the plastic section modulus of the gross section, elastic section modulus of the gross section and elastic section modulus of the effective section, α is the shape factor, η is the correction factor and ε_{csm} is the CSM limiting strain.

The curves showing the design capacities of the traditional plastic design, the plastic hinge method and the CSM, normalized by the theoretical plastic collapse load F_{coll}, are plotted in Fig. 6.20, as a function of cross-section slenderness $\bar{\lambda}_p$.

143

These illustrative curves are derived based on loading configuration I and the average measured values of material properties and cross-sectional dimensions.

The predictions of the three international design specifications are particularly conservative for the stocky (plastic and compact) sections, while among the specifications considered in this study, the AS/NZS (1997) specification provides the most conservative predictions and EC9 (2007) (see Table 6.8 - Table 6.12) yields the most accurate results among the three specifications. Moreover, the other three design methods - the traditional plastic design method, the plastic hinge method given in Annex H of EC9 (2007) and the continuous strength method - have been found to estimate the ultimate loads more accurately, due partly to their adoption of global plastic analysis for stocky sections. Overall, for comparisons made herein, the continuous strength method was shown to provide the most accurate and consistent predictions. Besides the employment of global plastic design, the explanation for the good predictions relate to the systematic exploitation of strain hardening at the cross-sectional level and the deformation-based design approach.

Table 6.7   Design Concepts for different design approaches

Design approach	Section capacity and analysis type	Class 1	Class 2	Class 3	Class 4
AA	Cross-section capacity	Lesser of ($M_{nc}=f_c I_f/c_{cf}+f_b I_w/c_{cw}$, $M_{nt}=f_t I_f/c_{tf}+f_b I_w/c_{tw}$), where f_c, f_b and f_t are slenderness dependent.			
	Global analysis	Elastic			
AS/NZS	Cross-section capacity	Lesser of ($W_{el}f_{bc}$, $W_{el}f_{bt}$), where f_{bc} and f_{bt} are slenderness dependent			
	Global analysis	Elastic			
EC9	Cross-section capacity	$W_{pl}f_y$	$W_{pl}f_y$	$W_{el}f_y$	$W_{eff}f_y$
	Global analysis	Elastic			
EC9-Annex H	Cross-section capacity	$\alpha\eta W_{el}f_y$	$W_{pl}f_y$	$W_{el}f_y$	$W_{eff}f_y$
	Global analysis	Plastic	Elastic		
Traditional plastic design	Cross-section capacity	$W_{pl}f_y$	$W_{pl}f_y$	$W_{el}f_y$	$W_{eff}f_y$
	Global analysis	Plastic	Elastic		
CSM	Cross-section capacity	M_{csm} for cross-section			
	Global analysis	Plastic, but with allowance for ratio of hinge rotations. (for $\varepsilon_{csm}/\varepsilon_y < 3.6$: elastic)			
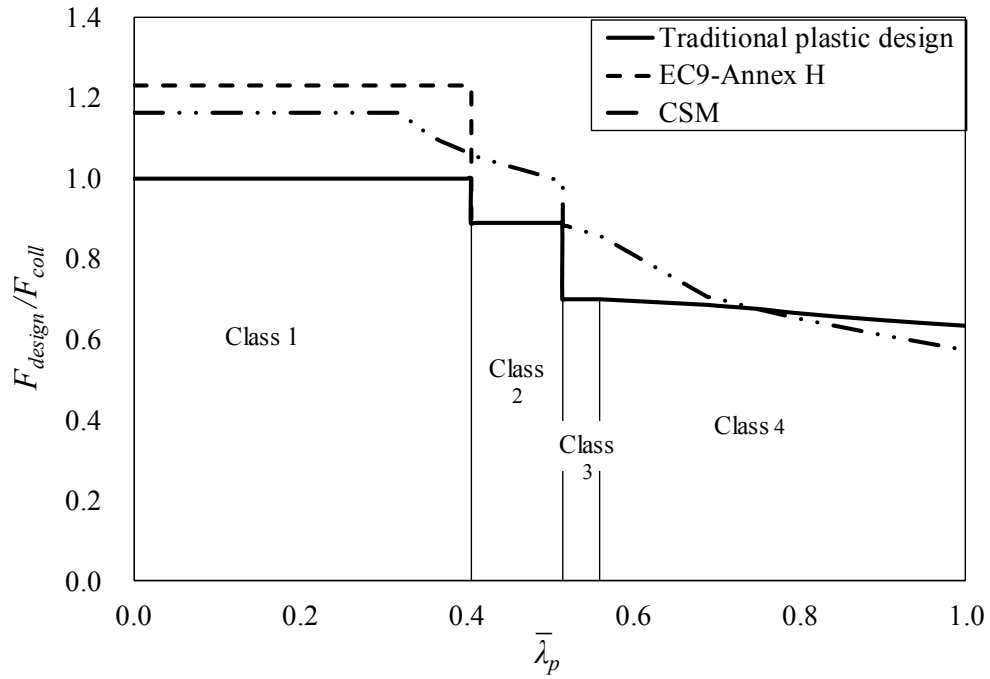
(a) normal-strength aluminium alloys
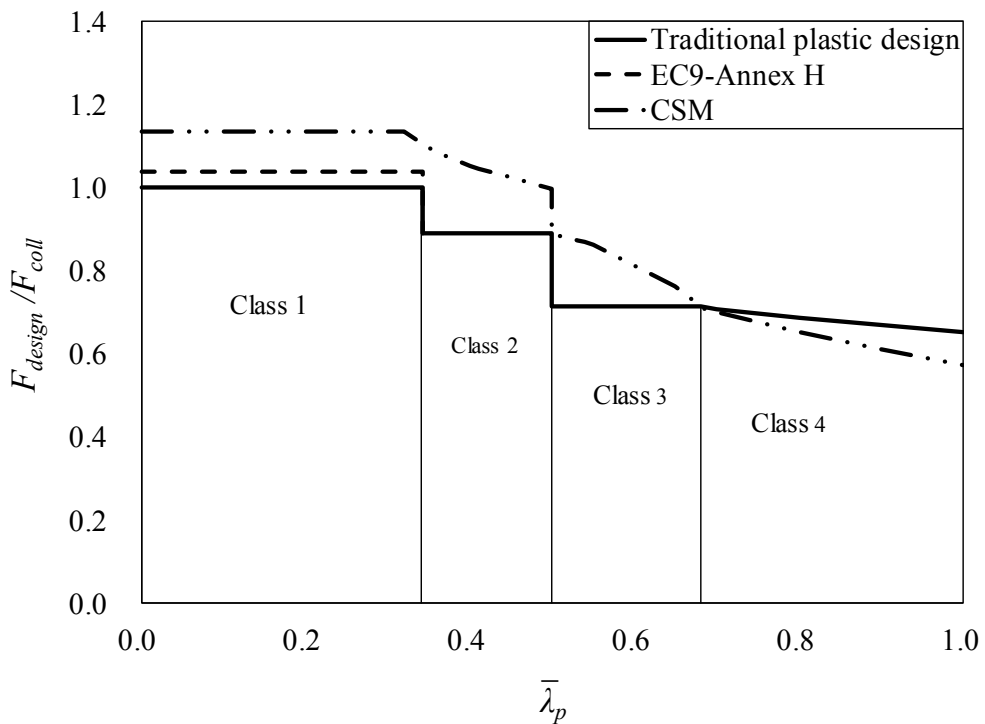
(b) high-strength aluminium alloys

Fig. 6.20   Curves indicating design capacities of different design approaches for

continuous beams

146

Table 6.8   Summary of comparisons between five-point bending test results and design strengths (configuration I)

Specimen	$\bar{\lambda}_p$	F_{exp} (kN)	$\dfrac{F_{exp}}{F_{AA}}$	$\dfrac{F_{exp}}{F_{AS/NZS}}$	$\dfrac{F_{exp}}{F_{EC9}}$	$\dfrac{F_{exp}}{F_{EC9-H}}$	$\dfrac{F_{exp}}{F_{pl}}$	$\dfrac{F_{exp}}{F_{csm}}$
H55×70×4.2B5I	0.35	114.1	1.58	1.77	1.45	1.46	1.46	1.20
H55×70×4.2B5I-R	0.35	112.3	1.57	1.75	1.40	1.40	1.40	1.15
H70×55×4.2B5I	0.44	84.9	1.41	1.52	1.29	1.29	1.29	1.12
H50×95×10.5B5I	0.05	329.9	2.18	2.58	1.87	1.58	1.67	1.44
H95×50×10.5B5I	0.22	188.2	2.24	2.38	1.83	1.49	1.63	1.40
H64×64×3.0B5I	0.58	65.3	1.41	1.54	1.55	1.55	1.55	1.37
N50×95×10.5B5I	0.05	306.7	2.21	2.61	1.96	1.73	1.74	1.49
N70×120×10.5B5I	0.13	532.9	2.45	2.84	2.19	1.75	1.95	1.65
N120×70×10.5B5I	0.22	362.0	2.64	2.82	2.22	1.80	1.97	1.66
N120×120×9.0B5I	0.29	655.2	1.79	1.98	1.64	1.27	1.46	1.24
+H70×120×10.5B5I	0.04	678.4	1.79	2.27	1.66	1.45	1.48	1.33
+H120×70×10.5B5I	0.11	416.3	1.74	2.18	1.66	1.44	1.48	1.32
+H95×95×4.3B5I	0.26	250.4	1.46	1.69	1.38	1.33	1.23	1.19
+N95×50×10.5B5I	0.09	171.1	1.84	2.45	1.78	1.51	1.59	1.42
+N50×95×10.5B5I	0.02	329.6	2.00	2.66	1.86	1.58	1.65	1.48
+H95×50×10.5B5I	0.10	220.9	1.78	2.37	1.72	1.65	1.53	1.44
+H50×95×10.5B5I	0.02	423.8	1.93	2.58	1.80	1.74	1.60	1.50
+H95×95×4.3B5I-R	0.26	250.6	1.43	1.65	1.34	1.26	1.19	1.14

Table 6.9 Summary of comparisons between five-point bending test results

and design strengths (configuration II)

Specimen	$\overline{\lambda}_p$	F_{exp} (kN)	$\dfrac{F_{exp}}{F_{AA}}$	$\dfrac{F_{exp}}{F_{AS/NZS}}$	$\dfrac{F_{exp}}{F_{EC9}}$	$\dfrac{F_{exp}}{F_{EC9-H}}$	$\dfrac{F_{exp}}{F_{pl}}$	$\dfrac{F_{exp}}{F_{csm}}$
H55×70×4.2B5II	0.35	141.5	1.90	2.12	1.74	1.74	1.74	1.18
H55×70×4.2B5II-R	0.35	130.6	1.81	2.02	1.66	1.66	1.66	1.13
H70×55×4.2B5II	0.44	120.2	1.97	2.14	1.80	1.80	1.80	1.28
H50×95×10.5B5II	0.05	436	2.61	3.11	2.31	1.70	1.66	1.47
H95×50×10.5B5II	0.20	222.1	2.64	2.80	2.15	1.42	1.55	1.37
H64×64×3.0B5II	0.57	80.83	1.75	1.91	1.91	1.91	1.91	1.69
N70×120×10.5B5II	0.13	693.9	3.20	3.71	2.87	1.86	2.07	1.80
N120×70×10.5B5II	0.22	450.8	3.16	3.39	2.73	1.75	1.96	1.69
N120×120×9.0B5II	0.30	657.8	1.74	1.92	1.58	1.00	1.14	0.99
+H70×120×10.5B5II	0.04	922.7	2.38	3.02	2.22	1.56	1.99	1.46
+H120×70×10.5B5II	0.11	530.4	2.19	2.75	2.10	1.48	1.89	1.38
+H95×95×4.3B5II	0.25	319.4	1.84	2.13	1.73	1.31	1.56	1.20
+N95×50×10.5B5II	0.09	199.1	2.16	2.88	2.09	1.56	1.88	1.37
+N50×95×10.5B5II	0.02	438.9	2.05	2.75	1.91	1.49	1.72	1.31
+H95×95×4.3B5II-R	0.26	326.0	1.84	2.13	1.73	1.35	1.56	1.22

Table 6.10   Summary of comparisons between five-point bending test results
and design strengths (configuration III)

Specimen	$\overline{\lambda}_p$	F_{exp} (kN)	$\dfrac{F_{exp}}{F_{AA}}$	$\dfrac{F_{exp}}{F_{AS-NZS}}$	$\dfrac{F_{exp}}{F_{EC9}}$	$\dfrac{F_{exp}}{F_{EC9-H}}$	$\dfrac{F_{exp}}{F_{pl}}$	$\dfrac{F_{exp}}{F_{csm}}$
H55×70×4.2B5III	0.32	91.6	1.48	1.66	1.36	1.36	1.31	1.23
H55×70×4.2B5III-R	0.35	109.6	1.41	1.57	1.29	1.29	1.29	1.16
H70×55×4.2B5III	0.39	72.1	1.49	1.62	1.36	1.36	1.36	1.27
H50×95×10.5B5III	0.05	346.2	1.90	2.27	1.68	1.66	1.62	1.42
H95×50×10.5B5III	0.20	191.4	1.92	2.05	1.57	1.54	1.51	1.32
H64×64×3.0B5III	0.58	64.3	1.29	1.41	1.41	1.41	1.41	1.25
N70×120×10.5B5III	0.13	589.7	2.47	2.86	2.22	1.92	2.14	1.84
N120×70×10.5B5III	0.22	377.7	2.45	2.63	2.11	1.81	2.04	1.74
+H70´120´10.5B5III	0.02	708.2	1.62	2.05	1.50	1.53	1.45	1.34
+H120´70´10.5B5III	0.12	420.2	1.49	1.87	1.43	1.51	1.38	1.32
+H95´95´4.3B5III	0.24	274.3	1.61	1.86	1.52	1.44	1.47	1.33
+N50´95´10.5B5III	0.01	358.4	1.56	2.09	1.45	1.51	1.40	1.32
+H95´95´4.3B5III-R	0.25	253.4	1.36	1.58	1.29	1.30	1.24	1.19

Table 6.11   Summary of comparisons between experimental and numerical
results with design strengths (for five point bending beams on SHS/RHS)

	$\dfrac{F_u}{F_{AA}}$	$\dfrac{F_u}{F_{AS-NZS}}$	$\dfrac{F_u}{F_{EC9}}$	$\dfrac{F_u}{F_{EC9-H}}$	$\dfrac{F_u}{F_{pl}}$	$\dfrac{F_u}{F_{csm}}$
Mean, P_m	1.71	1.88	1.63	1.42	1.47	1.34
COV, V_p	0.256	0.275	0.212	0.203	0.196	0.161

Table 6.12   Summary of comparisons between experimental and numerical
results with design strengths (for five point bending beams on SHS/RHS with
internal cross stiffeners)

	$\dfrac{F_u}{F_{AA}}$	$\dfrac{F_u}{F_{AS-NZS}}$	$\dfrac{F_u}{F_{EC9}}$	$\dfrac{F_u}{F_{EC9-H}}$	$\dfrac{F_u}{F_{pl}}$	$\dfrac{F_u}{F_{csm}}$
Mean, P_m	1.70	2.02	1.63	1.37	1.55	1.25
COV, V_p	0.251	0.276	0.236	0.178	0.210	0.165

6.5 Cross-section classifications

6.5.1 Introduction

Cross-section classification addresses the susceptibility of a cross-section to local buckling and defines its appropriate design resistance (Gardner and Theofanous, 2008). Eurocode 9 (2007) provides different treatments of local buckling for cross-sections in different classes. The codified treatments in EC9 were initially developed based on elastic-perfectly plastic material models. Slenderness parameter β/ε is used in the EC9 framework as an indicator to determine the class that a cross-section belongs to. Given the neglect of the nonlinear stress-strain relationship and the interaction between elements in favour of simplicity in EC9, the existing slenderness limits for aluminium alloy cross-sections are conservative. The purpose of this study is to re-evaluate the slenderness limits that define the classes on the basis of substantial experimental and numerical data on aluminium alloy cross-sections, which were newly generated in recent years. The conservatism in the existing limits is illustrated in this chapter.

As an alternative framework to the EC9 classification, the cross-section plate slenderness $\overline{\lambda}_p$, which has been used by the continuous strength method (CSM) and the direct strength method (DSM) (Schafer and Peköz, 1998), is employed in this study to define the cross-section slenderness level. Hence, it is called the CSM slenderness framework in the following discussion. Departing from the traditional slenderness parameter, this slenderness parameter $\overline{\lambda}_p$ considers the element interaction between flanges and webs, different cross-section shapes and stress distribution. Based on a large number of experimental and numerical results, new class limits are developed according to the definition of each behaviour class. Reliability analyses have also been performed to assess the new slenderness limits

150

for both compression and bending sections. The development and statistical analyses of the new limits are described herein.

As a part of cross-section capacity design, effective thickness formulae are proposed for Class 4 sections in compatibility of Class 3 limit. The effective thickness t_{eff} is obtained by multiplying the measured thickness t by the local buckling factor ρ_c. In the EC9 framework, existing functions with β/ε being the variable is modified to satisfy the requirement that when β/ε is equal to the new Class 3 limit, the local buckling factor should be unity. In the CSM slenderness framework, the feasibility of applying the CSM design curve to the effective thickness is studied. Efforts have been made to maintain the consistency in format with the Winter curve and the DSM design curve; only slight modifications have been made on the DSM curve for aluminium alloys proposed by Zhu and Young (2009). Detailed discussions on the design curves are presented in the later part of this chapter.

6.5.2 EC9 classification framework

As for aluminium alloy sections, EC9 (2007) is one of the major international specifications providing clear and quantitative classification definitions, concerning the attainment of local buckling. The cross-section class, according to EC9, is that of the lowest class of its elements, with Class 1 being the highest possible and Class 4 being the lowest. While the American (2010) and Australian/New Zealand (1997) specifications only define three types of cross-section classes: yielding (refereed to Classes 1 and 2 in EC9), inelastic buckling (equivalent to Class 3 in EC9) and elastic buckling (refereed to Class 4 in EC9). There are two principal reasons for the variation in the slenderness limits between different specifications: the first relates to the pool of available data; the

second reason relates to the different regional practices in terms of structural reliability (Law and Gardner, 2009).

According to EC9, cross-sections are assigned to one of the four classes according to their susceptibility to local buckling as estimated by comparing a slenderness parameter to codified class limits. The classification of a cross-section depends on the slenderest element, which means that a Class 1 cross-section has all of its elements of being Class 1, while a Class 4 cross-section has at least one Class 4 element. The classification of an element is individually classified based on the width-to-thickness b/t ratio independently of other constituent elements in a cross-section.

The slenderness indicator used in EC9 is β/ε, which includes the flat width-thickness ratio b/t and the yield stress f_y. Eq. 6.8 is used in EC9 to determine the slenderness β/ε for elements under compression. In terms of elements under bending, a reduction factor is used to account for the compression parts. For example, flexural elements with neutral axis in the middle of the section should multiply a reduction factor of 0.4 to the element width b, as defined by Eq. 6.9.

$$\frac{\beta}{\varepsilon} = \frac{b/t}{\sqrt{250/f_y}} \qquad\qquad \text{(Eq. 6.8)}$$

$$\frac{\beta}{\varepsilon} = \frac{0.4b/t}{\sqrt{250/f_y}} \qquad\qquad \text{(Eq. 6.9)}$$

Sections are classified by comparing the slenderness of each element with the limits in EC9, which are also shown in Table 6.13. These limits depend on the way in which the element are supported (either one edge supported as outstands or two edges supported as internal flange element), the stress distribution (uniform compression or varying stresses) and the forming process (heat-treated or non-heat-treated). Since the stress distribution effect has been considered when

calculating the slenderness parameter, the class limits are adopted for both uniform compressive or flexural elements. Table 6.13 also presents slenderness limits from EN1993-1-3 (2006), EN1993-1-4 (2006) and harmonised limits proposed by Gardner and Theofanous (2008), which were designed for carbon steel, stainless steel and both materials, respectively. However, owing to the differences in the Young's Modulus, the Poisson's ratio and the coefficient that is used to normalize the yield stress between steels and aluminium alloys, the aforementioned limits have been converted to a common basis, using the character values for aluminium alloys adopted in EC9 (2007), as shown in Table 6.13.

Table 6.13   Existing and proposed slenderness limits for cross-section classification

Slenderness parameter	Reference	Material	Class 1		Class 2		Class 3	
			Internal	Outstand	Internal	Outstand	Internal	Outstand
β/ε	EC9	Aluminium-Class A	11	3	16	4.5	22	6
		Aluminium-Class B	13	3.5	16.5	4.5	18	5
	EN1993-1-1	Carbon Steel	19	5	22	6	24	8
	EN1993-1-4	Stainless Steel	15	6	15	6	18	7
	Gardner and Theofanous (2008)	Carbon Steel & Stainless Steel	19	5	20	6	21	8
	Proposed	Aluminium-Class A & B	15		16		22	
$\bar{\lambda}_p$	EC9	Aluminium-Class A	0.34	0.28	0.50	0.43	0.68	0.57
		Aluminium-Class B	0.40	0.33	0.51	0.43	0.56	0.47
	Proposed	Aluminium-Class A & B	0.45		0.50		0.68	

6.5.2.1 Cross-section subjected to compression

As for cross-sections under compression, the only concern of classification is whether it has been fully effective. Compressive cross-sections which yield prior to local buckling are considered as 'effective', and defined in EC9 (2007) as being either of Class 1, Class 2, or Class 3. Sections of Classes 1, 2 and 3 are capable of reaching their yield stress before the onset of local buckling, while Class 4 sections fail by local buckling before reaching the yield stress. Hence, the design capacities for Classes 1, 2 and 3 sections are the yield limit Af_y. As for Class 4 sections, the gross area A is replaced by the effective area A_{eff}, which is based on effective cross-sections containing elements of effective thickness. A local buckling factor ρ_c is employed to reduce the thickness t to the effective thickness t_{eff} in any parts wholly or partly in compression, which is discussed in Chapter 6.5.4.

Although the Class 3 limit is the only boundary that can be identified from compressive sections, it is indicated in Annex F of EC9 (2007) that the capacities of Class 1 sections might be capable of reaching ultimate strength (Af_u) due to its allowance for strain hardening. However, it is only an alternative approach for Class 1 sections but not the codified definition of Class 1 sections; thus, Class 1 limit for sections in compression is not considered in this study. Further investigation is needed to determine the Class 1 limit for sections in compression according to the design criteria in Annex F (EC9, 2007).

● **Class 3 limit**

The normalized ultimate load P_u/Af_y against the slenderness β/ε for internal or outstand elements of Buckling Class A or B materials are plotted in Fig. 6.21. These three figures have followed the theoretical trend: greater slenderness, lower normalised capacity. The existing Class 3 limits are also plotted in the graphs,

which are $\beta/\varepsilon = 22$ for internal elements of Buckling Class A material, $\beta/\varepsilon = 18$ for internal elements of Buckling Class B material and $\beta/\varepsilon = 6$ for outstand elements of Buckling Class A material, respectively. No compression tests have been found on cross-sections with outstand elements of Buckling Class B material. These limits were seen to be accurate boundaries between sections with capacities greater than the yield limit and sections with capacities less than the yield limit. Fig. 6.21(b) indicates that the limit of 22 for Class A aluminium alloys may be safely applied to Class B aluminium alloys, although the number of test results for internal elements of Class B material is rather limited at this stage and further test and/or numerical results are required. Table 6.13 also reveals that the Class 3 limit of aluminium alloy ($\beta/\varepsilon = 22$) is fairly consistent with carbon steel ($\beta/\varepsilon = 24$) (EN1993-1-3, 2006), stainless steel ($\beta/\varepsilon = 18$) (EN1993-1-3, 2006) and the new limit proposed by Gardner and Theofanous (2008) ($\beta/\varepsilon = 21$). It is therefore recommended to harmonise the limits of Buckling Class A and B materials as 22 for internal elements. In terms of outstand elements, it is suggested to remain the Class 3 limit as 6 for Buckling Class A material (see Fig. 6.21(c)), due to lacking of data for Buckling Class B material.
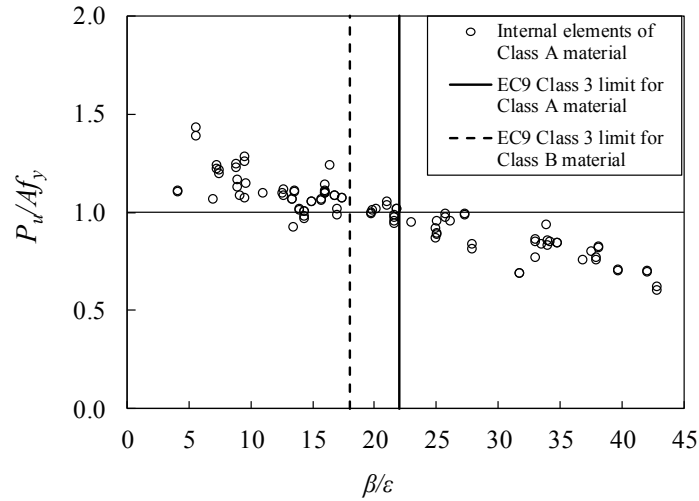
(a) Internal elements of Buckling Class A material
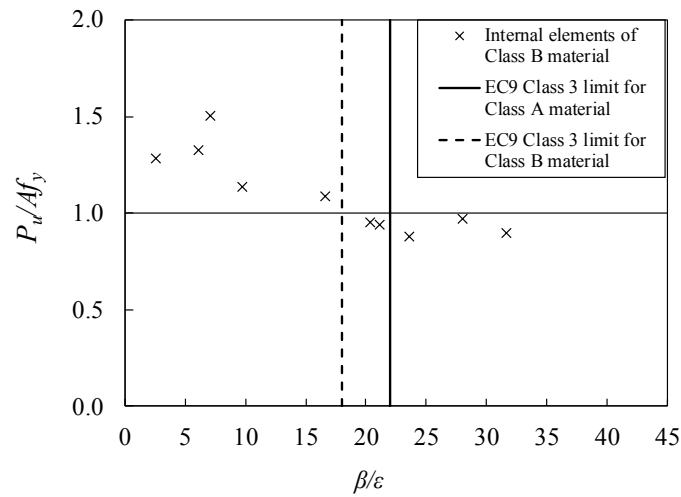
(b) Internal elements of Buckling Class B material
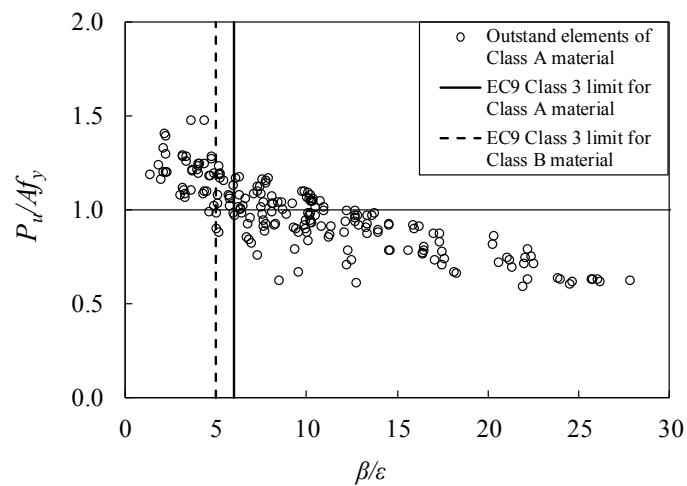
(c) Outstand elements of Buckling Class A material

Fig. 6.21 Comparison between stub column results and yield strength together

with EC9 Class 3 boundaries

156

6.5.2.2 Cross-section subjected to bending

Cross-section classification criteria for bending sections relate to rotation capacities and resisted strengths. As mentioned earlier, class limits in EC9 (2007) are categorised in four cases (internal or outstand elements of Buckling Class A or B materials) for non-welded elements. Relevant data have been collected to verify each of these limits, except only scarce data for outstand elements of Buckling Class A material and no data for outstand elements of Buckling Class B material. Thus, discussions made herein are only focused on internal elements. Fig. 6.22 - Fig. 6.24 are plotted as the ultimate moment capacity to elastic moment ratio ($M_u/W_{el}f_y$), the ultimate moment capacity to plastic moment ratio ($M_u/W_{pl}f_y$) and the rotation capacity R against the slenderness β/ε, respectively. The limits for classification can therefore be adjusted accordingly.

● **Class 3 limit**

Class 3 sections are defined as those capable of reaching the first yield, but buckle locally before becoming fully plastic. Thus, the flexural capacities of Class 3 sections are the product of yield stress f_y and the elastic section modulus W_{el}. On the contrary, Class 4 sections buckle locally before reaching the first yield, and have the resistances reduced below their yield resistance due to local buckling effects. For a beam containing slender elements, the effective section modulus W_{eff} may be determined from calculating the elastic section modulus of an effective cross-section obtained based on an effective thickness approach.

Analyses of the presented data reveals that the current Class 3 limit for internal elements of Buckling Class A material can accurately represent the transaction between semi-compact and slender sections, as illustrated in Fig. 6.22(a), and it is indicated in Fig. 6.22(b) that this limit ($\beta/\varepsilon=22$) also works well with internal elements of Buckling Class B material. The idea of harmonising Classes A and B

materials seems to be reasonable for bending sections, as compression sections in the previous section. Fig. 6.22(c) shows that the current Class 3 limit for outstand elements of Class A material may be safely adopted, though the available data is scarce and further investigation is required.
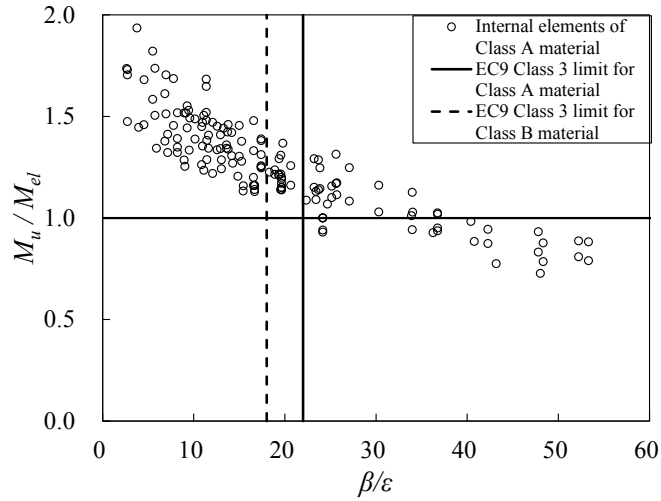
(a) Internal elements of Class A material
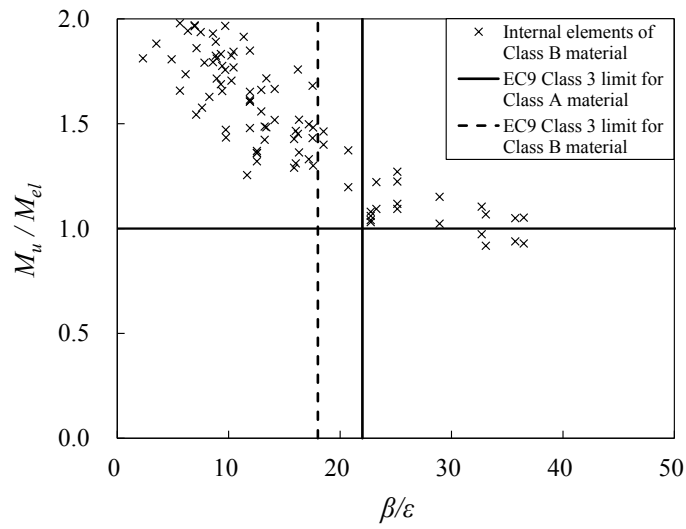
(b) Internal elements of Class B material
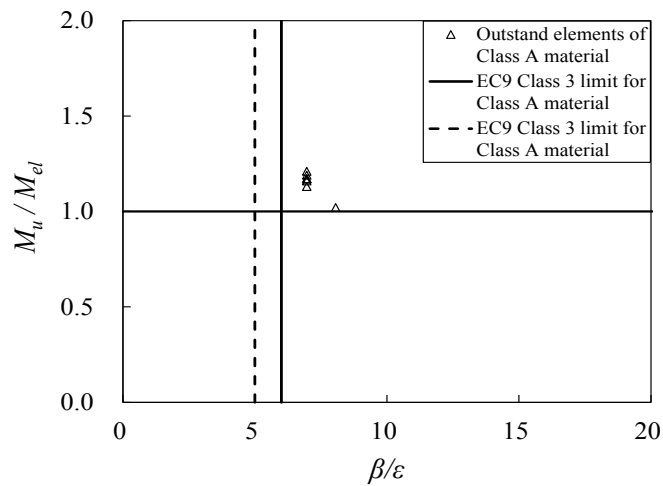
(c) Outstand elements of Class A material

Fig. 6.22   Comparison between experimental and numerical results and

elastic moments together with EC9 class 3 boundaries

159

● **Class 2 limit**

Class 2 sections are defined as sections which are able to develop their fully plastic capacities and thus form the first plastic hinge, but may not be able to maintain their capacities since the subsequent moment redistribution is affected by inelastic local buckling. As codified in EC9, the design capacities of Class 2 cross-sections equal to the product of the plastic section modulus W_{pl} and the yield stress f_y. Following this concept, the ultimate moment M_u normalised by the plastic moment $W_{pl}f_y$ are plotted against the slenderness β/ε in Fig. 6.23, as well as the Class 2 limits.

The available test results in Fig. 6.23 display the anticipated trend of decreasing normalised moment capacity $M_u/W_{pl}f_y$ with increasing slenderness β/ε. The distinction made between Class 2 and Class 3 sections is whether the capacity reaches plastic moment. In Fig. 6.23, it is found that the current Class 2 limits in EC9 can appropriately separate these cross-sections based on the class definitions. Furthermore, the Class 2 limits for internal elements of Class A ($\beta/\varepsilon=16$) and Class B ($\beta/\varepsilon=16.5$) materials are consistent, thus it is sensible to harmonise both limits and adopt the value of 16 as the unified limit. The test results of outstand elements are shown in Fig. 6.23(c), though scarce, but also demonstrate the suitability of the current limit. Hence, it is recommended to remain the current Class 2 limit for outstand elements until more results are reported.
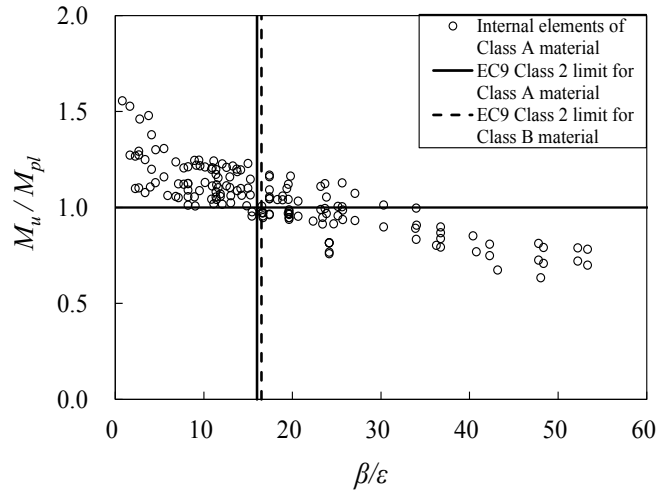
(a) Internal elements of Class A material
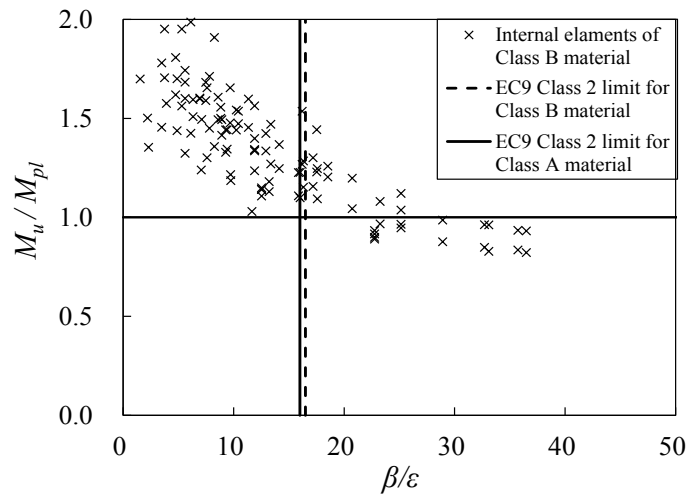
(b) Internal elements of Class B material
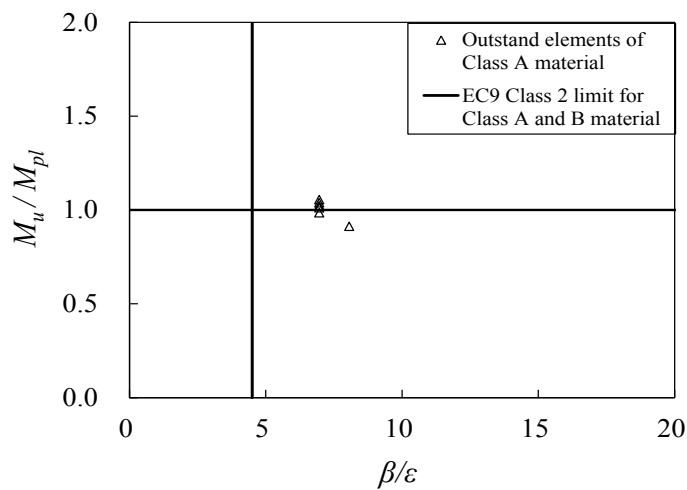
(c) Outstand elements of Class A material

Fig. 6.23 Comparison between collected results and plastic moments together

with EC9 Class 2 boundaries

161

● **Class 1 limit**

Class 1 cross-sections are defined as those which are capable of reaching and maintaining their full plastic moment capacities with sufficient deformation capacity, and thus moment redistribution is allowed to take place in the indeterminate structures of Class 1 sections for a collapse mechanism. Since Class 2 sections might be limited by local buckling on their deformation capacity (Gardner and Theofanous, 2008), distinction made between Class 1 and Class 2 sections is on the basis of the rotation capacity R, as defined by Eqs. 6.10 and 6.11, where sufficient rotation capacity has to be demonstrated in Class 1 sections (Chan and Gardner, 2008). Chan and Gardner (2008) have conducted an integrated investigation into previous literature and background documents of steel design codes, and finally concluded that a rotation capacity $R=3$ was sufficient to define Class 1 sections. In this study, a rotation capacity of three was also adopted for the development of Class 1 limit for aluminium alloys.

It should be noted that the definition of the rotation capacity R related to rotation θ_{rot} at the theoretical plastic hinge location for the three-point bending tests (Eq. 6.10) or to constant curvature κ_{rot} developed in the uniform moment region for the four-point bending tests (Eq. 6.11). The definitions of rotation capacity based on the moment-rotation and the moment-curvature relationships have been explained and employed by Chan and Gardner (2008).

$$R = \frac{\theta_{rot}}{\theta_{pl}} - 1 \qquad\qquad \text{(Eq. 6.10)}$$

$$R = \frac{\kappa_{rot}}{\kappa_{pl}} - 1 \qquad\qquad \text{(Eq. 6.11)}$$

\where θ_{pl} and κ_{pl} are the elastic rotation and curvature corresponding to the plastic moment $M_{pl} = W_{pl}f_y$ and θ_{rot} and κ_{rot} are the rotation and curvature at the point where the moment resistance drops back below M_{pl}, respectively.

Similar to the carbon steel and stainless steel results (Gardner and Theofanous, 2008), significant scatter exists in the rotation capacities of aluminium alloy beams, as plotted in Fig. 6.24. It is believed to be largely related to the effects of moment gradient, material properties, the interaction of constituent plates as well as the earlier tensile fracture before the moment resistance fully dropping back to the plastic moment M_{pl}. However, the anticipated trend is clear, and the Class 1 limits for Buckling Class A and B materials, currently lying on 11 and 13 respectively, might be seen to be strict and conservative. It can be observed in Table 6.13 that Class 1 limits for carbon steel (EN1993-1-3, 2006) and stainless steel (EN1993-1-4, 2006) are more relax than that for aluminium alloys (EC9, 2007). As an intermediate limit, the equivalent stainless steel limit of 15 is suggested to adopt for both Buckling Classes A and B materials. Fig. 6.24 suggests that the limit of 15 is reasonable and supported by the available data. Unfortunately, no rotation capacity of outstand elements is reported and thus corresponding limit cannot be assessed.
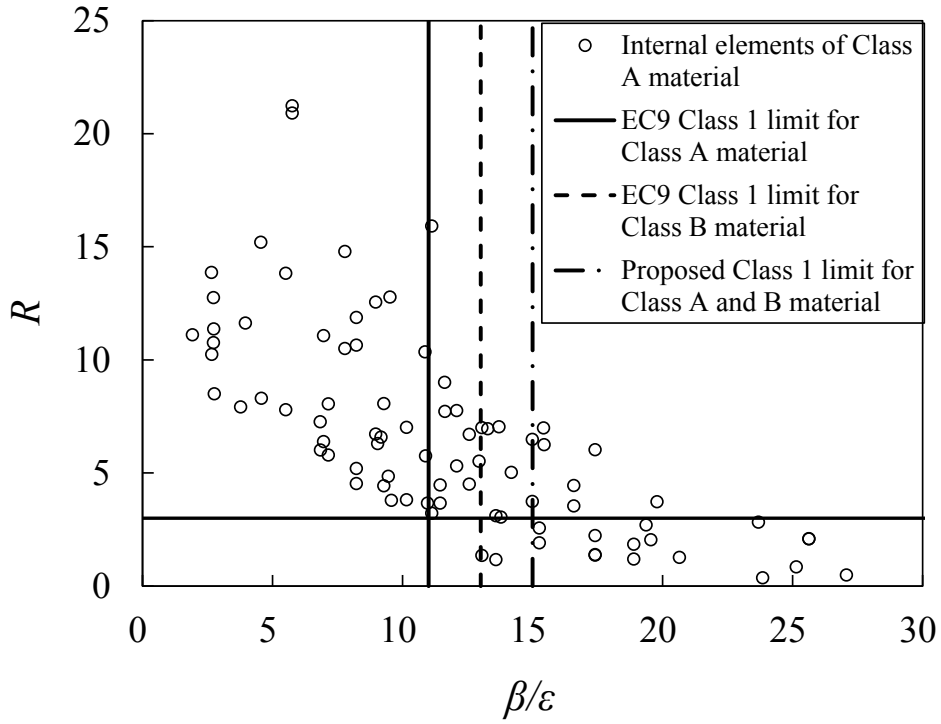
(a) Internal elements of Class A material
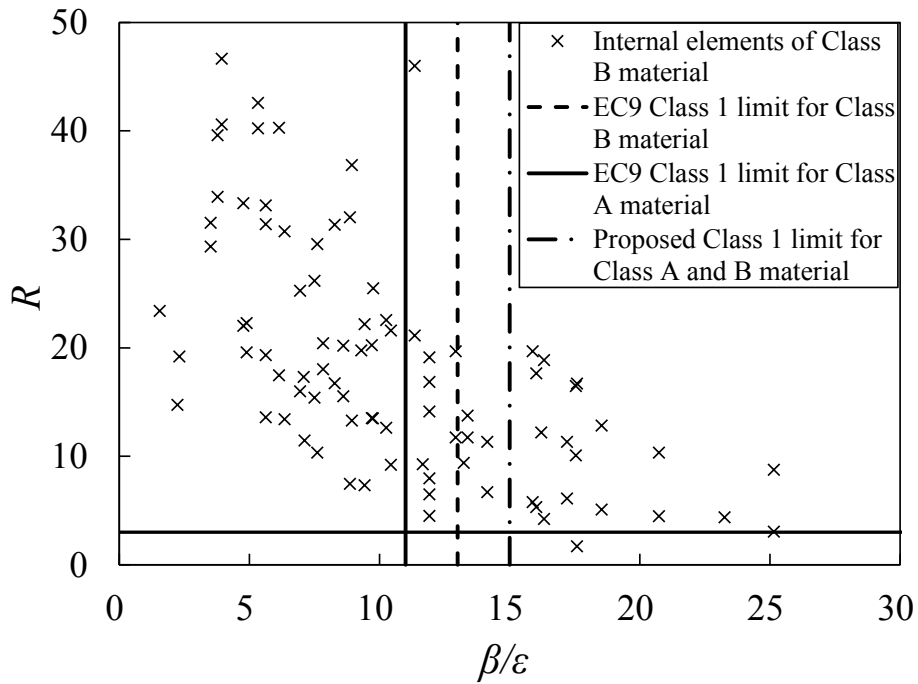
(b) Internal elements of Class B material

Fig. 6.24   Comparison between experimental/numerical results and plastic

moments together with EC9 Class 1 boundaries

6.5.2.3 Concluding remarks

The aforementioned recommendations are summarised in Table 6.13, where harmonised limits for internal elements of Classes A and B materials are given. The judgement of each behaviour class has considered all available data and also referred to current codified limits in other design specifications. Statistical analyses are presented in the coming chapter to assess these newly proposed limits. Regarding to the outstand elements, only Class 3 limit of Class A material was assessed by some compression test results and very limited bending test results; this existing limit may be seen to be reasonable and thus is recommended to remain herein.

6.5.3 Proposed CSM slenderness classification framework

The main drawback of the existing EC9 classification (2007) is that the slenderness parameter β/ε cannot account for the element interaction and the existing limits were determined based on the testing results of SHS members only (Faella et al., 2000), where RHS has different plate slenderness in the flange and web. In this study, analyses of the presented available data reveal that current slenderness limits for aluminium alloys are conservative. Furthermore, the current EC9 classification provides different sets of class limits according to the boundary conditions and type of materials. By following the well accepted characteristics of the four classes, a new classification framework is proposed. The new system includes a slenderness parameter $\overline{\lambda}_p$ considering element interaction and stress gradients, as well as a unified set of class limits applicable for all aluminium alloy tempers.

165

6.5.3.1 Slenderness parameter

Slenderness parameter is one of the key parameters to the section classification. In company with the continuous strength method (CSM) and the direct strength method (DSM) (Schafer and Peköz, 1998), the proposed classification uses the cross-section plate slenderness $\bar{\lambda}_p$ to replace the EC9 slenderness parameter β/ε, as defined in Eq. 6.12. The elastic local buckling stress σ_{cr} is not only based upon any individual element that makes up the cross-section, but also including the interaction between elements. The elastic buckling stress can be determined according to analytical approximations (Seif and Schafer, 2010) or a numerical approach, such as CUFSM (Li and Schafer, 2010). It should be noted that when using the hand calculation functions by Seif and Schafer (2010), the local plate buckling coefficients k is calculated by the centreline geometry of sections and the calculation of σ_{cr} employs flat width geometry. This approach was developed based on finite strip analysis and had been verified for hot-rolled steel sections (Seif and Schafer, 2010). In this study, the software CUFSM (Li and Schafer, 2010) was used.

$$\bar{\lambda}_p = \sqrt{f_y / \sigma_{cr}}$$
(Eq. 6.12)

6.5.3.2 Class 3 limit

To determine the Class 3 limit for stub columns, the yield limit Af_y is adopted. Classes 1, 2 and 3 sections should be capable of reaching this yield limit prior to the onset of local buckling, and meanwhile Classes 1 and 2 sections might benefit from strain hardening when experiencing large plastic strains. On the contrary, stub columns with Class 4 sections failed before reaching the yield limit. Fig. 6.25 indicates that the limit from the CSM, $\bar{\lambda}_p$ =0.68, is seen to be a reasonable boundary between slender and non-slender sections. In the CSM, the

166

slenderness $\overline{\lambda}_p$ =0.68 precisely leads to the cross-section limiting stress f_{csm} equal to the yield stress f_y, while $\overline{\lambda}_p$ ≤0.68 leads to f_{csm} greater than f_y, and vice versa. The slenderness limit between slender and non-slender sections in the DSM for aluminium alloy is also consistent, which is determined as 0.713 (Zhu and Young, 2009).

Regarding the sections in flexural, although local buckling triggers Class 3 and Class 4 sections reaching the plastic moment capacity, but Class 3 sections can still achieve yield limits (i.e. elastic moment capacity $W_{el}f_y$). Class 4 sections encounter local buckling in the elastic range and their bending resistances are lower than elastic moment capacities (Chan and Gardner, 2008). The proposed Class 3 limit $\overline{\lambda}_p$ =0.68, which has been validated by stub column results, is also appropriate for aluminium alloy sections in flexural, as indicated in Fig. 6.26. The moment capacities are higher than the elastic moment $W_{el}f_y$ when $\overline{\lambda}_p$ is not greater than 0.68, but start to fall below the elastic moment $W_{el}f_y$ for the case of $\overline{\lambda}_p$ greater than 0.68.
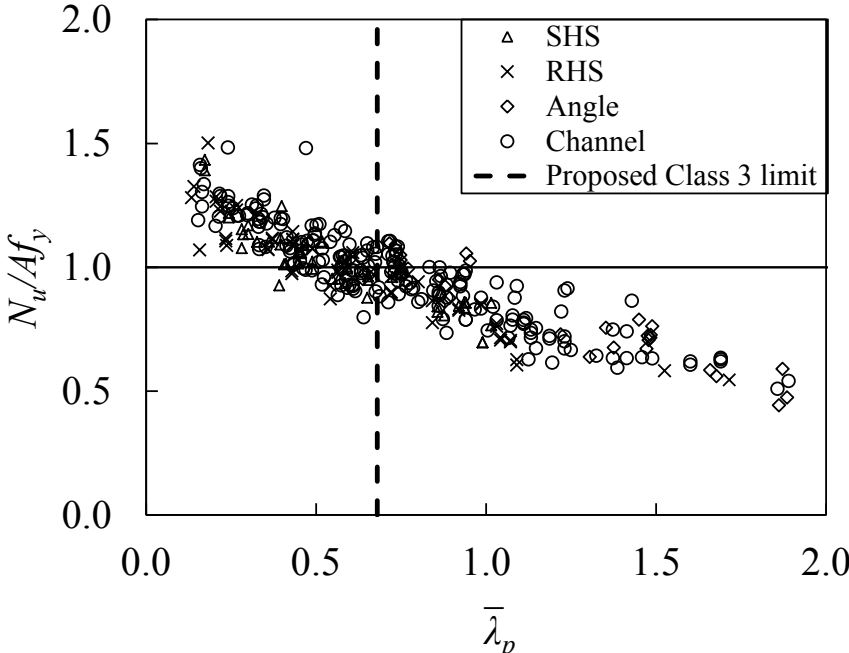
Fig. 6.25   Comparison between stub column test results and yield stress together with the proposed Class 3 limit

167
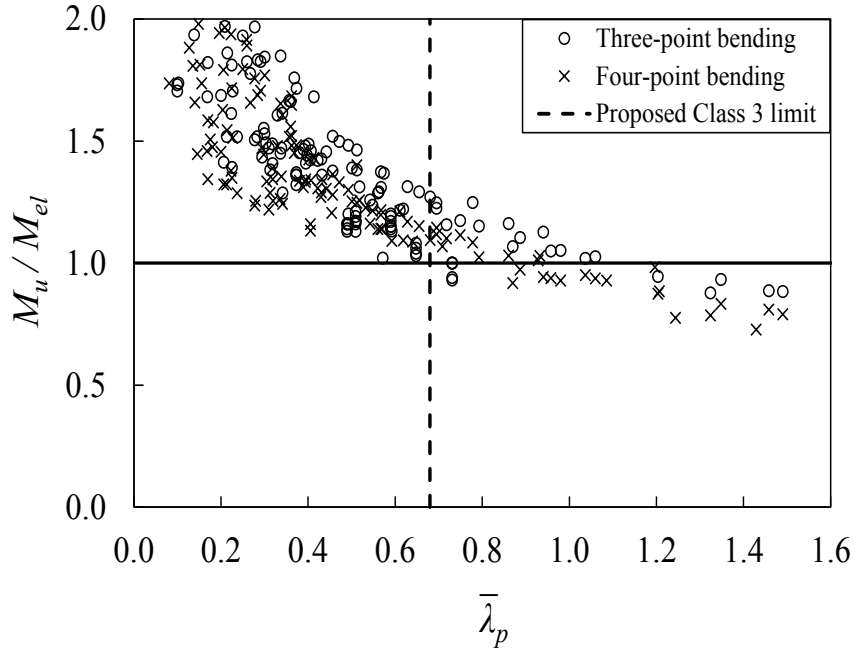
Fig. 6.26   Comparison between simply supported beam results and elastic moment together with the proposed Class 3 limit

6.5.3.3 Class 2 limit

Class 2 sections are able to reach the plastic moment but have less rotation capacity compared with Class 1 sections. The bifurcation between Class 2 and Class 3 is dependent on the cross-section capacities. Hence, the plastic moment level $W_{pl}f_y$ is used herein to determine the new Class 2 limit. A slenderness limit $\bar{\lambda}_p = 0.50$ is equivalent to the Class 2 limit in the EC9 framework (i.e. $\beta/\varepsilon=16$) through the relation shown in Eq. 6.13.

$$\bar{\lambda}_p = \frac{\sqrt{12(1-v^2)}\sqrt{250}}{\pi\sqrt{E}\sqrt{k}}(\frac{\beta}{\varepsilon})$$
(Eq. 6.13)

where v is the Poisson's Ratio.

It is indicated in Fig. 6.27 that the plotted data clearly agree with the codified definitions of Classes 2 and 3 sections. The Class 2 limit of $\bar{\lambda}_p= 0.50$ is supported

by the presented experimental and numerical bending results: the proposed limit is able to accurately identify the transaction between Class 2 and Class 3 sections.
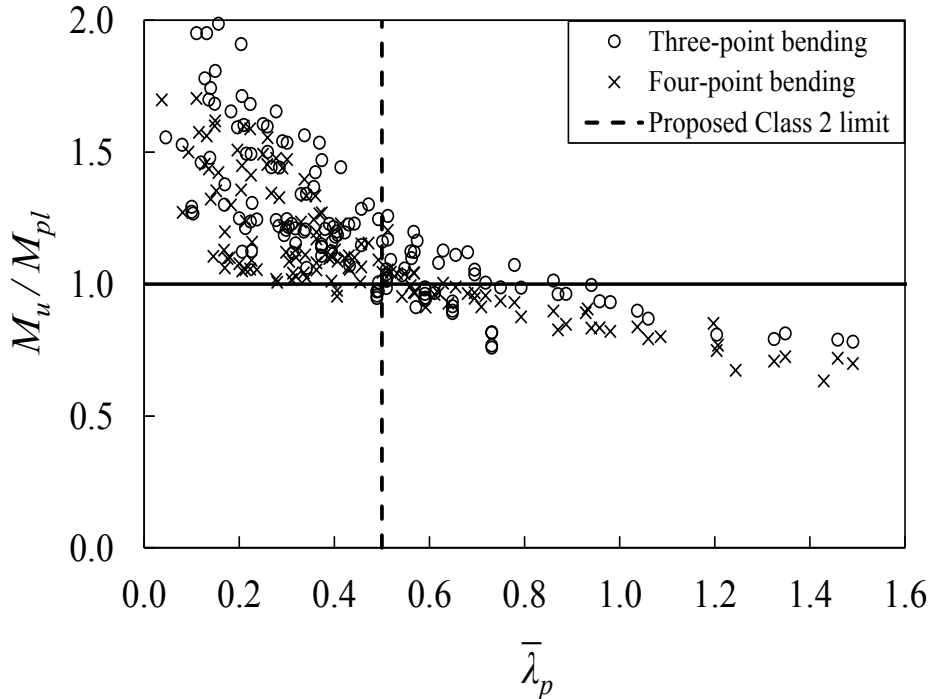
Fig. 6.27   Comparison between simply supported beam results and plastic moment with the proposed Class 2 limit

6.5.3.4 Class 1 limit

As discussed in Chapter 6.5.2.2, distinction between Class 1 and Class 2 cross-sections is the sustainability of their plastic moments with increasing rotation or deformation. To identify the Class 1 limit for bending sections, rotation capacity R of simply supported beams is employed. It should be noted that in some cases, specimens were failed by fracture on tension flange and the full rotation capacities were not reached. Hence, the data have been seen quite scattered, and a degree of engineering judgement has been required for the determination of the Class 1 limit of 0.45. Fig. 6.28 shows the rotation capacity R against slenderness $\overline{\lambda}_p$, together with the proposed Class 1 limit $\overline{\lambda}_p = 0.45$. A trend can be observed in Fig. 6.28:

Class 1 cross-sections generally have greater rotation capacity than the required value of 3, while sections of other classes clearly sustain less deformation capacity.
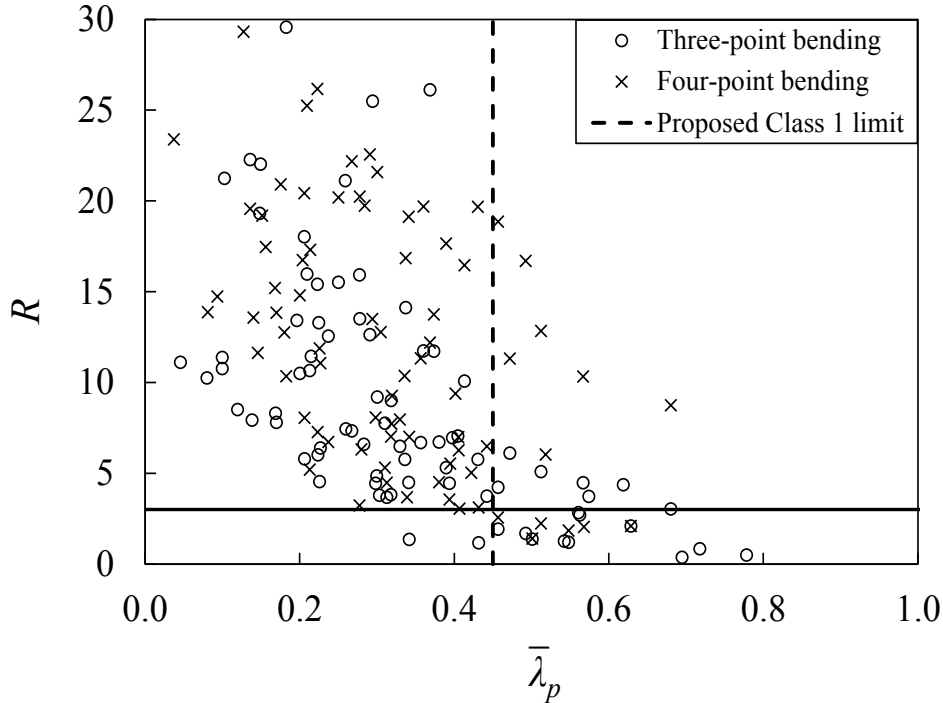
Fig. 6.28   Comparison between test results and rotation capacity with the proposed Class 1 limit

6.5.3.5 Concluding remarks

By following the codified characteristics of the four classes, a new classification parameter $\bar{\lambda}_p$ and its corresponding slenderness limits have been recommended and summarized in Table 6.13. The proposed classification framework overwhelms the EC9 framework by considering element interaction and unifying class limits for different supported conditions, aluminium alloy tempers and stress distribution. Additional merit of the slenderness limits in the $\bar{\lambda}_p$ framework (i.e. 0.45, 0.50 and 0.68) is the close match with the newly proposed slenderness limits in the β/ε framework (i.e. 15, 16 and 22). The consistency of different classification frameworks demonstrates the rational logic and harmonization behind the numbers.

170

6.5.4 Effective thickness formulae

Class 4 sections of compressive or flexural members may buckle locally before reaching their yield limits. According to EC9 (2007), local buckling in Class 4 members is generally compromised by replacing the true section with an effective section. The effective section is obtained by employing a local buckling factor ρ_c to reduce the thickness, and this reduction factor is applied to any uniform thickness of Class 4 component that is wholly or partly in compression. Within a cross-section, each element might have its own local buckling factor ρ_c, which is directly related to its corresponding slenderness. The formulae should also satisfy that when the slenderness of an element equals to Class 3 limit, its local buckling factor ρ_c should be equal to unity. For stub columns of Class 4 sections, the normalized capacity P_u/Af_y can be deemed as equal to the local buckling factor ρ_c, as illustrated in Eq. 6.14.

$$\frac{P_u}{Af_y} = \frac{A_{eff}\,f_y}{Af_y} = \frac{A_{eff}}{A} \approx \rho_c \qquad\qquad \text{(Eq. 6.14)}$$

6.5.4.1 EC9 framework

In the EC9 framework, the effective thickness formulae can be reassessed by plotting the data in P_u/Af_y versus β/ε. Regarding to the internal elements, the Class 3 limit for Class B material (β/ε=18) has been harmonized by the limit for Class A material (β/ε=22), as recommended in Section 7.5.2 herein. For consistency, it is proposed that the effective thickness formula for Buckling Class A material, specified in Clause 6.1.5 of EC9 (see Eq. 6.15), should also replace the existing function for Buckling Class B material. It is demonstrated in Fig. 6.29 (a) and (b) that Class 4 sections of both Classes A and B aluminium alloys can be accurately represented by the same design curve of Eq.6.15.

171

As for outstand elements, the current EC9 Class 3 limit ($\beta/\varepsilon=6$) has been suggested to remain for Class A material. In this case, the effective thickness formula (Eq. 6.16) codified in Clause 6.1.5 of EC9 is assessed herein by more than 200 compression test results. The curve in Fig. 6.29(c) may be seen to provide a good and safe fit to the test data. Hence, it is suggested to remain the current effective thickness formula for outstand elements of Buckling Class A aluminium alloys.

$$\rho_c = \frac{32}{(\beta/\varepsilon)} - \frac{220}{(\beta/\varepsilon)^2} \quad \text{for } \beta/\varepsilon > 22 \qquad \text{(Eq. 6.15)}$$

$$\rho_c = \frac{10}{(\beta/\varepsilon)} - \frac{24}{(\beta/\varepsilon)^2} \quad \text{for } \beta/\varepsilon > 6 \qquad \text{(Eq. 6.16)}$$
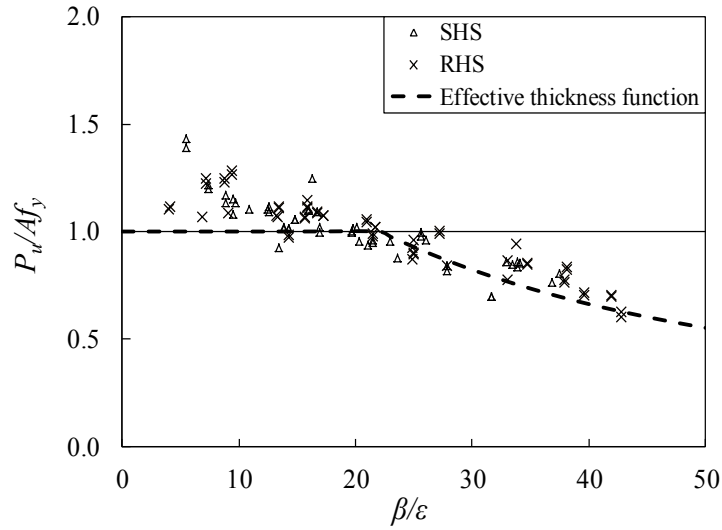
(a) Internal element of Buckling Class A material
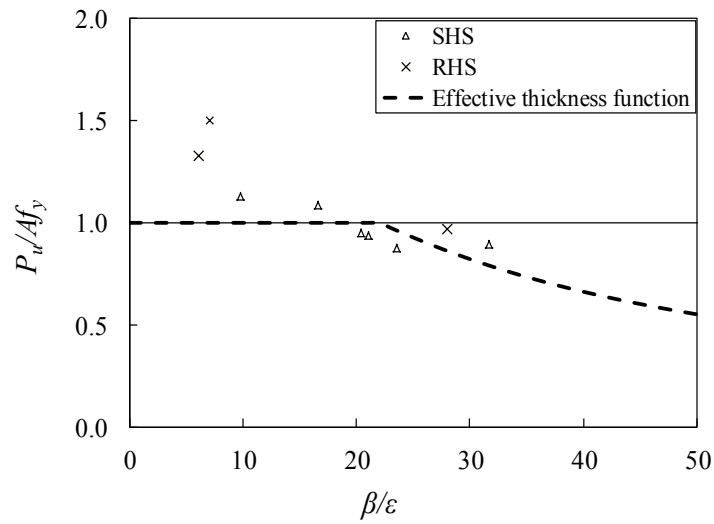
(b) Internal element of Buckling Class B material
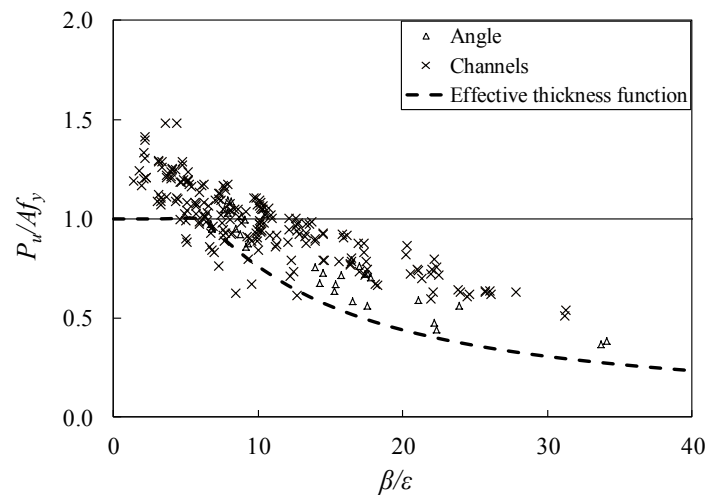
(c) Outstand element of Buckling Class A material

Fig. 6.29   Relationship between P_u/Af_y and β/ε

173

6.5.4.2 CSM slenderness framework

In the CSM slenderness framework, the effective thickness formula adopting the slenderness parameter $\bar{\lambda}_p$ is also proposed for compatibility. As explained earlier, the relationship between local buckling factor ρ_c and slenderness $\bar{\lambda}_p$ can be treated as that between the normalised capacity P_u/Af_y and $\bar{\lambda}_p$. Thus, the formula is indeed in the identical format of the DSM design curve (Schafer and Peköz, 1998), the CSM design curve as well as the Winter curve.

The design curve for aluminium alloy cross-sections has been proposed in the CSM approach, which was modified from the DSM design curve for cold-formed carbon steel members (Schafer and Peköz, 1998). The CSM base curve includes two parts, one for non-slender (Classes 1, 2 and 3) sections and the other one for slender (Class 4) sections. In this study, only the feasibility of the latter part is examined. Additional feature of this existing curve is that the transaction limit between the non-slender section and slender section is $\bar{\lambda}_p$=0.68, which is exactly the same as the proposed Class 3 limit. The expression of this curve is shown in Eq.6.17. More than 350 available results from compression tests are plotted in Fig. 6.30, including Buckling Class A and B materials as well as internal and outstand elements. It can be clearly observed in the graph that the suggested base curve was seen to provide a good fit to the data which belonged to different categories in the EC9 framework. The harmonisation with the CSM approach as well as the accuracy of predictions both suggest that Eq.6.17 is a good choice for the effective thickness prediction for aluminium alloy Class 4 sections.

$$\rho_c = \frac{1}{\bar{\lambda}_p^{0.8}} - \frac{0.195}{\bar{\lambda}_p^{1.6}} \qquad \text{for } \bar{\lambda}_p > 0.68 \qquad \text{(Eq. 6.17)}$$

174
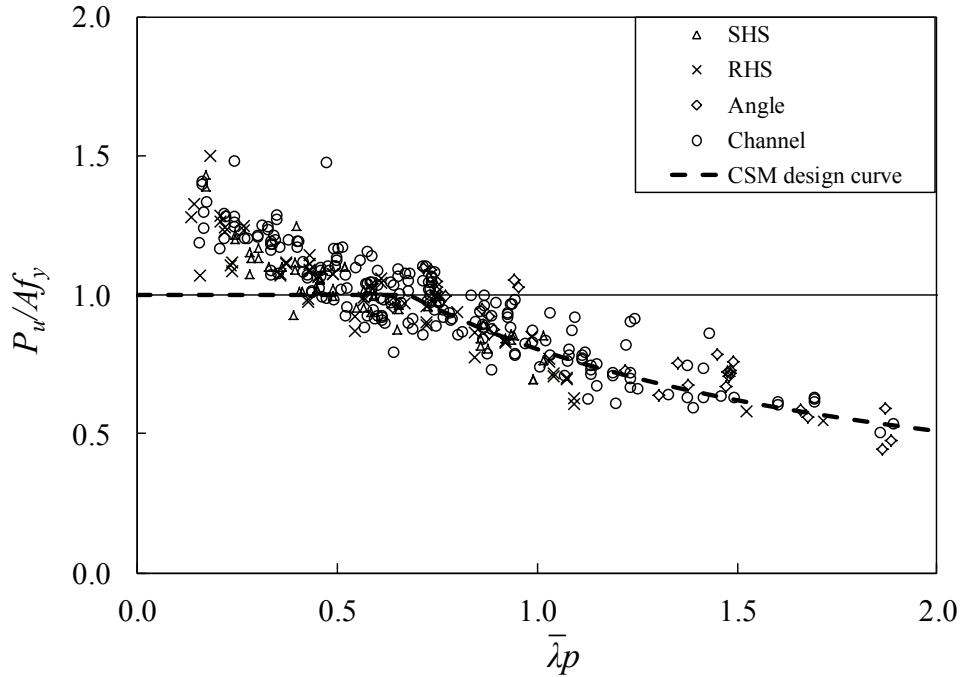
Fig. 6.30　　　Relationship between ρ_c and $\overline{\lambda}_p$ for all compressive cross-sections

6.5.5 Results comparison

In this section, the design strengths in main contents of EC9 and Annex F (or Annex H) of EC9 were predicted based on the existing limits, the proposed new limits in the EC9 framework as well as the proposed new limits in the CSM slenderness framework. Mean values and COV of the comparative results for stub columns, simply supported beams and continuous beams are presented in Table 6.14 - Table 6.16.

6.5.5.1 Stub columns

By observing the results in Table 6.14, the predicted capacities are more accurate when adopting both newly proposed classification systems. When considering only the design methods in the main text of EC9 (2007), the mean values of N_u/N_{EC9} are 1.12 and 1.06 for the proposed limits in the EC9 framework and the CSM slenderness framework, which are better than the existing classification

(mean value = 1.18). Meanwhile, the coefficients of variation (COV) also become less scatted when using the proposed limits (COV = 0.113 or 0.114). Similar results are also achieved for the predictions of Annex F of EC9. It is therefore concluded that both newly proposed classification systems are beneficial to the cross-section compressive capacity design.

Table 6.14   Stub column results (346 data) comparison with Eurocode 9 design strengths based on existing limits and proposed limits

Stub columns		Existing limits	New limits in EC9 framework	CSM slenderness framework
P_u/P_{EC9}	Mean Value	1.18	1.12	1.06
	COV	0.168	0.113	0.114
P_u/P_{EC9-F}	Mean Value	1.17	1.10	1.04
	COV	0.169	0.112	0.093

6.5.5.2 Simply supported beams

The cross-section flexural resistances obtained from experiments and simulations are compared with the design strengths predicted by EC9 (2007), as summarized in Table 6.15. On average, the main design guidance in EC9 predicted less than 75% of the test and numerical results with a coefficient of variation (COV) of 0.158, and both proposed classifications have slightly helped to improve design accuracy. Meanwhile, when employing the design method in Annex F for Class 1 sections, the mean value of M_u/M_{EC9-F} was found to be 1.23 for current class limits, whereas became 1.22 and 1.19 for new class limits in the EC9 framework and the CSM slenderness framework, respectively. However, the very similar scatter levels (COV = 0.128 and 0.127) were achieved by the three cases. It seems that the harmonised limits work well for both Buckling Class A and B materials.

Table 6.15   Simply supported beam results (283 data) comparison with Eurocode 9 design strengths based on existing limits and proposed limits

Simply supported beams		Existing limits	New limits in EC9 framework	CSM slenderness framework
M_u/M_{EC9}	Mean Value	1.28	1.27	1.25
	COV	0.152	0.158	0.163
M_u/M_{EC9-F}	Mean Value	1.23	1.22	1.19
	COV	0.121	0.128	0.127

6.5.5.3 Continuous beams

Even though the class limits are determined from the stub column and simply supported beam data, continuous bending test and numerical results are used herein to demonstrate the applicability of the new limits for indeterminate members. A summary of the comparisons for all continuous bending test and numerical results is presented in Table 6.16. Overall, the proposed class limits generally allow the predictions of EC9 (F_{EC9} and F_{EC9-H}) to achieve slightly better or equally the same mean values and COV. The predictions adopting the Annex H approach – the plastic hinge method – were found to be more than 20% better than the predictions of the main contents in EC9.

Table 6.16   Continuous beam results (256 data) comparison with Eurocode 9 design strengths based on existing limits and proposed limits

Simply supported beams		Existing limits	New limits in EC9 framework	CSM slenderness framework
F_u/F_{EC9}	Mean Value	1.63	1.63	1.61
	COV	0.223	0.222	0.224
F_u/F_{EC9-H}	Mean Value	1.40	1.38	1.33
	COV	0.193	0.204	0.185

6.5.6 Summary

Eurocode 9 (2007) is currently one of the popular aluminium alloy design specifications, which provides the classification for cross-sections subjected either partly or fully to compression. Following discussion of codified treatments of local buckling in each behaviour class, a comprehensive assessment of the existing cross-section classification in EC9 was performed. Analyses the combined experimental and numerical data set have highlighted the conservatism in the current classification system. Based on the experimental and numerical data, the feasibility of harmonising limits for Buckling Class A and B aluminium alloys was studied, after which a set of unified limits for Buckling Class A and B aluminium alloys are recommended in the EC9 framework for internal elements. The existing effective thickness formula for internal elements of Buckling Class A aluminium alloys is illustrated to be applicable for Buckling Class B aluminium alloys. In addition, a classification framework, using the CSM slenderness as the parameter, has been proposed herein. Corresponding class limits and effective thickness formulae for Class 4 sections are determined in harmonisation with the CSM approach. Within the CSM slenderness framework, element interaction is considered, and furthermore, effects from material tempers, section geometries and stress gradients are incorporated in a unified set of slenderness limits. Results show that the proposed limits are beneficial to the cross-sectional capacity prediction. Given the more accurate and consistent predictions resulted from the new classifications, more efficient design can be anticipated after adopting the new classifications.

CHAPTER 7
STRUCTURAL RELIABILITY

7.1 Introduction

Reliability is defined as the ability of a structure or a structural member to fulfil the specified requirements (EN1990, 2002). The concept of reliability analyses was firstly introduced at the end of 1960s, after which, the structural design rules and expressions can be assessed by a rationalised and unified approach. In addition, an identical notional reliability level should be achieved by the design rules to demonstrate their reliability and safety. This target reliability formed the basis for the probability-based design criteria and the code rationalisation.

This chapter explains the concept, some background information, calculation procedure and the derived results of reliability analyses according to the standardized approaches. The aim of the reliability analyses is to derive the partial safety factor γ_{M0} and the reliability index β, so that to assess whether the level of reliability of the resistance functions have conformed to EN1990 (2002) and the AISC (2010).

7.2 Background of reliability analyses

There are three categories of reliability methods, termed Level I to III. An overview of reliability methods is shown below. The probabilistic calibration procedures for partial factors can be subdivided into two main classes: (1) Full probabilistic methods (Level III), and (2) First order reliability methods (FORM) (Level II) (see Fig. 7.1).
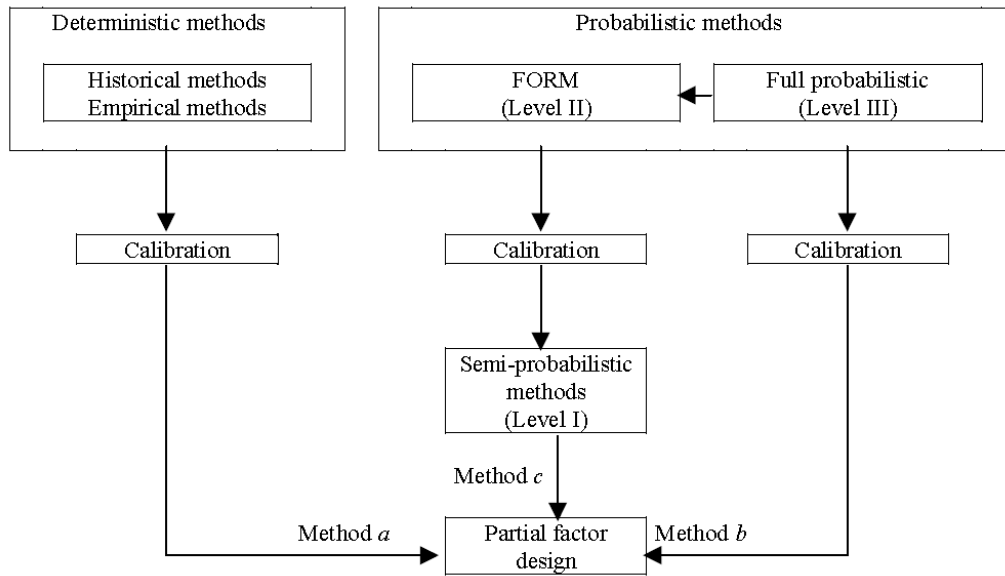
Fig. 7.1   Overall of Reliability methods (EN1990, 2002)

The Level I method was adopted in previous allowable stress design specifications. Appropriate levels of structural reliability, on a structural element (member) basis, are provided by the specification of a number of partial safety factors related to some pre-defined characteristic values of the basic variables (CIRIA No.63, 1977).

In both the Level II and Level III methods the measure of reliability should be identified with the survival probability $P_s = (1 - P_f)$, where P_f is the failure probability for the considered failure mode and within an appropriate reference period. If the calculated failure probability is greater than a pre-set target value P_0, then the structure should be considered to be unsafe (EN1990, 2002). The first order reliability method (Level II) is adopted in this study; thus, the detail explanation of FORM is given in the following section.

The Level III method is based on an exact probabilistic analysis of structural systems, using a full distributional approach. All design variables in this analysis should be expressed in terms of their full probability distribution functions and

180

probabilities of failure are computed by the evaluation of the appropriate convolution integrals (CIRIA No. 63, 1977). This method is difficult to apply in practice and not suitable for normal design purpose.

7.3 First order reliability method (FORM)

The Level II method, also termed the First Order Reliability Method (FORM), is a design method incorporating safety checks only at a selected point (or points) on the failure boundary (as defined by the appropriate limit state equation), and the key feature of FORM is to identify the design point on the failure boundary where the failure probability is maximum (Law, 2010). The Level II method assembles the statistics of the basic variables in terms of means, standard deviations and normal/log-normal distributions. Reliability levels are estimated in Level II either in terms pf a reliability index or a notional probability. With due regard for both operational and reliability considerations, FORM has been employed in the calibration of most modern specifications (e.g. Eurocodes and the AA). Some basic assumptions should be made before implementing the Level II reliability analyses.

Assumptions:

1. A sufficient number of test results is available;
2. All relevant geometric and material properties are measured;
3. There is no statistical dependence between the variables in the resistance function and
4. All variables follow either a normal or log-normal distribution

The statistical evaluation model in FORM is given by Eq. 7.1,

$$P(X < x_p) = p \qquad \text{(Eq. 7.1)}$$

For a specified probability p, the general format of the fractile x_p can be estimated as below:

$$x_p = \mu - \sigma k_n \qquad \text{(Eq. 7.2)}$$

where μ is the mean value of the population, k_n is the fractile factor and σ is standard deviation of the population and n is the sample size.

7.4 Reliability analyses by Eurocode approach (EN1990, 2002)

7.4.1 General

Design working life for building structures and other common structures is 50 years in EN1990 (2002), while the minimum reliability index for a 50-years structure is 3.8, as presented in Table B2 of Annex D (EN1990, 2002). All the designs using EN 1990 with the partial factors given in Annex A1 (EN1990, 2002) can be considered generally leading to a structure with a β value greater than 3.8 for a 50-years reference period (EN1990, 2002). According to the codified value in Annex C, the fractile factor of normal distribution of reliability index relating to the resistance α_R is 0.8; thus, for a global reliability index $\beta=3.8$, this leads to a desired reliability index for the resistance of $\alpha_R\beta = 0.8\times3.8 = 3.04$, which is roughly corresponding to the probability of failure 0.1% for a single property (see Table 7.1). Only resistance model is considered in the reliability analyses of EN1990 (2002).

Table 7.1　　Relation between β and P_f (EN1990, 2002)

P_f	10^{-1}	10^{-2}	10^{-3}	10^{-4}	10^{-5}	10^{-6}	10^{-7}
β	1.28	2.32	3.09	3.72	4.27	4.75	5.20

The derivation from tests of the design values for a material property, a model parameter or a resistance should be carried out in one of the following ways, according to EN1990 (2002):

a) by assessing a characteristic value, which is then divided by a partial factor and possibly multiplied if necessary by an explicit conversion factor (see D7.2 and D8.2 in EN1990);

b) by direct determination of the design value, implicitly or explicitly accounting for the conversion of results and the total reliability required (see D7.3 and D8.3 in EN1990).

Method (b) is used herein to evaluate the reliability level of the design rules.

7.4.2 Key input parameters

Some statistical parameters adopted in the EN1990 analyses were based on the recommended values in the Aluminum Design Manual (AA, 2010), including: the ratio of mean to nominal yield strengths (i.e. the material over-strength) is 1.10 and the coefficients of variation of yield strength and geometric properties could be taken as 0.06 and 0.05 respectively. These values were adopted in the statistical analyses of the test results in this study. Note that one of the key parameters $k_{d,n}$ is the design (ultimate limit state) fractile factor for the case "V_x unknown" for n tests, where n is the population of test data under consideration.

7.4.3 Calculation procedure

A total of seven steps, codified in EN1990 (2002), are needed to derive the reliability index:

Step 1: Develop a design model

(1) Develop a design model for the theoretical resistance r_t of the member or structural detail considered, represented by the resistance function:

$$r_t = g_{rt}(X)$$ (Eq. 7.3)

(2) The resistance function should cover all relevant basic variables X that affect the resistance at the relevant limit state.

(3) All basic parameters should be measured for each test specimen and should be available for use in the evaluation.

Step 2: Compare experimental and theoretical values

Substitute the actual measured properties into the resistance function so as to obtain theoretical values r_{ti} to form the basis of a comparison with the experimental values r_{ei} from the tests and plot the points of (r_{ti}, r_{ei}) on a diagram.

Step 3: Estimate the mean value correction factor b

(1) Represent the probabilistic model of the resistance r in the format:

$$r = br_t\delta$$ (Eq. 7.4)

where b is the "Least Squares" best-fit to the slope given by $b = \dfrac{\sum r_e r_t}{\sum r_t^2}$ and δ is the error term related to the deviation of the experimental resistance values to the mean strength function

(2) The mean value of the theoretical resistance function, calculated using the mean values X_m of the basic variables can be obtained from:

$$r_m = br_t(X_m)\delta = bg_{rt}(X_m)\delta$$ (Eq. 7.5)

Step 4: Estimate the coefficient of variation of the errors

(1) The error term δ_i for each experimental value r_{ei} should be determined:

$$\delta_i = \frac{r_{ei}}{br_{ti}}$$ (Eq. 7.6)

184

(2) From the values of δ_i, the coefficient of variation V_δ of the δ_i error terms.is defined as:

$$V_\delta = \sqrt{\exp\left(s_\Delta^2\right) - 1}$$ (Eq. 7.7)

where

$$\Delta_i = \ln(\delta_i)$$

$$\overline{\Delta} = \frac{1}{n}\sum_{i=1}^{n}\Delta_i$$

$$s_\Delta^2 = \frac{1}{n\text{-}1}\sum_{i=1}^{n}(\Delta_i - \overline{\Delta})^2$$

Step 5: Analyse compatibility

(1) The compatibility of the test population with the assumptions made in the resistance function should be analysed.

(2) If the scatter of the (r_{ei}, r_{ti}) values are too high to give economical design resistance functions, this scatter may be reduced in one of the following ways:

a) by correcting the design model to take into account parameters which had previously been ignored ;

b) by modifying b and V_δ by dividing the total test population into appropriate sub-sets for which the influence of such additional parameters may be considered to be constant.

(3) To determine which parameters have most influence on the scatter, the test results may be split into subsets with respect to these parameters.

(4) When determining the fractile factors k_n (see step 7), the k_n value for the sub-sets may be determined on the basis of the total number of the tests in the original series.

Step 6: Determine the coefficients of variation V_{Xi} of the basic variables

V_{xi} of the basic variables are generally determined on the basis of some prior knowledge. The Aluminum Design Manual (AA, 2010) proposed that the coefficients of variation of yield strength and geometric properties of aluminium alloy sections can be taken as 0.05 and 0.02 respectively. These values are adopted in this study.

Step 7: Determine the characteristic value r_d of the resistance

(1)   For the case of a limited number of tests, the design value r_d should be obtained from :

$$r_d = b g_{rt}(\underline{X}_m) \exp(-k_{d,\infty} \alpha_{rt} Q_{rt} - k_{d,n} \alpha_\delta Q_\delta - 0.5 Q^2)$$ (Eq. 7.8)

where:

$k_{d,n}$ is the design fractile factor from table D2 for the case "V_X unknown";

$k_{d,\infty}$ is the value of $k_{d,n}$ for $n \text{---}>\infty$ [$k_{d,\infty} = 3,04$].

NOTE the value of V_X is to be estimated from the test sample under consideration.

(2) For the case of a large number of tests the design value r_d may be obtained from:

$$r_d = b g_{rt}(\underline{X}_m) \exp(-k_{d,\infty} Q - 0.5 Q^2)$$ (Eq. 7.9)

where b is the mean value correction factor, $g_{rt}(X_m)$ is the design resistance model evaluated for the mean value of basic variables from tests, $k_{d,n}$ is the design fractile factor, $k_{d,\infty}$ is the design fractile factor for n tending to infinity, α_{rt} is the weighting factor for Q_{rt}, α_δ is the weighting factor for Q_δ. The values of Q_{rt}, Q_δ and Q are defined by Eq. 7.10, Eq. 7.11 and Eq. 7.12 respectively.

$$Q_{rt} = \sigma_{\ln(r_t)} = \sqrt{\ln(V_{rt}^2 + 1)}$$ (Eq. 7.10)

$$Q_\delta = \sigma_{\ln(r_\delta)} = \sqrt{\ln(V_\delta^2 + 1)}$$ (Eq. 7.11)

$$Q = \sigma_{\ln(r)} = \sqrt{\ln(V_r^2 + 1)} \qquad \text{(Eq. 7.12)}$$

$$\alpha_{rt} = \frac{Q_{rt}}{Q} \qquad \text{(Eq. 7.13)}$$

$$\alpha_\delta = \frac{Q_\delta}{Q} \qquad \text{(Eq. 7.14)}$$

Step 8: Obtain the partial safety factor γ_m

The partial factor is given by:

$$\gamma_m = \frac{r_n}{r_d} \qquad \text{(Eq. 7.15)}$$

where r_n is the nominal resistance which is obtained by putting the representative or nominal values of all the basic variables into the resistance function.

The partial factors γ_{M0} (for resistance of cross-sections and for resistance of members to instability) were recommended to be 1.10 in Clause 6.1.3 of EC9 (2007). A calculated partial safety factor lower than that specified in EC9 (i.e. 1.10) indicates a higher degree of reliability (>99.9%) for a design formulation.

7.5   Reliability analyses by the AISC approach (2010)

7.5.1 General

For the design methods of steel structural members in the AISC (2010) Standard, the partial factors of both member resistances for compression and flexure were recommended to be 0.9 and the implied safety index is approximately 2.60 (Law, 2010). In terms of aluminium alloy columns and beams, the reliability level for the design rules in the Aluminum Design Manual (2010) is 2.50 with partial factor ϕ being 0.9. The AISI Commentary (2000) also recommend β_0 be taken as 2.5 for structural members. In this study, a target reliability index of 2.5 is also applied to EC9 (2007). Thus, if the reliability index is greater than or equal to 2.5, the design

method is deemed to be reliable. According to the relation between reliability index β and the probability value ($P_f = \phi(-\beta)$) shown in Table 7.1, the corresponding probability of failure is 0.5%.

The general limit state design principle in the AISC (2010) is given in Eq. 7.16:

$$\sum_{i=1}^{j} r_i Q_{im} \leq \phi R_n \qquad \text{(Eq. 7.16)}$$

where Q_{im} is the mean load effect, γ_i is the load factor corresponding to Q_{im}, R_n is the nominal resistance and ϕ is the resistance factor corresponding to R_n.

The statistical models for resistances and load effects in the AISC (2010) are log-normal distribution. The reliability index β and partial reliability index ϕ defined by Ravindra and Galambos (1978) as:

$$\beta = \frac{\ln\left(R_m / Q_m\right)}{\sqrt{V_R^2 + V_Q^2}} \qquad \text{(Eq. 7.17)}$$

where Q_m and R_m are the mean values of the total load effect and resistance respectively and V_Q and V_R are the coefficient of variation of the total load effect and resistance respectively.

$$\phi = \left(R_m / R_n\right) \exp(-\alpha \beta V_R) \qquad \text{(Eq. 7.18)}$$

where R_m is the nominal resistance and α is the weighting factor.

7.5.2 Key input parameters

The input parameters were taken from Clause 1.3.2 of Appendix 1, Part I in the AA (2010) specification, where the mean values and COV for material properties and fabrication variables are taken as $M_m = 1.10$ (for behaviour governed by the yield stress) or 1.10 (for behaviour governed by the ultimate stress), $F_m = 1.00$, $V_M = 0.06$, and $V_F = 0.05$. In addition, the COV of loads V_Q is taken as 0.21. It should

be noted that the over-strength parameter is a key factor in the reliability analyses, the value of 1.10 is recommended by the AA (2010) and Galambos (1979). However, Galambos (1979) also reported other different values for the material properties, i.e. $M_m = 1.19$ for f_u and $M_m = 1.21$ for f_y for 6061-T6 extrusions, which are suggested by the Military Handbook and Clark (1974).

Since the analyses in the AISC include the load statistics, the load combination between Dead Load (DL) and Live Load (LL) should be considered. A load combination of 1.2DL + 1.6LL is used for the AA (2010), while 1.25DL + 1.50LL and 1.35DL + 1.50LL are used for the AS/NZS (1997) and EC9 (2007), respectively, which lead to the following results:

$$Q_m \le 0.691\phi R_n \qquad \text{AS/NZS} \qquad \qquad \text{(Eq. 7.19)}$$

$$Q_m \le 0.657\phi R_n \qquad \text{AA} \qquad \qquad \text{(Eq. 7.20)}$$

$$Q_m \le 0.683\phi R_n \qquad \text{EC9} \qquad \qquad \text{(Eq. 7.21)}$$

It should be noted that Eqs. 7.19 - 7.21 are derived from Eq. 7.16 by extending the load combination expressions. The detail investigation of Eqs. 7.19 - 7.21 has been described by Rogers and Hancock (1996)

The resistance factor ϕ, which is also a necessary parameter to derive β, depends on the structural scenario being addressed and the design specification under consideration. For aluminium alloy beams, the AA (2010) specification uses a resistance factor ϕ of 0.90, the AS/NZS (1997) specification uses a resistance factor ϕ of 0.85 and EC9 employs a resistance factor ϕ of 0.91 (Rogers and Hancock, 1996).

In order to have a direct comparison among different design approaches, all parameters (a constant resistant factor $\phi_2 = 0.90$ and a load combination of 1.2DL+1.6LL) were set to those given in the AA (2010) specification to calculate the reliability index. For this direct comparison, the calculated reliability index is denoted as β_2.

7.5.3 Calculation procedure

After substituting the load parameters of Eqs. 7.19 - 7.21 into the reliability index equation Eq. 7.17, the reliability expression may be restated as Eqs. 7.22 - 7.24:

$$\beta = \frac{1}{\sqrt{V_R^2 + V_Q^2}} \ln\left[\frac{R_m}{0.691\phi R_n}\right] \qquad \text{AS/NZS} \qquad \text{(Eq. 7.22)}$$

$$\beta = \frac{1}{\sqrt{V_R^2 + V_Q^2}} \ln\left[\frac{R_m}{0.657\phi R_n}\right] \qquad \text{AA} \qquad \text{(Eq. 7.23)}$$

$$\beta = \frac{1}{\sqrt{V_R^2 + V_Q^2}} \ln\left[\frac{R_m}{0.683\phi R_n}\right] \qquad \text{EC9} \qquad \text{(Eq. 7.24)}$$

where

$$V_R = \sqrt{V_M^2 + V_F^2 + C_P V_P^2} \qquad \text{(Eq. 7.25)}$$

$$C_p = \frac{n^2 - 1}{n^2 - 3n} \qquad \text{(Eq. 7.26)}$$

$$\frac{R_m}{R_n} = M_m \times F_m \times P_m \qquad \text{(Eq. 7.27)}$$

where C_P is a correction factor taking into account the number of tests, n, P_m is the mean values of tested-to-predicted load ratios, and V_P is the coefficients of variation of tested-to-predicted load ratios.

7.6   Comparison of EN1990 and AISC approaches

In worldwide, specifications of practice have been developed to provide authoritative guidelines to designers and contractors and to provide a basis of compliance. However, different specifications for various structural materials, loadings and types of construction have been prepared by different committees. Consequent anomalies resulted in different levels of safety and performance from various specifications, and comparison of economy of alternative approaches would become impossible to make (Law, 2010). There was obviously a need for rationalisation in structural design specifications (CIRIA, 1977). In this study, both the AISC (2010) and EN1990 (2002) reliability analysis approaches are employed to assess the design methods. Although these two reliability analyses approaches are based on the FORM principle, differences are still existed between them.

7.6.1 Weighting factors

Action and resistance weighting factors α_Q and α_R, as defined in Eqs.7.28 and 7.29 for normally distributed variables, are generated in FORM to solve reliability problems. The exact solutions of the weighting factors can be obtained from rigorous reliability equations with the given action and resistance functions (Law, 2010). However, in most cases, it would be difficult to identify the most critical action for the design and therefore a semi-probabilistic safety concept, in which no explicit reliability calculations are undertaken, is adopted (Law, 2010). The EN1990 approach sets the sensitivity factors of the action and resistance sides, α_Q and α_R to -0.7 and 0.8 respectively (IABSE Colloquium, 1996). The values of α_R adopted in the AISC approach to determine ϕ (see Eq. 7.18) is 0.55 (Ravindra and Galambos, 1978).

$$\alpha_Q = \frac{-\sigma_Q}{\sqrt{\sigma_Q{}^2 + \sigma_R{}^2}} \qquad \text{(Eq. 7.28)}$$

$$\alpha_R = \frac{\sigma_R}{\sqrt{\sigma_Q{}^2 + \sigma_R{}^2}} \qquad \text{(Eq. 7.29)}$$

where σ_Q and σ_R are the standard deviation of actions and resistances.

7.6.2 Resistance factor ϕ and γ_{M0}

Resistance factors have been defined in different expressions in American and European design specifications, to account for uncertainties and variability associated with the limit state models, material properties, geometry and fabrication. In the American specifications, the resistance factor ϕ is to factor down the nominal strength, as illustrated in Eqs. 7.30 and 7.31. Thus, the resistance factor should be a value smaller than unity, with the codified values of 0.9 and 0.85 for the American and Australian/New Zealand standards, respectively. The Eurocode system adopts a partial safety factor γ_{M0} to factor down the nominal strength R_n derived from characteristics values (Eq. 7.32). Since the partial safety factor is the ratio between nominal strength and design strength (Eq. 7.33), it should be a value greater than unity, with the codified value of 1.1 in EC9. The relation between ϕ and γ_{M0} is given in Eq. 7.34.

$\phi R_n \geq \gamma Q$ (Eq. 7.30)

$\phi = \gamma Q/R_n$ (Eq. 7.31)

$R_d \leq R_n / \gamma_{M0}$ (Eq. 7.32)

$\gamma_{M0} = R_n/R_d$ (Eq. 7.33)

$$\phi = \frac{1}{\gamma_{M0}} \qquad \text{(Eq. 7.34)}$$

Thus, in the AISC approach, resistance factor ϕ adopts different values for the AA, AS/NZS and EC9 specifications, as mentioned in Chapter 7.5.2.

7.6.3 Reliability level

The target reliability value depends on a number of factors (CIRIA Report, 1977), as briefly outlined in ISO 2394 (1998).

In EN1990 (2002), as mentioned earlier, the reliability index β for a 50-years design working life for building structures is derived as 3.8, which is adopted as the basis for the derivation of partial safety factors in the European specifications. Hence, a global reliability index β=3.8 results in a desired reliability index for the resistance $\alpha_R\beta = 0.8 \times 3.8 = 3.04$. The European specifications aim to restrict the probability of the actual resistance of structural components falling below the design resistance to 1 in 845 (approximately 10^{-3}) (Byfield and Nethercot, 2001). As mentioned earlier, a partial safety factor γ_M is the reliability indicator for EN1990 approach, where a target value of 1.10 is codified in EC9 for aluminium structural members. It is indicated that a design method with the calculated partial safety factor of smaller than 1.10 is a safe method with 1 in 1000 failure possibility. Thus, in this study, design rules with $\gamma_M \leq 1.10$ are deemed safe according to EN1990.

In terms of the AISC approach, the reliability index β is adopted as the reliability level indicator. The Aluminum Design Manual (2010) and AISI Commentary (2000) recommend that the target reliability index β_0 be taken as 2.50 for structural members. From Table 7.1, we can know that the probability of failure is 0.5%. In this study, based on corresponding ϕ values in different design specifications, the design rules with $\beta_0 \geq 2.50$ are deemed reliable according to the AISC (2010).

However, the reliability index β from EN1990 and the AISC cannot be compared directly, since these two statistical analyses systems are developed based on

different assumptions and treatments, such as load combination and the resistance factor (Rogers and Hancock, 1996). The analyses in EN1990 only focus on the resistance part, excluding the load combinations; while the AISC considers reliability index including uncertainties from both resistance and action effects.

7.7 Special treatments to the dependent variables in Eurocodes

7.7.1 Compression design of Class 4 sections

A major assumption of the standard statistical analyses outlined in EN1990 (2002) is that the resistance equation is a function of independent variables. From the design equations in EC9 (2002) for the slender sections, the resistance of stub columns is seen to depend on the effective area A_{eff} and the material yield stress f_y (Eq. 6.4). However, the yield stress has influence on the effective thickness, which means that the basic variables are not independent in these design expressions. A procedure of separating the dependence of the basic variables is described herein for compression design of Class 4 SHS/RHS (see Fig. 3.1).

First, some assumptions have to be made:

1) $\because\ t \ll\quad$ and H
   $\quad \therefore$

$$A = BH - (B - 2t)(H - 2t)$$
$$= t(2B + 2H - 4t)$$
$$\approx 2t(B + H)$$

$$\Rightarrow\ \frac{A_{eff}}{A} = \frac{2(B+H)t_{eff}}{2(B+H)t} = \frac{t_{eff}}{t} = \rho_c \qquad \text{(Eq. 7.35)}$$

2) $\because t \ll\quad$ and H

$$\therefore \frac{b_2}{b_1} = \frac{(B_2 - 2t_2)}{(B_1 - 2t_1)} \approx \frac{B_2}{B_1} \qquad \text{(Eq. 7.36)}$$

194

The procedure for separating the dependence of the basic variables is shown below:

$$
\begin{aligned}
P &= A_{eff}\,f_y \\
&= 2(B+H)t_{eff}\,f_y \\
&= 2(B+H)t\rho_c f_y \\
&= Xf_y{}^a t^b (B+H)^c
\end{aligned}
$$

(Eq. 7.37)

where X is a constant, independent of f_y, t and $(B+H)$. The powers a, b and c vary for different slenderness and should be computed for each test specimen. In order to evaluate the power a, two columns of the same geometrical properties, but different material properties, $f_{y,1}$ and $f_{y,2}$ are considered. The ratio of their capacities is given by:

$$
\begin{aligned}
\frac{P_2}{P_1} &= \frac{Xf_{y,2}{}^a t^b (B+H)^c}{Xf_{y,1}{}^a t^b (B+H)^c} \\[2mm]
&= \frac{f_{y,2}{}^a}{f_{y,1}{}^a} \\[2mm]
&= (\frac{f_{y,2}}{f_{y,1}})^a \\[2mm]
\Rightarrow \quad \ln(\frac{P_2}{P_1}) &= \ln(\frac{f_{y,2}}{f_{y,1}})^a \\[2mm]
&= a\ln(\frac{f_{y,2}}{f_{y,1}})
\end{aligned}
$$

$$
\therefore \quad a = \frac{\ln(\frac{P_2}{P_1})}{\ln(\frac{f_{y,2}}{f_{y,1}})}
$$

(Eq. 7.38)

And, due to the difference in f_y, the reduction factors for local buckling ρ_c of the two columns are also different:

$$\frac{\rho_{c,2}}{\rho_{c,1}} = \frac{\dfrac{C_1}{\left(\dfrac{\beta_2}{\varepsilon_2}\right)} - \dfrac{C_2}{\left(\dfrac{\beta_2}{\varepsilon_2}\right)^2}}{\dfrac{C_1}{\left(\dfrac{\beta_1}{\varepsilon_1}\right)} - \dfrac{C_2}{\left(\dfrac{\beta_1}{\varepsilon_1}\right)^2}}$$

(Eq. 7.39)

$$\frac{\dfrac{\beta_2}{\varepsilon_2}}{\dfrac{\beta_1}{\varepsilon_1}} = \frac{\dfrac{\left(\dfrac{b}{t}\right)}{\sqrt{\dfrac{250}{f_{y,2}}}}}{\dfrac{\left(\dfrac{b}{t}\right)}{\sqrt{\dfrac{250}{f_{y,1}}}}} = \sqrt{\frac{f_{y,2}}{f_{y,1}}}$$

(Eq. 7.40)

and,

$$\begin{aligned}\frac{P_2}{P_1} &= \frac{2(B+H)t\rho_{c,2}f_{y,2}}{2(B+H)t\rho_{c,1}f_{y,1}} \\ &= \frac{\rho_{c,2}}{\rho_{c,1}}\frac{f_{y,2}}{f_{y,1}}\end{aligned}$$

(Eq. 7.41)

By adopting small increments in f_y (e.g. $f_{y,2}/f_{y,1}$ = 1.001), an accurate approximation of the power a can be obtained for an instantaneous value of f_y.

The power a can then be found by the following steps:

1. Calculate $(\beta/\varepsilon)_{actual}$ (as $(\beta/\varepsilon)_1$), the cross-section slenderness of the test specimen, from the test data;

2. Calculate the reduction factor for local buckling $\rho_{c,actual}$ (as $\rho_{c,1}$), from $(\beta/\varepsilon)_1$;

3. Calculate $(\beta/\varepsilon)_2$, from $f_{y,2}/f_{y,1}$ =1.001 and Eq. 7.40;

4. Calculate $\rho_{c,2}$ from Eq. 7.39;

4. Calculate $\dfrac{P_2}{P_1}$ from Eq.7.41;

5. Find a by Eq.7.38.

The power *b* may be subsequently obtained as follows:

Considering two columns of the same geometrical properties except different thickness t_1 and t_2, and different material properties, $f_{y,1}$ and $f_{y,2}$, the ratio of their capacities is given by:

$$\frac{P_2}{P_1} = \frac{Xf_{y,2}{}^a t_2{}^b (B+H)^c}{Xf_{y,1}{}^a t_1{}^b (B+H)^c}$$

$$= \frac{f_{y,2}{}^a}{f_{y,1}{}^a} \frac{t_2{}^b}{t_1{}^b}$$

$$= (\frac{f_{y,2}}{f_{y,1}})^a (\frac{t_2}{t_1})^b$$

$$\Rightarrow \quad \ln(\frac{P_2}{P_1}) = \ln[(\frac{f_{y,2}}{f_{y,1}})^a (\frac{t_2}{t_1})^b]$$

$$= a\ln(\frac{f_{y,2}}{f_{y,1}}) + b\ln(\frac{t_2}{t_1})$$

$$\therefore \quad b = \frac{\ln(\frac{P_2}{P_1}) - a\ln(\frac{f_{y,2}}{f_{y,1}})}{\ln(\frac{t_2}{t_1})} \qquad \text{(Eq. 7.42)}$$

And, due to the difference in f_y and t, the reduction factor for local buckling ρ_c of the two columns is also different:

$$\frac{\frac{\beta_2}{\varepsilon_2}}{\frac{\beta_1}{\varepsilon_1}} = \frac{\dfrac{(\frac{b}{t_2})}{\sqrt{\dfrac{250}{f_{y,2}}}}}{\dfrac{(\frac{b}{t_1})}{\sqrt{\dfrac{250}{f_{y,1}}}}} = \sqrt{\frac{f_{y,2}}{f_{y,1}}}\frac{t_1}{t_2} \qquad \text{(Eq. 7.43)}$$

and,

$$\frac{P_2}{P_1} = \frac{2(B+H)t_2\rho_{c,2}f_{y,2}}{2(B+H)t_1\rho_{c,1}f_{y,1}}$$

$$= \frac{\rho_{c,2}}{\rho_{c,1}} \frac{f_{y,2}}{f_{y,1}} \frac{t_2}{t_1}$$

(Eq. 7.44)

The power b can be obtained by following similar steps as those to determine the power a and taking $t_2 / t_1 = 1.001$ and $f_{y,2} / f_{y,1} = 1.001$.

The power c may be subsequently obtained as follows.

Considering two columns of the same height but different outer-dimensions B_1 and B_2, H_1 and H_2, different thickness t_1 and t_2, and different material properties, $f_{y,1}$ and $f_{y,2}$, the ratio of their capacities is given by:

$$\frac{P_2}{P_1} = \frac{Xf_{y,2}{}^a t^b (B+H)^c}{Xf_{y,1}{}^a t^b (B+H)^c}$$

$$= \frac{f_{y,2}{}^a}{f_{y,1}{}^a} \frac{t_2{}^b}{t_1{}^b} \frac{(B_2+H_2)^c}{(B_1+H_1)^c}$$

$$= (\frac{f_{y,2}}{f_{y,1}})^a (\frac{t_2}{t_1})^b (\frac{B_2+H_2}{B_1+H_1})^c$$

$$\Rightarrow \ln(\frac{P_2}{P_1}) = \ln[(\frac{f_{y,2}}{f_{y,1}})^a (\frac{t_2}{t_1})^b (\frac{B_2+H_2}{B_1+H_1})^c]$$

$$= a\ln(\frac{f_{y,2}}{f_{y,1}}) + b\ln(\frac{t_2}{t_1}) + c\ln(\frac{B_2+H_2}{B_1+H_1})$$

$$\therefore \quad c = \frac{\ln(\frac{P_2}{P_1}) - a\ln(\frac{f_{y,2}}{f_{y,1}}) - b\ln(\frac{t_2}{t_1})}{\ln(\frac{B_2+H_2}{B_1+H_1})}$$

(Eq. 7.45)

And, due to the difference in f_y, t, B and H, the reduction factor for local buckling ρ_c of the two columns is also different:

$$\frac{\dfrac{\beta_2}{\varepsilon_2}}{\dfrac{\beta_1}{\varepsilon_1}} = \frac{\dfrac{(\dfrac{b_2}{t_2})}{\sqrt{\dfrac{250}{f_{y,2}}}}}{\dfrac{(\dfrac{b_1}{t_1})}{\sqrt{\dfrac{250}{f_{y,1}}}}} \approx \sqrt{\frac{f_{y,2}}{f_{y,1}}}\,\frac{t_1}{t_2}\,\frac{B_2}{B_1} \qquad \text{(Eq. 7.46)}$$

and,

$$\frac{P_2}{P_1} = \frac{2(B_2 + H_2)t_2\rho_{c,2}f_{y,2}}{2(B_1 + H_1)t_1\rho_{c,1}f_{y,1}}$$

$$= \frac{\rho_{c,2}}{\rho_{c,1}}\,\frac{f_{y,2}}{f_{y,1}}\,\frac{t_2}{t_1}\,\frac{(B_2 + H_2)}{(B_1 + H_1)} \qquad \text{(Eq. 7.47)}$$

The power c can be obtained by following similar steps as those to determine the power a and taking $B_2/B_1 = H_2/H_1 = 1.001$, $t_2/t_1 = 1.001$ and $f_{y,2}/f_{y,1} = 1.001$.

The relationship between the three powers (a, b and c) and the cross-section slenderness β/ε is plotted in Fig. 7.2. The values of the parameters are calculated based on high strength aluminium alloys, which is Class A material. By observing the figure, it is found that non-slender sections with low slenderness ($\beta/\varepsilon \le 22$), ρ_c is a constant equal to 1.0 and hence the powers $a = b = c = 1$. While regarding for slender sections with high slenderness ($\beta/\varepsilon > 22$), as the section becomes more slender, the capacity of stub columns P is more dependent on thickness, but less dependent on the material properties (f_y) and outer dimensions (B and H).

The curves can be interpreted that when a section becomes more slender, its yield strength becomes less important in calculating its capacity; on the other hand, its thickness becomes more sensitive, but its outer dimensions become less sensitive. The slenderness of a very slender section is more important than strength.

199
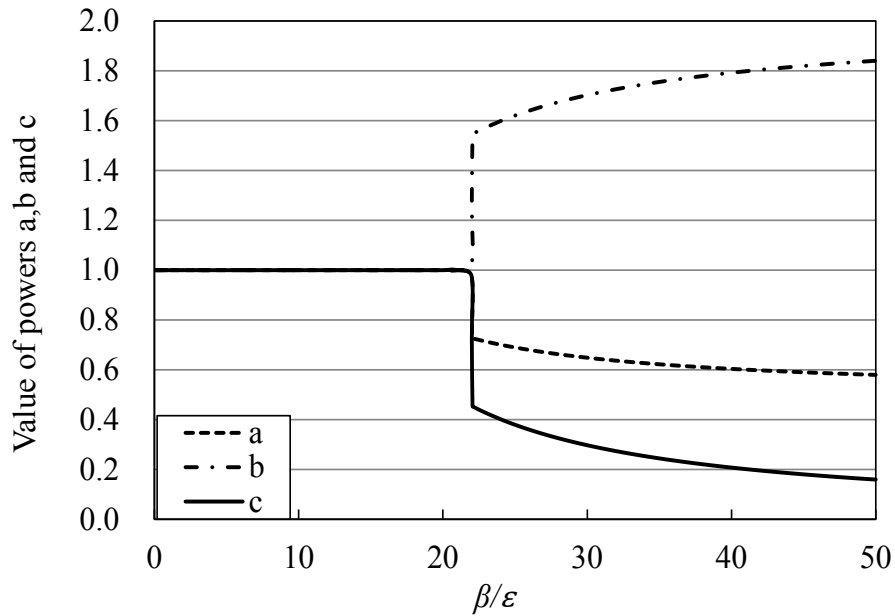
Fig. 7.2   The powers *a*, *b* and *c* versus non-dimensional slenderness

parameter β/ε for stub columns

7.7.2 Pure bending of Class 4 sections

Similar to stub columns, the flexural resistance of Class 4 sections is seen to depend on the reduction factor ρ_c, the material yield strength f_y and the section modulus W_{el} (see Chapter 6.3.4). However, the basic variables are not independent on these design expressions. The dependence of the basic variables in the flexural resistance function should be separated. A procedure for separating the dependence of the basic variables for bending design of Class 4 SHS/RHS (see Fig. 3.1) is described herein.

Some assumptions have to be made:

1) Negligible movement for neutral axis.
2) $t \ll B$ and H

$$W_{el} = \frac{I}{y}$$

$$= \frac{\dfrac{BH^3}{12} - \dfrac{bh^3}{12}}{\dfrac{H}{2}}$$

$$= \frac{2tH^3 + bH^3 - bh^3}{6H}$$

$$\because \quad h^3 = (H - 2t)^3 = H^3 - 6H^2 t + 12Ht^2 - 8t^3$$

$$H^3 - h^3 = 6H^2 t - 12Ht^2 + 8t^3$$

$$\therefore$$

$$Wel = \frac{2tH^3 + b(6H^2 t - 12Ht^2 + 8t^3)}{6H}$$

$$\approx \frac{2tH^3 + b(6H^2 t)}{6H}$$

$$= \frac{tH^2 + (B - 2t)3Ht}{3}$$

$$\approx \frac{tH^2 + 3HBt}{3}$$

$$= t(\frac{H^2 + 3HB}{3})$$

$$\frac{Weff}{Wel} = \frac{t_{eff}(\dfrac{H^2 + 3HB}{3})}{t(\dfrac{H^2 + 3HB}{3})} = \frac{t_{eff}}{t} = \rho_c \qquad \text{(Eq. 7.48)}$$

3) $\because \quad t << B$ and H

$$\therefore \frac{b_2}{b_1} = \frac{(B_2 - 2t_2)}{(B_1 - 2t_1)} \approx \frac{B_2}{B_1} \qquad \text{(Eq. 7.49)}$$

The procedure for separating the dependence of the basic variables is shown below:

$$M = W_{eff} f_y$$
$$= \rho_c W_{el} f_y$$
$$= (\frac{3BH + H^2}{3}) t \rho_c f_y \qquad \text{(Eq. 7.50)}$$
$$= K f_y{}^a t^b (3BH + H^2)^c$$

where K is a constant, independent of f_y, t and $(B+H)$. The powers a, b and c vary for different slenderness and should be computed for each test specimen.

Similar approaches are adopted to derive the power a, b and c. Key expressions are listed below.

The power a can be found by:

Assumptions: $t_2 = t_1$, $3B_1 H_1 + H_1{}^2 = 3B_2 H_2 + H_2{}^2$ and $f_{y,2}/f_{y,1} = 1.001$

$$a = \frac{\ln(\frac{M_2}{M_1})}{\ln(\frac{f_{y,2}}{f_{y,1}})} \qquad \text{(Eq. 7.51)}$$

$$\frac{M_2}{M_1} = \frac{\rho_{c,2}}{\rho_{c,1}} \frac{f_{y,2}}{f_{y,1}} \qquad \text{(Eq. 7.52)}$$

$$\frac{\frac{\beta_2}{\varepsilon_2}}{\frac{\beta_1}{\varepsilon_1}} = \sqrt{\frac{f_{y,2}}{f_{y,1}}} \qquad \text{(Eq. 7.53)}$$

The power b can be found by:

Assumptions: $3B_1 H_1 + H_1{}^2 = 3B_2 H_2 + H_2{}^2$, $f_{y,2}/f_{y,1} = 1.001$ and $t_2/t_1 = 1.001$

$$b = \frac{\ln(\frac{M_2}{M_1}) - a \ln(\frac{f_{y,2}}{f_{y,1}})}{\ln(\frac{t_2}{t_1})} \qquad \text{(Eq. 7.54)}$$

$$\frac{M_2}{M_1} = \frac{\rho_{c,2}}{\rho_{c,1}} \frac{f_{y,2}}{f_{y,1}} \frac{t_2}{t_1}$$

(Eq. 7.55)

$$\frac{\dfrac{\beta_2}{\varepsilon_2}}{\dfrac{\beta_1}{\varepsilon_1}} = \sqrt{\frac{f_{y,2}}{f_{y,1}}} \frac{t_1}{t_2}$$

(Eq. 7.56)

The power c can be found by:

Assumptions: $f_{y,2}/f_{y,1} = 1.001$, $t_2/t_1 = 1.001$ and $B_2/B_1 = H_2/H_1 = 1.001$

$$c = \frac{\ln(\dfrac{M_2}{M_1}) - a \ln(\dfrac{f_{y,2}}{f_{y,1}}) - b \ln(\dfrac{t_2}{t_1})}{\ln(\dfrac{3 B_2 H_2 + H_2^{\,2}}{3 B_1 H_1 + H_1^{\,2}})}$$

(Eq. 7.57)

$$\frac{M_2}{M_1} = \frac{\rho_{c,2}}{\rho_{c,1}} \frac{f_{y,2}}{f_{y,1}} \frac{t_2}{t_1} \frac{(3 B_2 H_2 + H_2^{\,2})}{(3 B_1 H_1 + H_1^{\,2})}$$

(Eq. 7.58)

$$\frac{\dfrac{\beta_2}{\varepsilon_2}}{\dfrac{\beta_1}{\varepsilon_1}} = \sqrt{\frac{f_{y,2}}{f_{y,1}}} \frac{t_1}{t_2} \frac{B_2}{B_1}$$

(Eq. 7.59)

The relationship between the three powers (a, b and c) and the cross-section slenderness β/ε is plotted in Fig. 7.3. Note that the curves for the powers a and c are overlay. The values of the parameters are calculated based on high strength aluminium alloys, which is Class A material. In terms of non-slender sections with low slenderness ($\beta/\varepsilon \le 22$), ρ_c equals to unity and $a = b = c = 1$, which indicates the independence between variables. As for slender sections with high slenderness ($\beta/\varepsilon > 22$), the capacity of simply supported beam is more dependent on thickness, in the other word, the change in thickness t is more sensitive than the change of f_y, B and H.
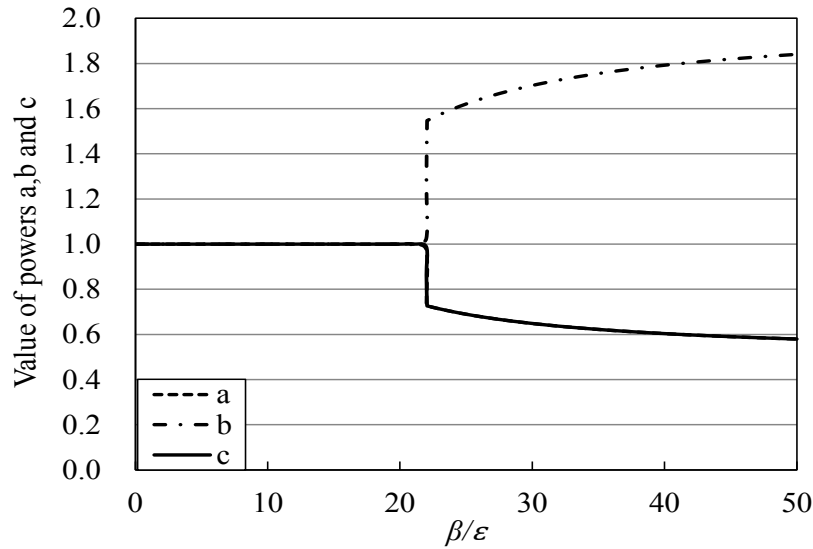
Fig. 7.3   The powers *a, b* and *c* versus non-dimensional slenderness parameter β/ε for simply supported beams

7.8 Results and discussions

Reliability analyses have been performed to verify the reliability level of the newly proposed CSM approach and the three exiting international specifications for the capacity prediction of stub columns, simply supported beams and continuous beams. Two analysis approaches, i.e. EN1990 (2002) and the AISC (2010), were employed.

7.8.1 Stub columns

A total of 346 stub column test results are used in the analyses. The reliability indices β were found to be 2.32, 2.61, 2.61 and 2.54 for the AA (2010), the AS/NZS (1997), EC9 (2007) and Annex F in EC9 (2007), when adopting their own specified load combination and resistance factors (see Table 7.2). If the load combination and resistance factor specified in the AA (2010) are adopted for all methods, the comparison is called direct comparison. It is found that the reliability indices β_2 of all methods satisfy the target value 2.50 except the AA.

204

Thus, all methods except the AA can be deemed to be reliable for aluminium alloy stub column capacity predictions. The reliability analyses by the EN1990 approach obtained partial factor γ_{M0} greater than 1.10 for all design methods (Table 7.2). The calculated partial factor γ_{M0} for the CSM (γ_{M0}=1.35) is the smallest one comparing with other specifications. The CSM is more reliable than the existing design specifications, and hence, it can be deemed to be a relatively safe design method for capacity prediction of cross-sections in compression.

Table 7.2   Results of statistical analyses of stub column design methods in the CSM and the three international design specifications

	$\dfrac{P_u}{P_{AA}}$	$\dfrac{P_u}{P_{AS/NZS}}$	$\dfrac{P_u}{P_{EC9}}$	$\dfrac{P_u}{P_{EC9-F}}$	$\dfrac{P_u}{P_{csm}}$
Mean, P_m	1.19	1.28	1.18	1.17	1.04
COV, V_p	0.251	0.250	0.168	0.169	0.090
ϕ	0.90	0.85	0.91	0.91	---
β	2.32	2.61	2.61	2.54	---
ϕ_2 (direct comparison)	0.90	0.90	0.90	0.90	0.90
β_2 (direct comparison)	2.32	2.54	2.74	2.67	2.57
γ_{M0}	1.60	1.52	1.38	1.51	1.35

7.8.2 Simply supported beams

A total of 208 simply supported beams on SHS/RHS and I-sections were used in the reliability analyses. The reliability index β of the CSM was found to be 2.79 by the AISC approach, and the partial factor γ_{M0} is 1.25 according to EN1990 (Table 7.3). The AA approach validates that the CSM is safe based on a resistance factor ϕ = 0.90, but the EN1990 approach negates the reliability of the five design models (i.e. the AA, the AS/NZS, EC9, Annex F of EC9 and the CSM) for a partial factor of 1.10 (equivalent to ϕ = 0.91). The calculated γ_{M0} of the CSM (γ_{M0} = 1.25) is smaller than those for the AA and the AS/NZS, which indicates that the design model of the CSM is reasonably acceptable.

A series of 71 experimental and numerical bending results on stiffened SHS/RHS were employed herein. The reliability index β is 2.63 for the CSM (Table 7.4), which is greater than 2.50 and thus the CSM can be deemed as reliable according to the AISC requirements. However, the calculated value of γ_{M0} for the CSM is found to be 1.48, which is greater than the target value of 1.10 (Table 7.4); other specifications also obtained similar values for γ_{M0}. It is therefore indicated that the bending resistance design functions for stiffened SHS/RHS in the CSM can achieve the similar level of reliability as the AA and AS/NZS.

Table 7.3   Results of statistical analyses of simply supported beam (of SHS/RHS) design methods in the CSM and the three international design specifications

	$\dfrac{M_u}{M_{AA}}$	$\dfrac{M_u}{M_{AS/NZS}}$	$\dfrac{M_u}{M_{EC9}}$	$\dfrac{M_u}{M_{EC9-F}}$	$\dfrac{M_u}{M_{csm}}$
Mean, P_m	1.27	1.39	1.26	1.21	1.14
COV, V_p	0.187	0.212	0.159	0.109	0.114
ϕ	0.90	0.85	0.91	0.91	---
β	2.88	3.09	2.90	2.92	---
ϕ_2 (direct comparison)	0.90	0.90	0.90	0.90	0.90
β_2 (direct comparison)	2.88	3.01	3.02	3.06	2.79
γ_{M0}	1.31	1.27	1.21	1.16	1.25

Table 7.4   Results of statistical analyses of simply supported beam (of SHS/RHS with internal cross stiffeners) design methods in the CSM and the three international design specifications

	$\dfrac{M_u}{M_{AA}}$	$\dfrac{M_u}{M_{AS/NZS}}$	$\dfrac{M_u}{M_{EC9}}$	$\dfrac{M_u}{M_{EC9-F}}$	$\dfrac{M_u}{M_{csm}}$
Mean, P_m	1.40	1.66	1.35	1.27	1.18
COV, V_p	0.207	0.233	0.188	0.150	0.153
ϕ	0.90	0.85	0.91	0.91	---
β	3.07	3.47	2.64	2.65	---
ϕ_2 (direct comparison)	0.90	0.90	0.90	0.90	0.90
β_2 (direct comparison)	3.07	3.40	2.76	2.78	2.63
γ_{M0}	1.48	1.38	1.47	1.42	1.49

7.8.3 Continuous beams

In terms of 147 five-point bending beams of SHS/RHS, results of the statistical analyses are tabulated in Table 7.5. By observing results of the CSM, the reliability index β was found to be 3.12, which is much greater than the target value of 2.50 and signifies safe predictions. The partial factor γ_{M0} was found to be 1.38, failed to satisfy the codified value of 1.10, but better than the calculated values of γ_{M0} for EC9 (γ_{M0} =1.49). The CSM may be adopted for continuous beams on tubular sections and provides results with similar reliability level as EC9.

The data pool for continuous beams of SHS/RHS with internal stiffeners contains 110 results. The design models for stiffened hollow sections all obtained the calculated index β greater than 2.50 (see Table 7.6). It is therefore recommended by the AISC that the CSM as well as the three aforementioned specifications can be safely applied to continuous beams on SHS/RHS with internal stiffeners. However, all the five design methods failed to satisfy the target partial safety factor (1.10) stated in EC9 (see Table 7.6). The partial factor γ_{M0} was found to be 1.43 for the CSM, which is slightly greater than EC9 (γ_{M0}=1.37). From the view of the EN1990 approach, the CSM is an unsafe design method for continuous beams on stiffened SHS/RHS. The large difference between the statistical results obtained from the AISC and EN1990 approaches suggested that further investigations are required to justify the CSM as a safe method for continuous beams with stiffened SHS/RHS. However, the reliability index β is greater than 2.5 for the CSM; therefore, the CSM can be assumed to provide similar reliability level as EC9.

Table 7.5   Results of statistical analyses of continuous beam (of SHS/RHS)

design methods in the CSM and the three international design specifications

	$\dfrac{F_u}{F_{AA}}$	$\dfrac{F_u}{F_{AS/NZS}}$	$\dfrac{F_u}{F_{EC9}}$	$\dfrac{F_u}{F_{EC9-H}}$	$\dfrac{F_u}{F_{csm}}$
Mean, P_m	1.71	1.88	1.63	1.42	1.34
COV, V_p	0.256	0.275	0.212	0.203	0.161
ϕ	0.90	0.85	0.91	0.91	---
β	3.34	3.53	3.42	2.91	---
ϕ_2 (direct comparison)	0.90	0.90	0.90	0.90	0.90
β_2 (direct comparison)	3.34	3.47	3.53	3.02	3.12
γ_{M0}	1.36	1.32	1.26	1.45	1.38

Table 7.6   Results of statistical analyses of continuous beam (of SHS/RHS

with internal cross stiffeners) design methods in the CSM and the three

international design specifications

	$\dfrac{F_u}{F_{AA}}$	$\dfrac{F_u}{F_{AS/NZS}}$	$\dfrac{F_u}{F_{EC9}}$	$\dfrac{F_u}{F_{EC9-H}}$	$\dfrac{F_u}{F_{csm}}$
Mean, P_m	1.70	2.02	1.63	1.37	1.25
COV, V_p	0.251	0.276	0.236	0.178	0.165
ϕ	0.90	0.85	0.91	0.91	---
β	3.34	3.70	3.24	2.88	---
ϕ_2 (direct comparison)	0.90	0.90	0.90	0.90	0.90
β_2 (direct comparison)	3.34	3.64	3.34	3.00	2.79
γ_{M0}	1.33	1.23	1.33	1.37	1.43

7.8.4 Cross-section class limits

In order to validate the slenderness limits proposed in Chapter 6.5 achieving a consistent level of safety, incorporating the uncertainty in the test and numerical results and variability of the basic variables in the design expressions, reliability analyses in accordance with EN1990 (2002) were performed.

The reliability analyses were performed for each class limit following three steps. First, the conventional partial safety factor γ_{M0}' is derived from the EN1990

approach (2002), and it means that the mean curve should be reduced by a factor of γ_{M0}' to provide a reliable design curve. Second, a least square regression is conducted to fit the data set, as plotted in Fig. 7.4 - Fig. 7.7. Third, the best fit model is then scaled down by the required safety factor γ_{M0}', and now the partial safety factor γ_{M0} for each class can be derived in accordance to the codified criteria for that behaviour class. In this approach, the reference line that the data points refer to is the best fit model curve instead of the mean curve, and it can be deemed to be a more rational way to estimate the variations. In addition, the merit of this statistical approach is that the partial safety factor can benefit from the over-strength results.

7.8.4.1 Stub columns

Due to the fact that the number of internal elements of Class B material is too scarce to perform reliability analyses, so the 11 results of Class B material were combined with those of Class A material, as shown in Fig. 7.4(a). A least squares regression fit to the available data set is also plotted in Fig. 7.4(a), which is then scaled down by the required safety factor of 1.26 obtained from the reliability analyses. The γ_{M0} for Class 3 limit of internal elements under uniform compression ($\beta/\varepsilon = 22$) was found to be 1.25, greater than 1.10. However, the proposed Class 3 limit maintains the same as the current codified value. Hence, it is indicated that although the evaluated value of γ_{M0} for internal elements is higher than 1.10, the proposed and existing Class 3 limits achieve similar reliability level. Following similar procedures, the evaluated safety factor γ_{M0} of 1.14 was found for outstand elements, as illustrated in Fig. 7.4 (b). Since the evaluated value is only slightly higher than 1.10, it is reasonably acceptable.

The reliability analyses were also performed to validate the Class 3 limit in the CSM slenderness framework. As demonstrated in Fig. 7.5, the calculated safety

factor for Class 3 limit including types of elements was found to be 1.32. The Class 3 limit is proposed as $\bar{\lambda}_p = 0.68$, which corresponds to the existing limit of β/ε=22. This proposed limit might be seen to achieve similar safety level, though evaluated safety factor is greater than the target value of 1.10. In addition, the transaction limit in the DSM between slender and non-slender sections is determined as $\bar{\lambda}_p = 0.776$ for carbon steel (Schafer and Peköz, 1998) and $\bar{\lambda}_p = 0.713$ for aluminium alloys (Zhu and Young, 2009). The proposed value of 0.68 is more conservative than both DSM limits, while the DSM (Schafer and Peköz, 1998; Zhu and Young, 2009) have been validated by reliability analyses and safely used by metallic materials.
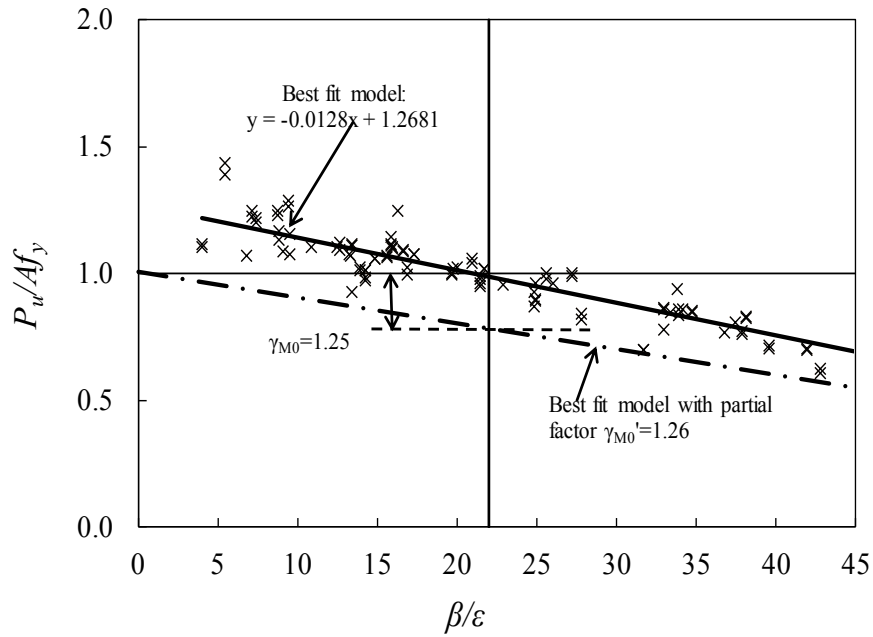
(a) Internal elements
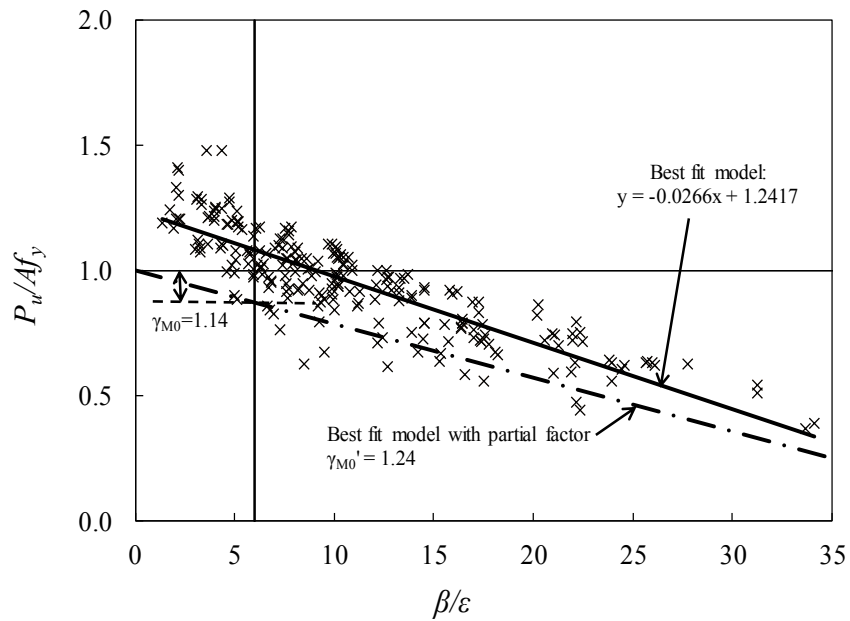
(b) Outstand elements

Fig. 7.4   Determination of γ_{M0} for the best fit model for class 3 limit in the

EC9 framework (by stub column data)
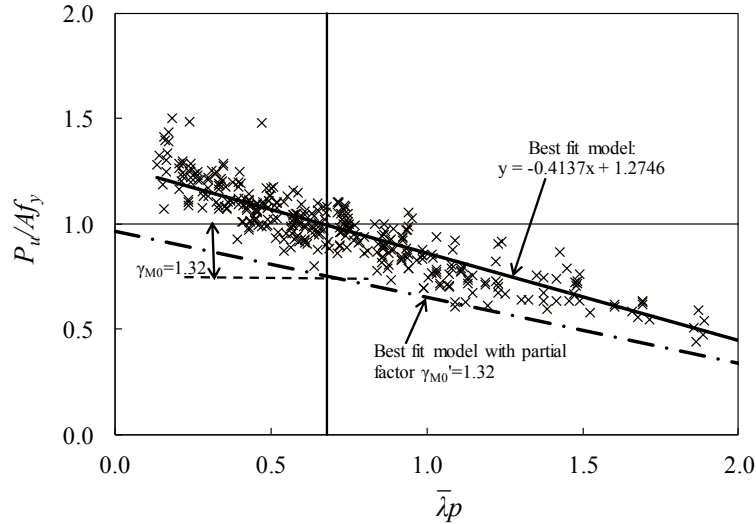
Fig. 7.5   Determination of γ_{M0} for the best fit model in the CSM slenderness

framework (by stub column data)

7.8.4.2 Simply supported beams

Statistical analyses were also performed based on the bending data to verify the proposed classification limits. In terms of the limits in the EC9 framework, the key statistical parameters and results are shown in Fig. 7.6. The calculated value of γ_{M0} for both Buckling Class A and B materials were found to be less than or equal to 1.10 for all class limits. Meanwhile, the limits in the CSM slenderness framework were also evaluated by means of statistical analyses (See Fig. 7.7). The evaluated values of γ_{M0} were found to be 0.45, 1.12 and 1.08 for Class 1, 2 and 3 limits, respectively, which were either smaller than 1.10 or slightly greater than 1.10. Hence, it can be concluded that the two newly proposed limit sets are reliable and applicable to aluminium alloy internal elements under bending. It might be noted that the reliability results assessed on the basis of bending tests are in contrast the findings of the stub column tests: the Class 3 limit is suitable and relax for bending sections, while it fails to achieve the target value of 1.10 for compressive sections. Similar observations have been reported by Gardner et al. (2010). Possible reasons can be the less onerous stress distribution in the web and therefore additional support offered to the compression flange (Gardner et al., 2010).

212
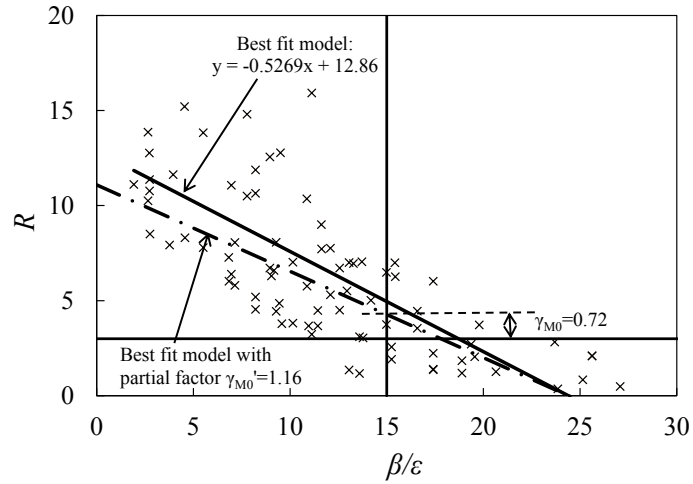
(a) Buckling Class A materials with Class 1 limit
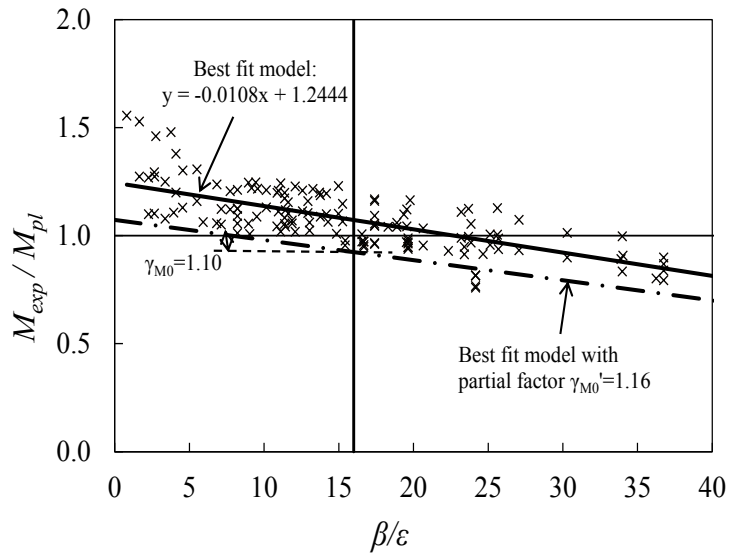
(b) Buckling Class A materials with Class 2 limit
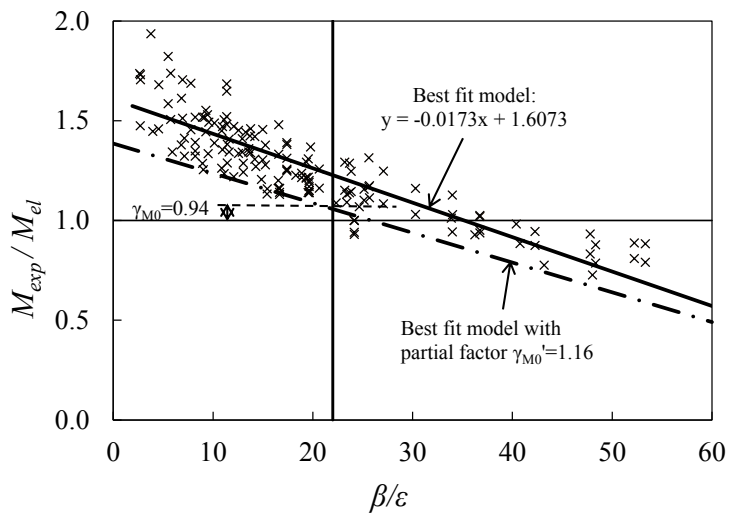
(c) Buckling Class A materials with Class 3 limit

Fig. 7.6 (cont'd)

213
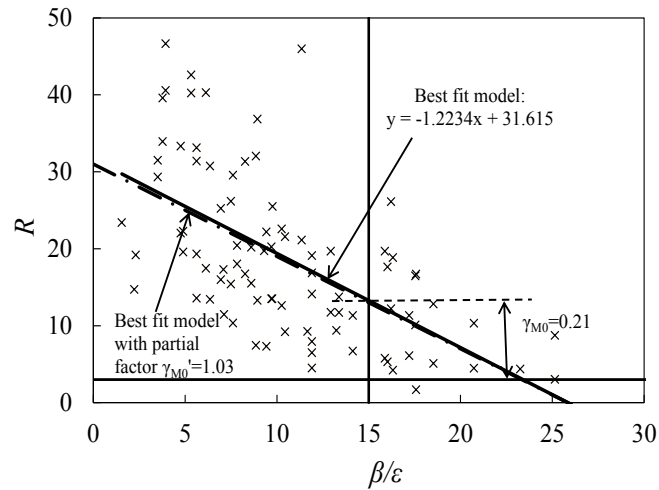
(d) Buckling Class B materials with Class 1 limit
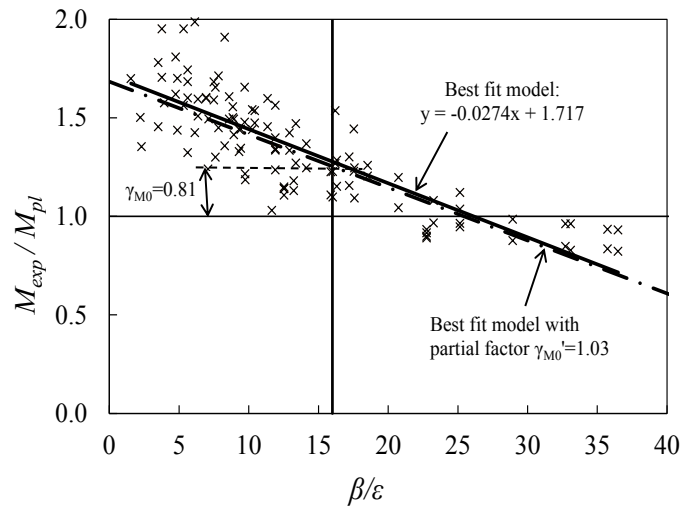
(e) Buckling Class B materials with Class 2 limit
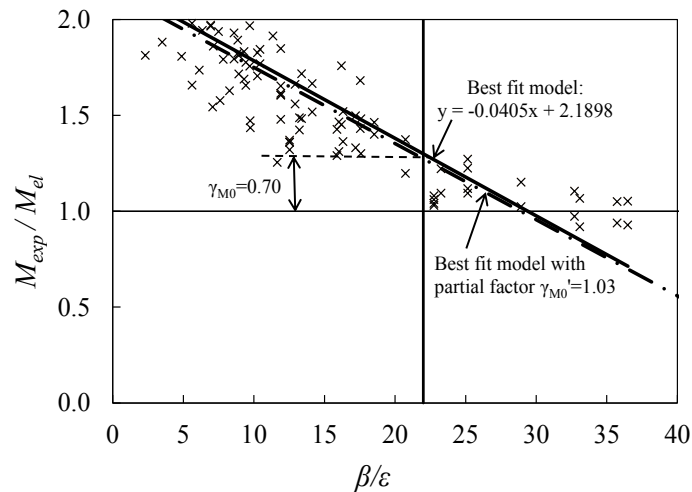
(f) Buckling Class B materials with Class 3 limit

Fig. 7.6   Determination of γ_{M0} for the best fit model for class limits of internal elements in the EC9 framework (by simply supported beam data)

(a) Class 1 limit

Best fit model:
y = -39.256x + 25.104

Best fit model with
partial factor $\gamma_{M0}'=1.30$

$\gamma_{M0}=0.45$

R

$\overline{\lambda}p$

(b) Class 2 limit

Best fit model:
y = -0.6379x + 1.4667

$\gamma_{M0}=1.12$

Best fit model with
partial factor $\gamma_{M0}'=1.30$

M_{exp}/M_{pl}

$\overline{\lambda}p$

(c) Class 3 limit

Best fit model:
y = -0.9295x + 1.8629

$\gamma_{M0}=1.08$

Best fit model with
partial factor $\gamma_{M0}'=1.30$

M_{exp}/M_{el}

$\overline{\lambda}p$
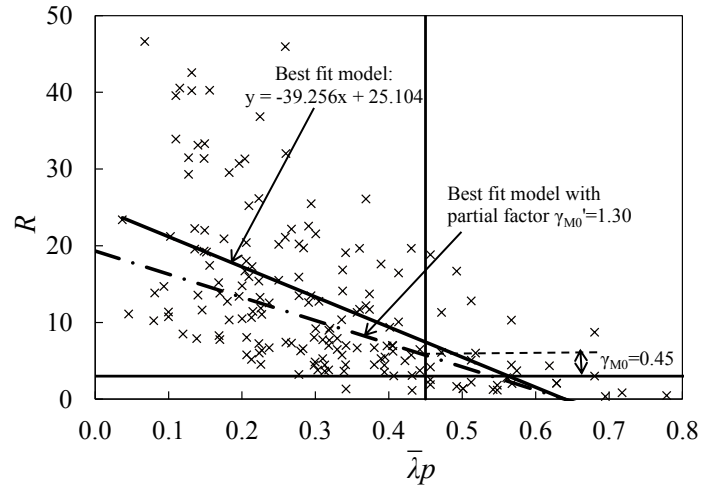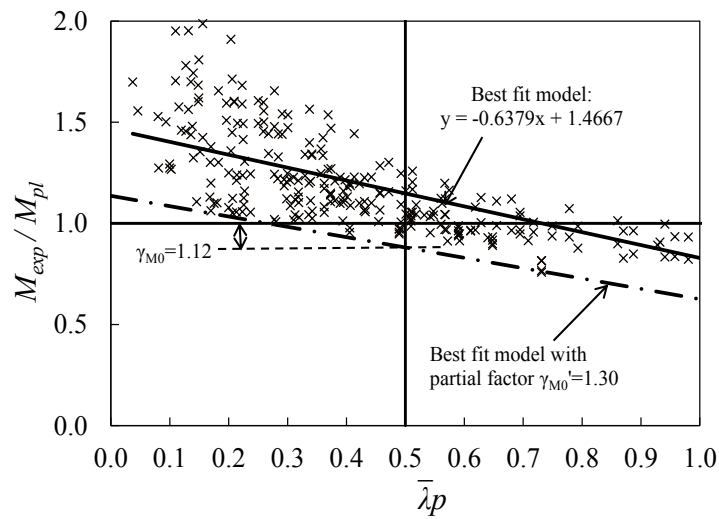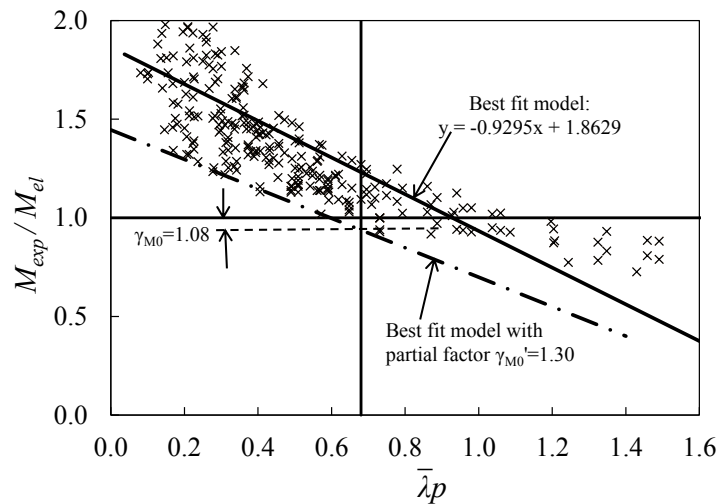
Fig. 7.7　　Determination of γ_{M0} for the best fit model for class limits of internal elements in the CSM slenderness framework (by simply supported beam data)

215

7.9 Summary

A large number of aluminium alloy test and FE results were used to evaluate the reliability level of the exiting design standards and the proposed CSM approach, including: 346 stub columns, 208 simply supported beams of SHS/RHS, 71 simply supported beams of stiffened SHS/RHS, 147 continuous beams of SHS/RHS and 110 continuous beams of stiffened SHS/RHS. Both European and American approaches were employed herein to assess the design methods in accordance to the specified reliability criteria.

When using the American approach, the reliability indices β of the three current specifications are from 2.32 to 3.53, with mostly greater than 2.50. The reliability indices of the CSM are all greater than 2.50. It may be concluded that the aforementioned three design specifications were found to be either too conservative in some cases or unsafe in others; however, the CSM can generally provide reliable design resistance predictions for aluminium alloy stub columns, using a resistance factor $\phi = 0.9$.

When using the Eurocode approach, the resistance factors γ_{M0} for the three specifications are from 1.16 to 1.51. The partial factors γ_{M0} were found to be between 1.25 and 1.49 for the CSM. It seems that the design methods are not considered sufficiently safe according to the criteria of EN1990. Since γ_{M0} of the CSM is generally smaller than those three specifications, the CSM can be considered as reasonably acceptable and offering similar reliability as existing design specifications.

Reliability analyses have also been performed to validate the proposed limits in two classification frameworks according to EN1990 (2002). Both stub column and simply supported beam results were used. The newly proposed class limits

have been shown to be safe and more accurate for aluminium alloy cross-sections.

CHAPTER 8

CONCLUSIONS AND SUGGESTIONS FOR

FUTURE RESEARCH

This chapter summarises the key research findings and overall conclusions of this project. Some recommendations for future research are also presented.

8.1   Concluding remarks

Current aluminium alloy structural design is based largely on elastic analysis. At the cross-sectional level, the yield limit has been determined as the upper bound of the section capacity, while at the global system level, the global elastic analysis (structure fails at the formation of the first hinge) is adopted by most of the design specifications. The primary objective of this study has therefore been to develop a more rational and efficient design method for aluminium alloy structures by safely exploiting strain hardening and moment redistribution. The process of developing the new method has involved the following: collecting available test results from previous studies, conducting laboratory tests, developing finite element models for parametric studies, reviewing existing design rules, proposing new design methods and validating it by reliability analysis. This process has predominantly defined the shape and flow of the thesis.

The literature review reveals the significant effect of strain hardening and moment redistribution, as well as the limited experimental data on aluminium alloy stocky sections, especially continuous beam tests. Meanwhile, some relevant data were collected from literature, including 331 stub column tests on SHS/RHS, angles and channels, 48 simply supported beam tests on SHS/RHS and I-sections.

The experimental investigation on the behaviour and strength of aluminium alloy structural members was performed. This test programme included 11 stub columns, 40 simply supported beams and 46 continuous beams. The cross-sections of specimens were square and rectangular hollow sections with or without internal cross stiffeners. Two aluminium alloys, namely 6061-T6 and 6063-T5, were involved in the investigation. The material properties of the test specimens were obtained from tensile coupon tests. More than 50% strain hardening in the aluminium alloy materials was observed from the tensile coupon tests. Meanwhile, all tested specimens achieved greater member capacities than the theoretical yielding limits.

Numerical investigations were performed on simply supported beams and continuous beams. A nonlinear finite element software ABAQUS was employed to develop numerical models. Numerical predictions of the key performance achieved a high degree of accuracy, with a mean value of tested-to-numerical ultimate load ratio within 5% and a low variation less than 10%. Upon validation against the experimental data, the FE models were employed in the parametric studies to generate 192 results for simply supported beams and 210 for continuous beams. The slenderness ratio b/t of the cross-sections has been extended to a wider range from 0.88 to 55.14, covering the four cross-section classes specified in Eurocode 9. The experimental and numerical data newly generated in this study have become a major contribution to the pool of available results on aluminium alloy structures.

The proposed design method, the continuous strength method (CSM), was initially developed for stainless steel structures, whereas the aforementioned data pool together with the data in the literature were used to study the feasibility of applying the CSM to aluminium alloy structural members. The CSM is a

219

deformation-based method and employs a base curve to define a continuous relationship between the cross-section slenderness and the deformation capacity. Two key components of the CSM, a base curve and a bi-linear material model, were examined, revised and proposed in this study. The base curve has been extended to the slender section range for all metallic materials and the elastic, linear hardening material model is calibrated specifically for aluminium alloys in the present study. The significance of strain hardening and moment redistribution in aluminium alloy structures was explored and rationally exploited by the continuous strength method (CSM). In addition, the interaction effect between component elements was also considered in the CSM using cross-section plate slenderness for the section as a whole, which has been suggested to be derived by analytical approximations or a numerical approach. Worked examples were provided to demonstrate the design steps in the proposed CSM approach for aluminium alloy structural members.

Comparisons of the experimental and numerical results with the design strengths of the American, Australian/New Zealand and European specifications as well as the continuous strength method (CSM) for aluminium alloy structures, have been performed. It was found that the predictions of the three design specifications are more conservative for stocky cross-sections with up to 50% underestimation, due to the occurrence of strain hardening. The design strengths predicted by the continuous strength method, which allows for the systematic exploitation of strain hardening, were found up to 30% more accurate and 40% more consistent than predictions of the existing design methods. The reasons for the good performance of the continuous strength method can also be directly related to the employment of global plastic design and the proposed base curve defining the continuous relationship between the cross-section slenderness and the deformation capacity.

A comprehensive assessment of the existing section classification in EC9 was carried out, and revealed the conservatism in the current classification system. The feasibility of harmonising limits for Buckling Class A and B aluminium alloys was investigated, after which a set of unified limits for different aluminium alloy tempers are recommended in the EC9 framework for internal elements. In addition, a classification framework, using the CSM slenderness as the parameter, has been proposed. Within the CSM slenderness framework, element interaction is considered, meanwhile effects from material tempers, section geometries and stress gradients are incorporated in a unified set of class limits. Corresponding effective thickness formulae for Class 4 sections were proposed for both classification frameworks.

In order to validate the proposed design method, reliability analyses have been performed for the CSM as well as the three existing design specifications. Standardized statistical evaluation procedures are provided in EN1990 (2002) and the AISC (2010) specifications. A series of reliability analyses has been performed for the design rules of stub columns, simply supported beams and continuous beams as well as cross-section class limits. The reliability of the CSM for determinate and indeterminate structures has been validated: the calculated reliability index of the CSM is either well passed the target value or better than the existing design specifications.

Overall, the objective of achieving a more rational and efficient design method for aluminium alloy structural members has been achieved. The proposed design method, the continuous strength method (CSM), has also been demonstrated to be safe and consistent for aluminium alloys. The CSM can be applied to cross-sections with a full range of slenderness. Furthermore, efforts have been made to keep consistency with the design of other metallic materials, such as

stainless steel and carbon steel. In the coming future, this improved design efficiency will lead to a considerable material saving in the industry.

8.2 Suggestions for future research

Based on the present study, suggestions for further work on design rules of aluminium alloys are proposed herein, relating to the extension of the proposed design method to some other potential application areas.

The current CSM is limited to flexural design of cross-sections symmetric about the bending axis. It has been assumed that strain hardening only influences the performance of non-slender sections. However, for other sections such as T-sections, angles or channels bent about un-symmetric axis, the slender sections might also be able to benefit from strain hardening on the tension flange in the case of the neutral axis being much closer to the compression flange. Further laboratory tests and numerical analyses are needed to validate the applicability of the CSM for sections bending about the un-symmetric axis.

Aluminium alloys are sensitive to high temperature; strength of aluminium alloys can be reduced by more than 50% at the heat affected zone. Thus, the design of aluminium alloy structural members at elevated temperatures should be investigated, and the CSM can be extended to cover aluminium alloy members at the fire limit state. Aluminium alloy material properties at elevated temperatures are also needed to be investigated.

In this study, an extension version of the CSM has been proposed for indeterminate structures. However, the CSM for indeterminate structures is currently restricted to continuous beams. Further investigations are however needed into other indeterminate configurations including frames. The internal moment redistribution

in indeterminate structures should be carefully examined before reaching more general conclusions for indeterminate structures.

The scope of the CSM is mainly focused on determination of cross-section resistance only. However, strain hardening has effects on the buckling resistance for members of non-slender sections. Further study is clearly required to extend the CSM to the global member level for both columns (flexural buckling and torsional buckling) and beams (lateral torsional buckling). The attainment of individual buckling modes as well as interaction between different buckling modes could be investigated and covered by the CSM design rules.

The existing and newly proposed classification limits were assessed based on mostly closed sections, due to the scope of the present study and limited experimental data. In this study, the assessment and revision of class limits were mainly focused on internal elements. Hence, cross-section compression and flexural capacity data on sections with outstand elements, of different material tempers, are needed. Subsequently, class limits for outstand elements could be reviewed and proposed.

REFERENCES

ABAQUS (2010). *Analysis user's manual, version 6.10-1*, Dassault Systemes Simulia Corp., USA

Afshan, S. and Gardner, L. (2013) "The continuous strength method for structural stainless steel design" *Thin-Walled Structures*, 68(2013): 42-49

Aluminum Association (2008), Tornado Tower Earns 'Best Tall Building' Award. Access on Feb27, 2012.
<http://www.tupian99.com/show-1-54-35a0d31d0156fe80.html>

Aluminum Association (AA). (2010). *Aluminum design manual*. Washington, D.C.

Aluminum Company of Canada, Ltd (1940) *Arvida Bridge: First Aluminum Highway Bridge in the World, Arvida, Quebec, Canada*, Published by Aluminum Company of Canada Ltd, Canada.

American Institute of Steel Construction (AISC) (2010), *Specification for Structural Steel Buildings*, *ANSI/AISC 360-10*, Chicago, IL.

American Institute of Steel Construction (AISC) (2013), *Design Guide 27: Structural Stainless Steel*, Chicago, IL.

American Iron and Steel Institute (AISI) Commentary (2000), *Commentary on the Load and Resistance Factor Design Specification for Cold-formed Steel Structural Members*, Washington D.C., USA.

American Iron and Steel Institute (AISI). (2007). *North American Specification for the design of cold-formed steel structural members*, Washington, D. C.

American Iron and Steel Institute (AISI). (2012) *North American Specification for the design of cold-formed steel structural members*, Washington, D. C.

American Society for Testing and Materials (ASTM). (1997). *"Standard test methods for tension testing of metallic materials" E 8M-97*, West Conshohocken, Pa.

American Society for Testing and Materials (ASTM). (2010), *"Standard Test method for indentation hardness of aluminum alloys by means of a Webster hardness gage" ASTM B647-10*, West Conshohocken, Pa.

Ashraf, M., Gardner, L. and Nethercot, D. A. (2006), "Finite element modelling of structural stainless steel cross-sections", *Thin-Walled Structures*. 44(10): 1048-1062.

Ashraf, M. and Young, B. (2011). "Design formulations for non-welded and welded aluminium stub columns using Continuous Strength Method" *Engineering Structures*, 33(12): 3197-3207

Australian Standard (AS). (2007). *Methods for tensile testing of metals, AS 1391-2007*, Standards Association of Australia, Sydney, Australia.

Australian/New Zealand Standard (AS/NZS). (1997). A*luminum structures part 1: Limit state design, AS/NZS 1664.1:1997*, Standards Australia, Sydney, Australia.

Australian/New Zealand Standard AS/NZS. (2005), *Cold-formed steel structures, Australian/New Zealand Standard, AS/NZS 4600*, Standards Australia, Sydney, Australia.

Baehre, R. (1966), "Compression between structural behaviour of elastoplastic materials", *Tekn. Dr Arne Johnson Ingenjosbyra, Report No. 16*.

Badger, P. (2009), Liverpool South Parkway Bus Station, Access on Dec 20th, 2013. <.http://www.flickr.com/photos/salford_ian/3937973457/>

Bijlaard, P. P. and Fisher, G. P. (1953), *Column strength of H-sections and square tubes in post buckling range of component plates,* National Advisory Committee for Aeronautics Technical Note 2994, Washington

Bruneau, M., Uang, C. M. and Whittaker, A. (1998). *Ductile design of steel structures*. McGraw-Hill. New York.

British Standards (BS) (1991) *Structural use of aluminium: Part 1- code practice for design BS8118,* UK

Byfield, M. P. and Nethercot, D. A. (2001) "Eurocodes - failing to standardise safety", *Proceedings of the Institution of Civil Engineers - Structures and Buildings,* 144(4): 186-188

Canadian Standards Association (CSA) (2005), *Strength Design in Aluminum CSA-S157*, Canada.

Chan, T.M. and Gardner, L. (2008). "Bending strength of hot-rolled elliptical hollow sections." *Journal of Constructional Steel Research* 64(9): 971-986.

CIRIA Report (1977). *Rationalisation of safety and serviceability factors in structural codes. CIRIA*, No. 63.

Clark, J. W. (1974), *Statistical Aspects of Strength of Aluminum*, ALCOA Report No. 76-74-10, June 20, 1974

Dawson, R. G. and Walker, A. C. (1972), "Post-buckling of geometrically imperfect plates", *Journal of the Structural Division, ASCE*, 98(1): 75-94.

De Matteis, G., Landolfo, R., Manganiello, M. and Mazzolani, F.M. (2004) "Inelastic behaviour of I-shaped aluminium beams: numerical analysis and cross-sectional classification", *Computers and Structures,* 82 (23-26): 2157–2171.

De Matteis, G., Moen, L.A., Langseth, M., Landolfo, R., Hopperstad, O.S. and Mazzolani, F.M. (2001), "Cross-sectional classification for aluminium beams—parametric study", *Journal of Structural Engineering, ASCE,* 127(3): 271-279.

Dumont, C. and Hill, H.N. (1940), "Lateral stability of equal flanged aluminum alloy I-beams subjected to pure bending" *NACA TN 770*

Dwight, J. (1999) *Aluminium design and structure*, E & FN SPON, London, UK

Ellobody, E. and Young, B. (2005) "Structural performance of cold-formed high strength stainless steel columns", *Journal of Constructional Steel Research* 61(12): 1631–1649

European Committee for Standardization (EN 1990) (2002), "*Eurocode: Basis of Structural Design.*" *EN 1990-2002,* CEN.

European Committee for Standardization (EC3). (2006) "*Eurocode 3: Design of steel structures—Part 1-3: General rules – Supplementary rules for cold-formed members and sheeting*". *EN 1993-1-3:2006*, CEN.

European Committee for Standardization (EC3). (2006) "*Eurocode 3: Design of steel structures—Part 1-4: General rules – Supplementary rules for stainless steels*". *EN 1993-1-4:2006,* CEN.

European Committee for Standardization (EC9). (2007). "*Eurocode 9: Design of aluminum structures—Part 1-1: General rules—General rules and rules for buildings.*" *BS EN 1999-1-1:2007*, CEN.

Faella, C., Mazzolani, F.M., Piluso, V. and Rizzano, G. (2000), "Local buckling of aluminum members: testing and classification" *Journal of Structural Engineering, ASCE* 126(3): 353-360

Frey, F. and Mazzolani, F. M. (1977), "Buckling behaviour of aluminium-alloy extruded members" *International Colloquium on Stability of Steel Structures*, Liège, pp.85-94.

Galambos, T. V. (1979) *Load and Resistance Factor Design for Aluminum Structures*, Progress report to the Aluminum Association, Research Report No. 54. US.

Gardner, L. and Nethercot, D. A. (2001), "Numerical modelling of cold-formed stainless steel sections", *Proceedings of the Ninth Nordic Steel Construction Conference* (Edited by Mäkeläinen et al.), Helsinki, Finland, pp.781-789

Gardner, L. (2002). *A new approach to structural stainless steel design*. PhD thesis, Department of Civil and Environmental Engineering, Imperial College of Science, Technology and Medicine, London

Gardner, L. and Ashraf, M. (2006). "Structural design for non-linear metallic materials", *Engineering Structures* 28(6):926–934.

Gardner, L. (2008). "The continuous strength method", *Proceedings of the Institution of Civil Engineers - Structures and Buildings* 161(3):127-133.

Gardner, L. and Theofanous, M. (2008), "Discrete and continuous treatment of local buckling in stainless steel elements" *Journal of Constructional Steel Research* 64(11): 1207-1216

Gardner, L., Saari, N. and Wang F. (2010) "Comparative experimental study of hot-rolled and cold-formed rectangular hollow sections" *Thin-Walled Structures*, 48 (7): 495–507

Gardner, L., Wang, F. and Liew, A. (2011), "Influence of strain hardening on the behavior and design of steel structures." *International Journal of Structural Stability and Dynamics* 11(5): 855-875

Hasan, S. W. and Hancock, G. J. (1989). "Plastic bending tests of cold-formed rectangular hollow", *Steel Construction*, 23(4): 2-19

Hassinen, P. (2000), "Compression strength of aluminum columns – Experimental and numerical studies" *Proceedings of the 3rd International Conference on Coupled Instabilities of Metal Structures,* 241-248, CIMS'2000, ICP, London, UK

Hill, H. N. (1944), "Determination of stress-strain relations from the offset yield strength values". *Technical Note No. 927*. National Advisory Committee for Aeronautics. Washington, D. C.

Hill, H. N. and Clark, J. W. (1955), "Straight-line column formulas for aluminum alloys." *Alcoa Technical Paper No. 12*, Pittsburgh, Pennsylvania.

IABSE Colloquium (1996), *Basis of Design and Actions on Structures - Background and application of Eurocode 1*, Delft, The Netherlands

ISO 2394 (1998), *International Organization for Standardization - General Principles on Reliability for Structures*.

Jandera, M., Gardner, L. and Machacek, J. (2008) "Residual stresses in cold-rolled stainless steel hollow sections." *Journal of Constructional Steel Research,* 64(11): 1255-1263

Jombock, J. R. and Clark, J. W. (1968), "Bending strength of aluminum formed sheet members." *Journal of Structural Division*, ASCE, 94, No. ST2.

Kemp, A. R., Byfield M. P. and Nethercot D. A. (2002) "Effect of strain hardening on flexural properties of steel beams", *The Structural Engineer*, 80(8): 29–35.

Kim, Y. and Peköz, P. (2010), "Ultimate flexural strength of aluminum sections" *Thin-walled structures* 48(10-11): 857-865.

Kissell, J.R. and Ferry, R. L. (1995) *Aluminum Structures: A Guide to Their Specifications and Design*, John Wiley & Sons.

Kuhlmann, U. (1989). "Definition of flange slenderness limits on the basis of rotation capacity values", *Journal of Constructional Steel Research* 14(1): 21–40.

Lai, Y.F.W. and Nethercot, D.A. (1992), "Strength of aluminium members containing local transverse welds", *Engineering Structures* 14(4): 241-254

Landolfo, R., Piluso, V., Langseth, M. and Hopperstad, O. S. (1999), "EC9 provisions for flat internal elements: comparison with experimental results", *Light-Weight Steel and Aluminum Structure*s, pp.515-522

Langseth, M. and Hopperstad, O. S. (1997), "Local buckling of square thin-walled aluminium extrusions", *Thin- Walled Structures* 27(1):117-126

Law, K. H. and Gardner, L. (2009), "Unified slenderness limits for circular hollow sections." *Proceeding of 6th International Conference on Advances in Steel Structures*, pp. 293-300, Hong Kong, China

Law K. H. (2010), *Instabilities in Structural Steel Elliptical Hollow Section Members*, PhD Thesis, Imperial College London, UK.

Lay, M.G. and Galambos, T.V. (1965). "Inelastic steel beams under uniform moment." *Journal of the Structural Division*, *ASCE* 91(6): 67–93.

Lay, M.G. and Galambos, T.V. (1967). "Inelastic beams under moment gradient" *Journal of the Structural Division, ASCE* 93(1): 381–99.

Li, Z. and Schafer, B.W. (2010) "Buckling analysis of cold-formed steel members with general boundary conditions using CUFSM: conventional and constrained finite strip methods." *Proceedings of the 20th Int;l. Spec. Conf. on Cold-Formed Steel Structures*, pp.17-31, St. Louis, MO. (Nov, 2010).

Manganiello, M., De Matteis, G. and Landolfo, R. (2006) "Inelastic flexural strength of aluminium alloys structures", *Engineering Structures*, 28(4): 593-608.

Mazzolani, F.M. (1972), "Characterization of the σ-ε law and buckling of aluminium columns", *Construction Metallic*, No.3

Mazzolani, F.M. (1995), *Aluminum alloy structures 2nd.* E&FN Spon Press.

Mazzolani, F.M., Faella, C., Piluso, V. and Rizzano, G. (1996), "Experimental analysis of aluminium alloy SHS-members subjected to local buckling under uniform compression." *Proceeding of 5th International Colloquium on Structural Stability*, 475-488, SSRC, Rio de Janeiro, Brazil (Apr, 1996).

Mazzolani, F. M., Faella, C., Piluso, V. and Rizzano, G. (1997a). "Local buckling of aluminium alloy RHS-members: experimental analysis." *Proceeding of XVI Congresso C.T.A., Italian Conference on Steel Construction*, pp.1-12, Collegio dei Tecnici dell'Acciaio, Ancona (Oct, 1997).

Mazzolani, F.M., Piluso, V. and Rizzano, G. (1997b), "Numerical simulation of aluminium stocky hollow members under uniform compression" *Proceeding of 5th International Colloquium on Stability and Ductility of Steel Structures*, SDSS'97, Nagoya, Japan (Jul, 1997).

232

Mazzolani, F. M., Piluso, V. and Rizzano, G. (2001), "Experimental analysis of aluminum alloy channels subjected to local buckling under uniform compression" *Proceeding of C.T.A., Italian Conference on Steel Construction*. ACS, 1-10, Acai Servizi, Milano, Italy (Sep, 2001).

Mazzolani, F.M., Piluso, V. and Rizzano, G. (2011), "Local buckling of aluminum alloy angles under uniform compression" *Journal of Structural Engineering, ASCE* 137(2):173-184.

Mennink, J. (2002). *Cross-Sectional Stability of Aluminum Extrusions: Prediction of the Actual Local Buckling Behaviour.* The Netherlands.

Mirambell, E. and Real, E. (2000) "On the calculation of deflections in structural stainless steel beams: an experimental and numerical investigation" *Journal of Constructional Steel Research*, 54(1): 109-133

Moen, L.A., Hopperstad, O.S. and Langseth, M. (1998), "Elastoplastic buckling of anisotropic aluminium plate elements" *Journal of Structural Engineering, ASCE,* 124(6):712-719

Moen, L.A., Langseth M. and Hopperstad, O.S. (1999a). "Rotational capacity of aluminium beams under moment gradient. I: experiments" *Journal of Structural Engineering, ASCE,* 125(8): 910-920.

Moen L.A., De Matteis, G., Hopperstad O.S., Langseth M., Landolfo, R. and Mazzolani, M. (1999b) "Rotational capacity of aluminium beams under moment gradient II: numerical simulations" *Journal of Structural Engineering, ASCE,* 125(8): 921-929

Nethercot, D. A., Li T. Q. and Choo, B. S. (1995) "Required rotations and moment redistribution for composite frames and continuous beams", *Journal of Constructional Steel Research*, 35(2): 121-163.

Opheim, B. S. (1996). *Bending of thin-walled aluminium extrusions*, PhD Dissertation, Division of Structure Engineering., Norwegian University of Science and Technology

Panlilo, F. (1947), "The theory of limit design applied to magnesium alloy and aluminum alloy structures", *J. Royal Aeronautical Soc*., pp.534–571.

Ramberg, W. and Osgood, W. R. (1943), "Description of stress-strain curves by three parameters", *Technical Note No. 902*, National Advisory Committee for Aeronautics, Washington, D.C.

Ravindra, M. K. and Galambos, T. V. (1978), "Load and resistance factor design for steel", *Journal of the Structural Division, ASCE*, 104(ST9): 1337–1353

Rogers, C. A. and Hancock, G. J. (1996), *Ductility of G550 Sheet Steels in Tension - Elongation Measurements and Perforated Tests, Research Report No R735*

Rasmussen, K.J.R. and Hancock, G.J. (1993) "Design of cold-formed stainless steel tubular members. I: Columns." *Journal of Structural Engineering, ASCE*, 119(8): 2349-2367.

Schafer, B.W. and Peköz, T. (1998), "Direct strength prediction of cold-formed steel members using numerical elastic buckling solutions", *Proceeding of 14th Int. specialty conference on cold-formed steel structures*, pp. 69–76. University of Missouri-Rolla, Rolla, Mo.

Seif, M. and Schafer, B.W. (2010), "Local buckling of structural steel shapes", *Journal of Constructional Steel Research* 66(10): 1232-1247

Sharp, M. L. (1999) "Chapter 8: Aluminum structures" in *Structural Engineering Handbook* (Edited by Wai-Fah Chen), Boca Raton: CRC Press LLC.

Solar Energy Development Programmatic EIS Information Centre, access on Dec 20th, 2013. <. http://solareis.anl.gov/guide/transmission/index.cfm>

Templin, R. L., Sturm, R. G., Hartmann, E. C. and Holt, M. (1938), "*Column strength of various aluminum alloys*." Alcoa Technical Paper No. 1, Pittsburgh, PA.

Theofanous, M., Chan, T.M. and Gardner, L. (2009), "Flexural behaviour of stainless steel oval hollow sections", *Thin-walled Structures* 47(6-7): 776-787

Theofanous, M., Saliba, N., Zhao, O. and Gardner, L. (2014) "Ultimate response of stainless steel continuous beams." *Thin-Walled Structures*.83:115-127

Wang, T., Hopperstad, O.S., Lademoa, O.G. and Larsen, P. K. (2007) "Finite element modelling of welded aluminium members subjected to four-point bending", *Thin-Walled Structures* 45 (2007) 307–320

Wang, F. (2011), *A Deformation Based Approach to Structural Steel Design*. PhD Thesis, Imperial College London, UK.

Welo T. (1991), *Inelastic deformation capacity of flexurally-loaded aluminium alloy structures*. Ph.D. thesis. Trondheim (Norway): Division of Structural Engineering, The Norwegian Institute of Technology.

Xiao, Y. and Menzemer, C. (2003) "Ultimate compressive strength of aluminum plate elements", *Journal of Structural Engineering, ASCE*, 129 (11): 1441-1447

Zhou, F. and Young, B. (2008) "Aluminum tubular sections subjected to web crippling—Part I: Tests and finite element analysis", *Thin-Walled Structures* 46 (4): 339–351

Zhu, J. H., and Young, B. (2006a). "Tests and design of aluminum alloy compression members", *Journal of Structural Engineering, ASCE* 132(7):1096–1107.

Zhu, J. H. and Young, B. (2006b). "Aluminum alloy tubular columns – Part II: parametric study and design using direct strength method." *Thin-Walled Structures* 44(9): 969-985.

Zhu, J. H. and Young, B. (2008). "Behavior and design of aluminum alloy structural members", *Advanced Steel Construction* 4(2):158-172

Zhu, J. H. and Young, B. (2009), "Design of aluminum alloy flexural members using direct strength method." *Journal of Structural Engineering, ASCE* 135(5): 558-566

Ziemian, R. D. (2010), *Guide to Stability Design Criteria for Metal Structures*, *6th Edition*, John Wiley & Sons, Inc., New Jersey, United States.

PUBLICATIONS

Ten supporting journal and conference papers have been published, accepted for publication, submitted or in preparation based on the work presented in this thesis.

Journal Papers

1. Su, M., Young, B. and Gardner, L. (2013) "Continuous strength method for aluminium alloy structures" *Advanced Material Research* 742(2013):70-75.

2. Su, M., Young, B. and Gardner, L. (in press) "Testing and design of aluminum alloy cross-sections in compression." *Journal of Structural Engineering, ASCE*.

3. Su, M., Young, B. and Gardner, L. (in press) "Deformation-based design of aluminium alloy beams" *Engineering Structures*.

4. Su, M., Young, B. and Gardner, L., "Aluminum alloy continuous beams of tubular cross-sections - Part I: tests and model validation", *Journal of Structural Engineering, ASCE,* submitted.

5. Su, M., Young, B. and Gardner, L., "Aluminum alloy continuous beams of tubular cross-sections - Part II: parametric study and design", *Journal of Structural Engineering, ASCE,* submitted.

Conference Papers

6. Su, M., Young, B. and Gardner, L. (2012) "Compression tests of aluminium alloy cross-sections", *Proceedings of the 13th International Symposium Tubular Structures* pp. 501-508 (London, 2012)

7. Su, M., Young, B. and Gardner, L. (2012). Bending tests of aluminium alloy cross-sections, *Proceedings of the 13th Inter-national Symposium Tubular Structures* pp. 509-516 (London, 2012)

8. Su, M., Young, B. and Gardner, L. (2012), "Continuous beam tests on aluminium alloy hollow sections", *Proceedings of the 6th International Conference on Coupled Instabilities in Metal Structures*. pp.119-126 (Glasgow, 2012)

9. Su, M., Young, B. and Gardner, L. (2013). "Continuous beam tests on aluminium alloy SHS and RHS with internal stiffeners", *Research and Application in Structural Engineering, Mechanics and Computation,* pp. 401-402 (Cape Town, 2013)

10. Su, M., Young, B. and Gardner, L. (2014). "Numerical study of aluminium alloy continuous beams", *Proceedings of the 12th International Conference on Steel, Space and Composite Structures,* pp. 351-360 (Prague, 2014)

APPENDIX A.   PHOTOGRAPHS OF DEFORMED TEST SPECIMENS

A.1   Stub column tests
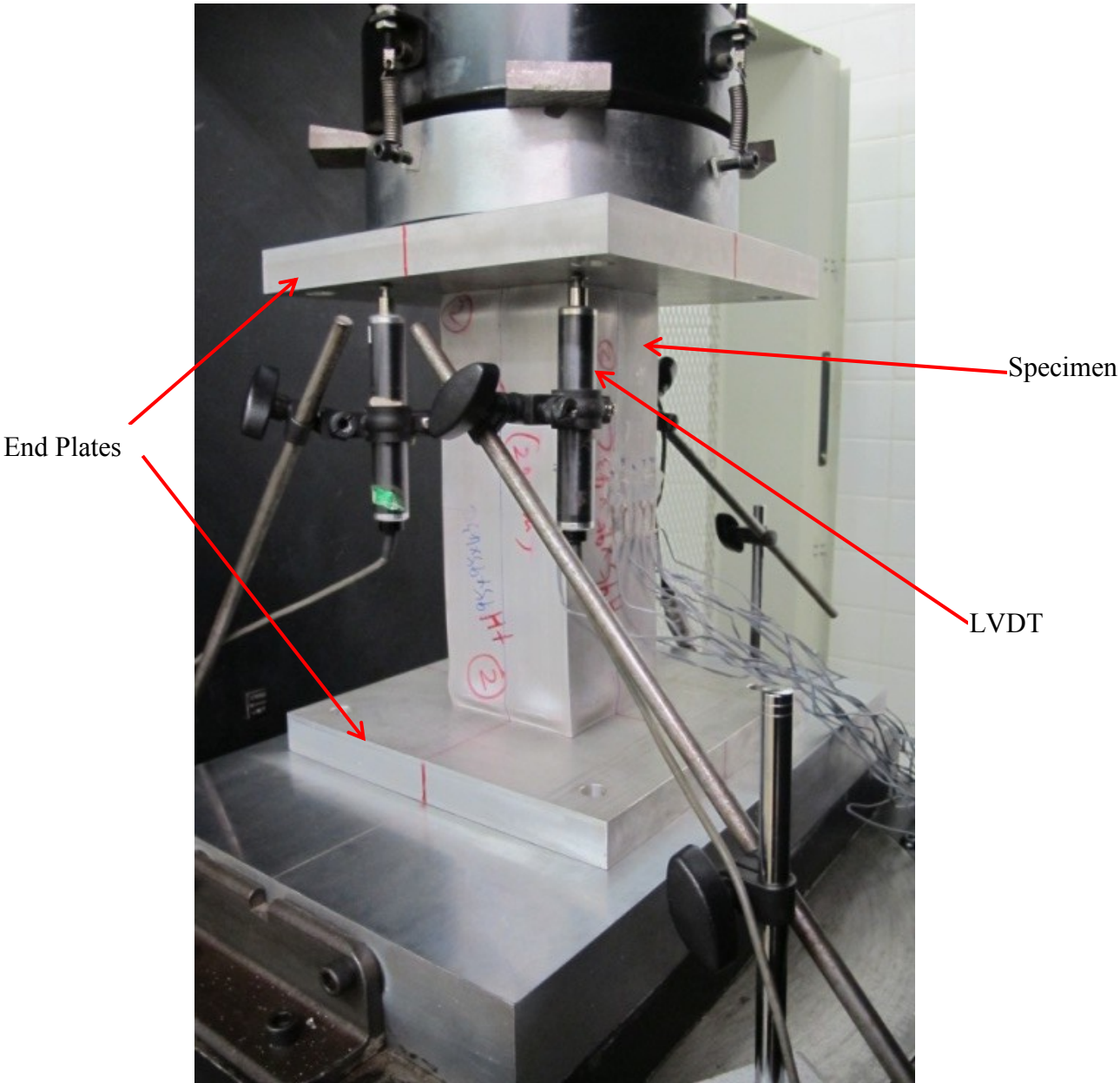
Fig. A.1.1 Experimental set-up for stub columns

Fig. A.1.2 Specimen attached with strain gauges at one quarter of the cross-section

at the mid-span

Fig. A.1.3 The attainment of global buckling on specimen (+H120×70×10.5C-R)

after ultimate load
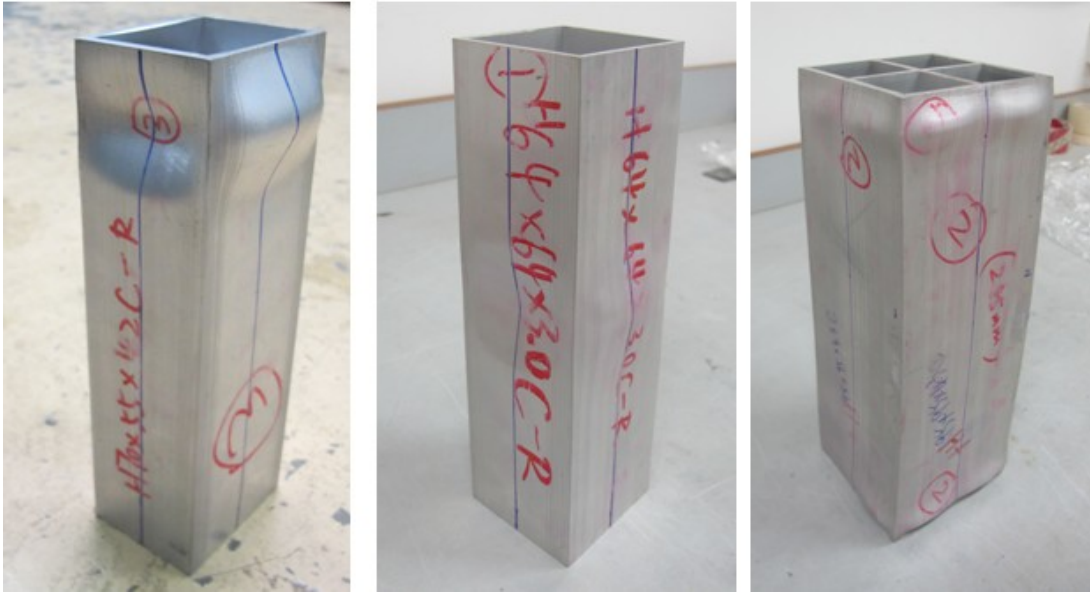
Fig. A.1.4 Stub column failure modes for specimens (a) H70×55×4.2C-R, (b)
H64×64×3.0C-R and (c) +H95×95×4.3C

A.2   Simply supported beam tests
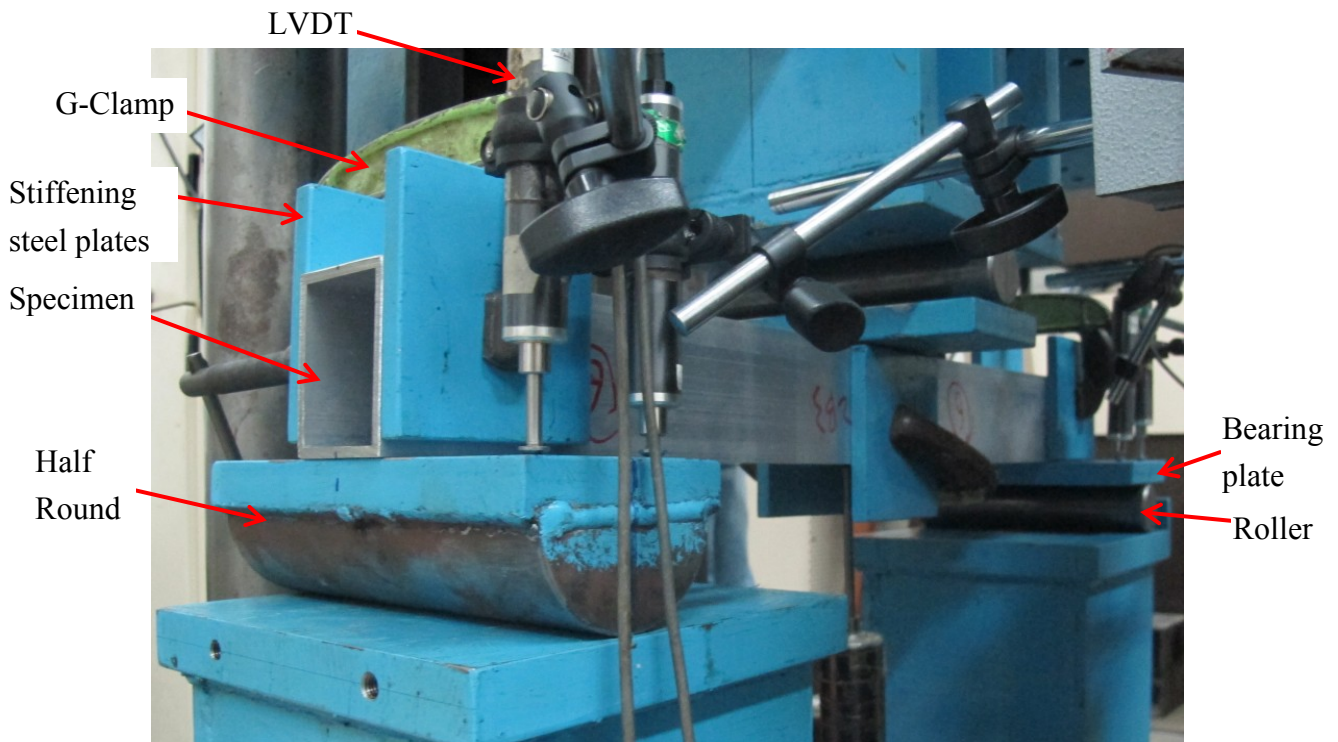
(a)

(b)

Fig. A.2.1 Experimental setup for three-point bending tests of (a) non-stocky sections (with stiffening steel plates) and (b) stocky sections (without stiffening steel plates)

(a)

(b)

Fig. A.2.2 Experimental setup for four-point bending tests of (a) non-stocky sections (with stiffening steel plates) and (b) stocky sections (without stiffening steel plates)

(a)
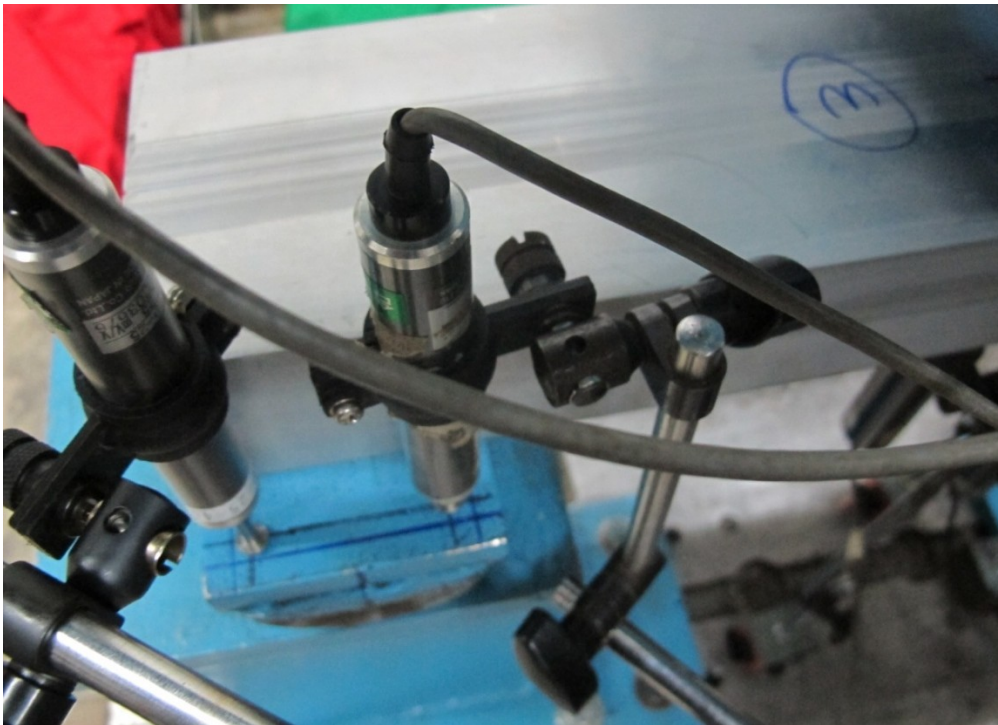
(b)

Fig. A.2.3 Arrangement of LVDTs at the beam ends to measure end rotations
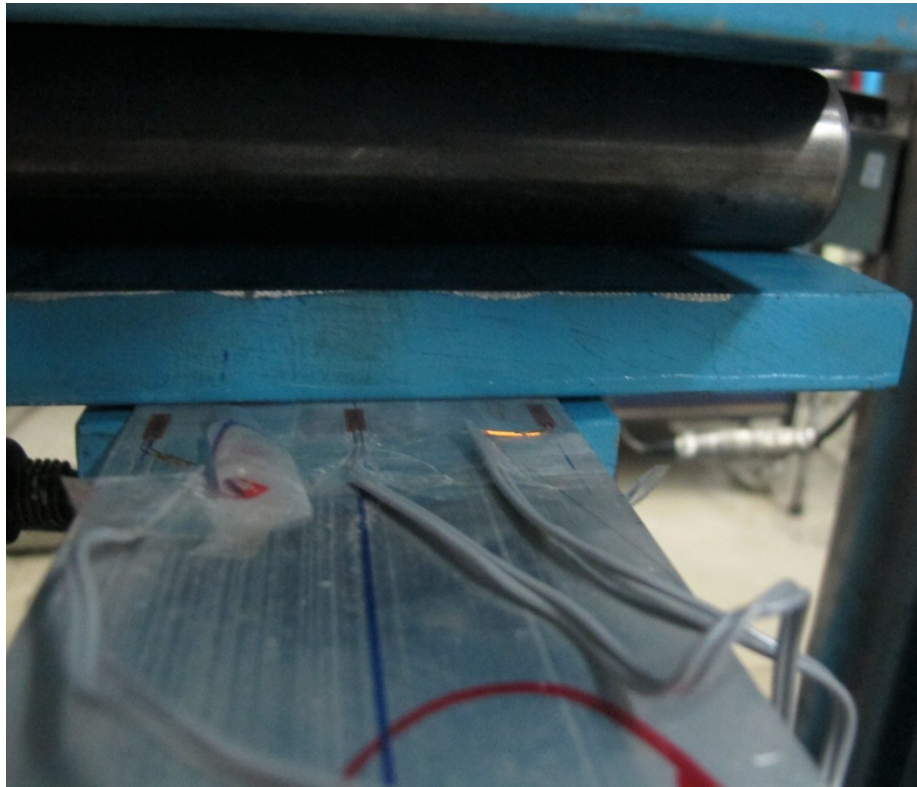
(a)
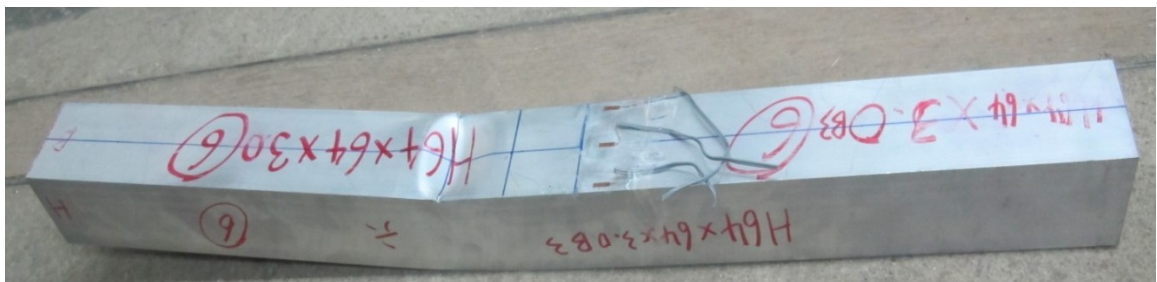
(b)

Fig. A.2.4 Strain gauges attached on the compression flange of the specimen

(H64×64×3.0B3) to measure local buckling if any
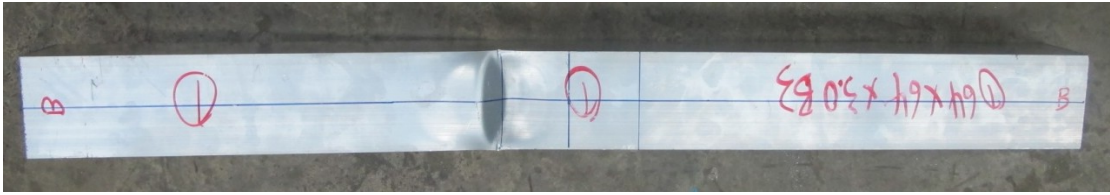
(a) Plane view

(b) Side view

Fig. A.2.5 Tested three-point bending beam (H64×64×3.0B3) with inelastic local

buckling on the compression flange of specimen
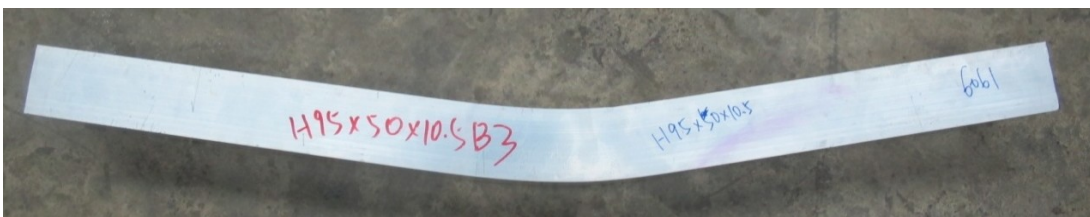
(a)Plane view

(b) Side view

Fig. A.2.6. Tested three-point bending beam (H95×50×10.5B3) without local

buckling on the compression flange of specimen
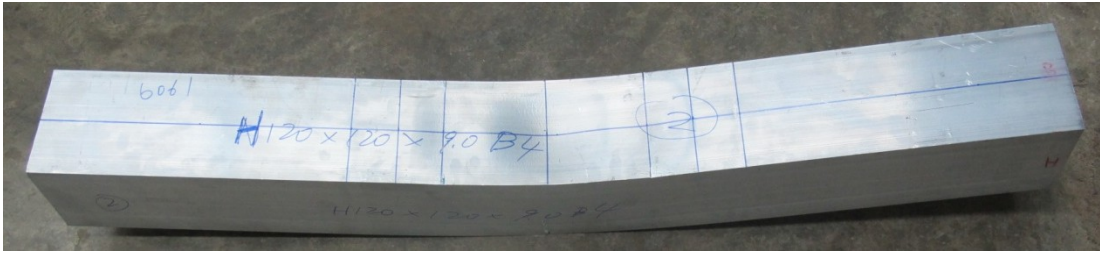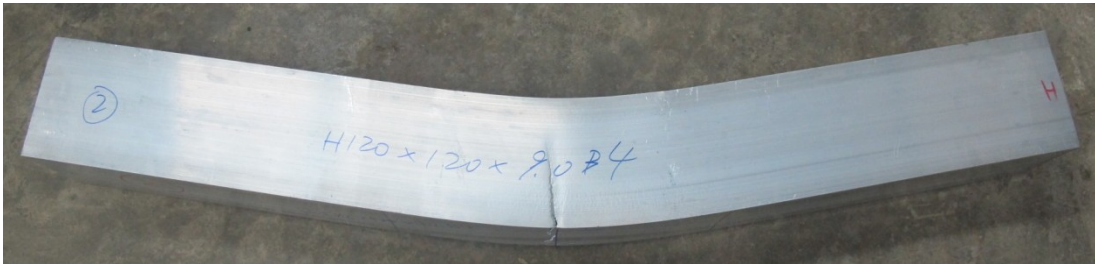
(a) Plane view

(b) Side view

Fig. A.2.7. Tested four-point bending beam (H120×120×9.0B4) with inelastic

local buckling on the compression flange of specimen
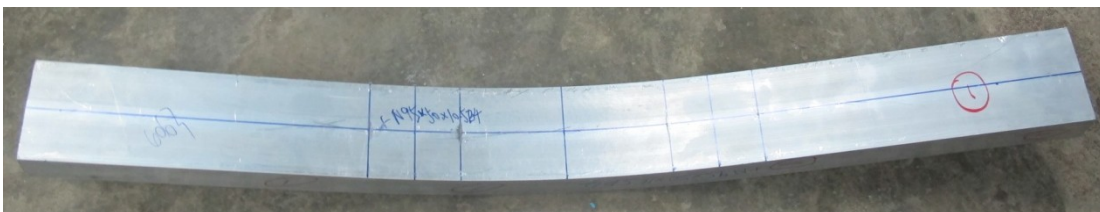
(a) Plane view
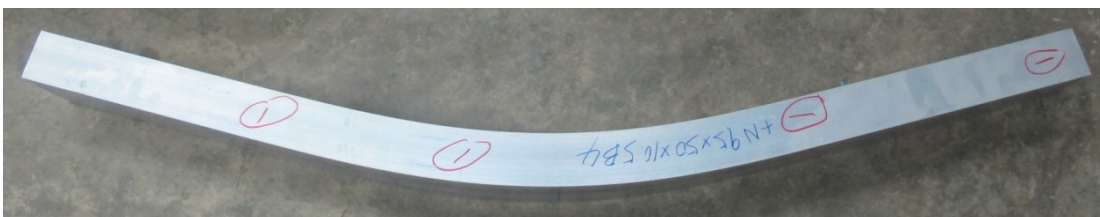
(b) Side view

Fig. A.2.8. Tested four-point bending beam (+N95×50×10.5B4) without inelastic

local buckling on the compression flange of specimen

(a)

(b)

(c)

Fig. A.2.9 Details of material fracture on the tension flanges

A.3 Continuous bending tests
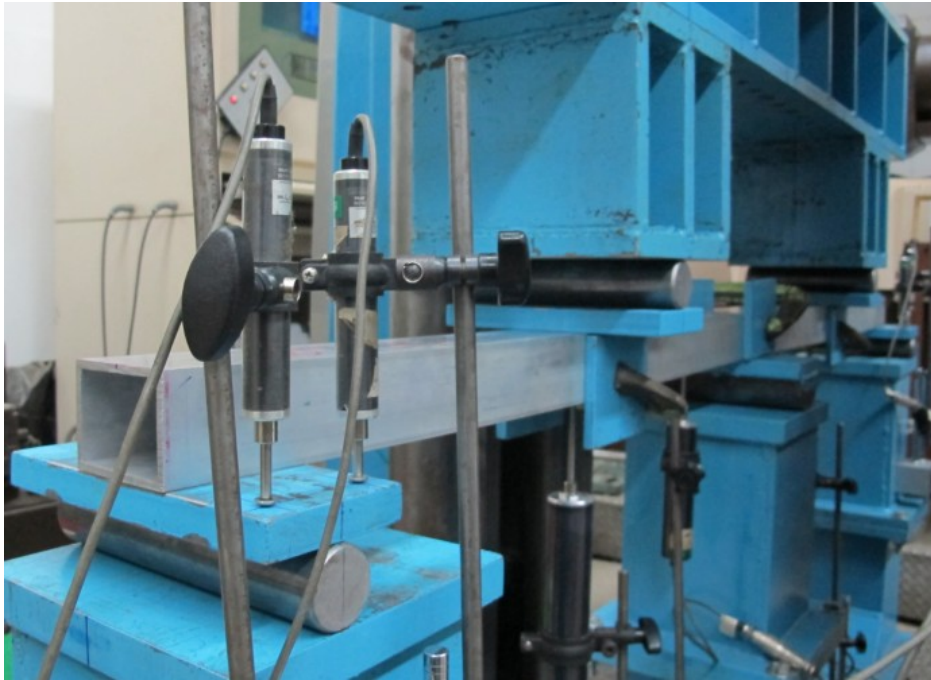
(a)
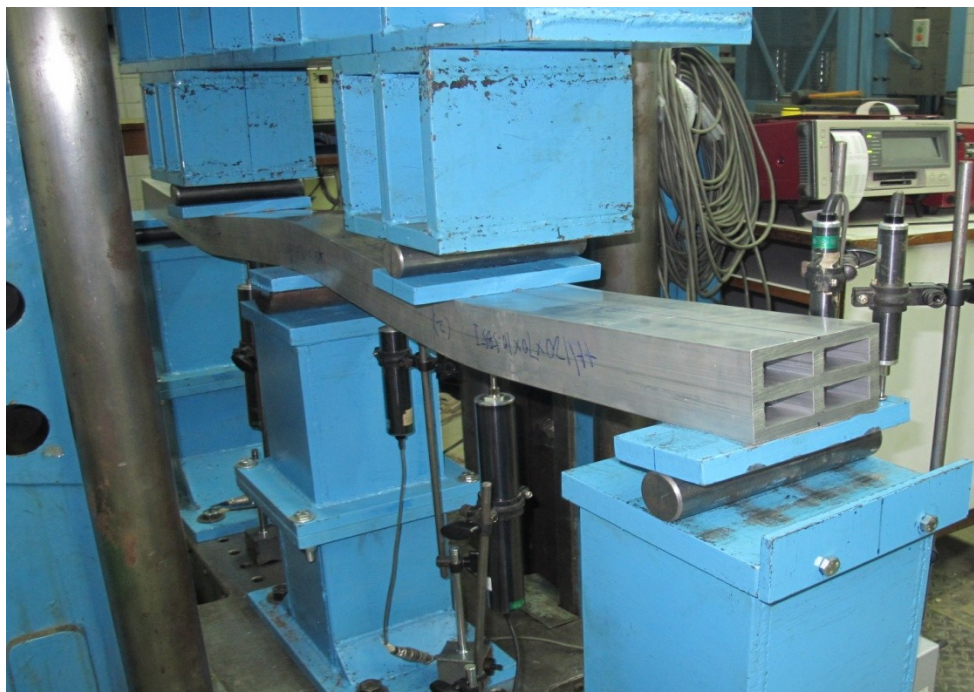
(b)

Fig. A.3.1 Experimental setup for five-point bending tests of (a) non-stocky sections (with stiffening steel plates) and (b) stocky sections (without stiffening steel plates)

Fig. A.3.2 Large deflection of specimen (+N50×95×10.5B5II) before failure
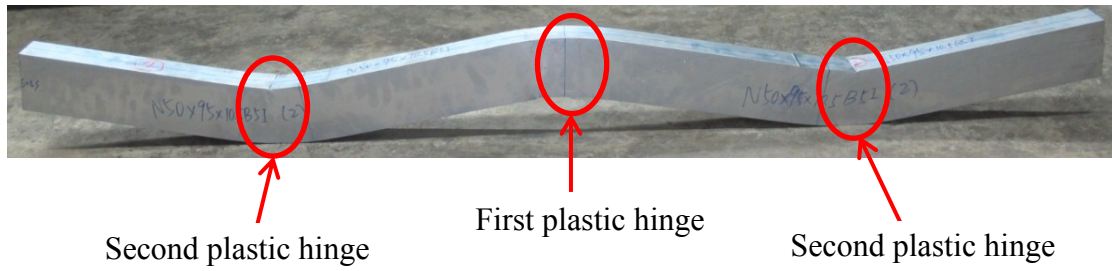
(a) Configuration I
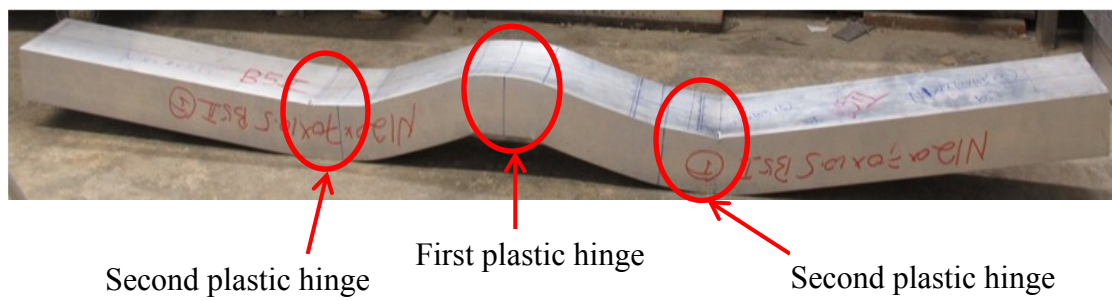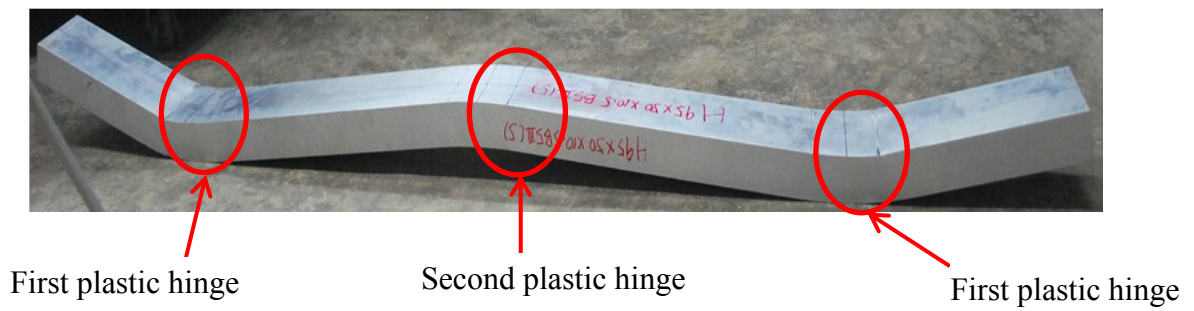
(b) Configuration II

(c) Configuration III

Fig. A.3.3 Three plastic hinges occurred on the five-point bending beams
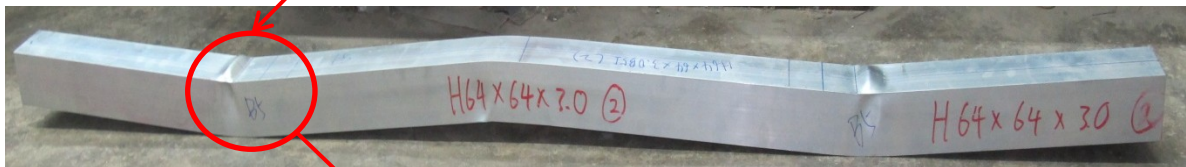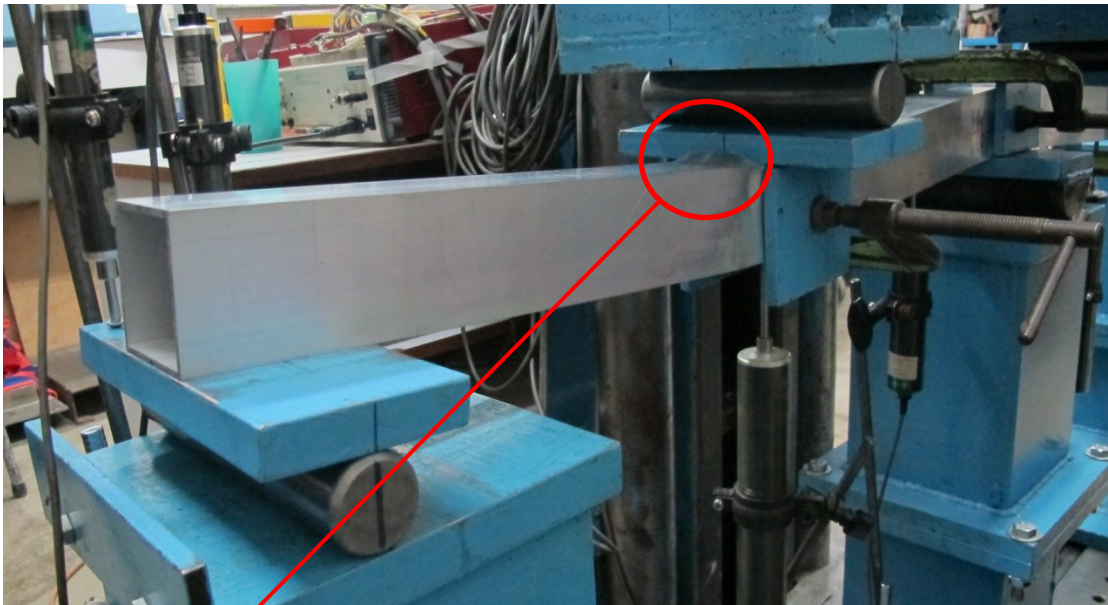
Fig. A.3.4 Inelastic local buckling on the compression flanges of five-point
bending beam (H64×64×3.0B5I)
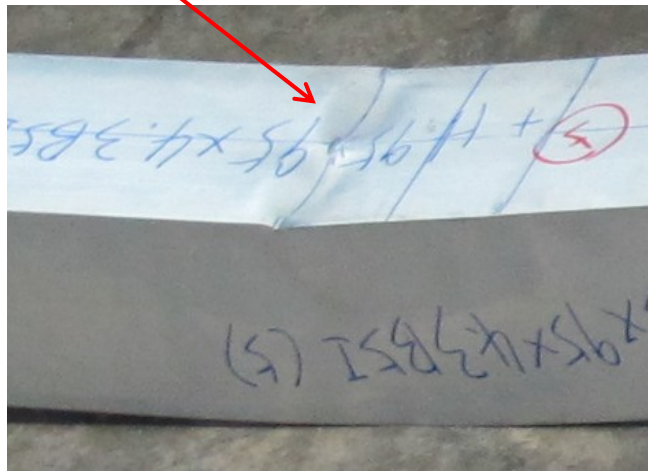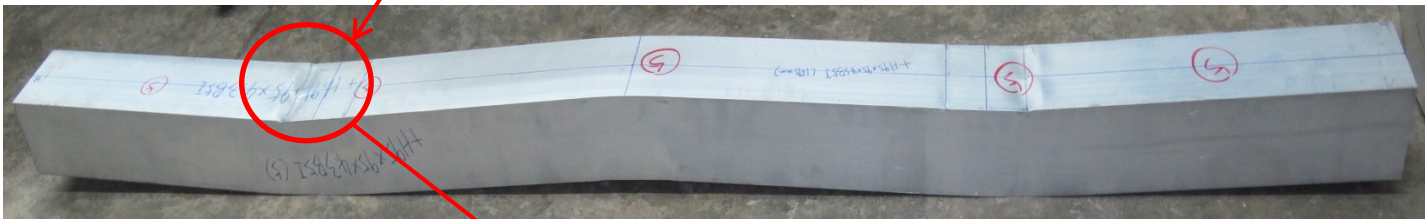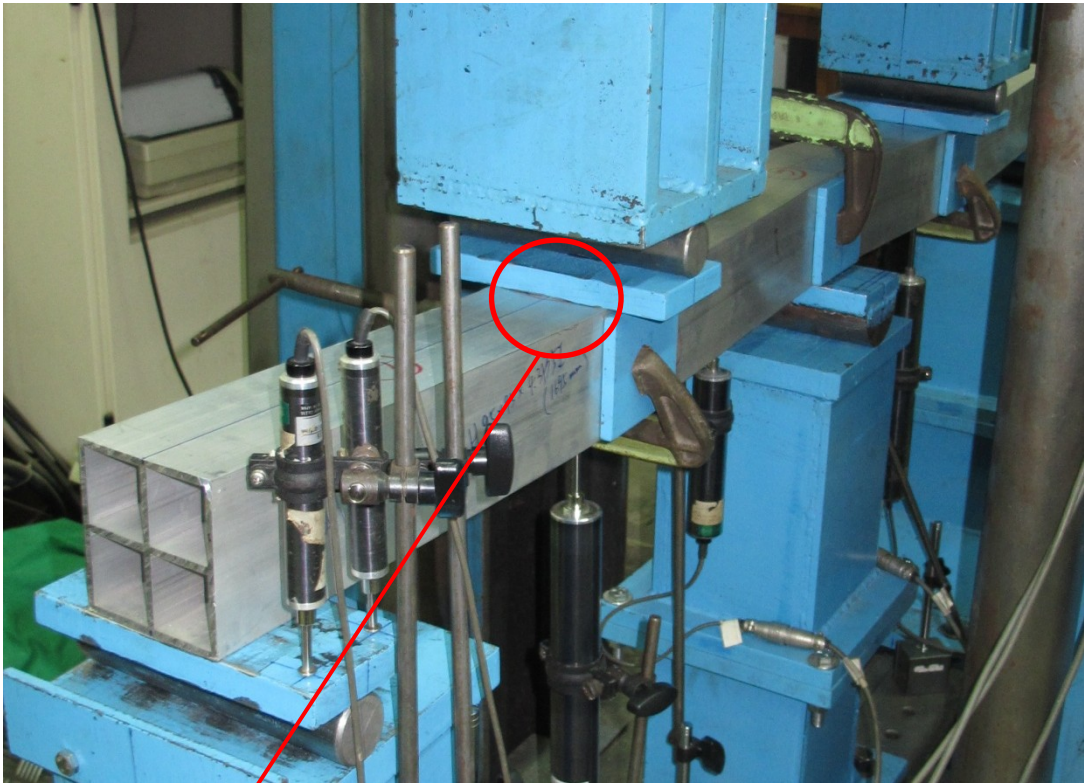
Fig. A.3.5 Inelastic local buckling on the compression flanges of five-point
bending beam (+H95×95×4.3B5I)
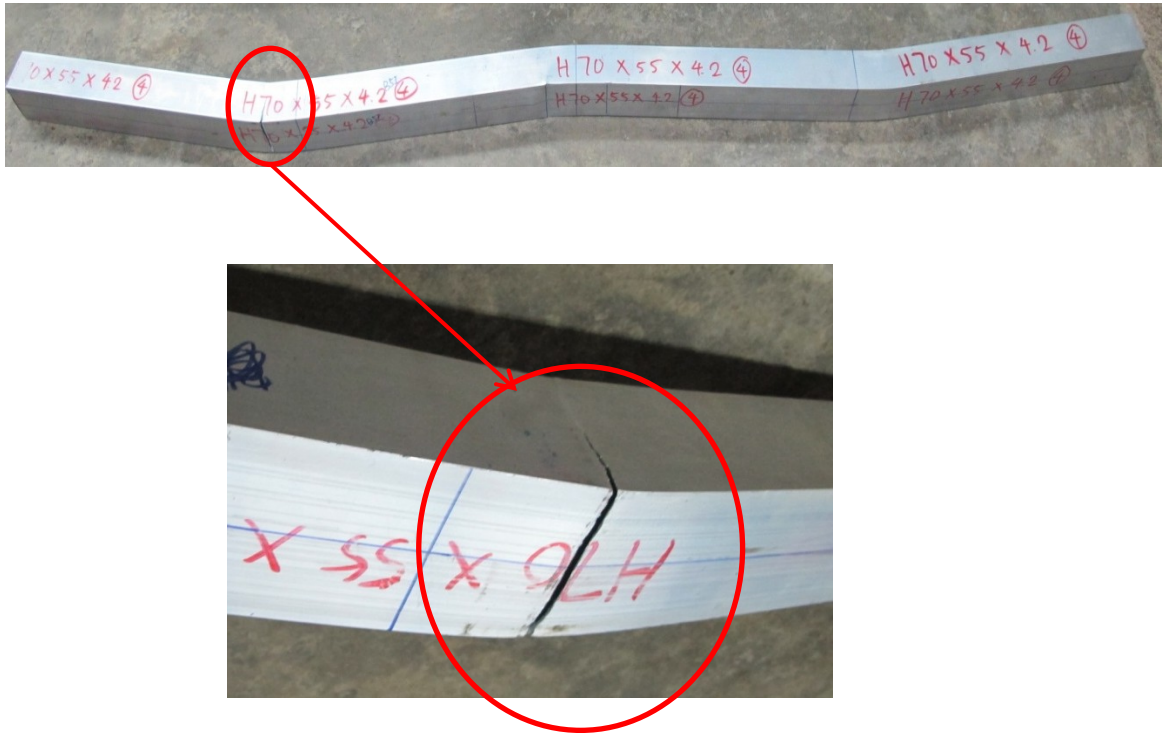
Fig. A.3.6 Details of material fracture on the tension flange of specimen
(H70×55×4.2B5III)

APPENDIX B. LOAD-DEFORMATION CURVES FROM STUB COLUMN TESTS
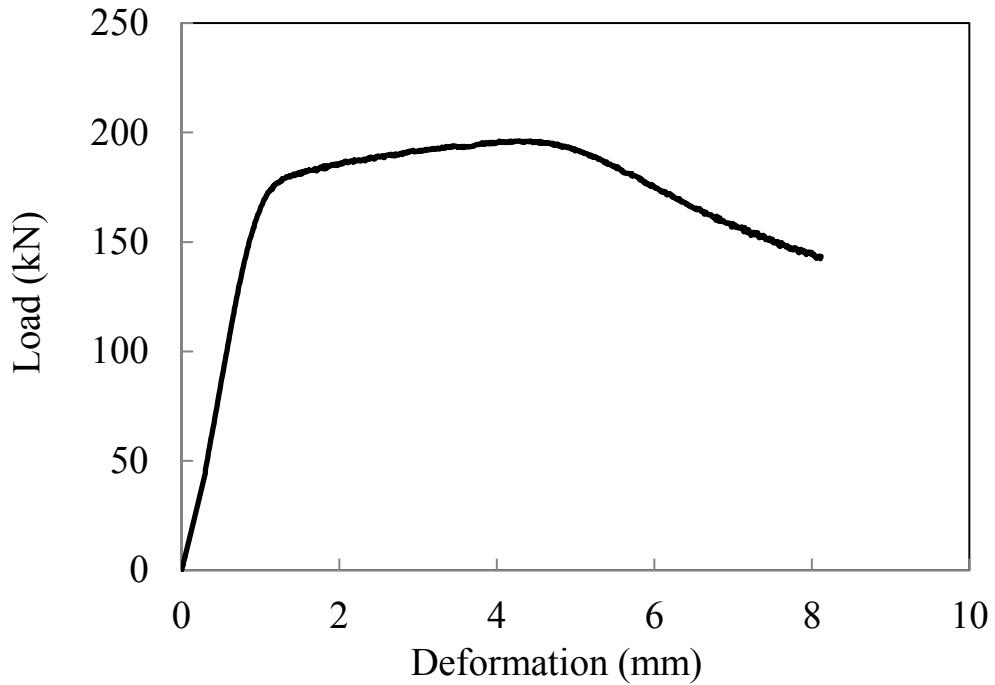
Fig. B.1 Axial load versus deformation curve for H70×55×4.2C
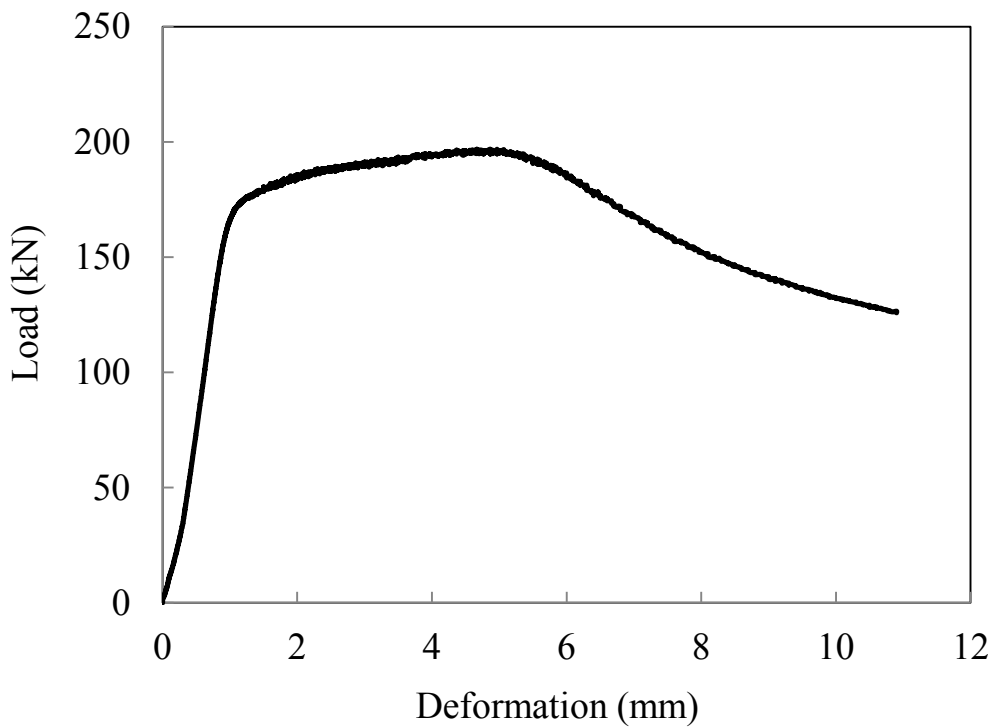
Fig. B.2 Axial load versus deformation curve for H70×55×4.2C-R
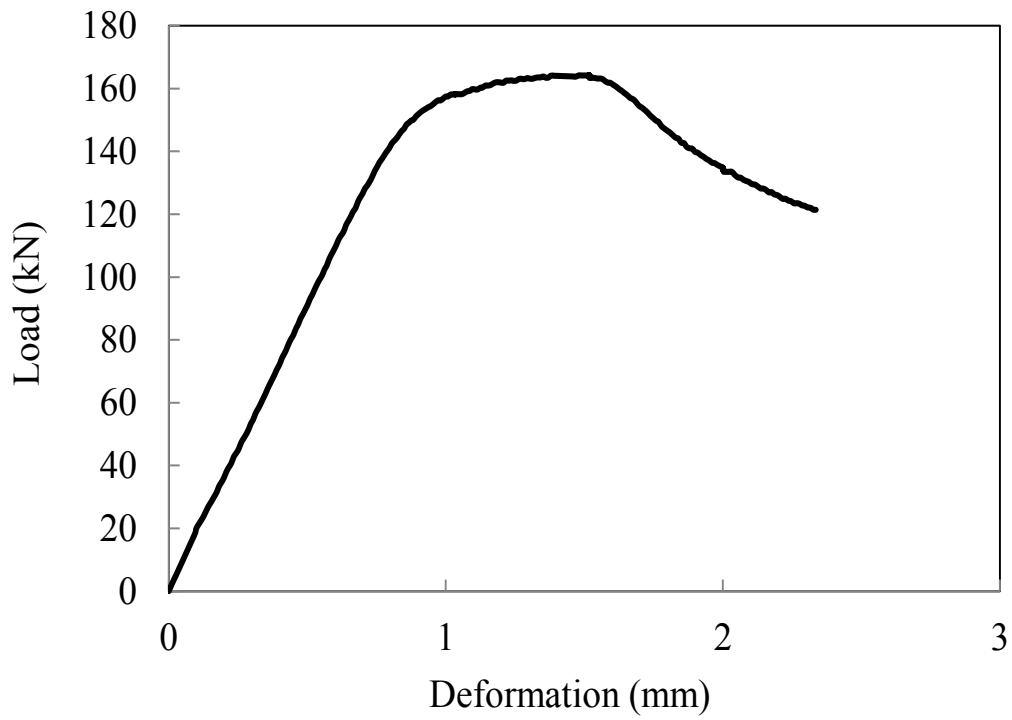
Fig. B.3 Axial load versus deformation curve for H64×64×3.0C
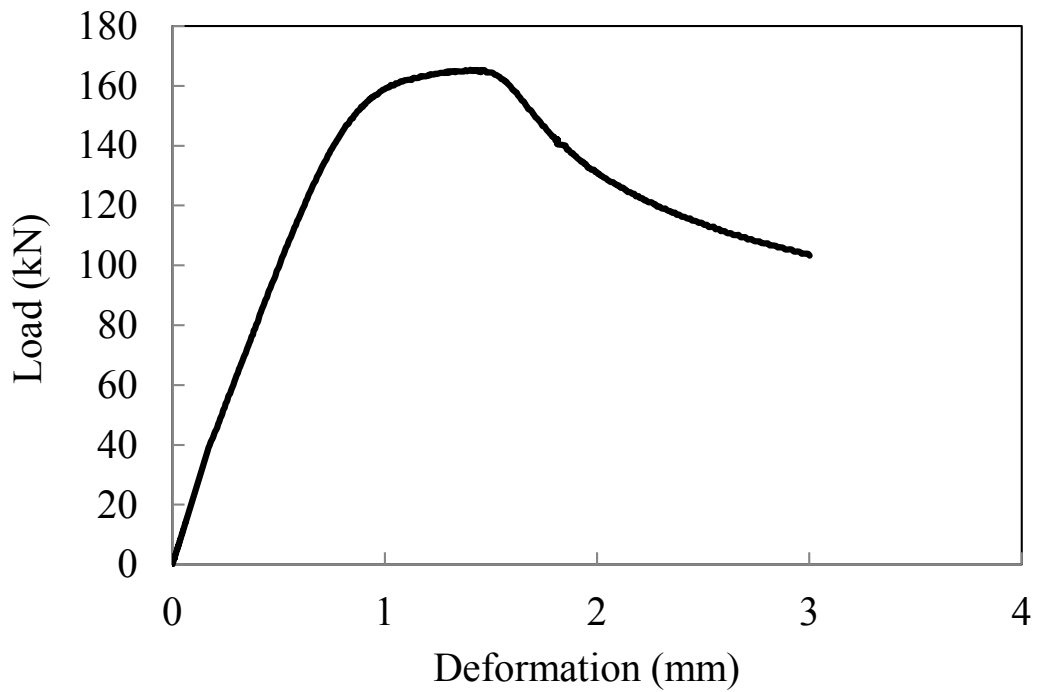
Fig. B.4 Axial load versus deformation curve for H64×64×3.0C-R
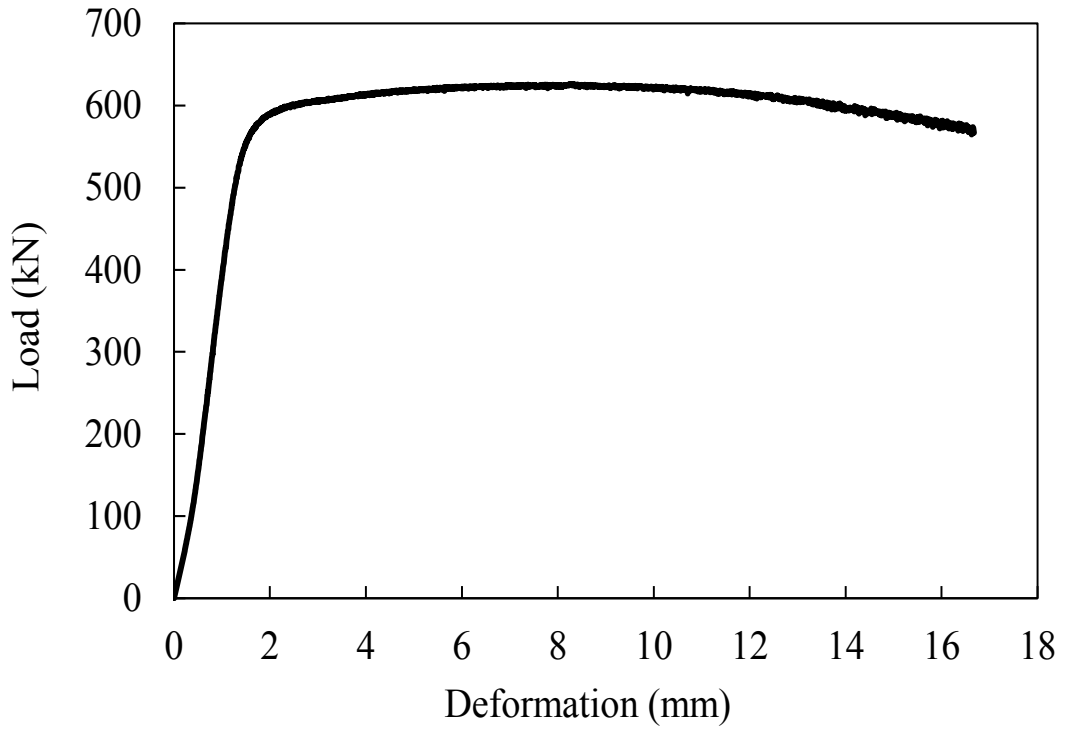
Fig. B.5 Axial load versus deformation curve for H95×50×10.5C
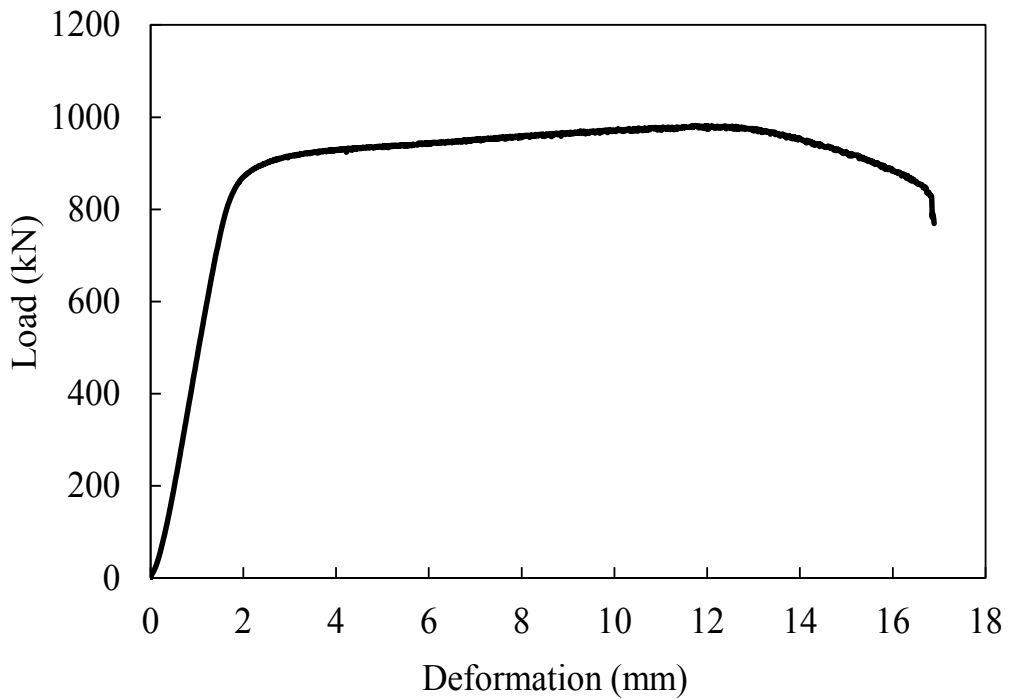
Fig. B.6 Axial load versus deformation curve for H120×120×9.0C
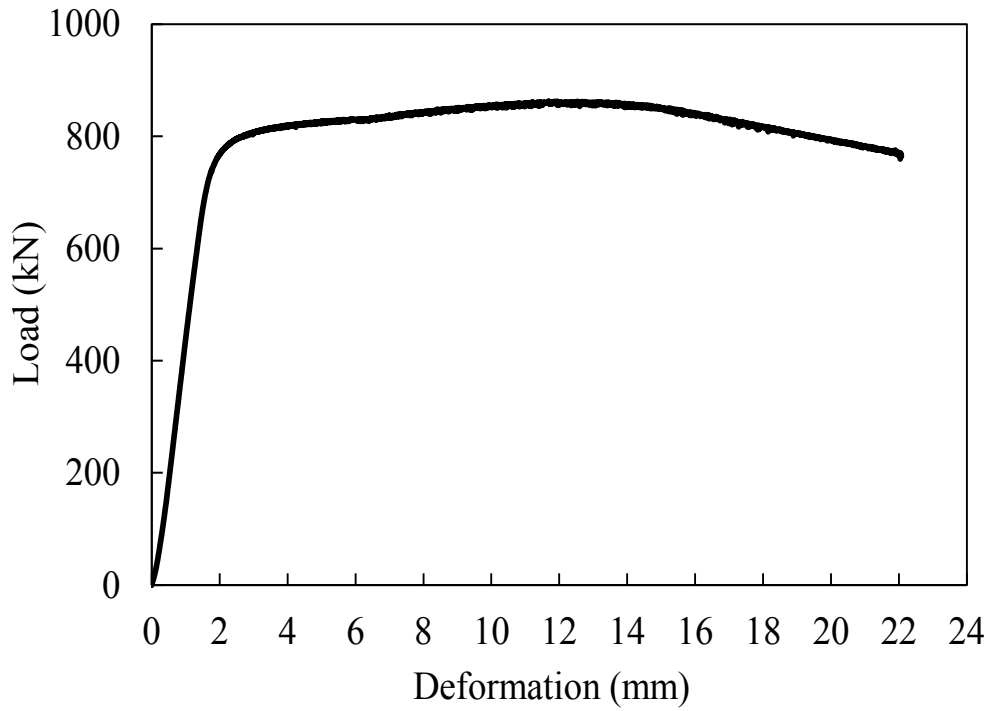
Fig. B.7 Axial load versus deformation curve for H120×70×10.5C
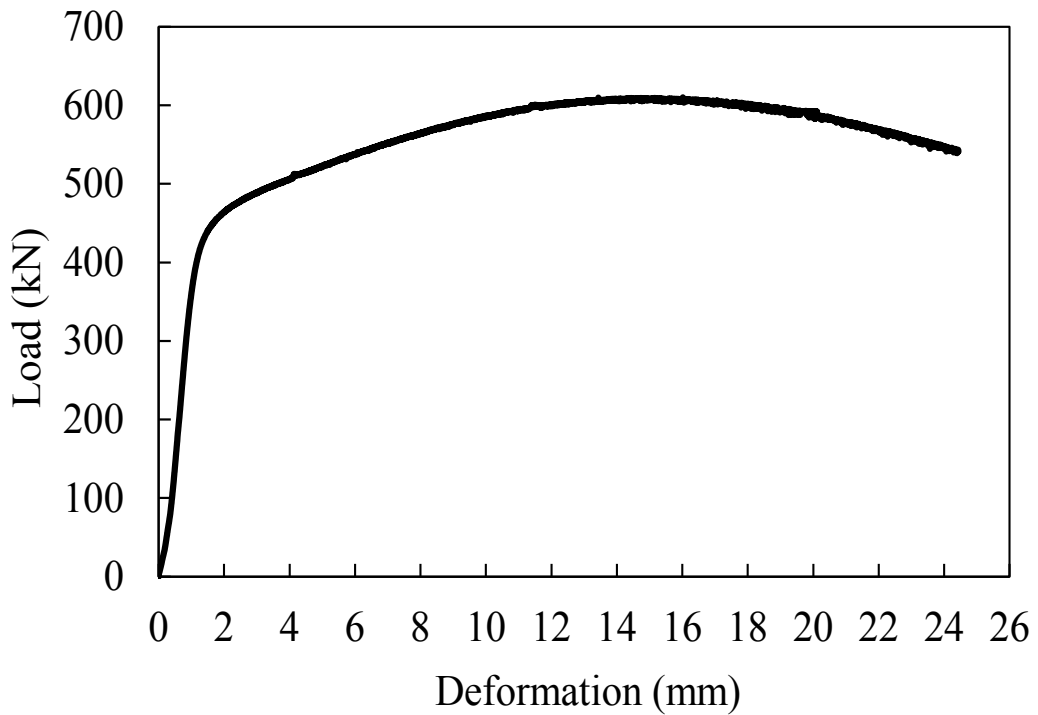
Fig. B.8 Axial load versus deformation curve for N95×50×10.5C

258
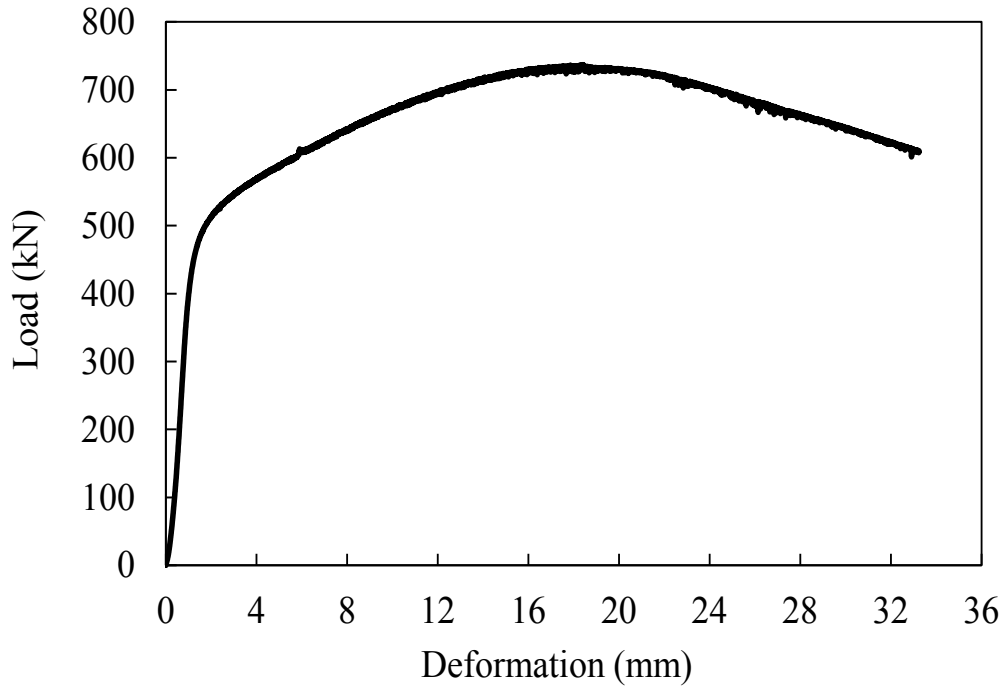
Fig. B.9 Axial load versus deformation curve for N120×70×10.5C
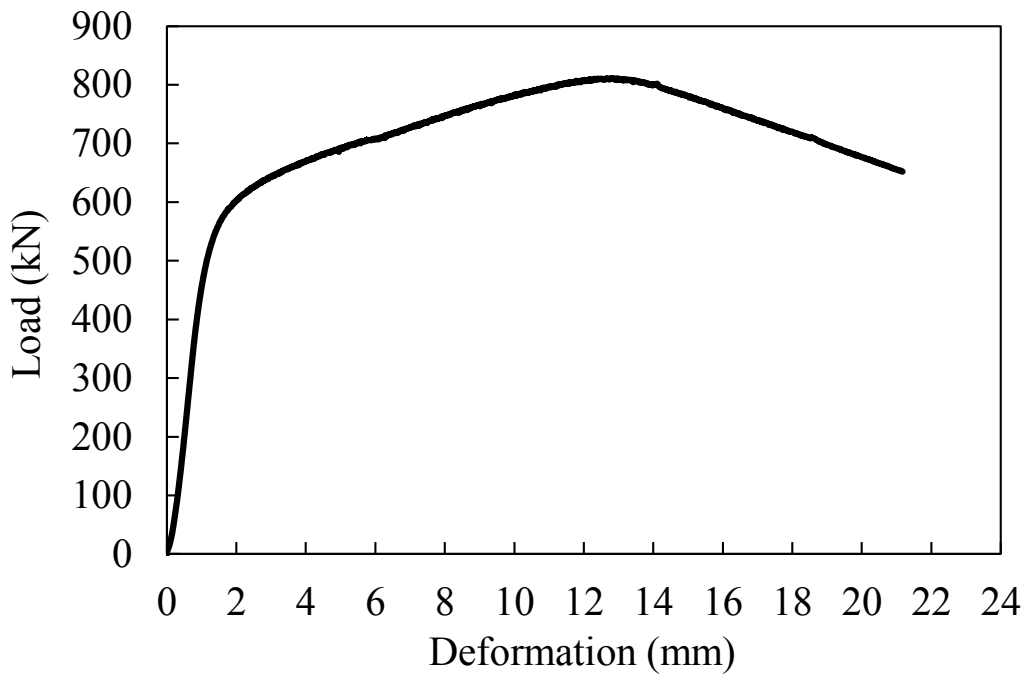
Fig. B.10 Axial load versus deformation curve for N120×120×9.0C
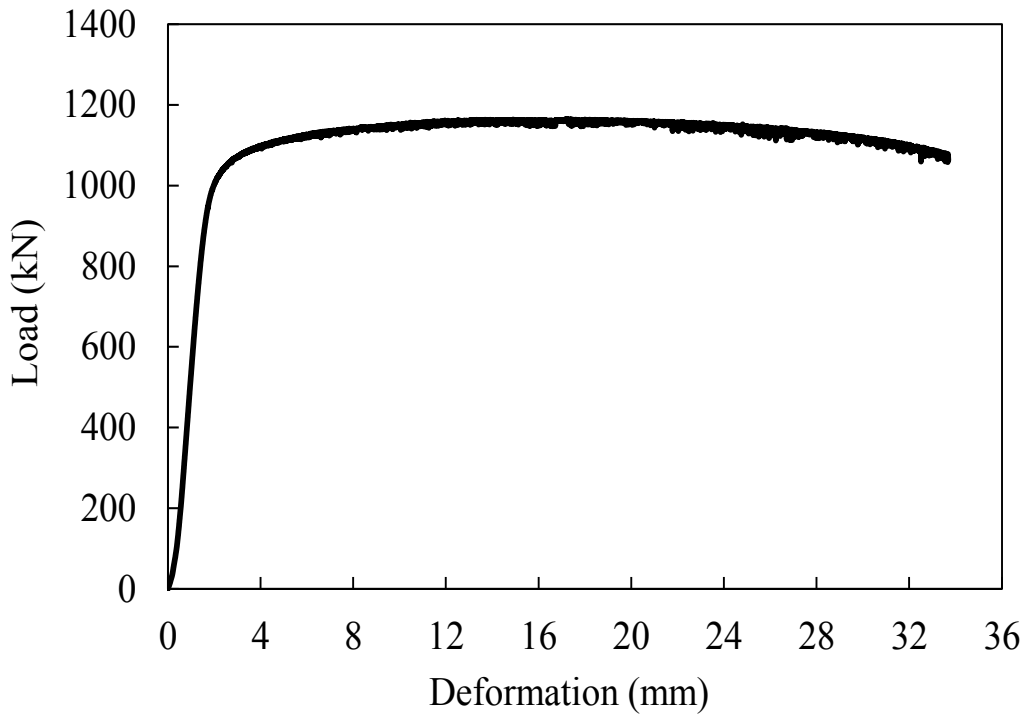
Fig. B.11 Axial load versus deformation curve for +H120×70×10.5C
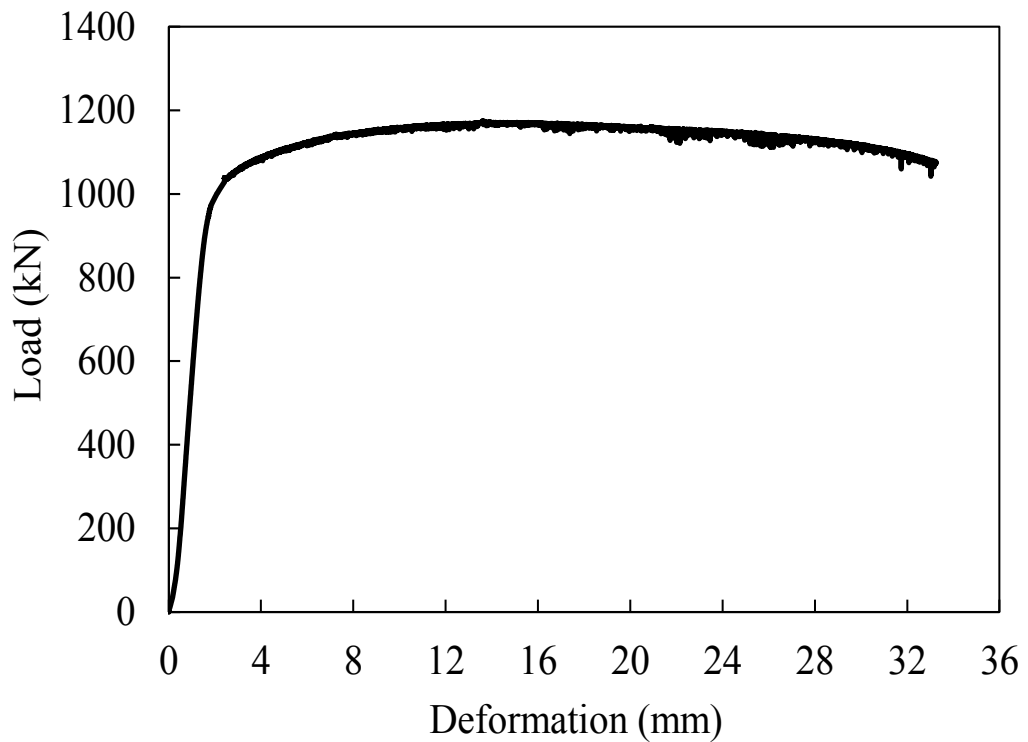
Fig. B.12 Axial load versus deformation curve for +H120×70×10.5C-R
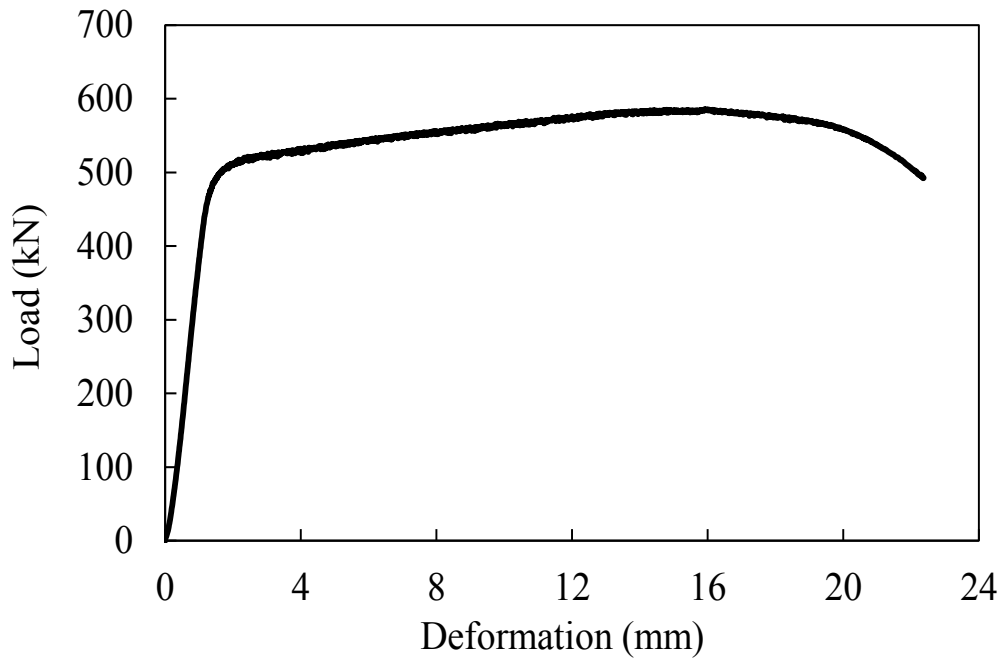
Fig. B.13 Axial load versus deformation curve for +H95×95×4.3C
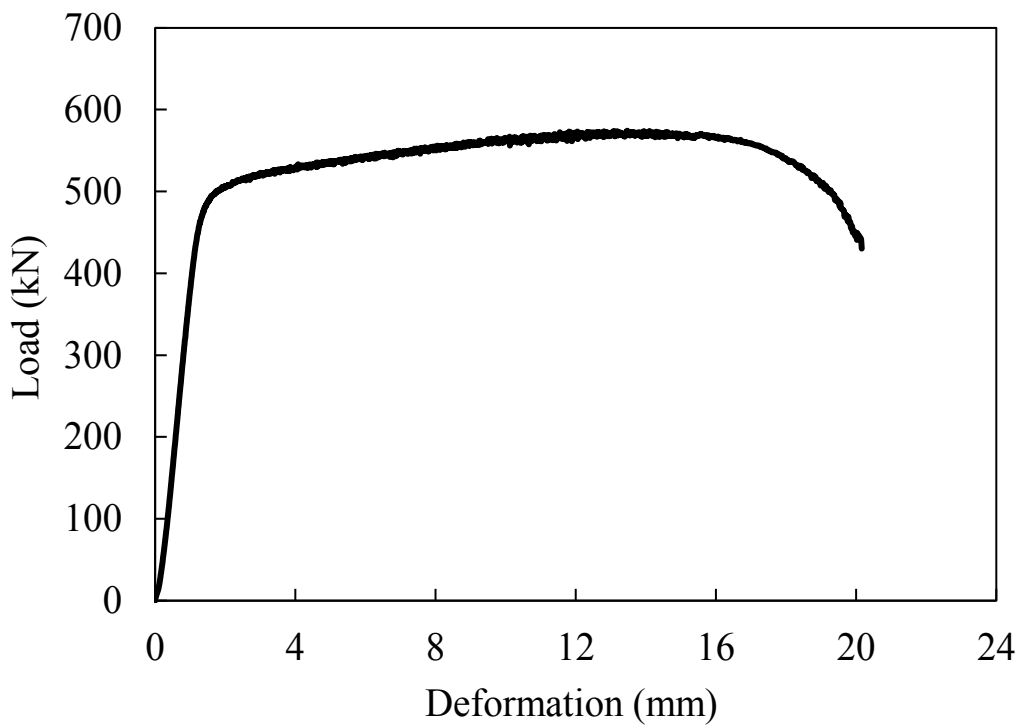
Fig. B.14 Axial load versus deformation curve for +H95×95×4.3C-R
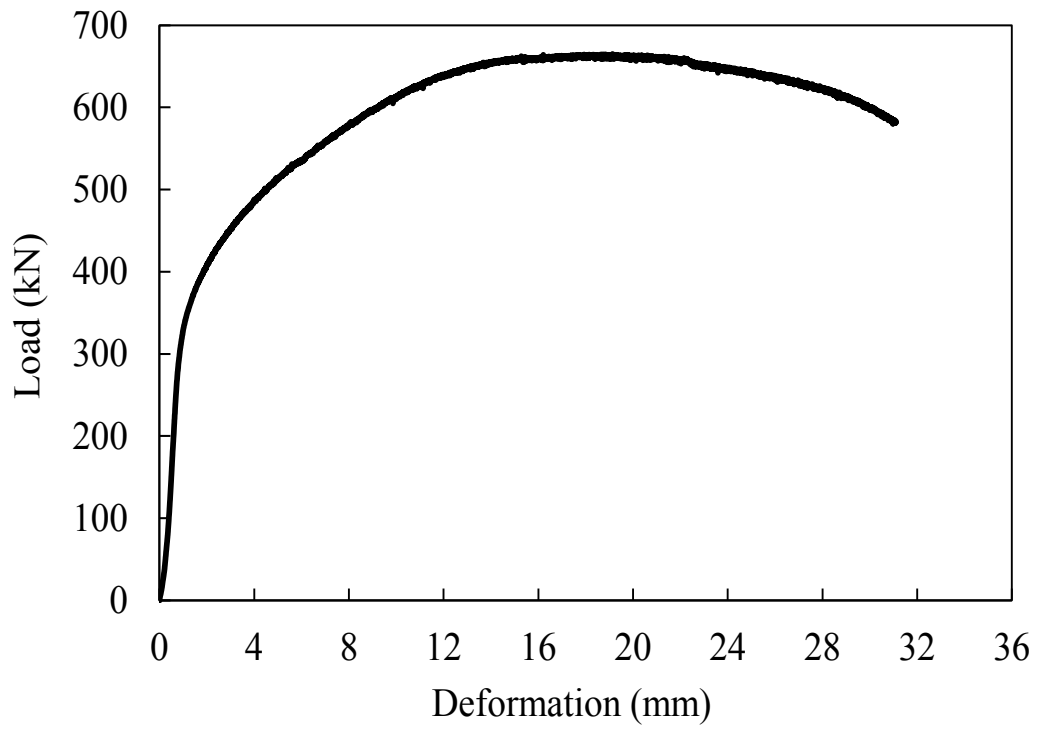
Fig. B.15 Axial load versus deformation curve for +N95×50×10.5C

APPENDIX C.

MOMENT-END ROTATION CURVES FROM THREE-POINT BENDING TESTS AND SIMULATIONS
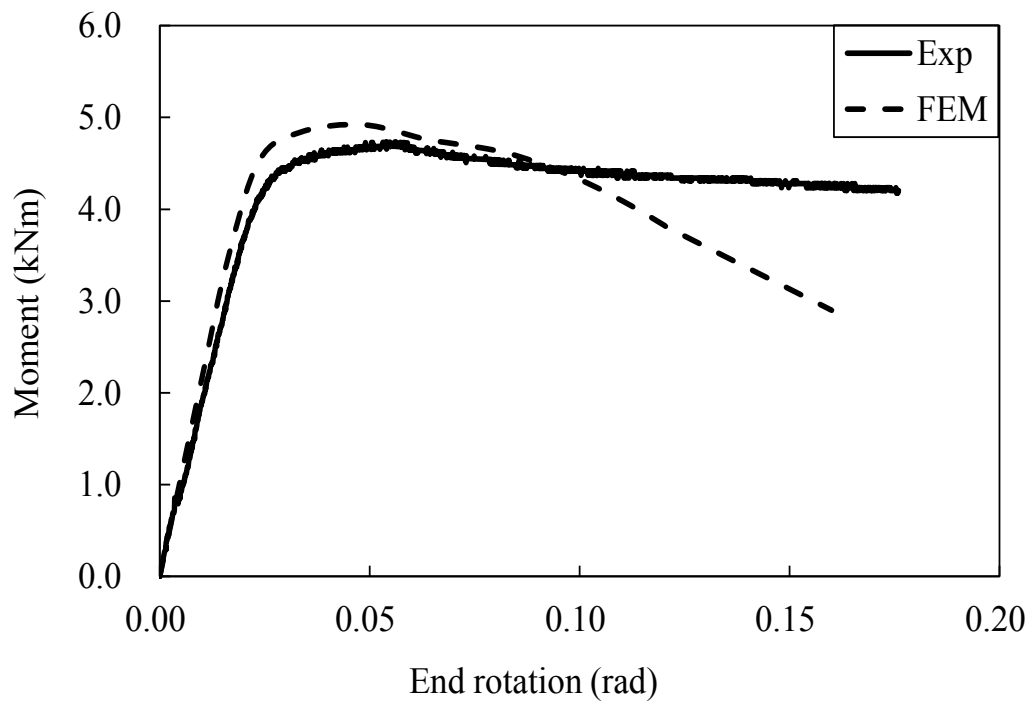
Fig. C.1 Moment versus end rotation curves for H70×55×4.2B3
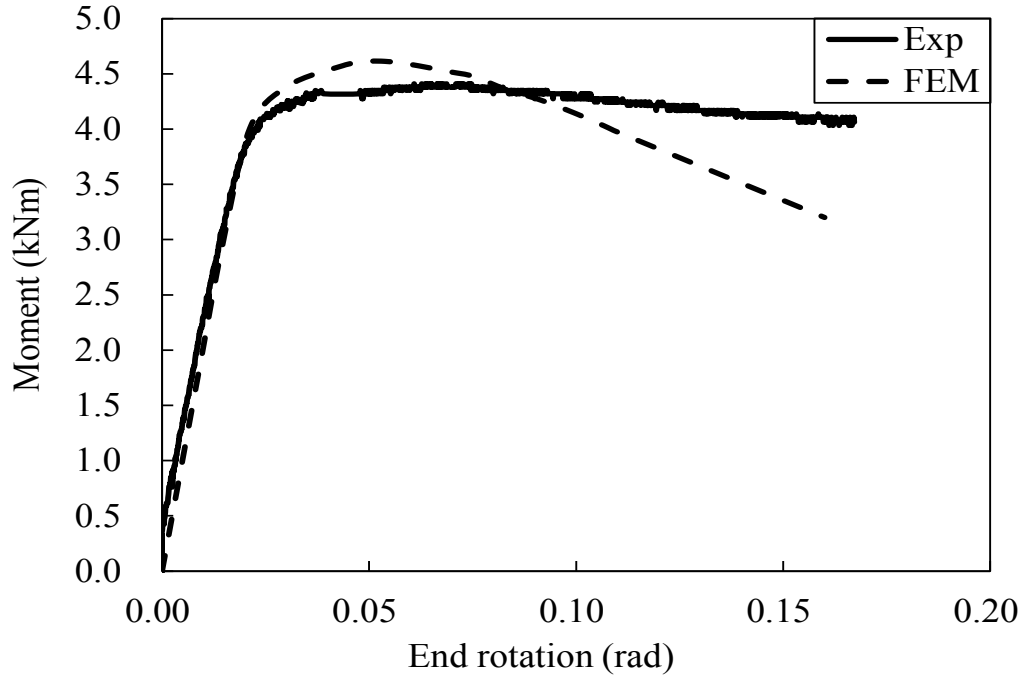
Fig. C.2 Moment versus end rotation curves for H70×55×4.2B3-R
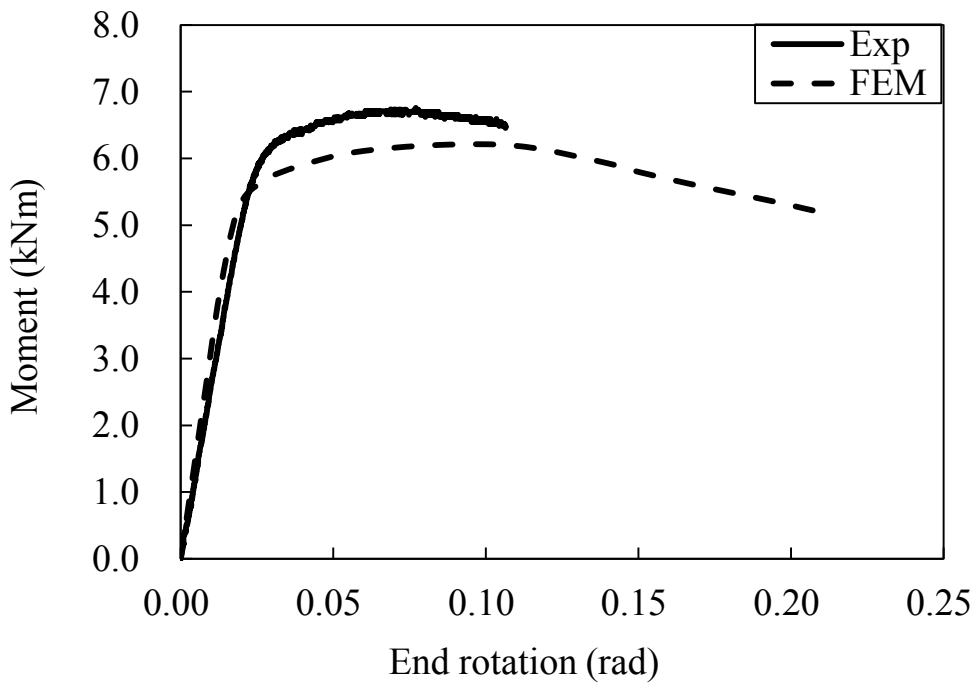
Fig. C.3 Moment versus end rotation curves for H55×70×4.2B3
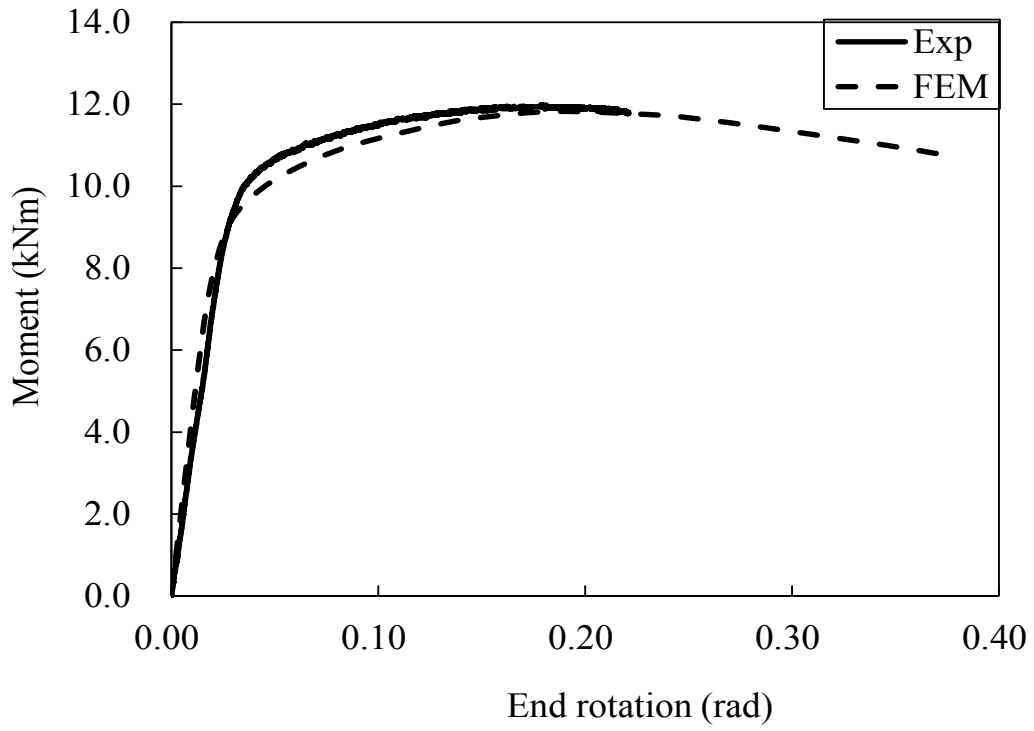
Fig. C.4 Moment versus end rotation curves for H95×50×10.5B3
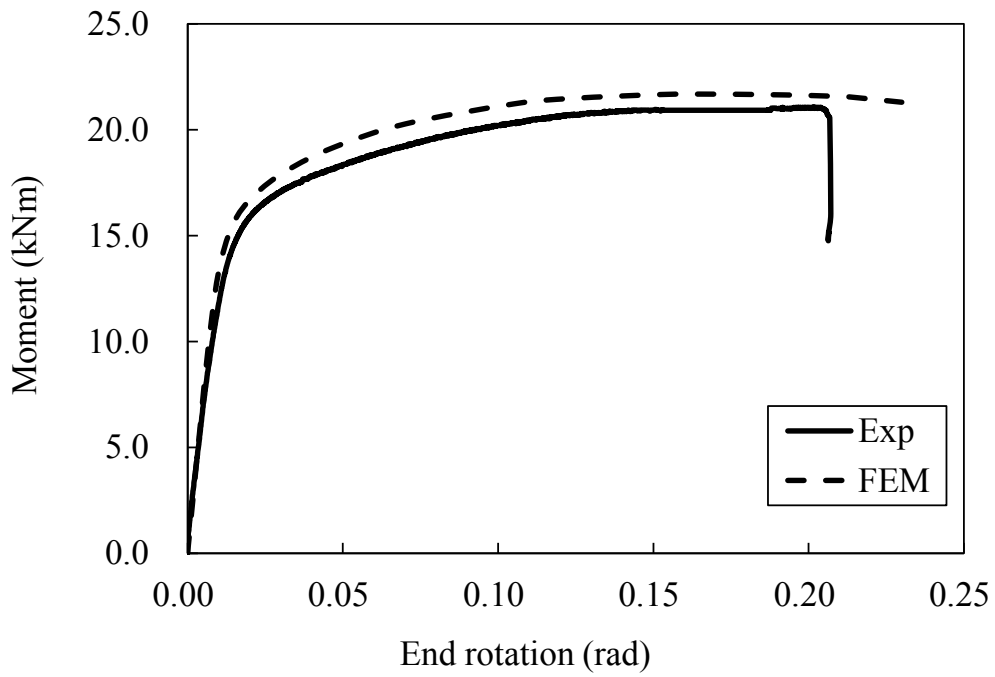
Fig. C.5 Moment versus end rotation curves for H50×95×10.5B3
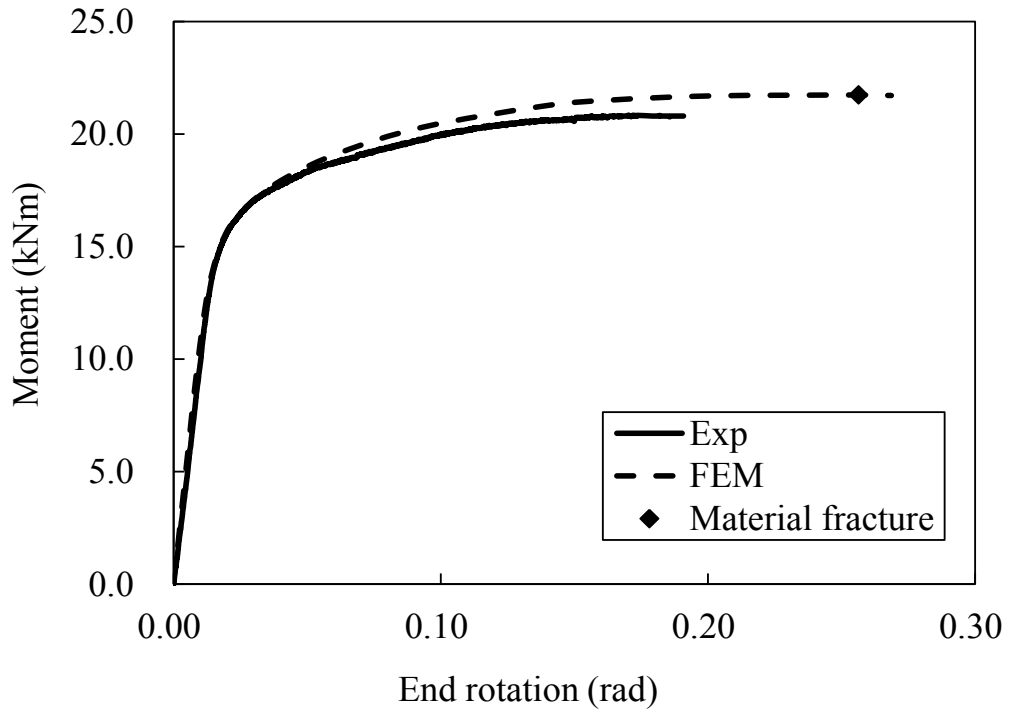
Fig. C.6 Moment versus end rotation curves for H50×95×10.5B3-R
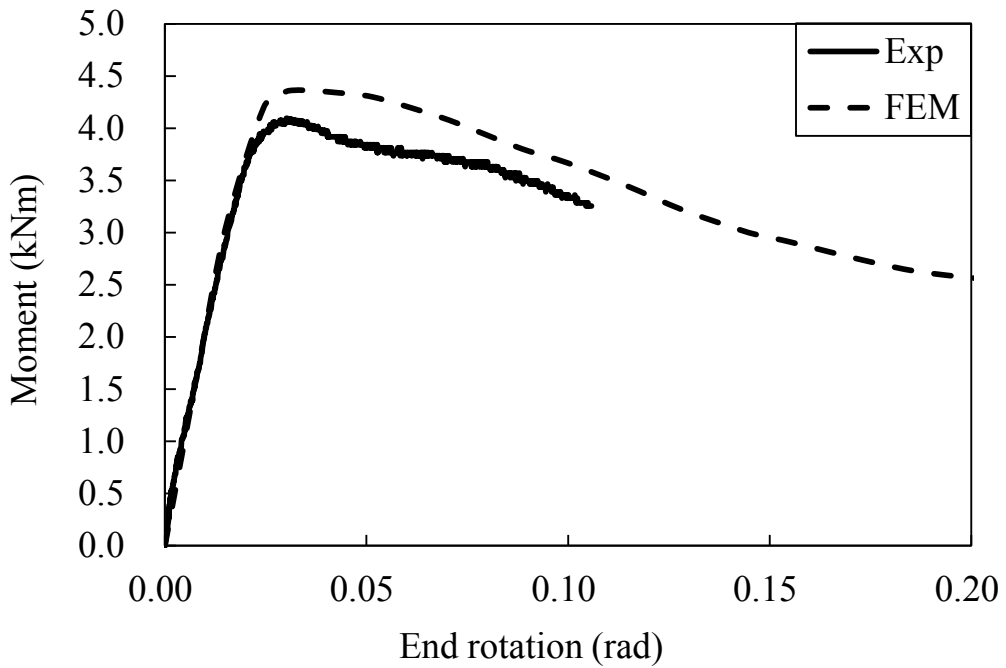
Fig. C.7 Moment versus end rotation curves for H64×64×3.0B3
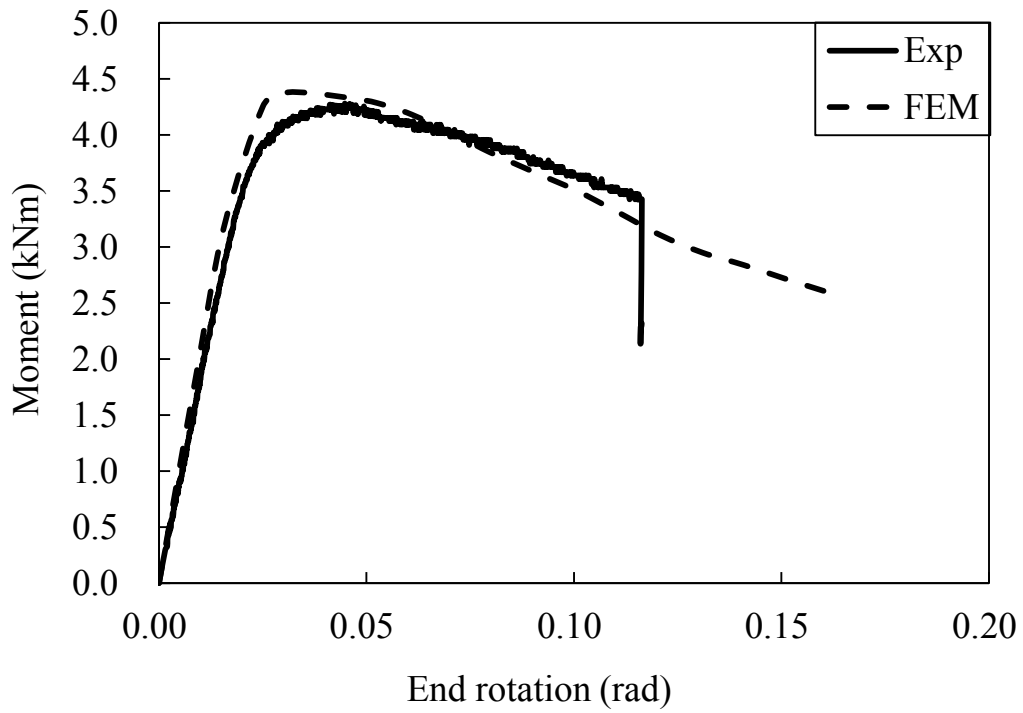
Fig. C.8 Moment versus end rotation curves for H64×64×3.0B3-R
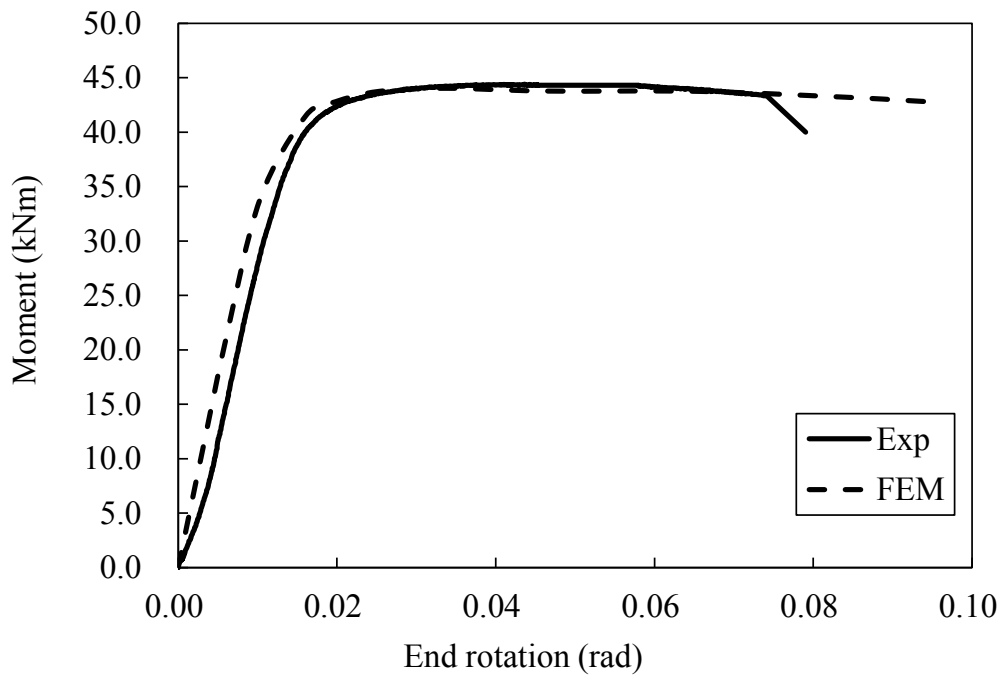
Fig. C.9 Moment versus end rotation curves for H120×120×9.0B3
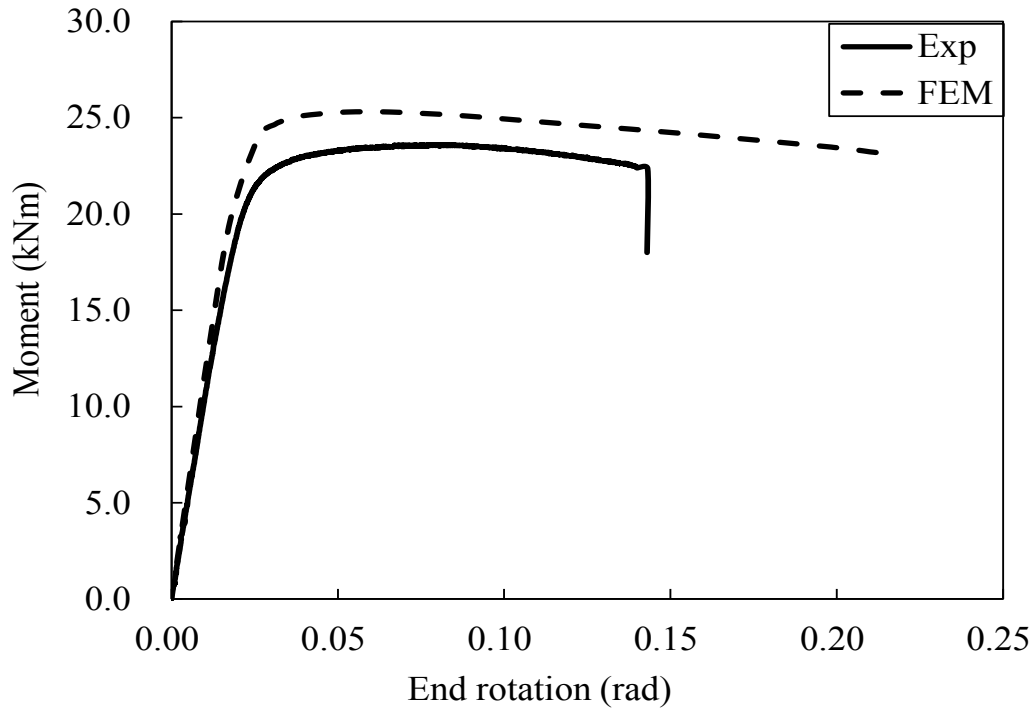
Fig. C.10 Moment versus end rotation curves for H120×70×10.5B3
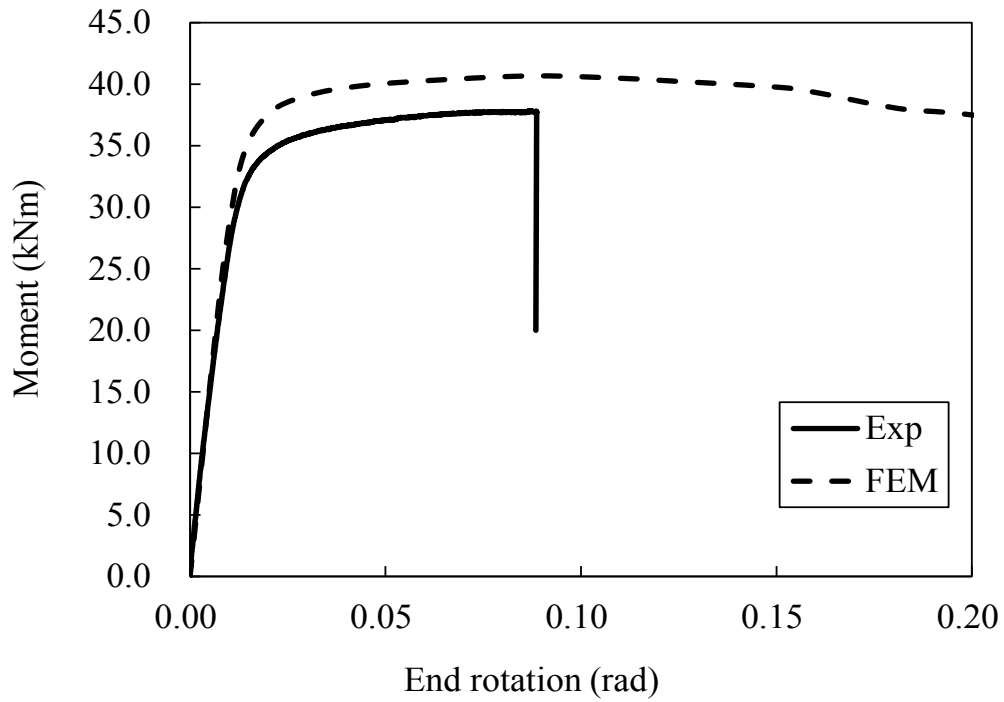
Fig. C.11 Moment versus end rotation curves for H70×120×10.5B3
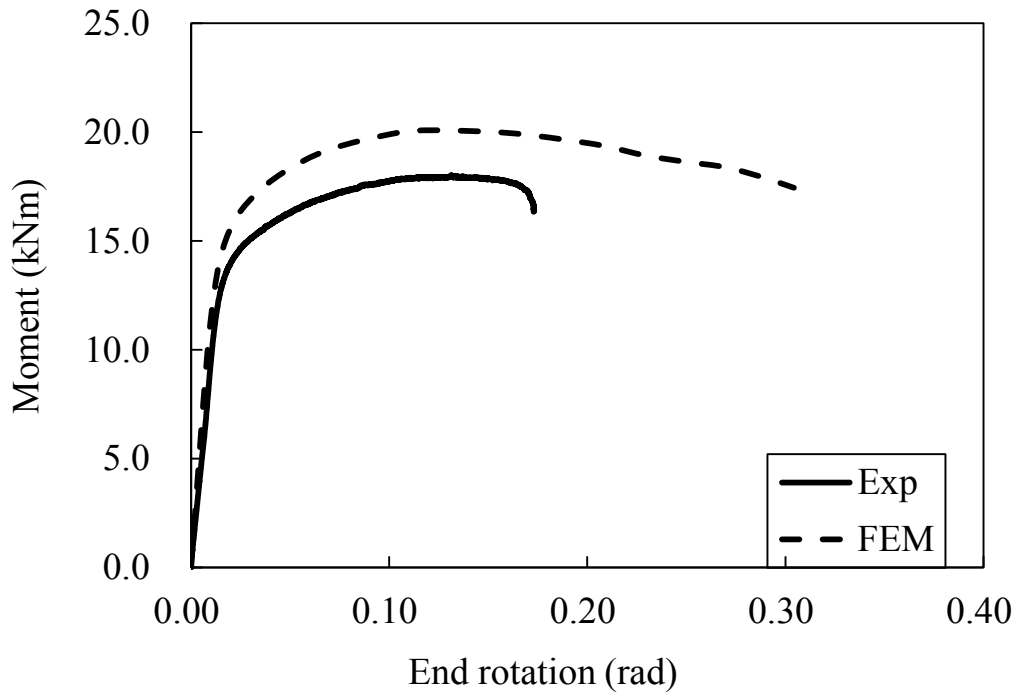
Fig. C.12 Moment versus end rotation curves for N120×70×10.5B3
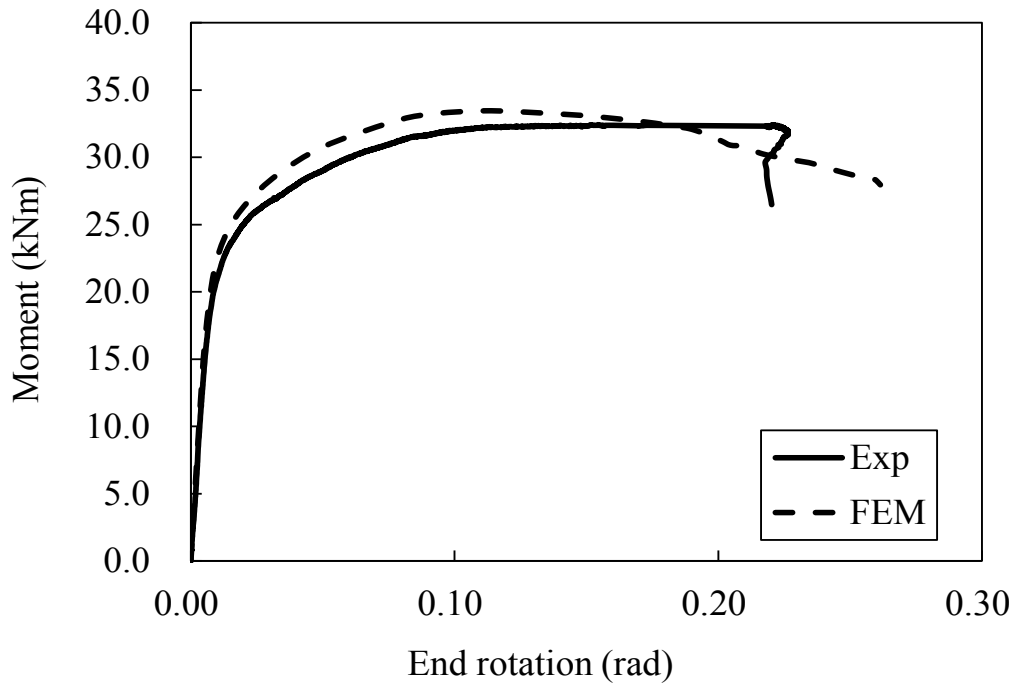
Fig. C.13 Moment versus end rotation curves for N70×120×10.5B3
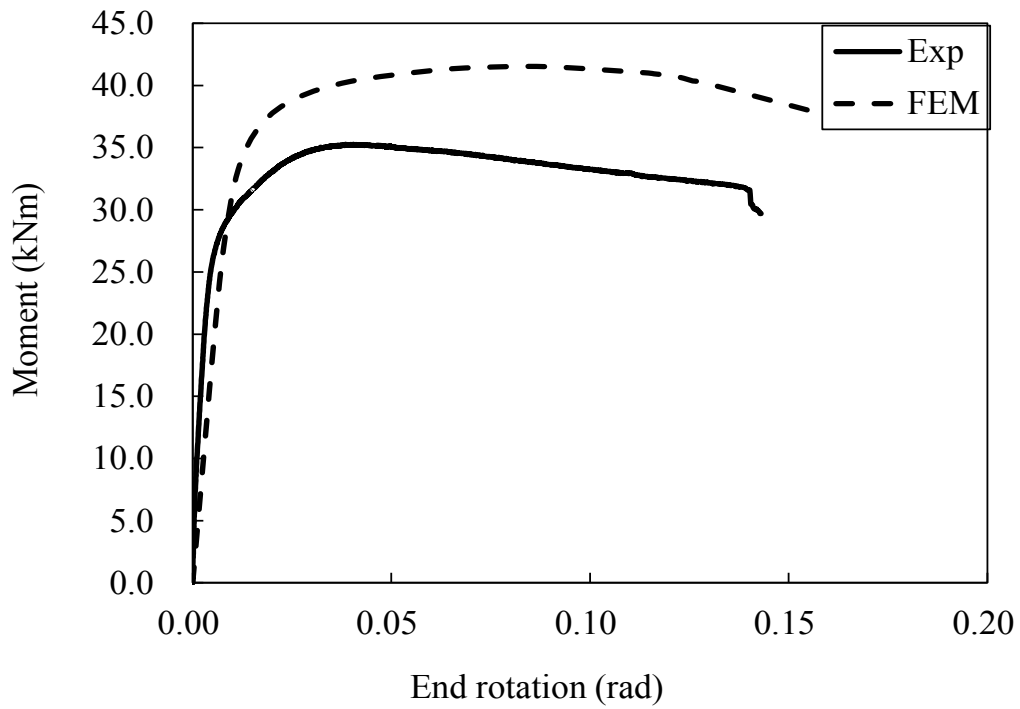
Fig. C.14 Moment versus end rotation curves for N120×120×9.0B3
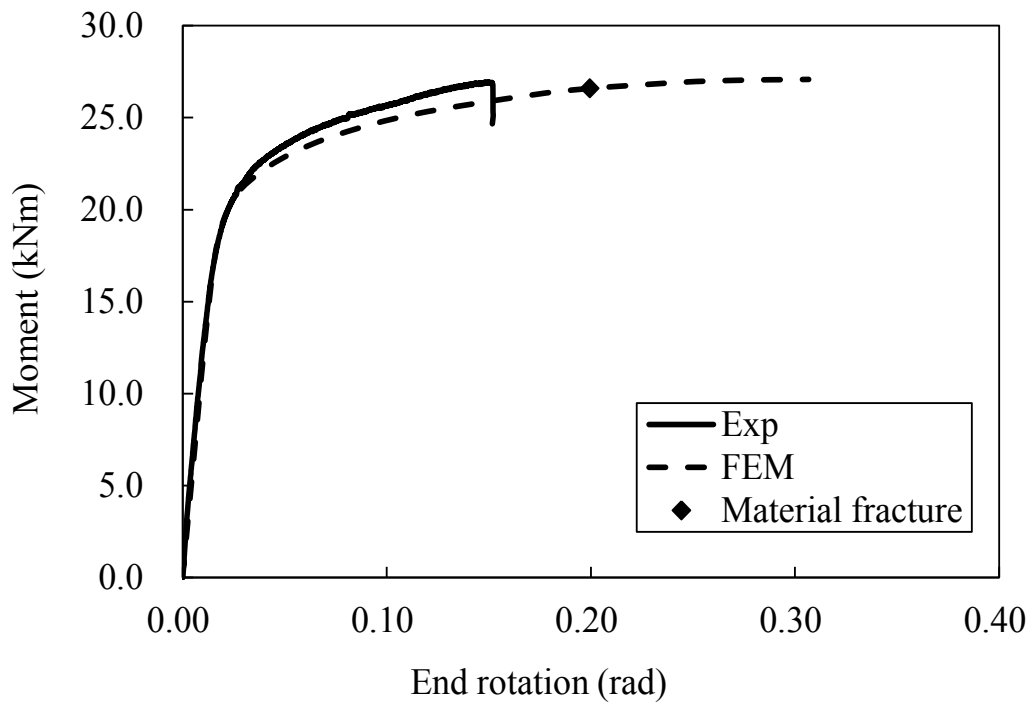
Fig. C.15 Moment versus end rotation curves for +H120×70×10.5B3
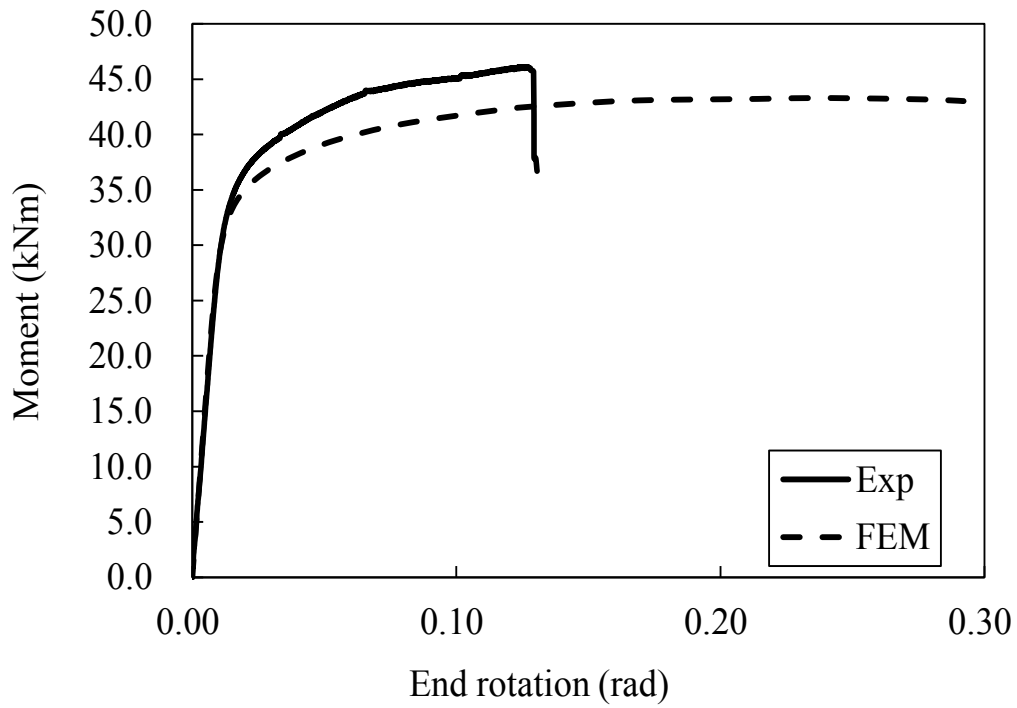
Fig. C.16 Moment versus end rotation curves for +H70×120×10.5B3
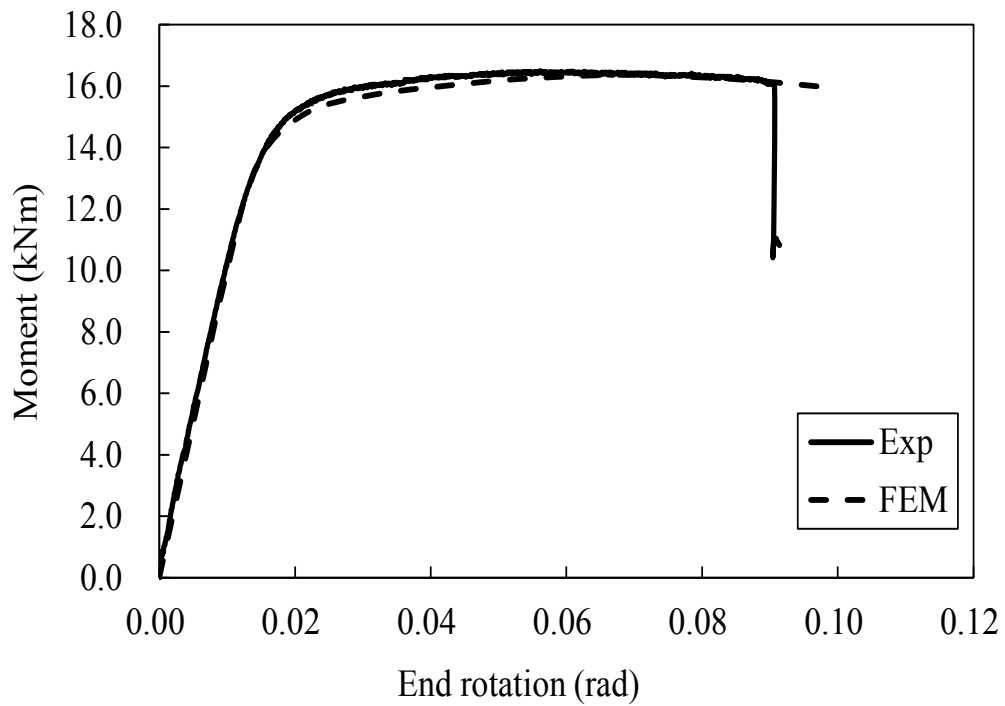
Fig. C.17 Moment versus end rotation curves for +H95×95×4.3B3

271
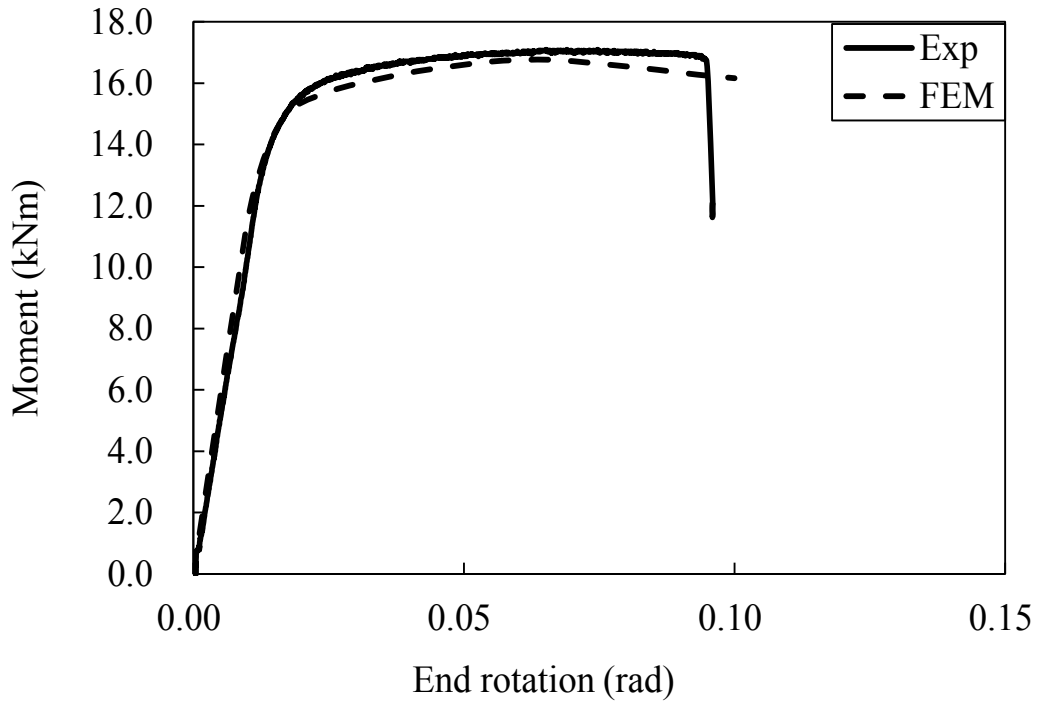
Fig. C.18 Moment versus end rotation curves for +H95×95×4.3B3-R
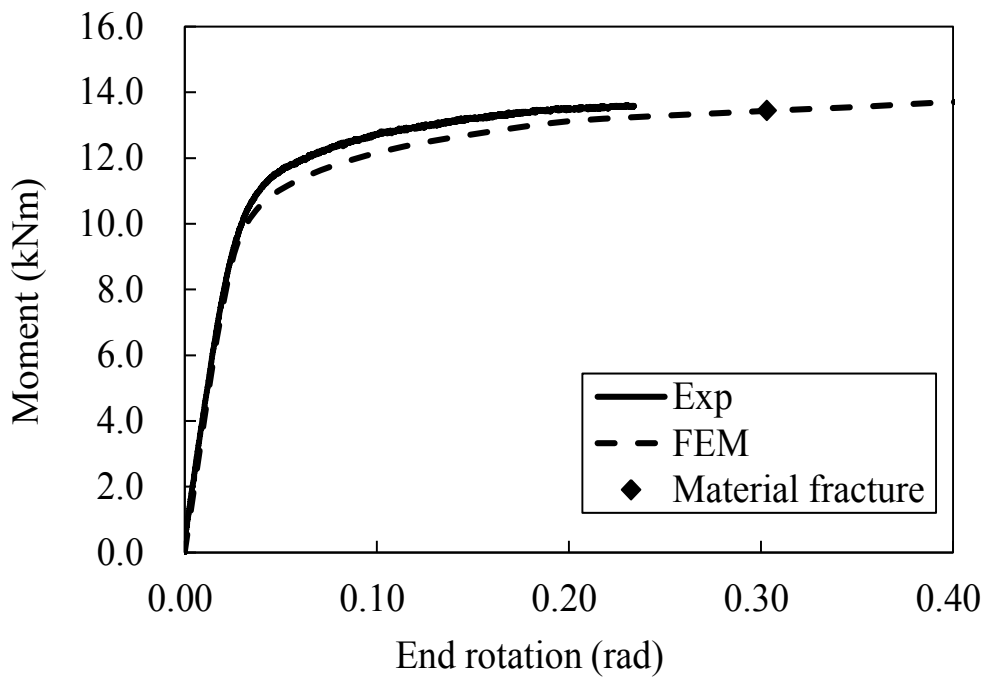
Fig. C.19 Moment versus end rotation curves for +H95×50×10.5B3

272
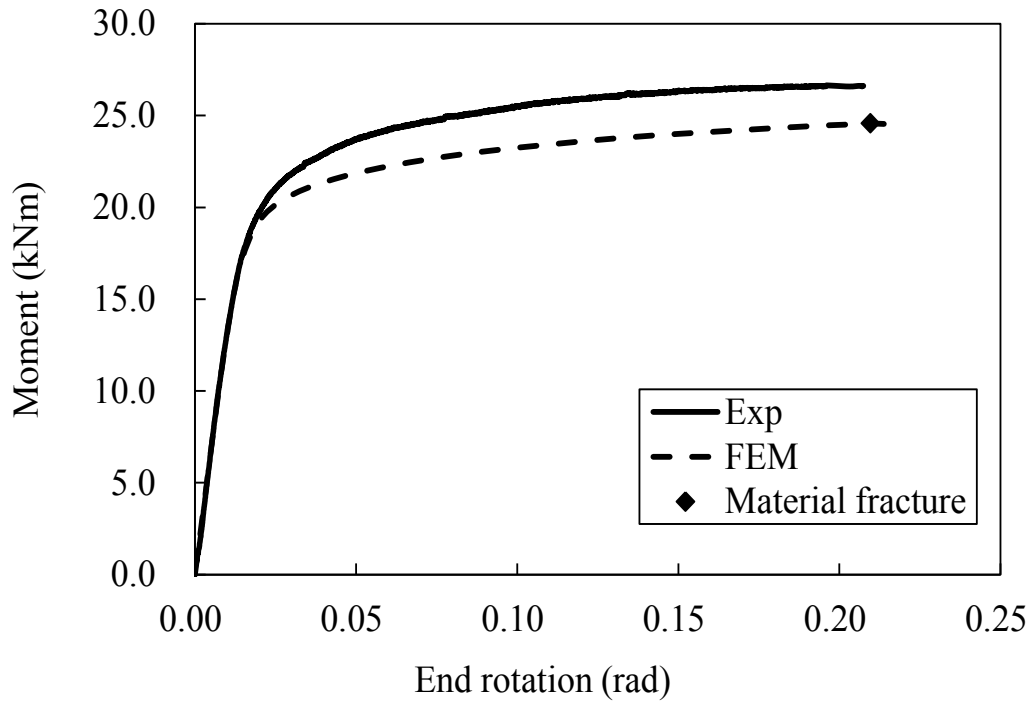
Fig. C.20 Moment versus end rotation curves for +H50×95×10.5B3

APPENDIX D.

MOMENT-CURVATURE CURVES FROM FOUR-POINT BENDING TESTS AND SIMULATIONS
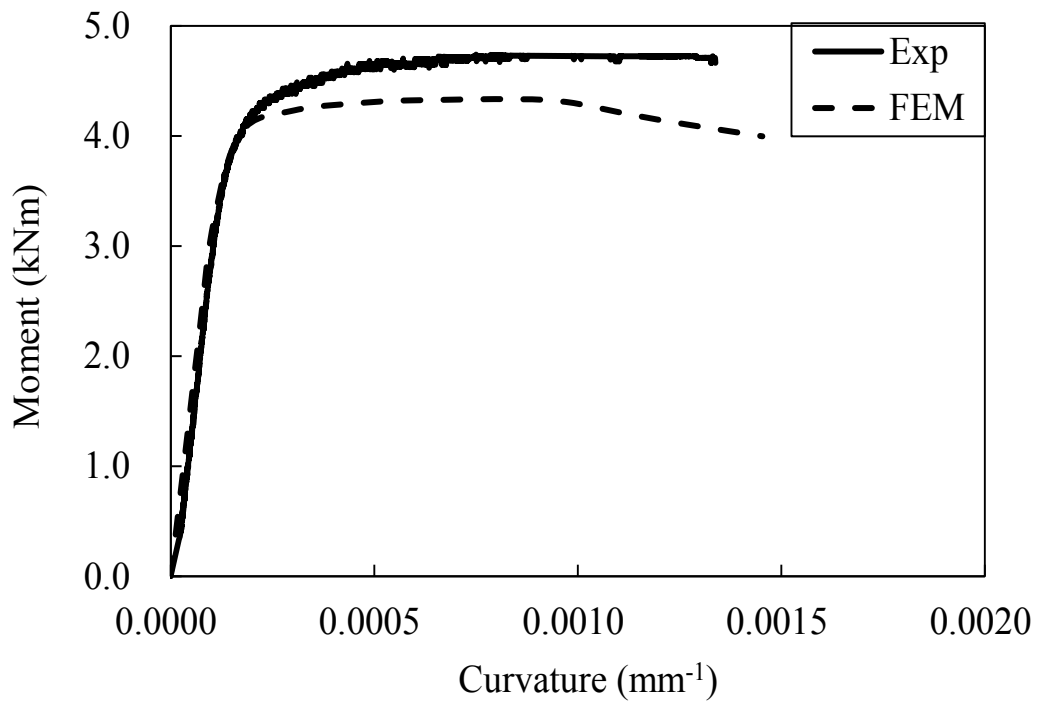
Fig. D.1 Moment versus curvature curves for H70×55×4.2B4
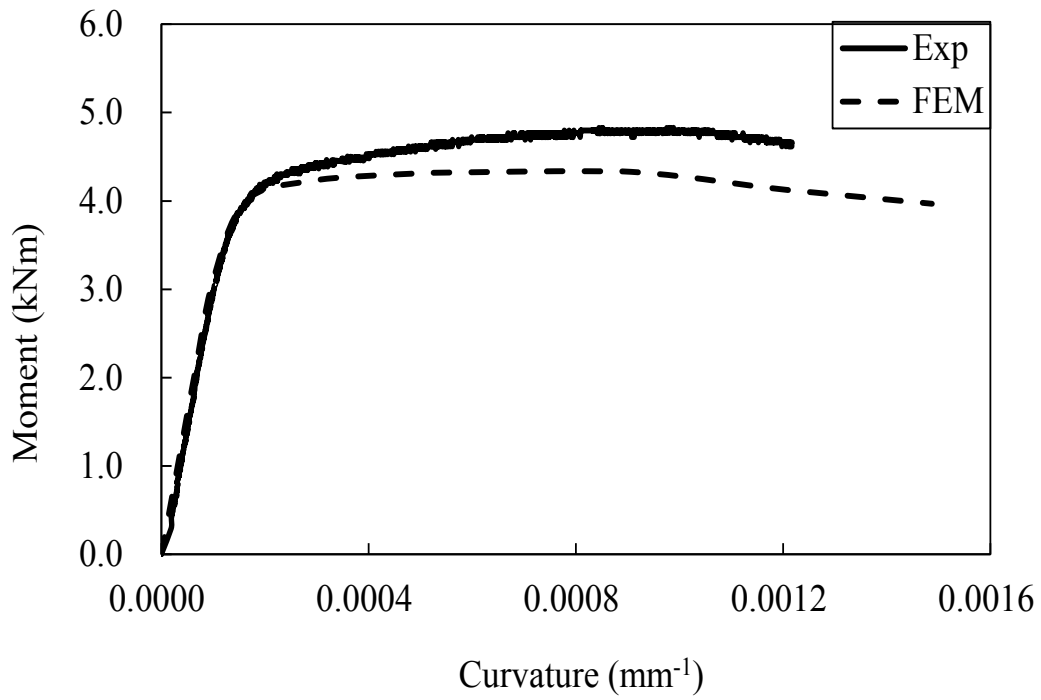
Fig. D.2 Moment versus curvature curves for H70×55×4.2B4-R
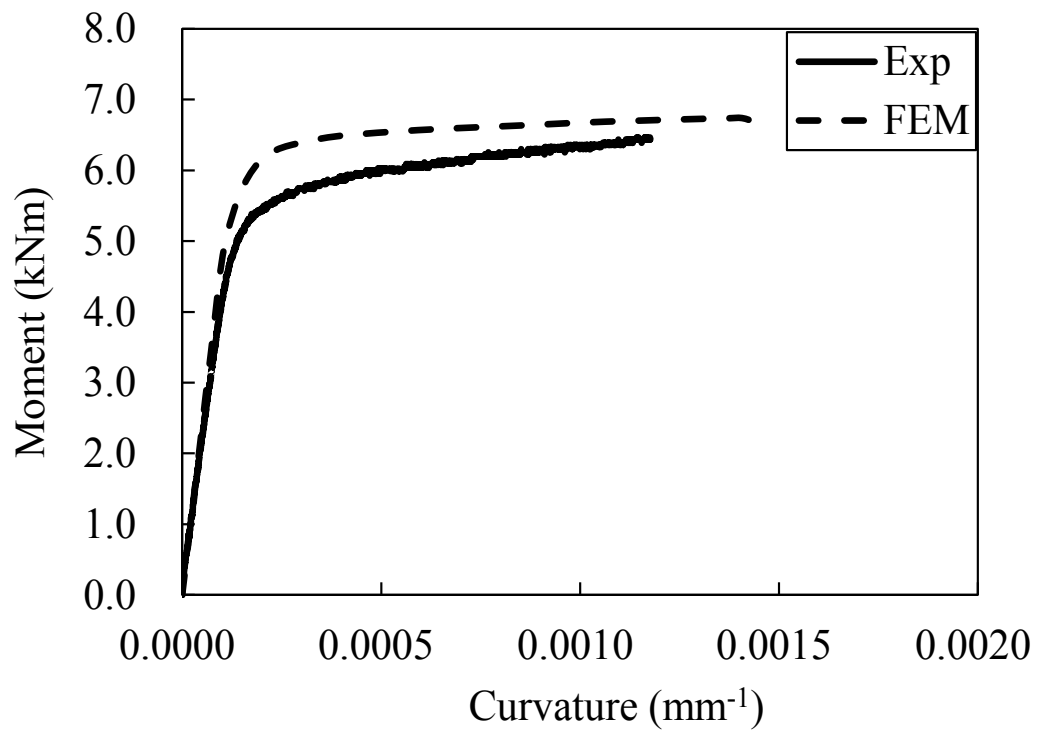
Fig. D. 3 Moment versus curvature curves for H55×70×4.2B4
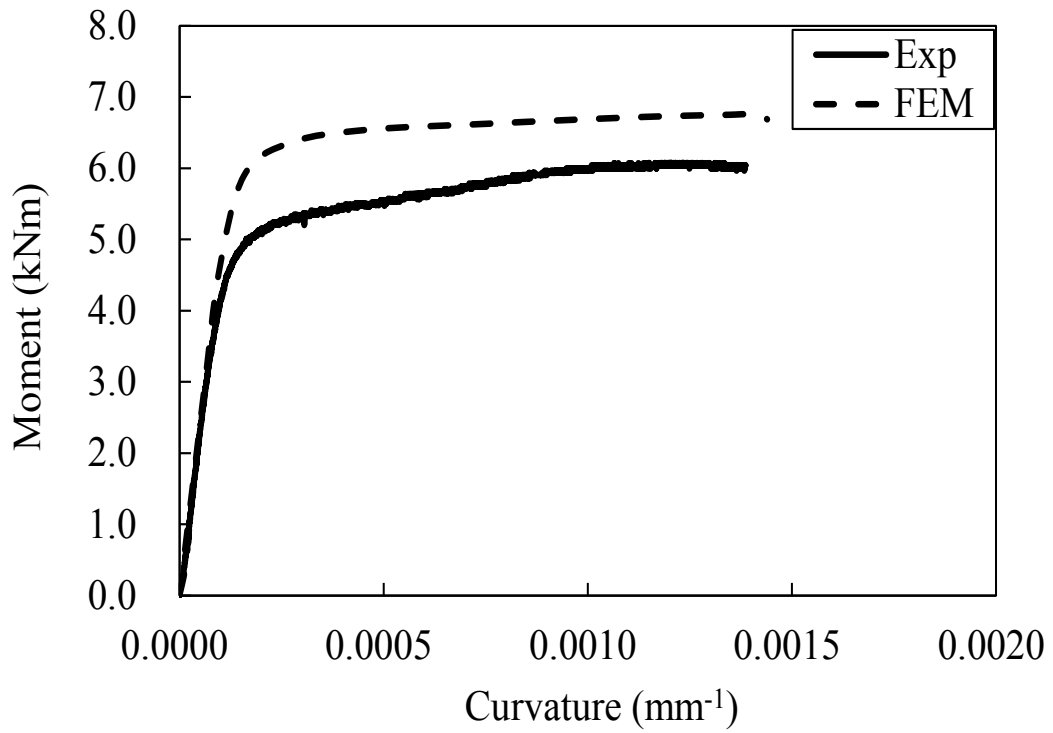
Fig. D. 4 Moment versus curvature curves for H55×70×4.2B4-R
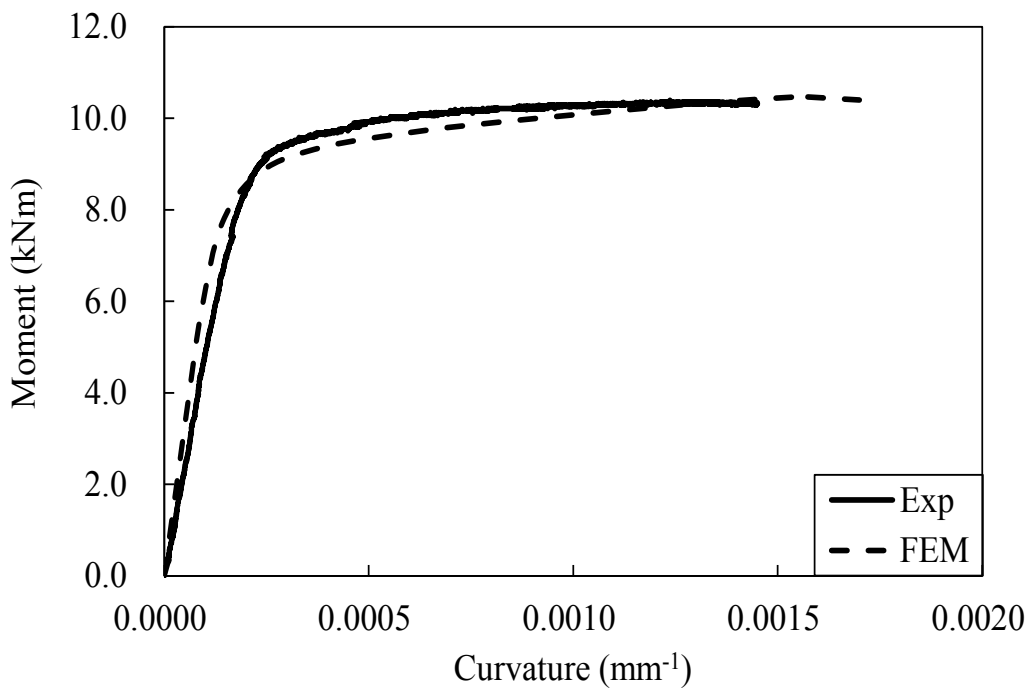
Fig. D.5 Moment versus curvature curves for H95×50×10.5B4

276
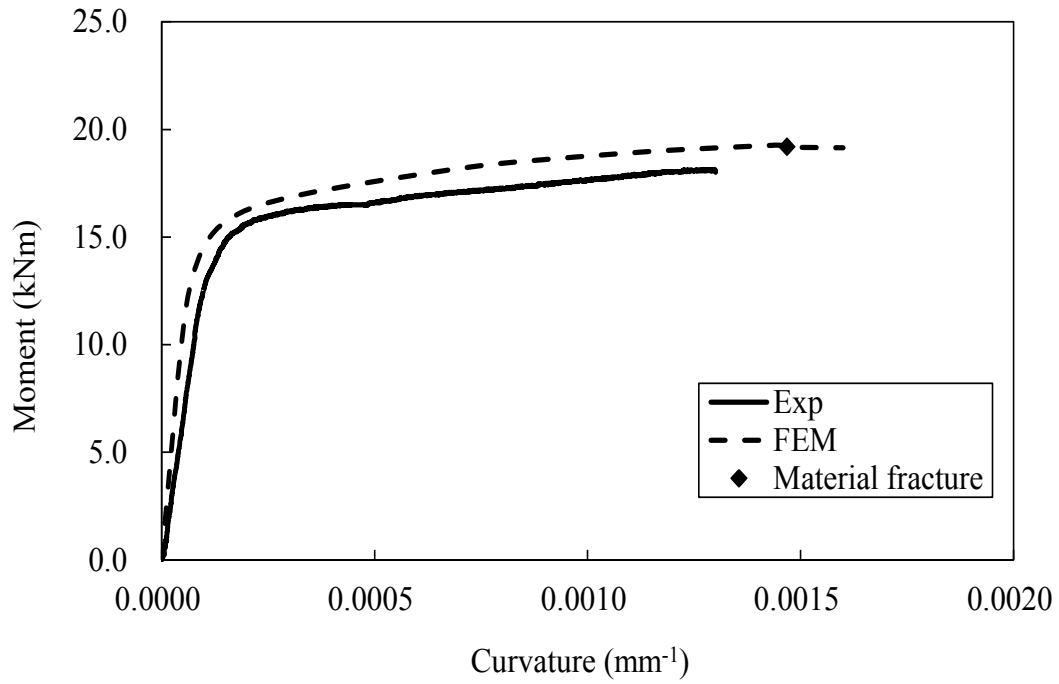
Fig. D.6 Moment versus curvature curves for H50×95×10.5B4
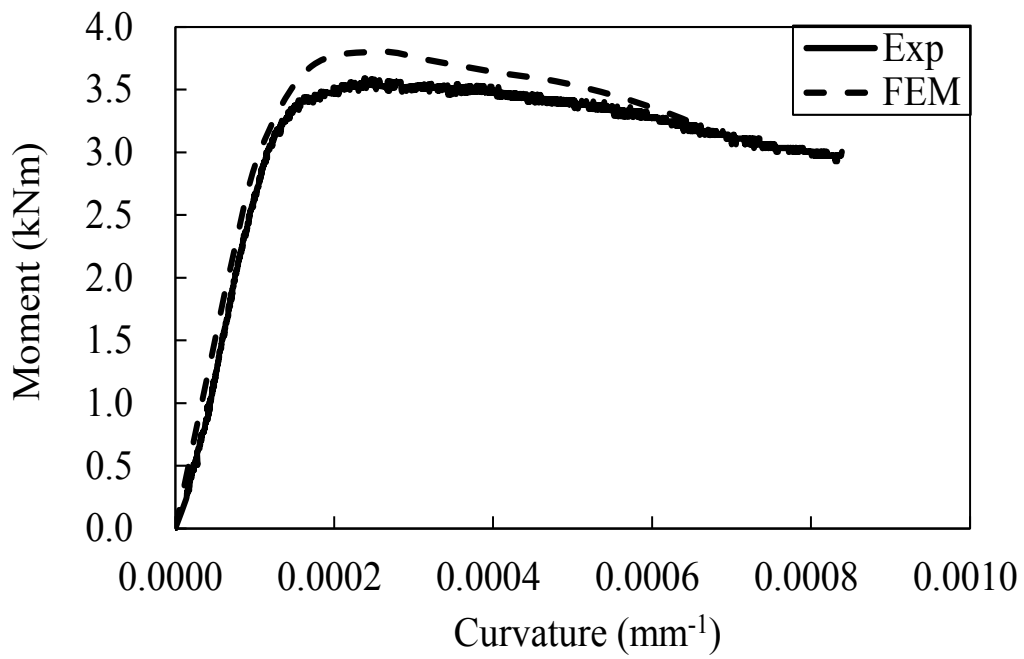
Fig. D.7 Moment versus curvature curves for H64×64×3.0B4
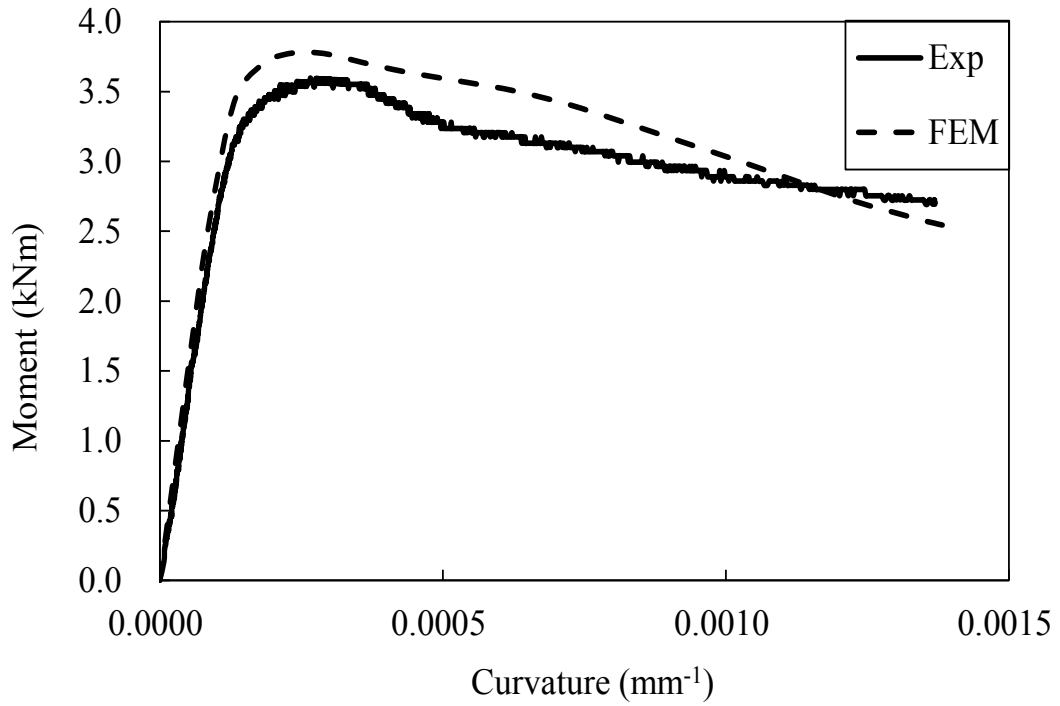
Fig. D.8 Moment versus curvature curves for H64×64×3.0B4-R
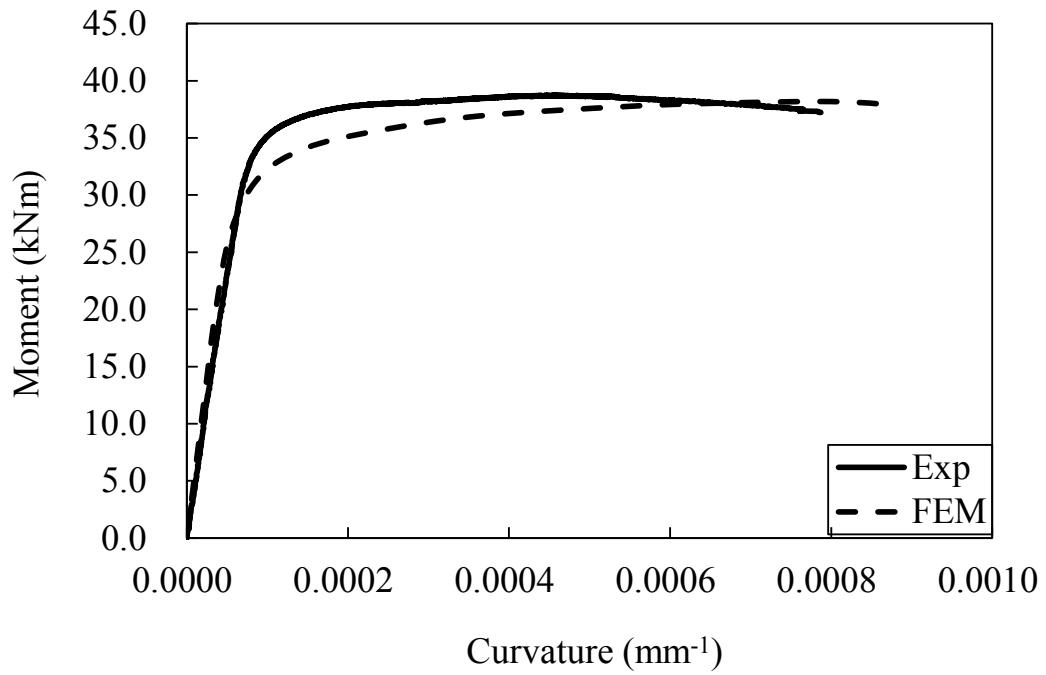
Fig. D.9 Moment versus curvature curves for H120×120×9.0B4
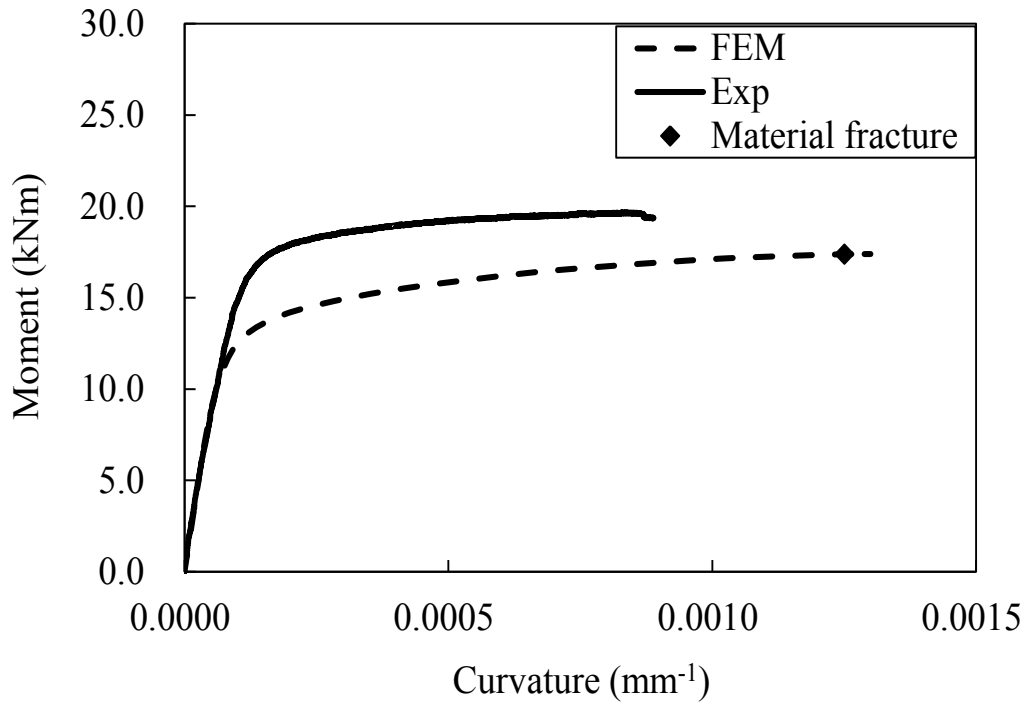
Fig. D.10 Moment versus curvature curves for H120×70×10.5B4
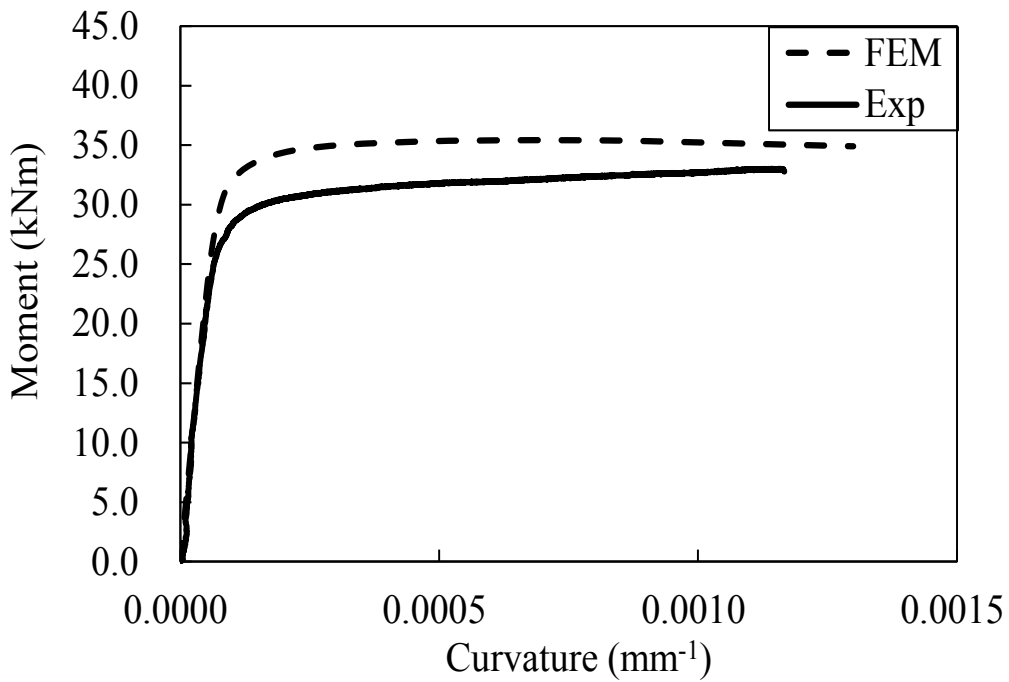
Fig. D.11 Moment versus curvature curves for H70×120×10.5B4
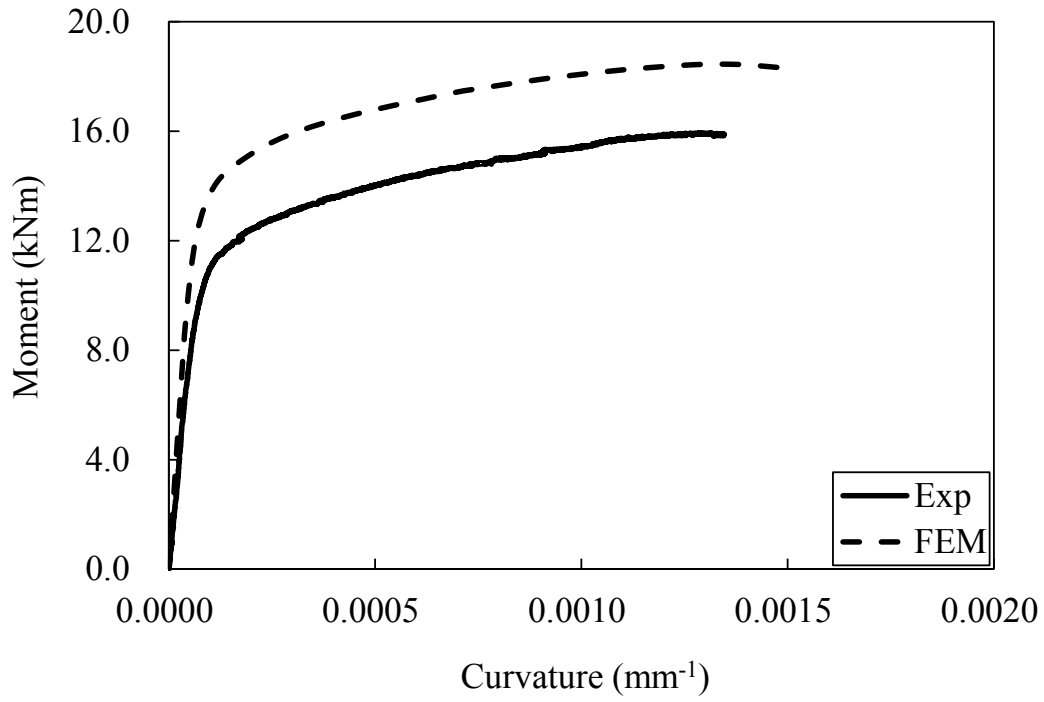
Fig. D.12 Moment versus curvature curves for N50×95×10.5B4
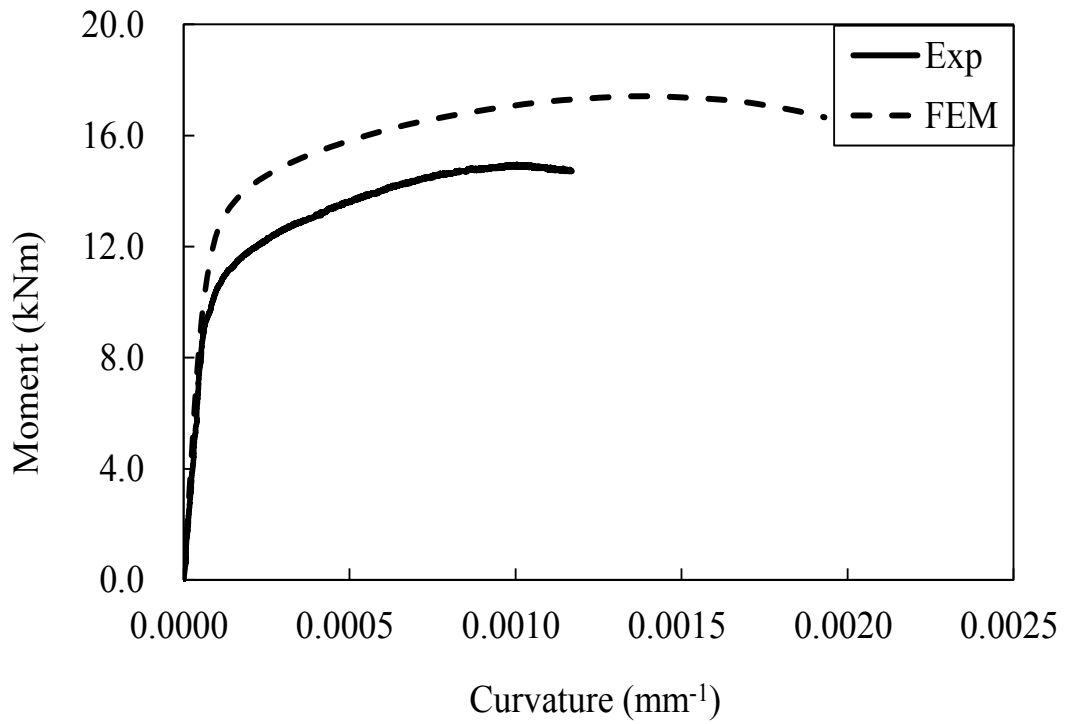
Fig. D.13 Moment versus curvature curves for N120×70×10.5B4
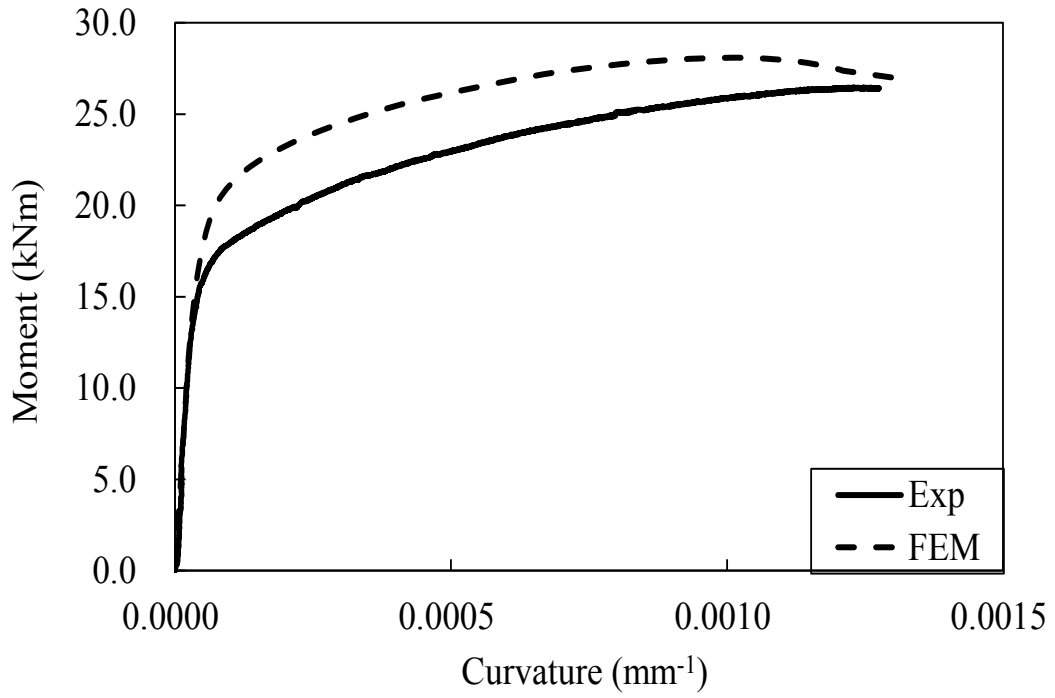
Fig. D.14 Moment versus curvature curves for N70×120×10.5B4
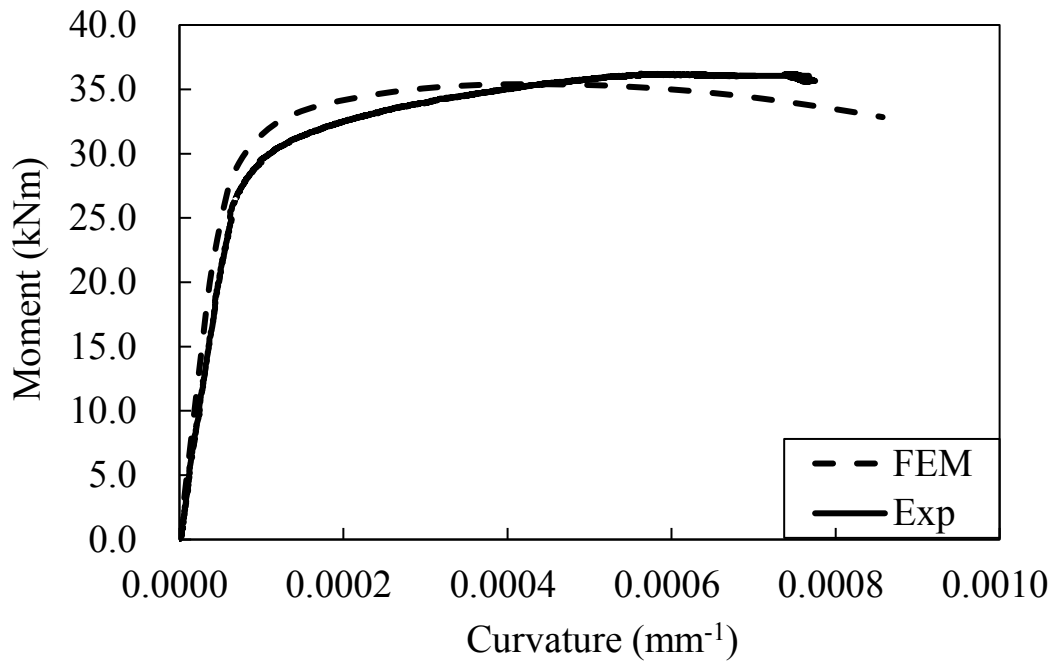
Fig. D.15 Moment versus curvature curves for N120×120×9.0B4
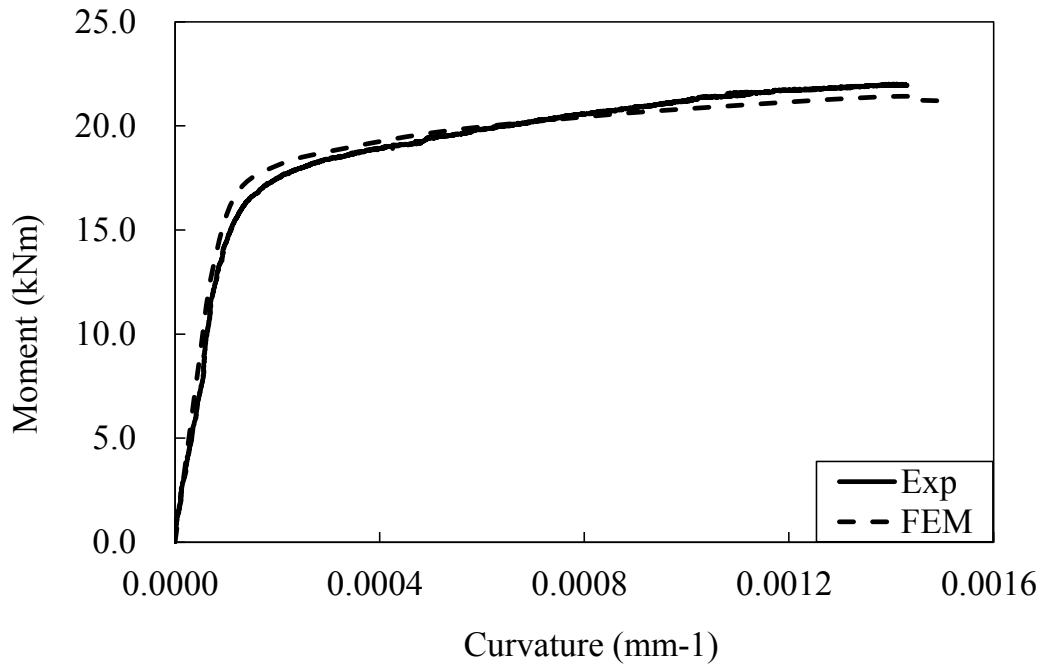
Fig. D.16. Moment versus curvature curves for +H120×70×10.5B4
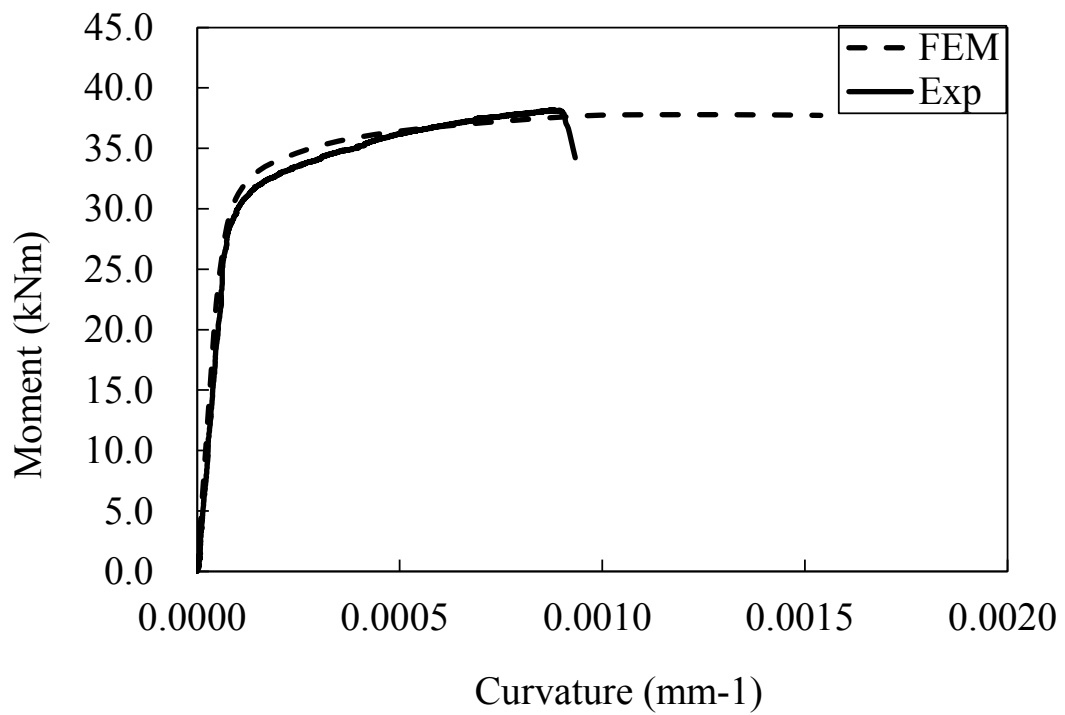
Fig. D.17. Moment versus curvature curves for +H70×120×10.5B4
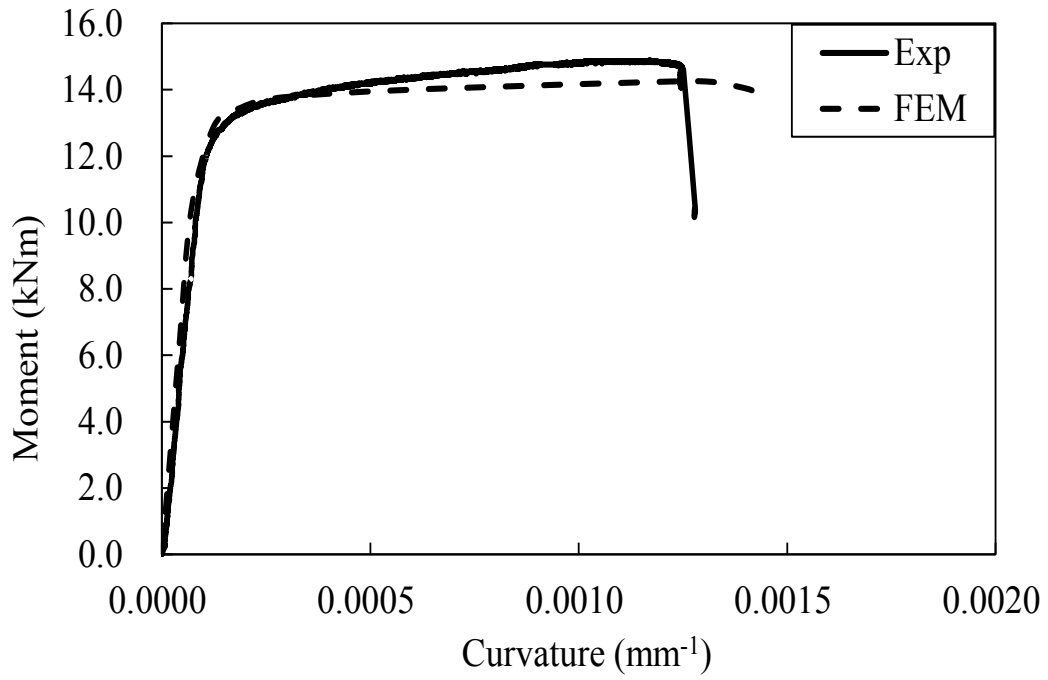
Fig. C.18. Moment versus curvature curves for +H95×95×4.3B4
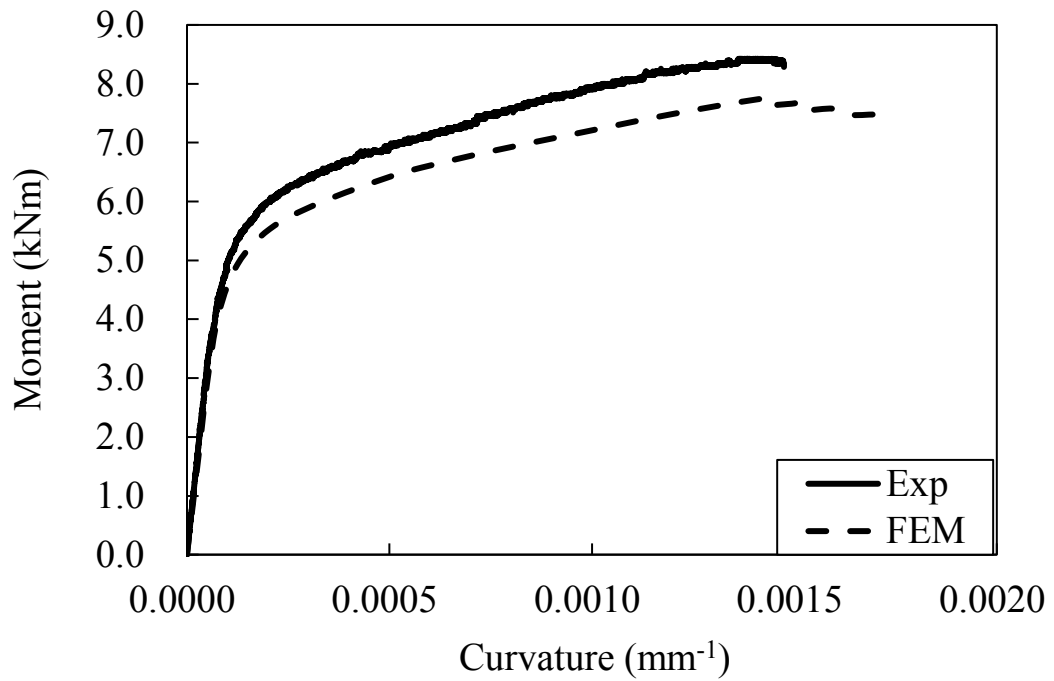
Fig. D.19. Moment versus curvature curves for +N95×50×10.5B4

283
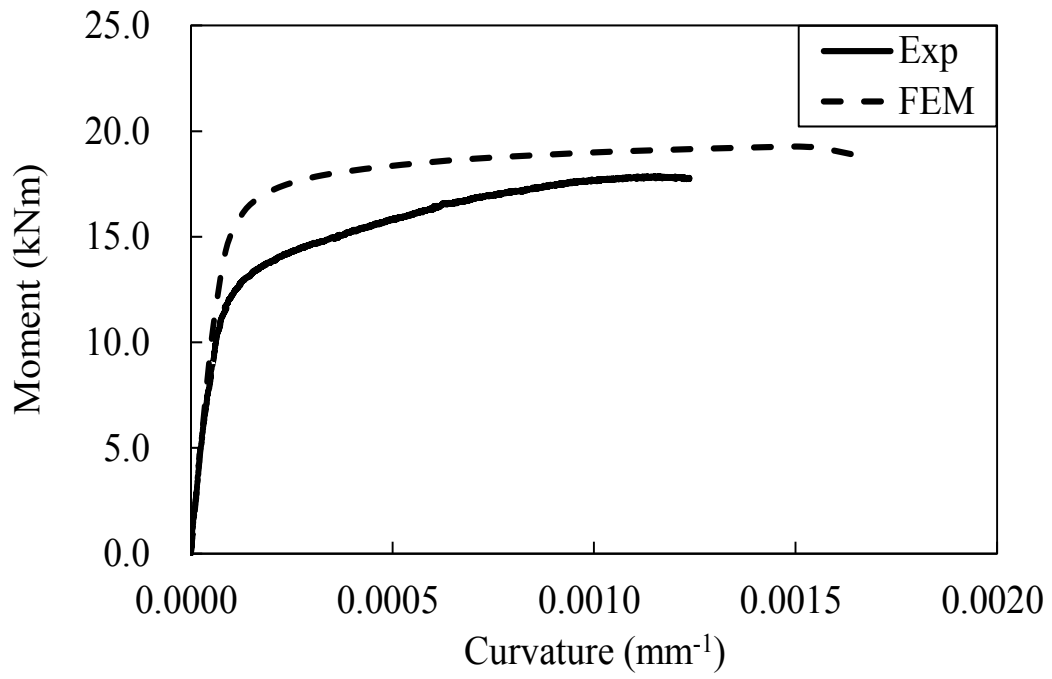
Fig. D.20. Moment versus curvature curves for +N50×95×10.5B4

APPENDIX E.

LOAD-DEFLECTION CURVES FOR CONTINUOUS BENDING TESTS AND SIMULATIONS

E.1   Loading configuration I
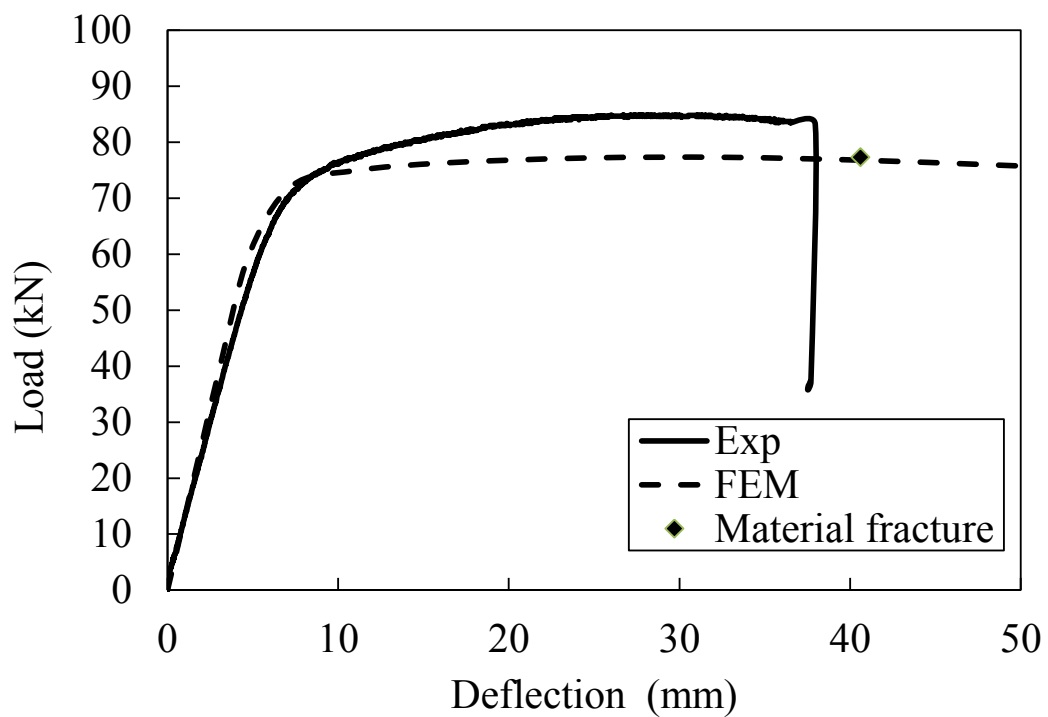
Fig. E.1.1 Load-deflection curves for H70×55×4.2B5I
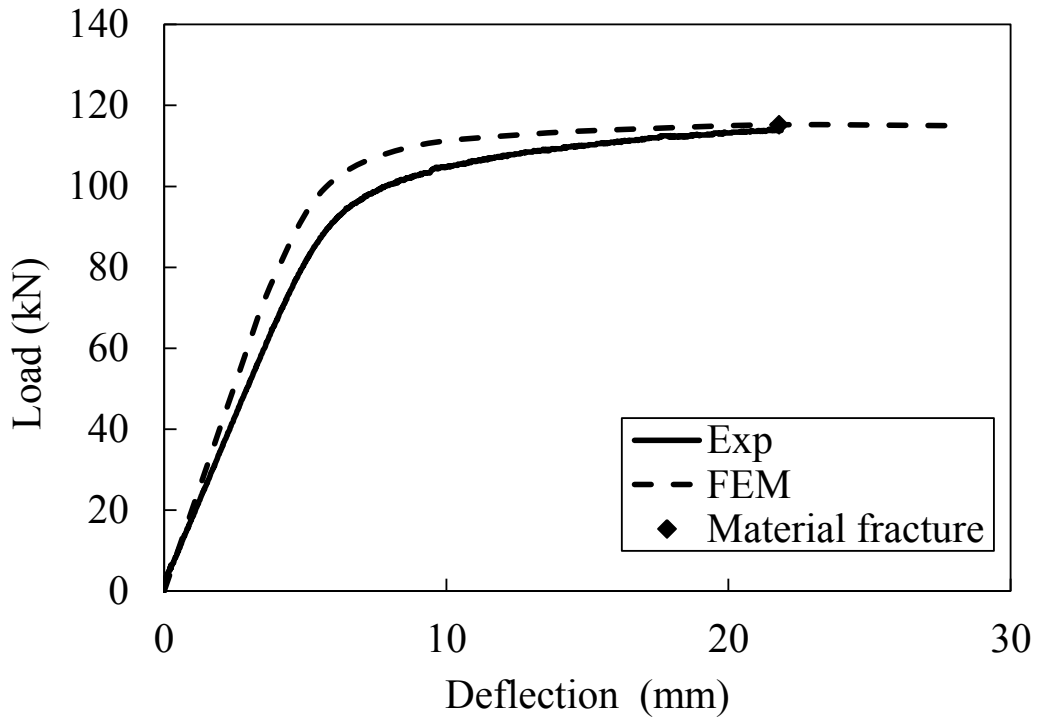
Fig. E.1.2 Load-deflection curves for H55×70×4.2B5I
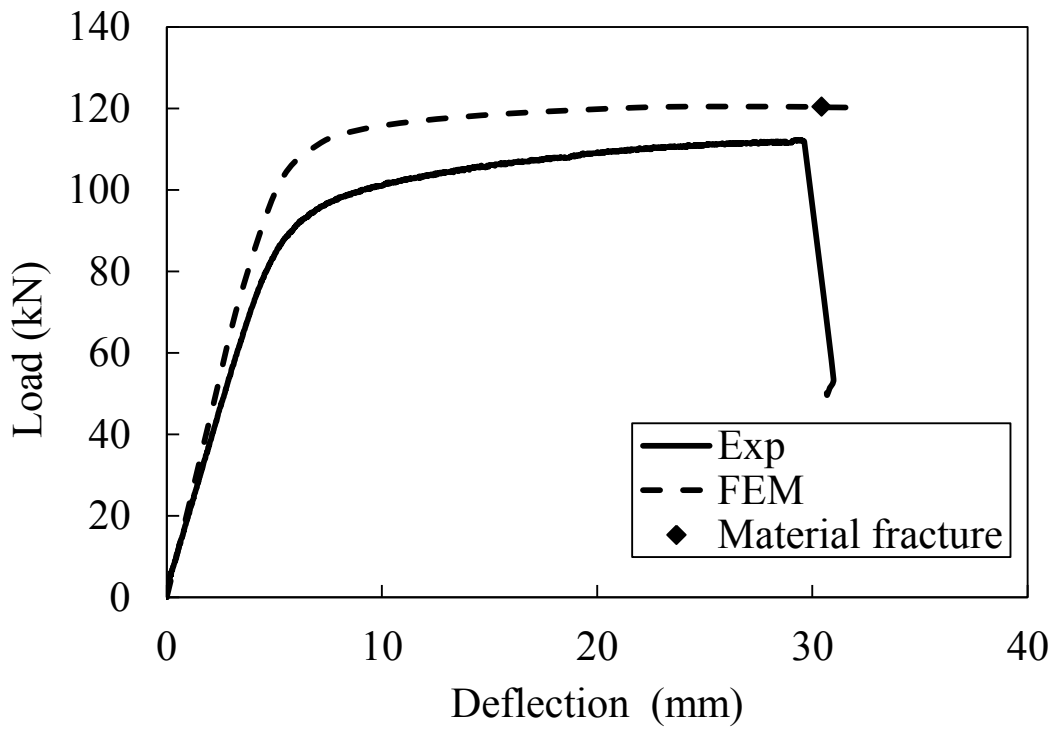
Fig. E.1.3 Load-deflection curves for H55×70×4.2B5I-R
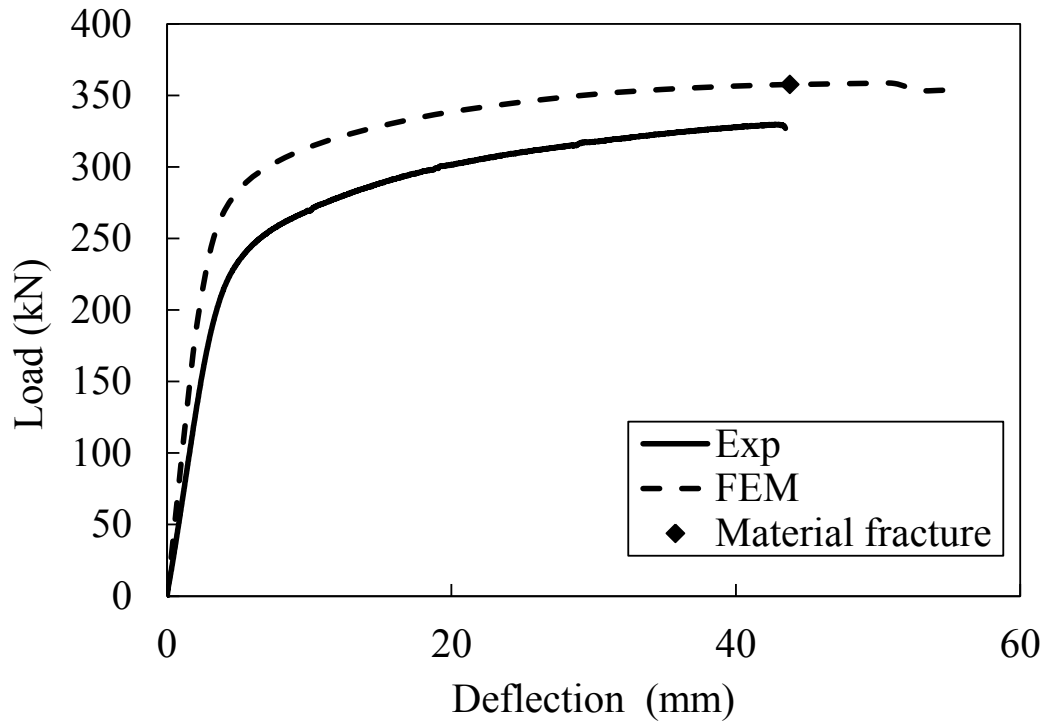
Fig. E.1.4 Load-deflection curves for H50×95×10.5B5I
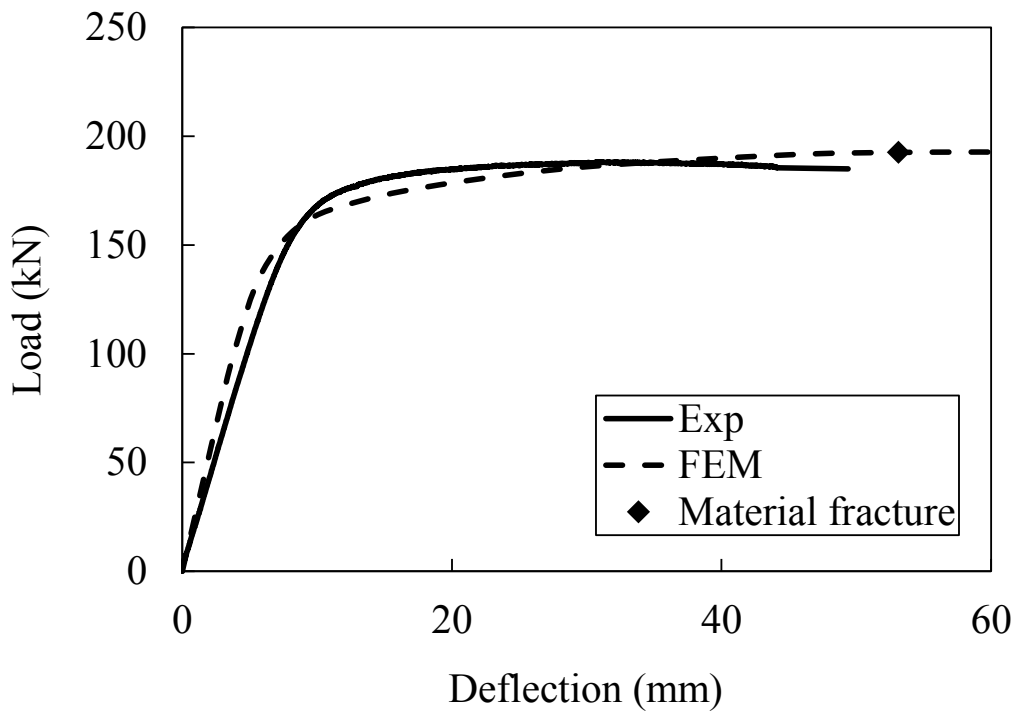
Fig. E.1.5 Load-deflection curves for H95×50×10.5B5I
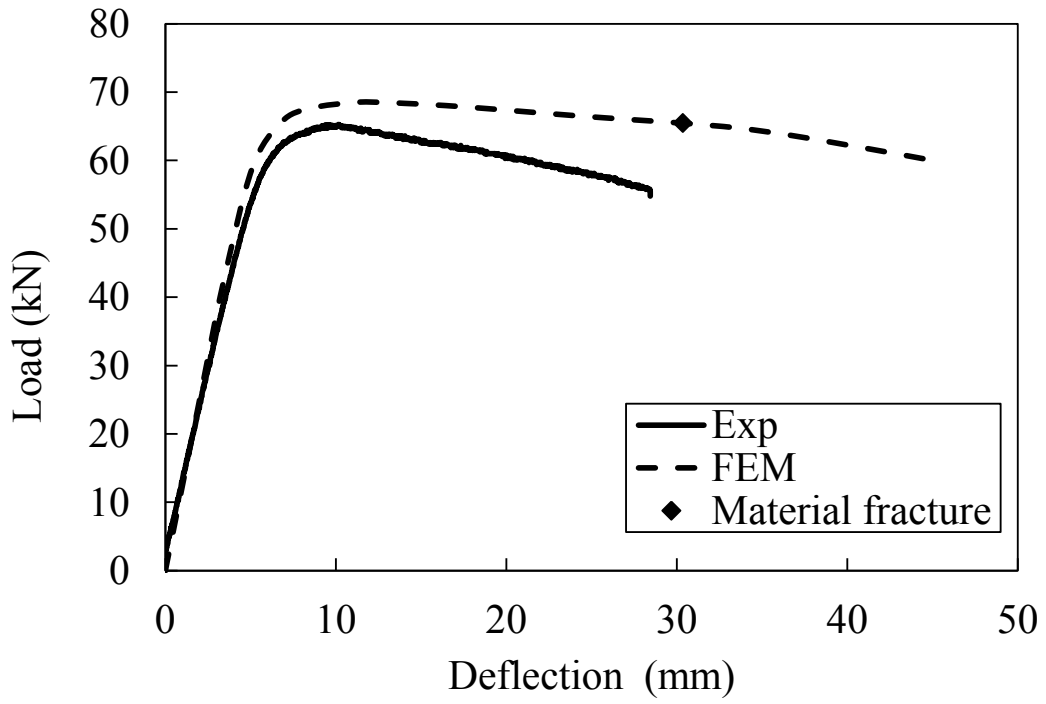
Fig. E.1.6 Load-deflection curves for H64×64×3.0B5I
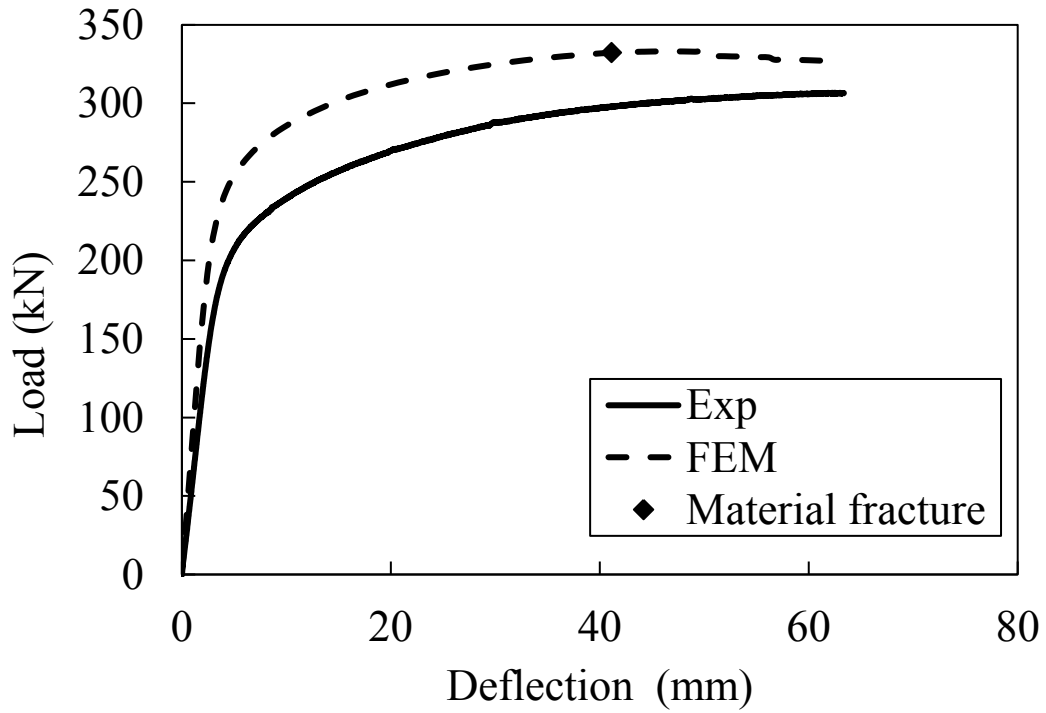
Fig. E.1.7 Load-deflection curves for N50×95×10.5B5I
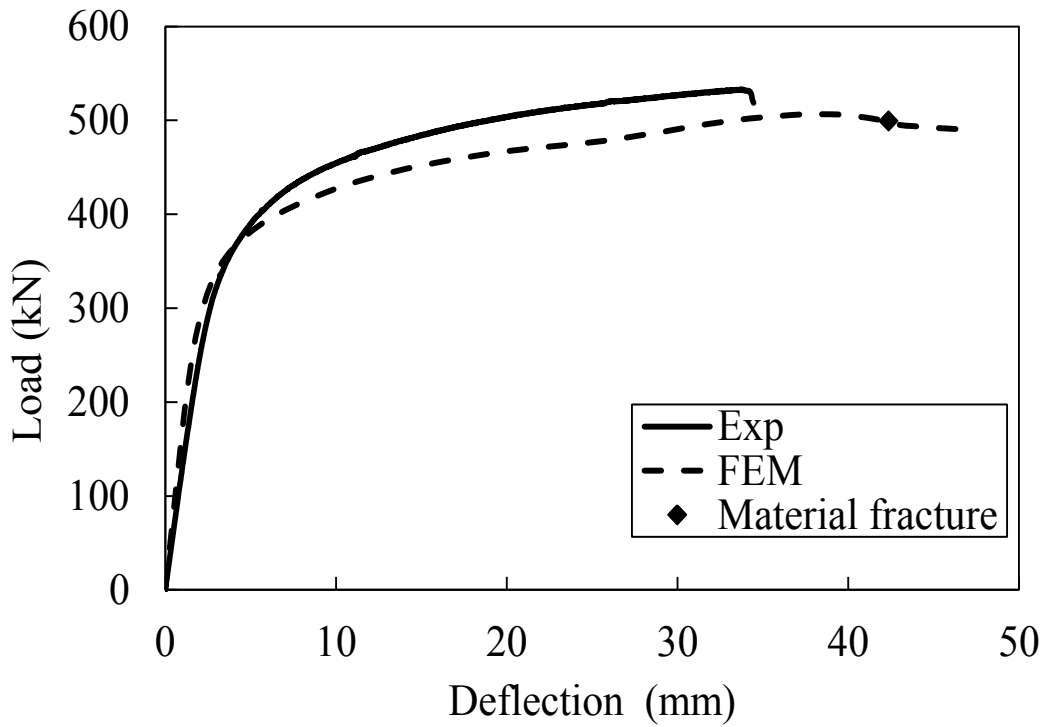
Fig. E.1.8 Load-deflection curves for N70×120×10.5B5I
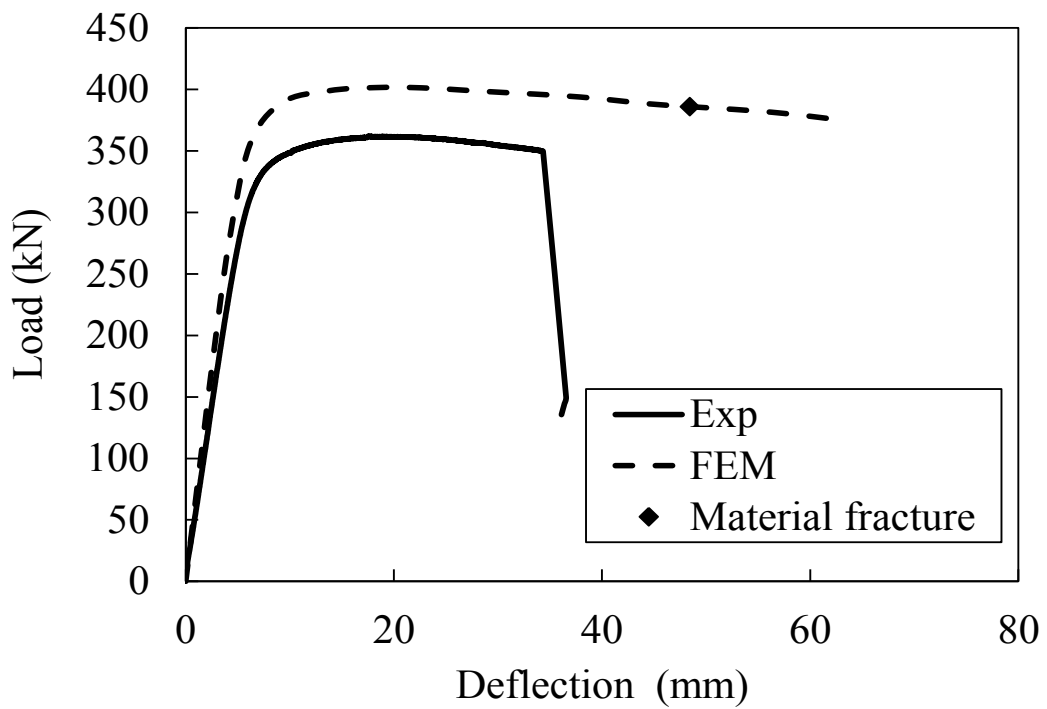
Fig. E.1.9 Load-deflection curves for N120×70×10.5B5I
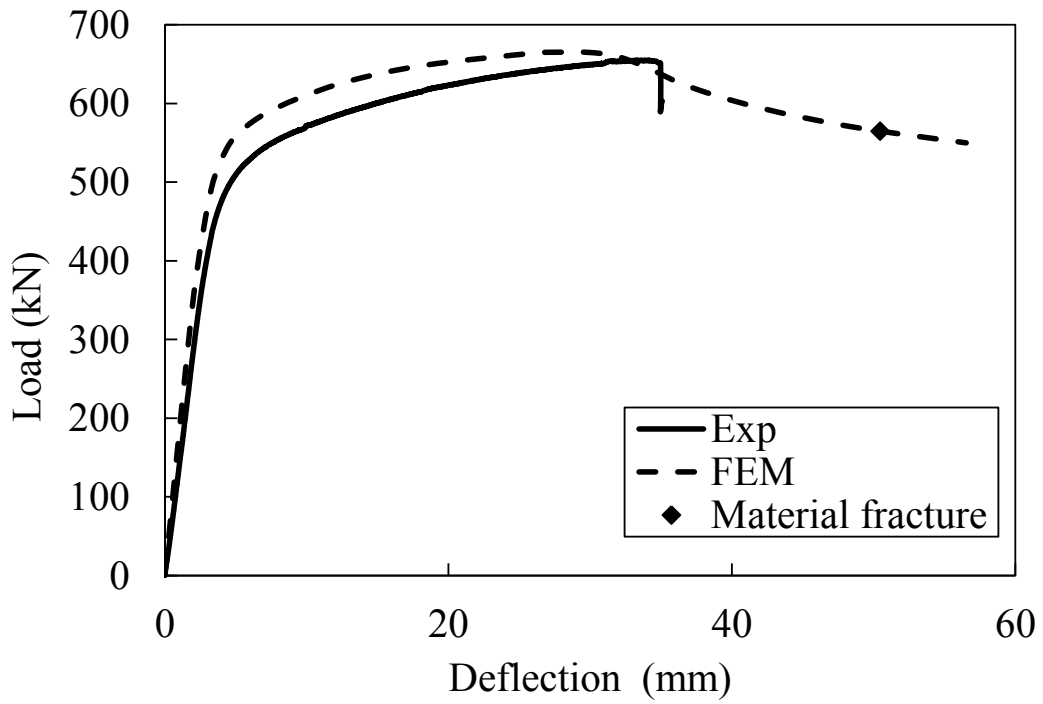
Fig. E.1.10 Load-deflection curves for N120×120×9.0B5I
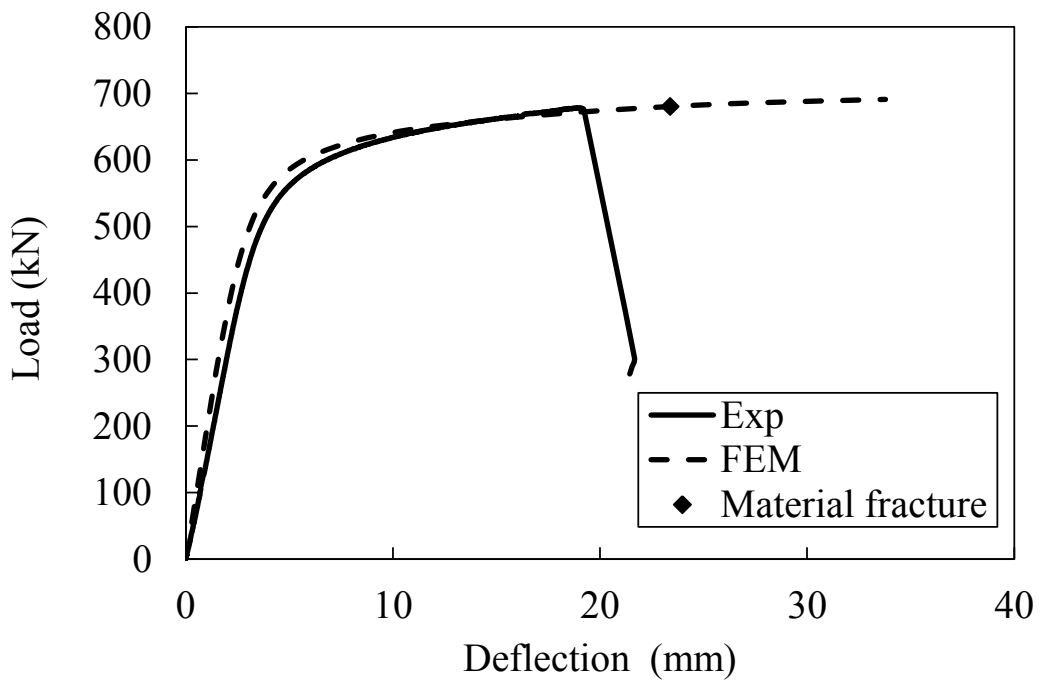
Fig. E.1.11 Load-deflection curves for +H70×120×10.5B5I
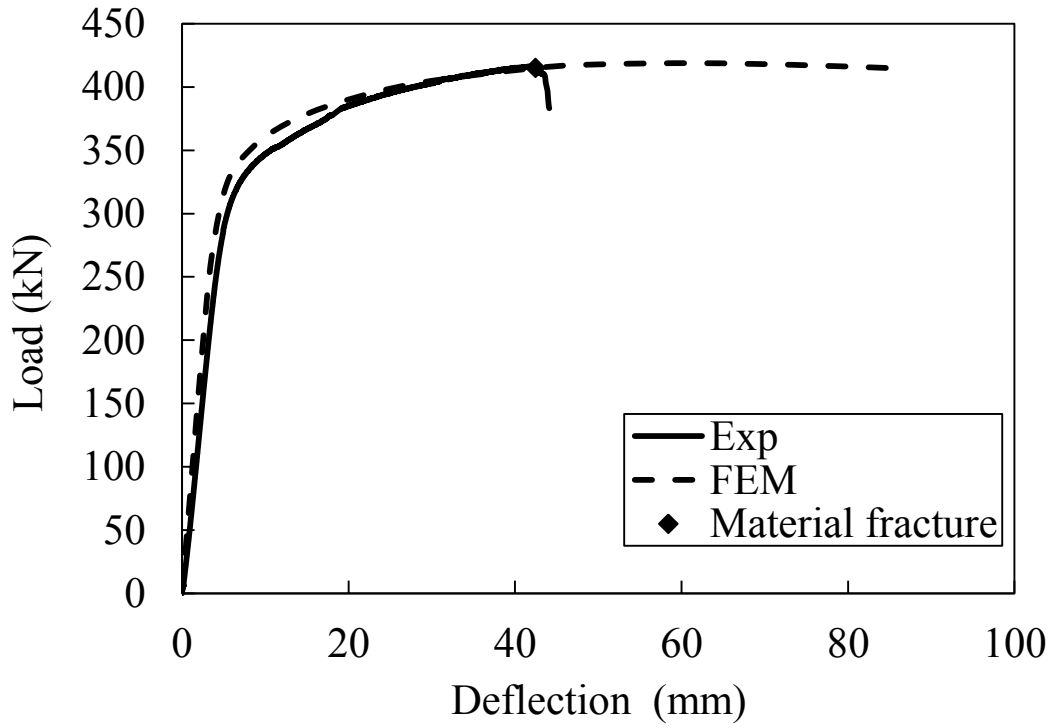
Fig. E.1.12 Load-deflection curves for +H120×70×10.5B5I
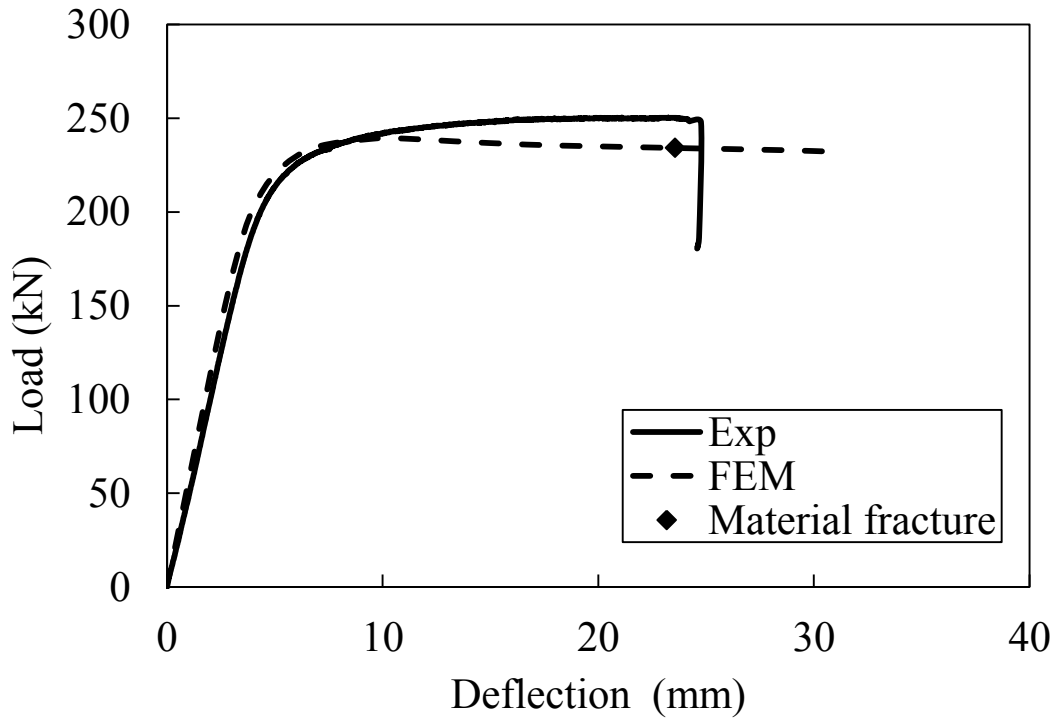
Fig. E.1.13 Load-deflection curves for +H95×95×4.3B5I
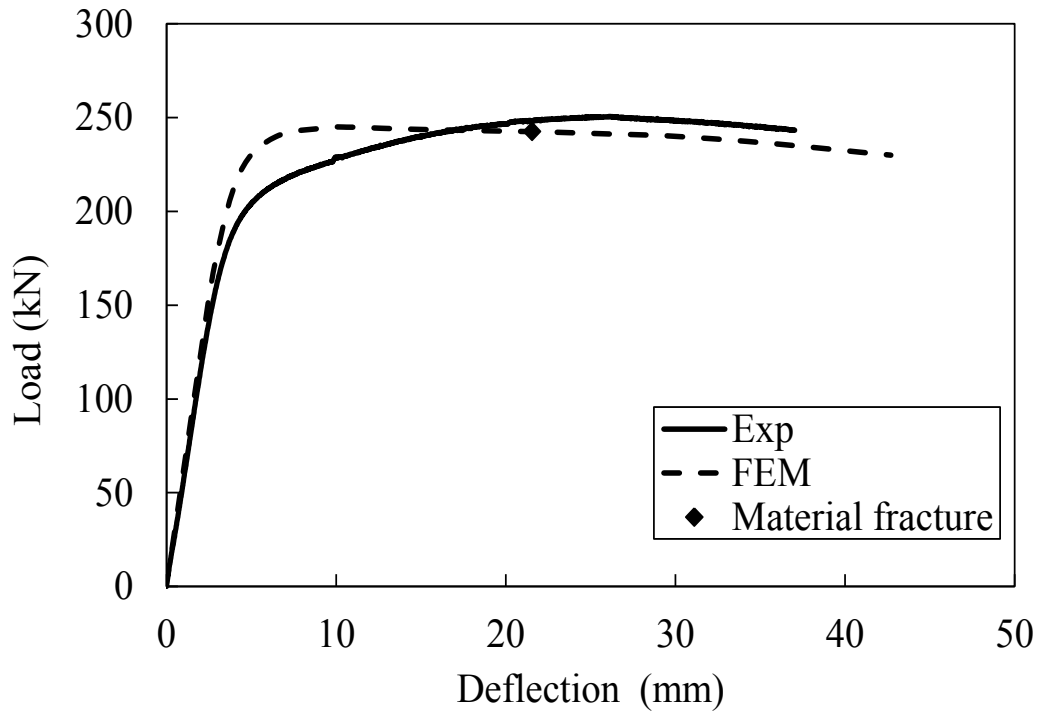
Fig. E.1.14 Load-deflection curves for +H95×95×4.3B5I-R
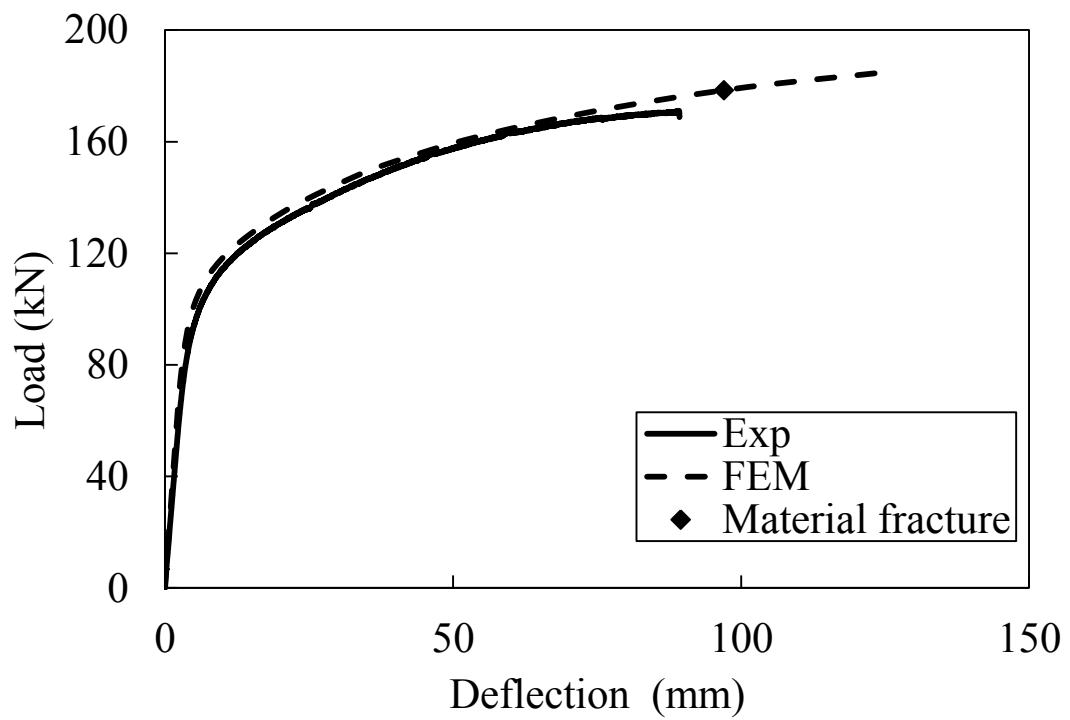
Fig. E.1.15 Load-deflection curves for +N95×50×10.5B5I
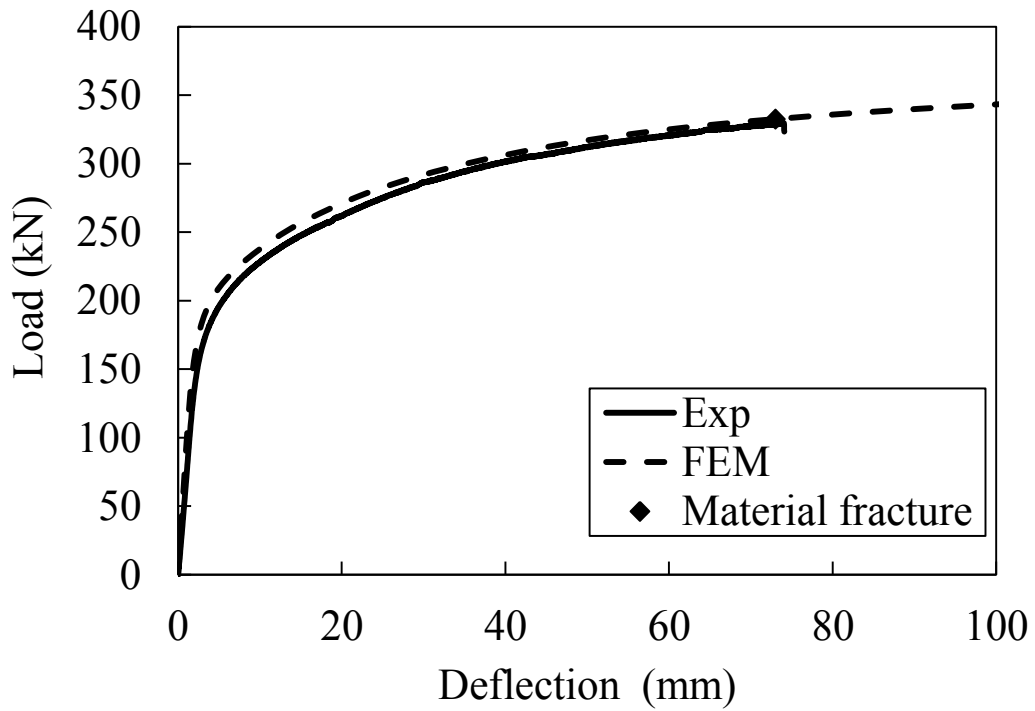
Fig. E.1.16 Load-deflection curves for +N50×95×10.5B5I
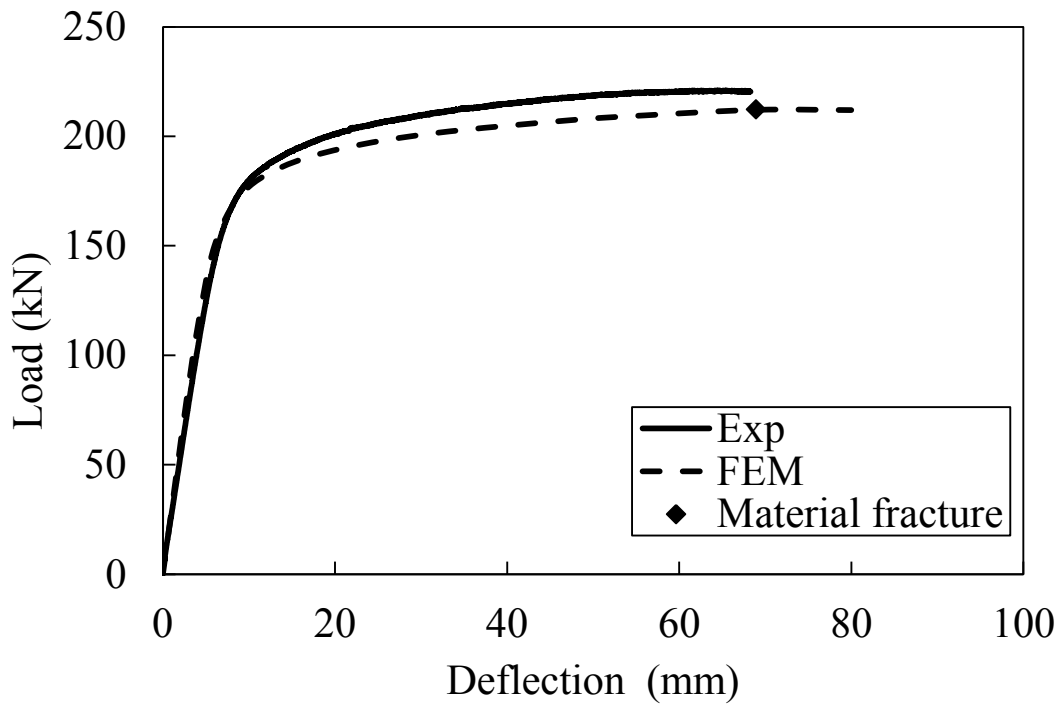
Fig. E.1.17 Load-deflection curves for +H95×50×10.5B5I
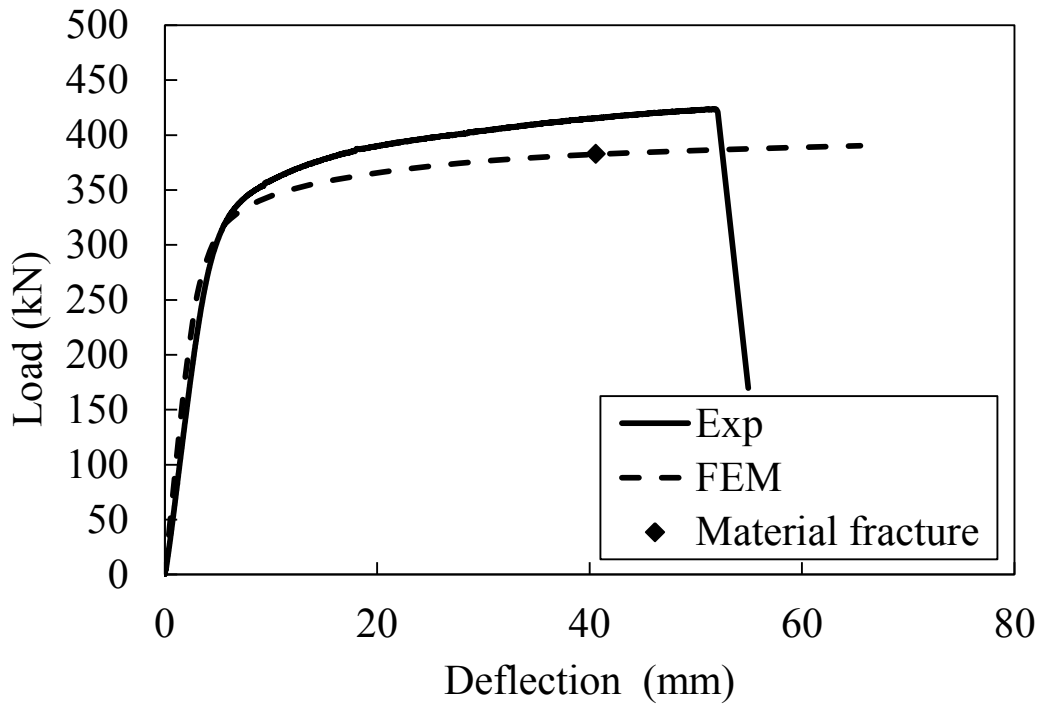
Fig. E.1.18 Load-deflection curves for +H50×95×10.5B5I

E.2 Loading configuration II
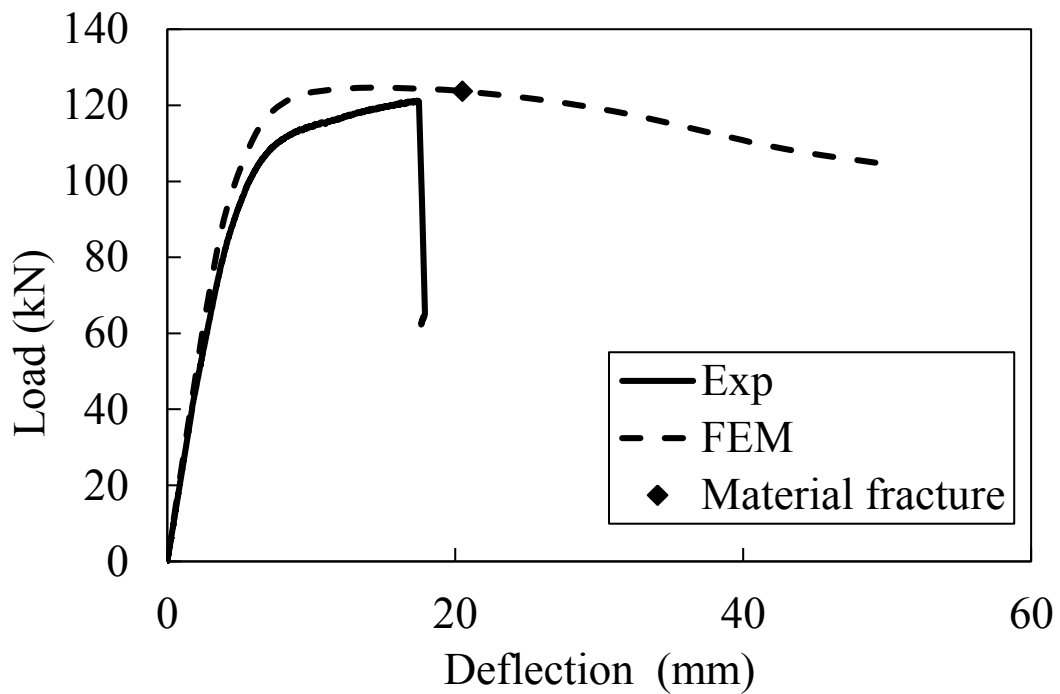
Fig. E.2.1 Load-deflection curves for H70×55×4.2B5II
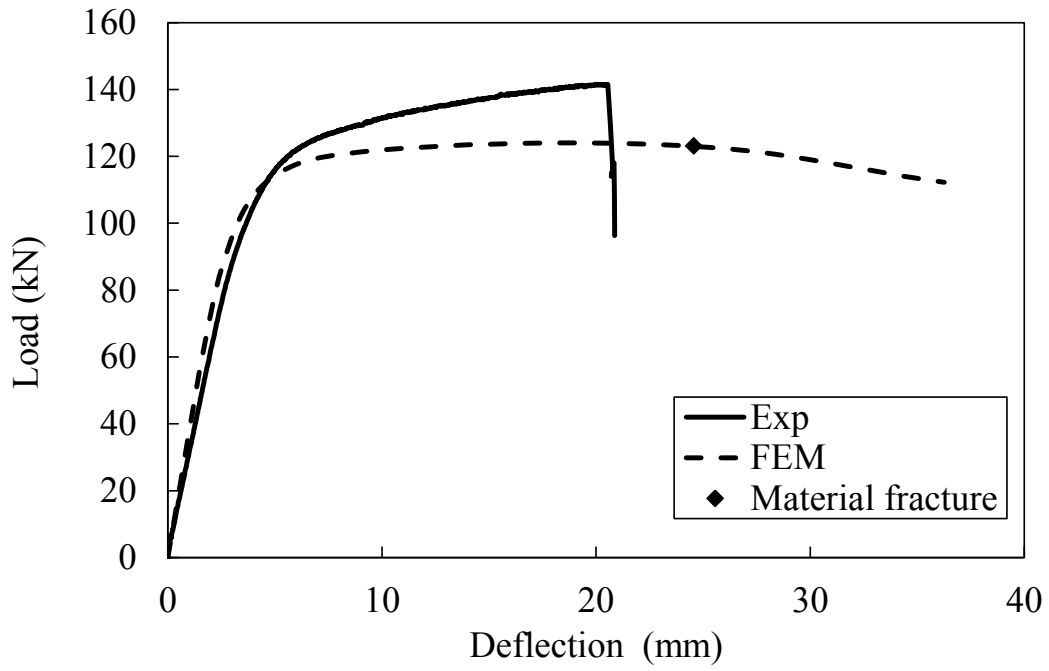
Fig. E.2.2 Load-deflection curves for H55×70×4.2B5II
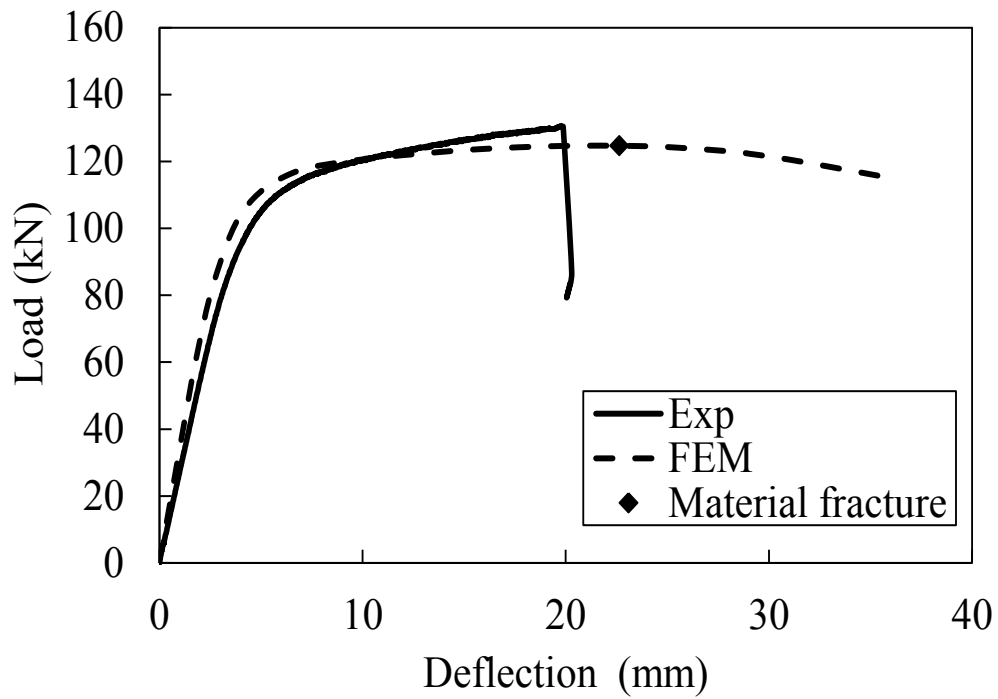
Fig. E.2.3 Load-deflection curves for H55×70×4.2B5II-R
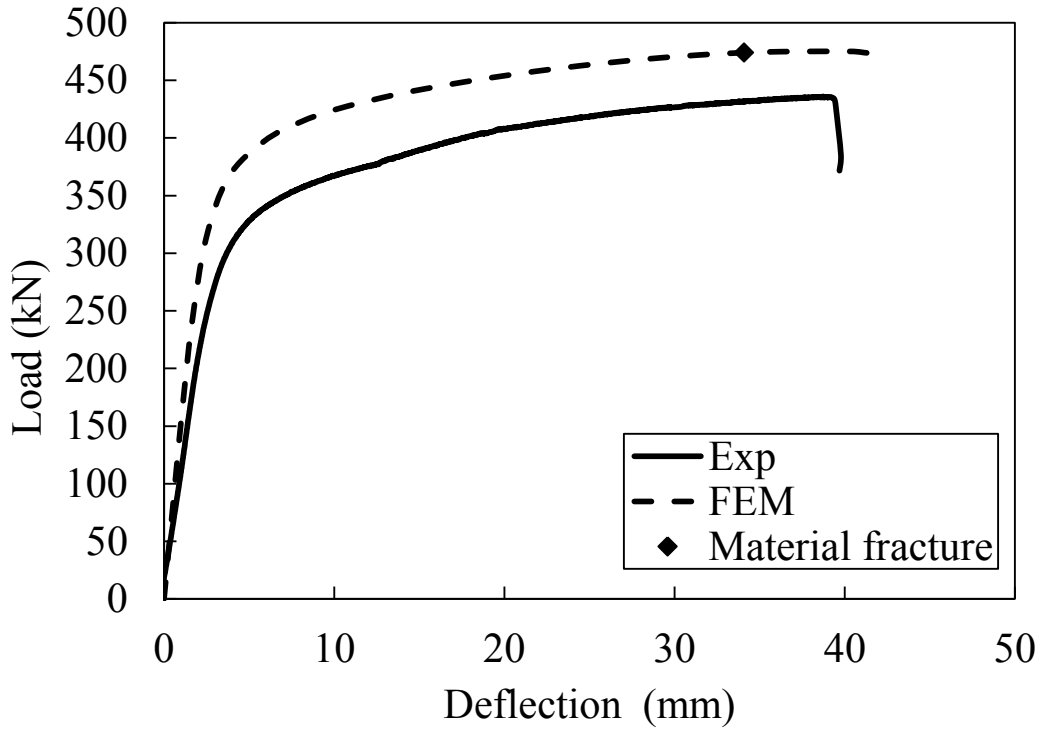
Fig. E.2.4 Load-deflection curves for H50×95×10.5B5II
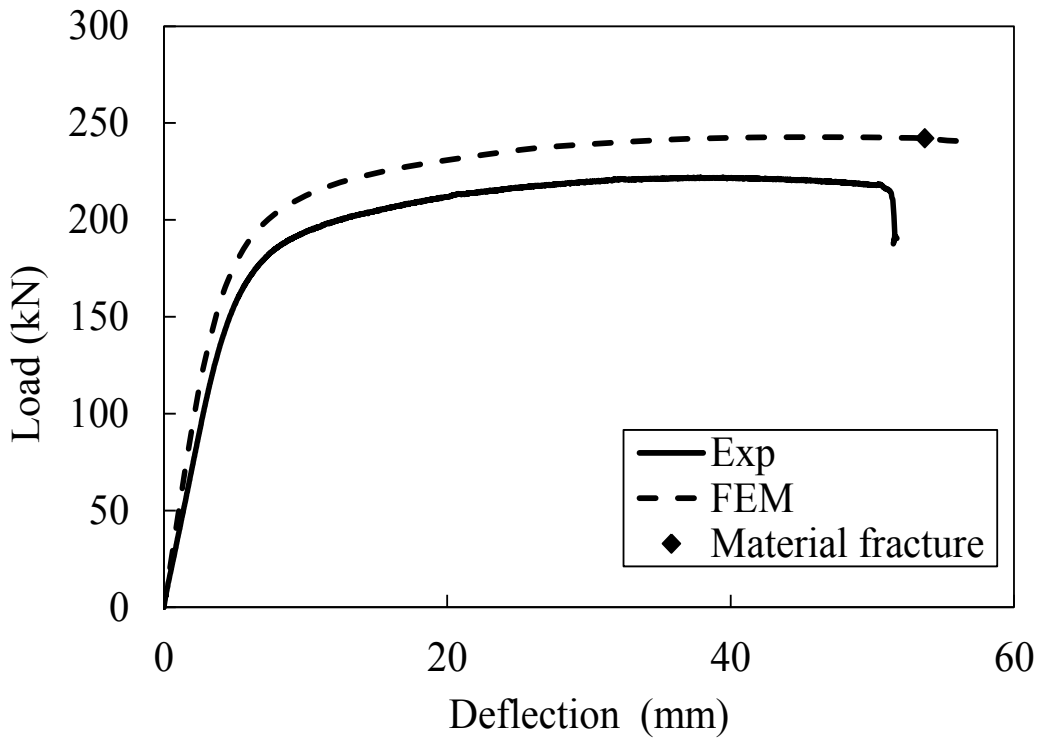
Fig. E.2.5 Load-deflection curves for H95×50×10.5B5II
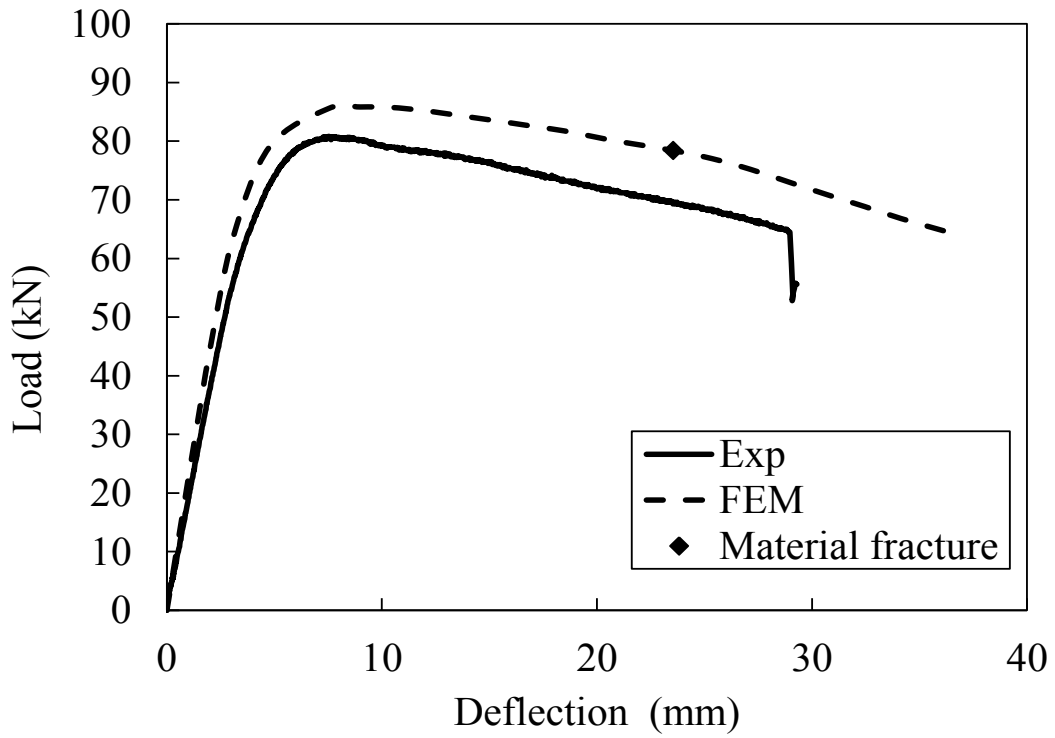
Fig. E.2.6 Load-deflection curves for H64×64×3.0B5II
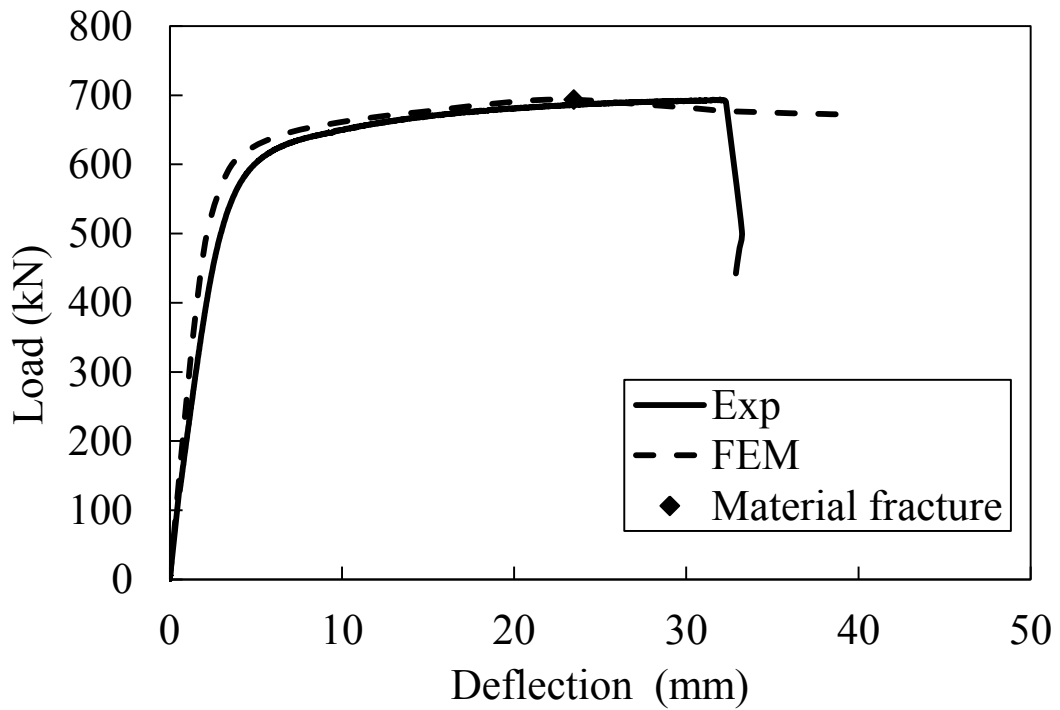
Fig. E.2.7 Load-deflection curves for N70×120×10.5B5II
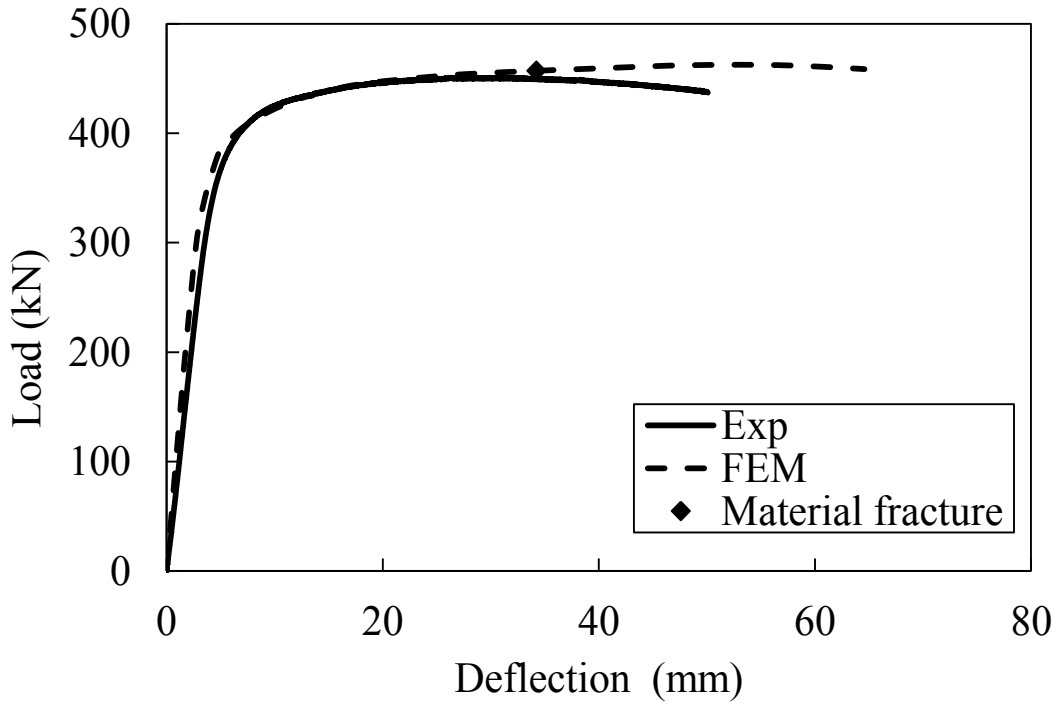
Fig. E.2.8 Load-deflection curves for N120×70×10.5B5II
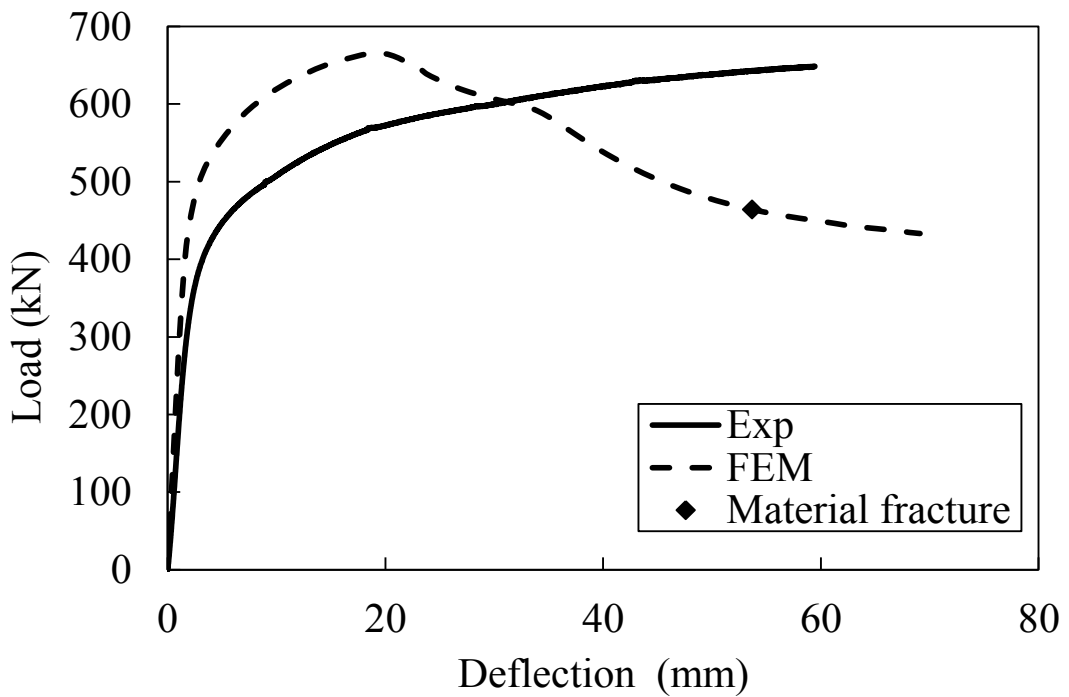
Fig. E.2.9 Load-deflection curves for N120×120×9.0B5II
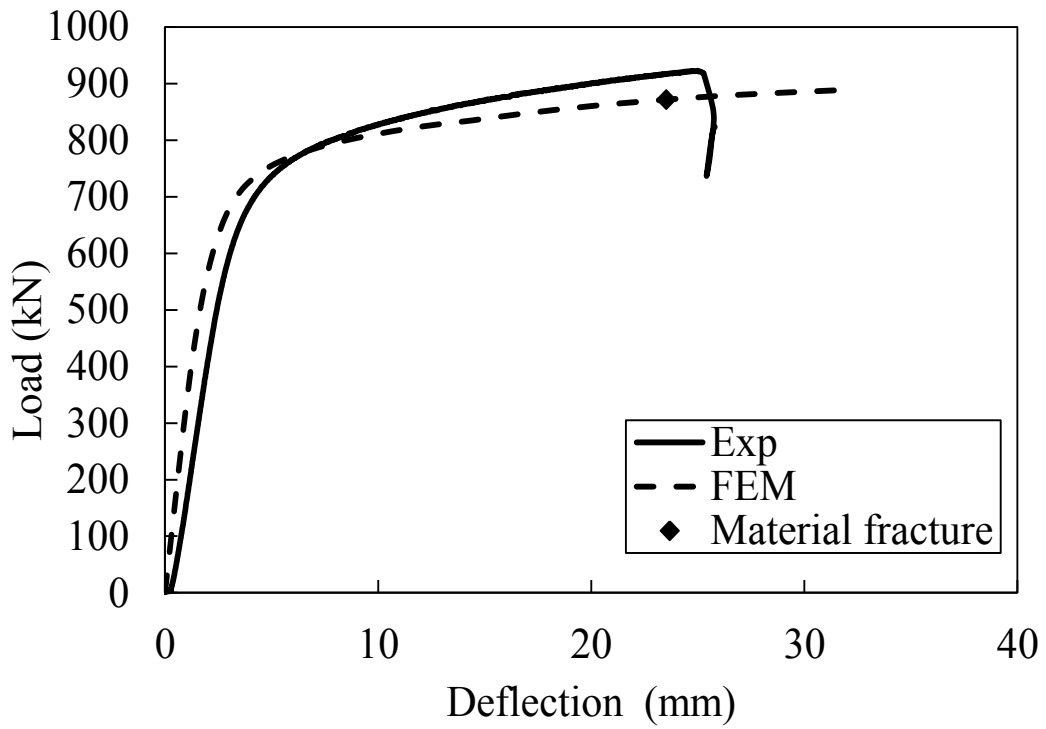
Fig. E.2.10 Load-deflection curves for +H70×120×10.5B5II
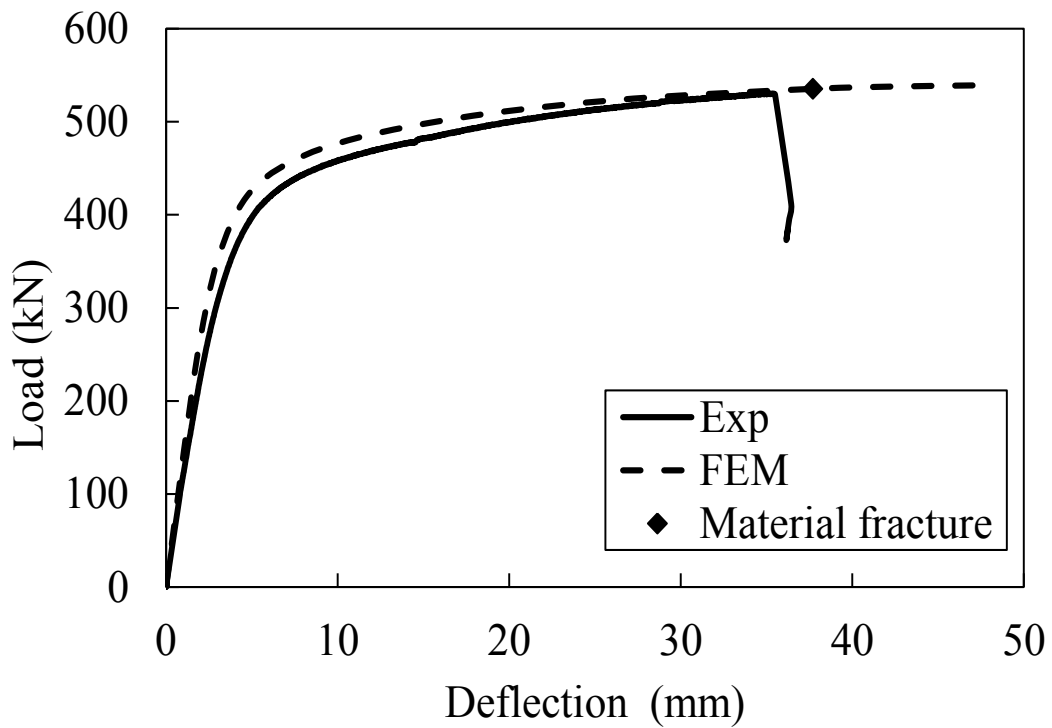
Fig. E.2.11 Load-deflection curves for +H120×70×10.5B5II
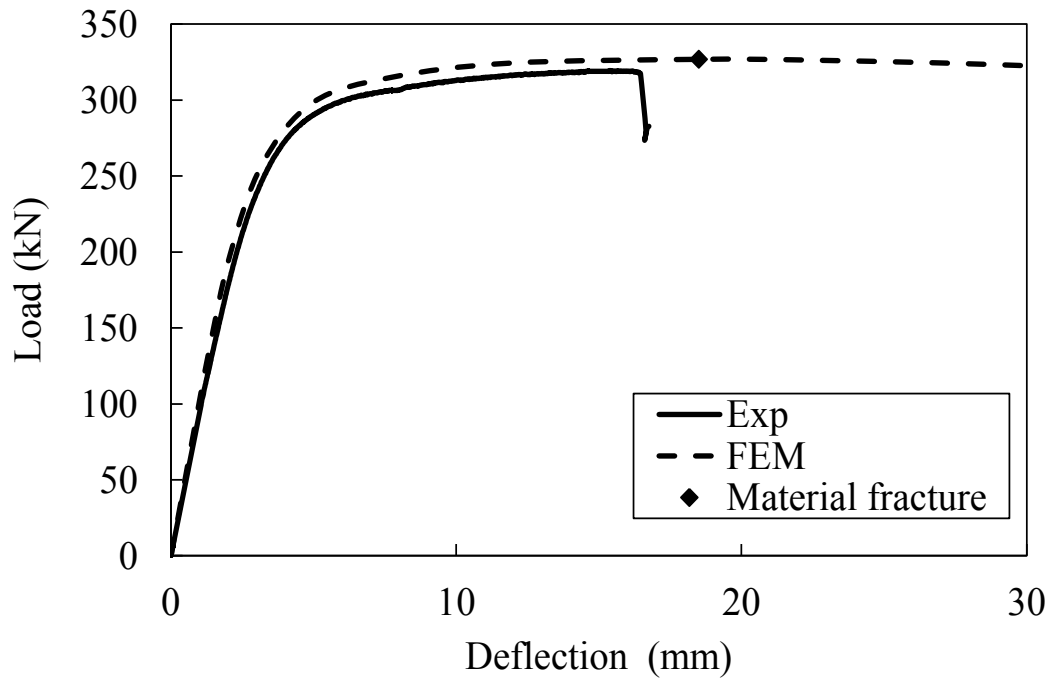
Fig. E.2.12 Load-deflection curves for +H95×95×4.3B5II
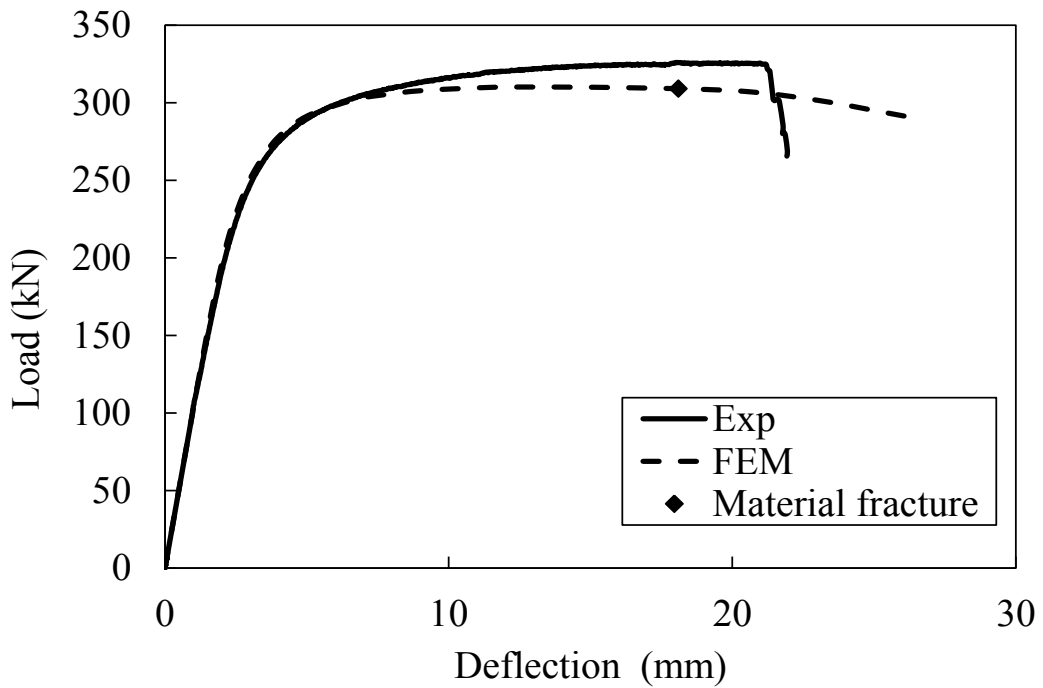
Fig. E.2.13 Load-deflection curves for +H95×95×4.3B5II-R

300
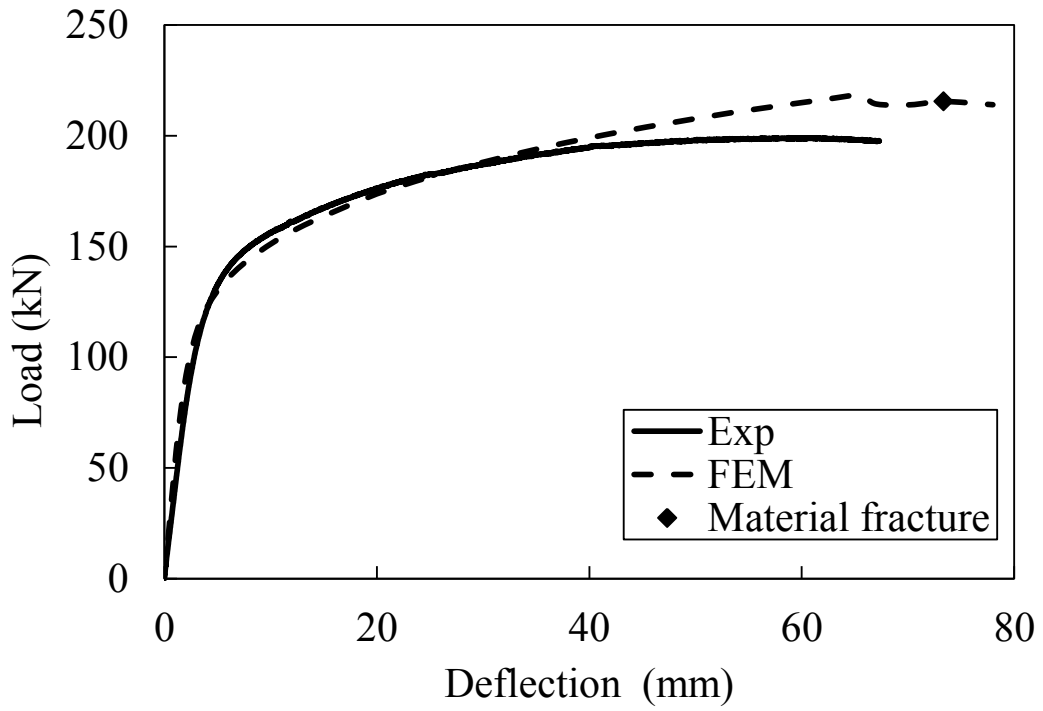
Fig. E.2.14 Load-deflection curves for +N95×50×10.5B5II
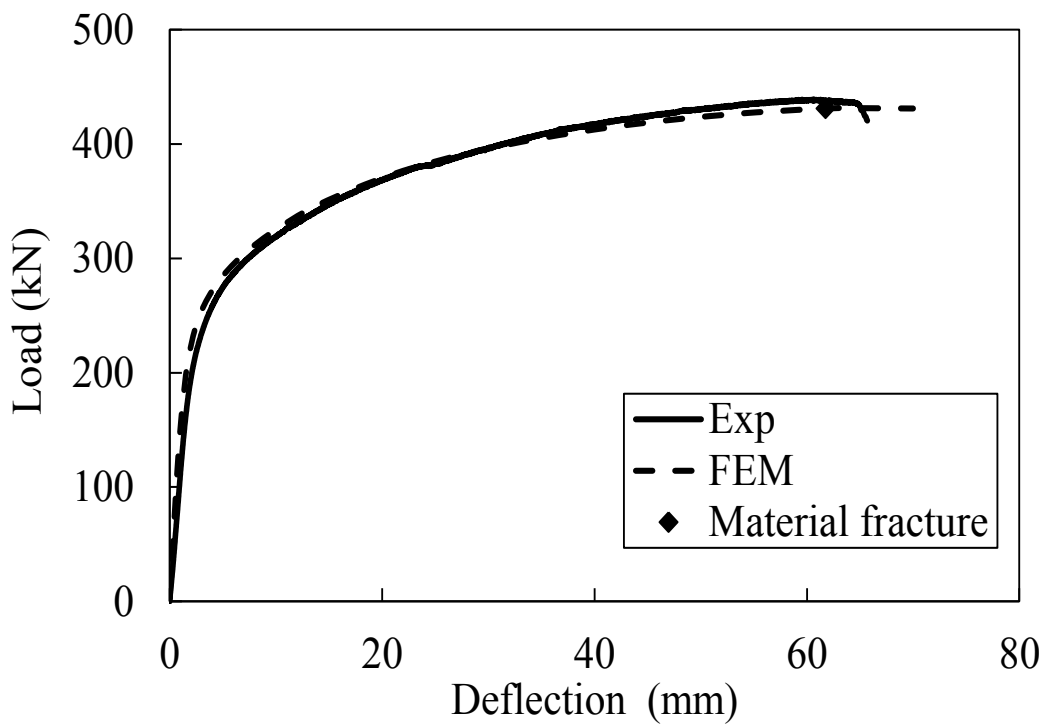
Fig. E.2.15 Load-deflection curves for +N50×95×10.5B5II

301

E.3 Loading configuration III
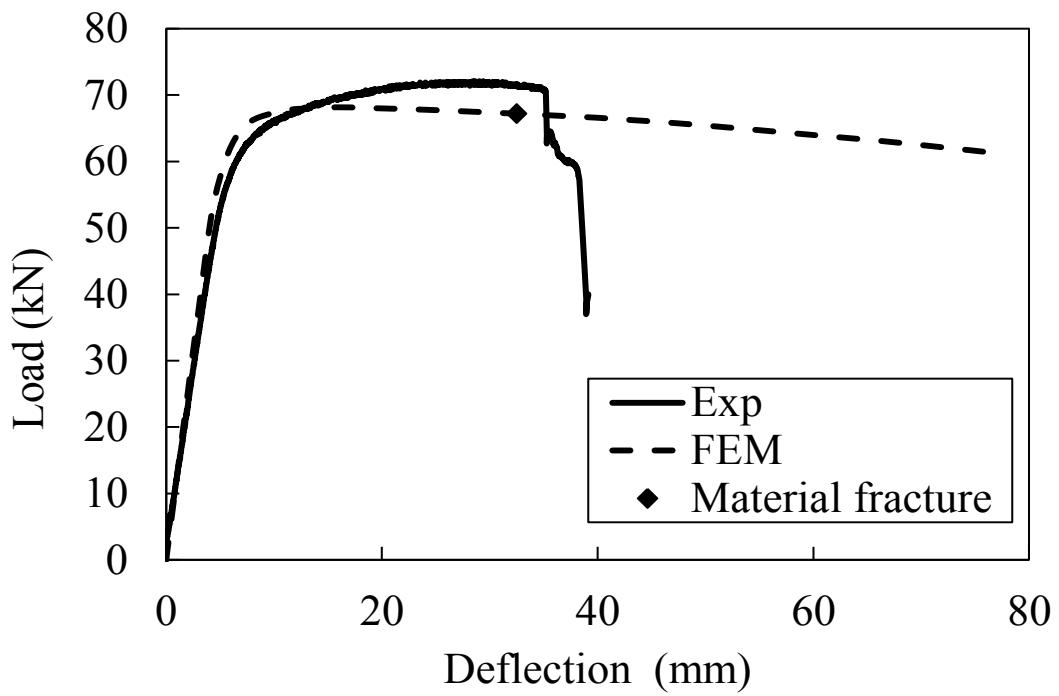
Fig. E.3.1 Load-deflection curves for H70×55×4.2B5III
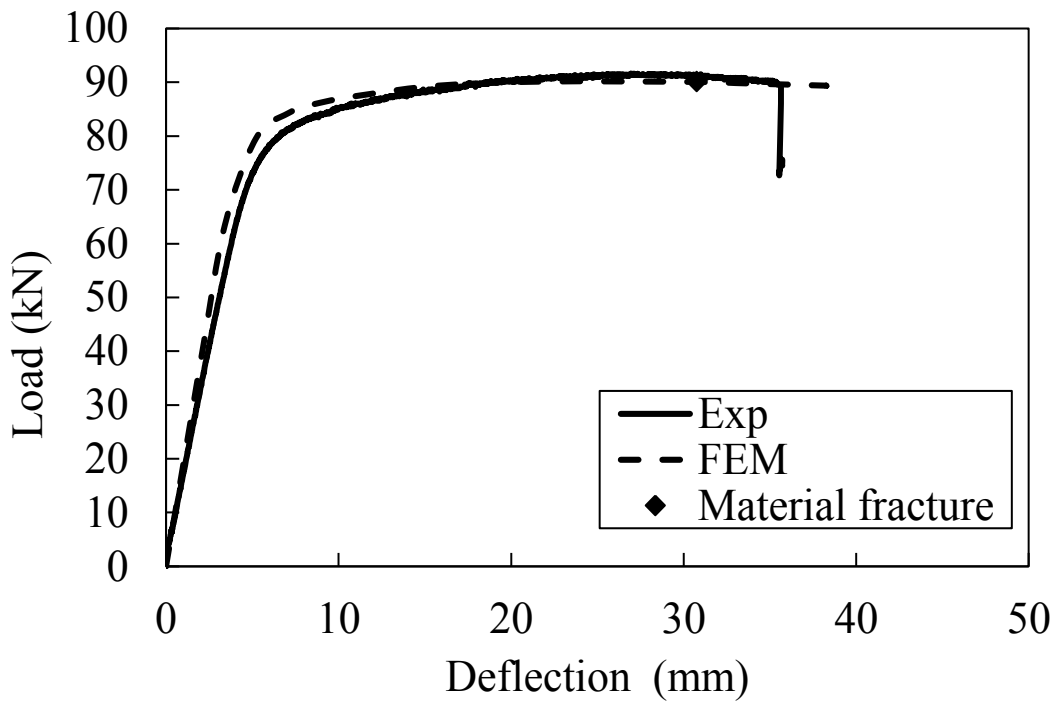
Fig. E.3.2 Load-deflection curves for H55×70×4.2B5III
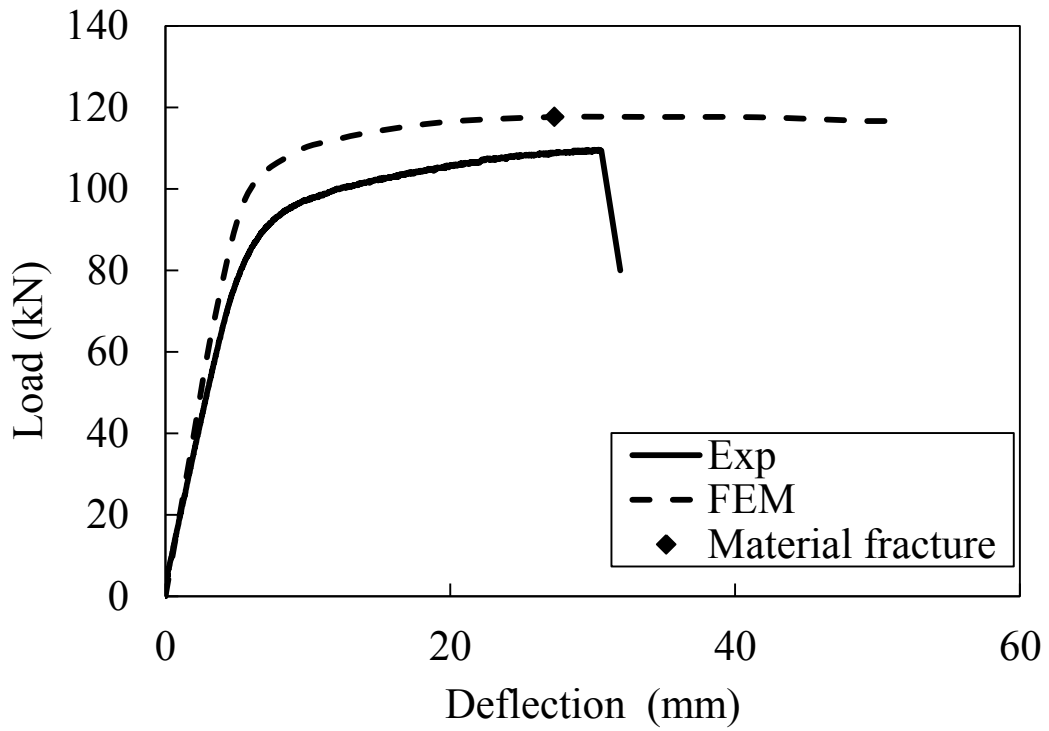
Fig. E.3.3 Load-deflection curves for H55×70×4.2B5III-R
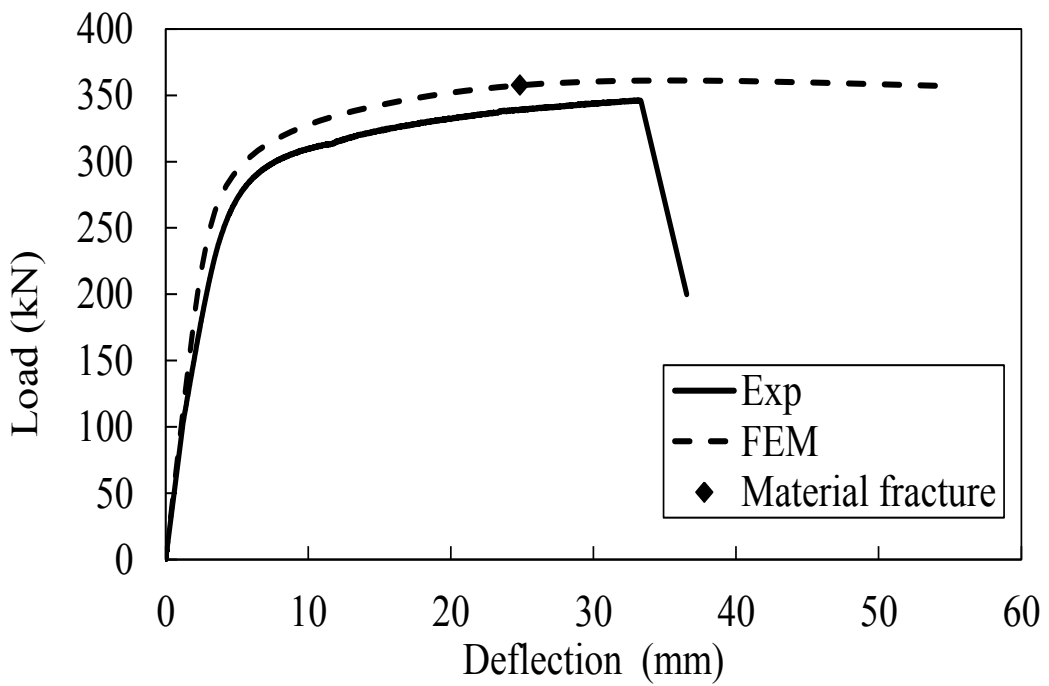
Fig. E.3.4 Load-deflection curves for H50×95×10.5B5III
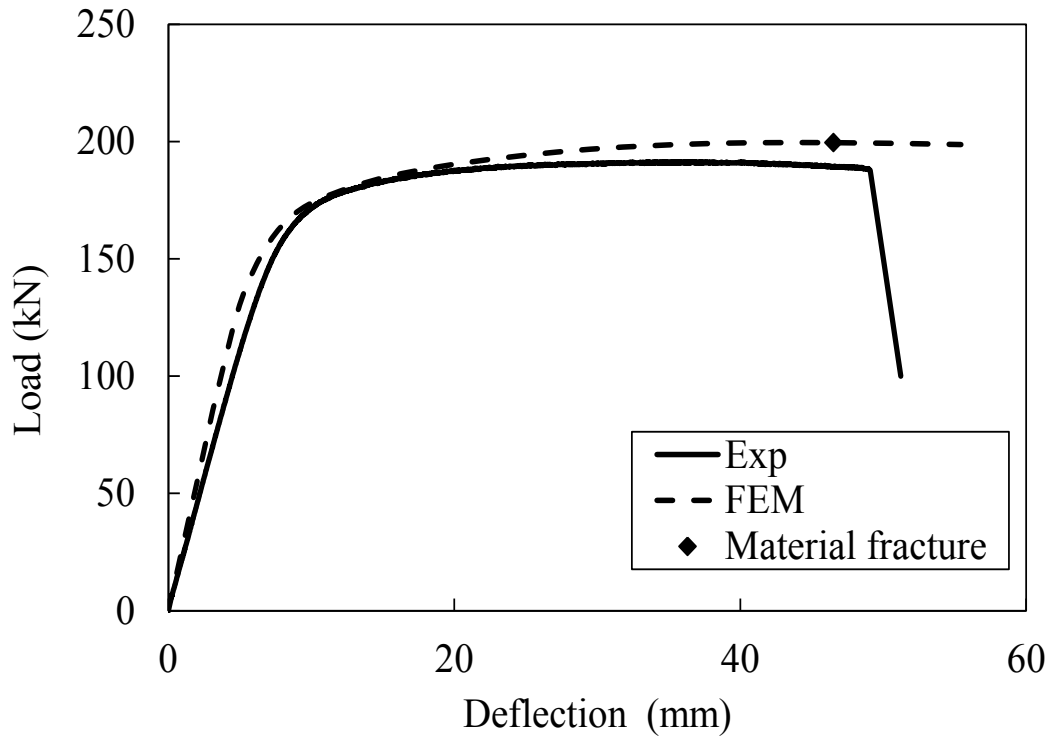
Fig. E.3.5 Load-deflection curves for H95×50×10.5B5III
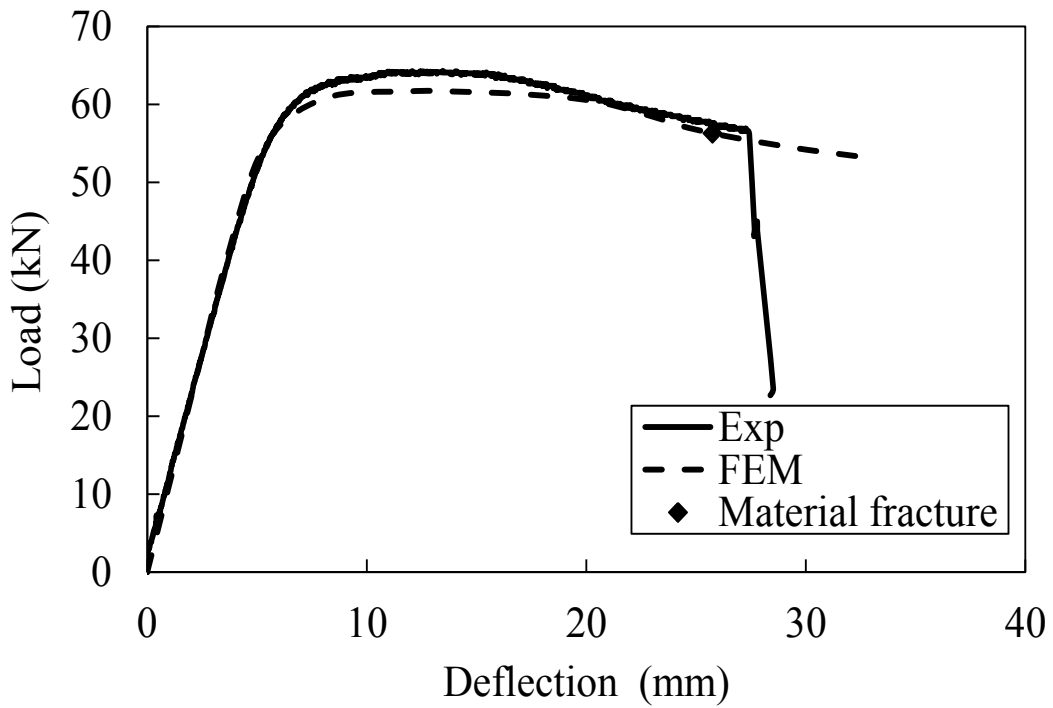
Fig. E.3.6 Load-deflection curves for H64×64×3.0B5III
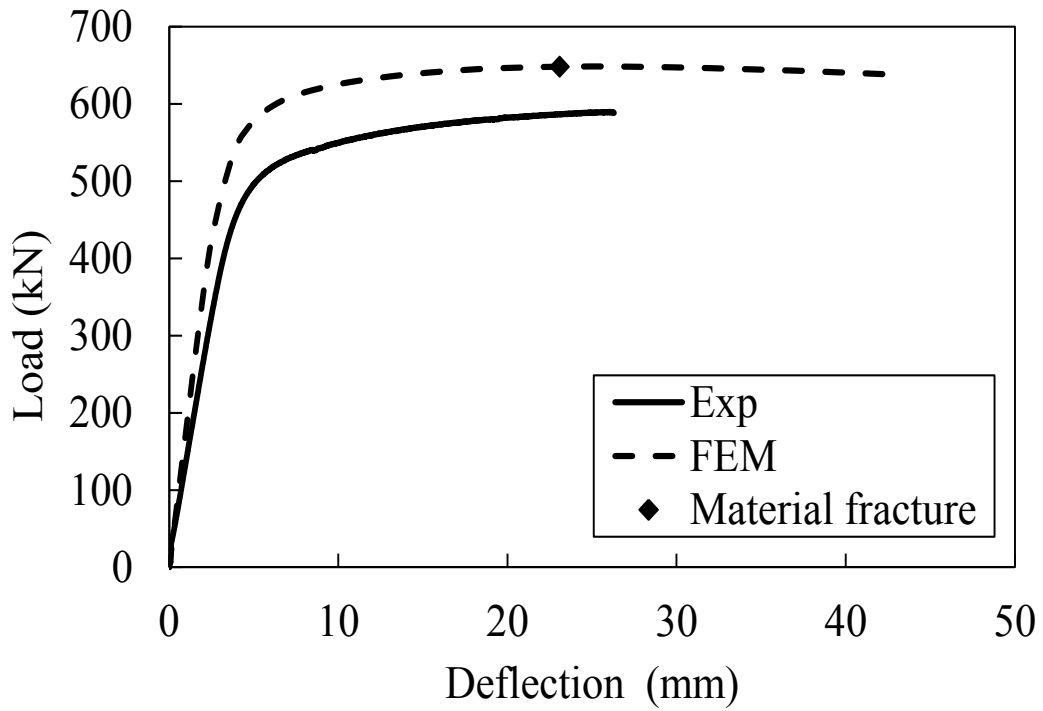
Fig. E.3.7 Load-deflection curves for N70×120×10.5B5III
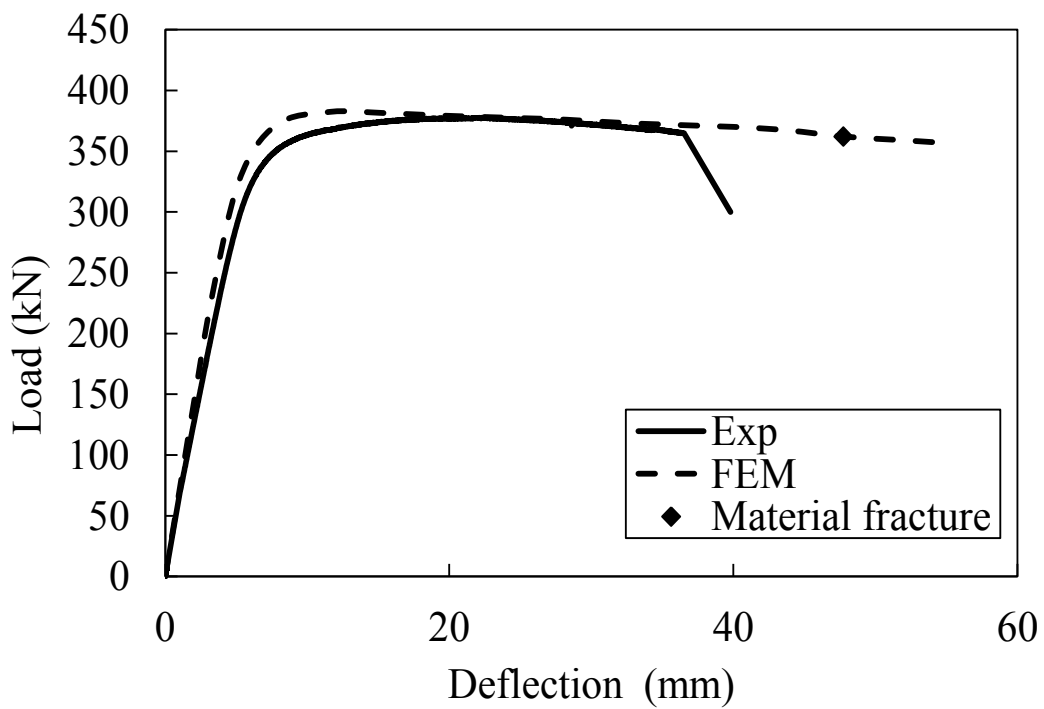
Fig. E.3.8 Load-deflection curves for N120×70×10.5B5III
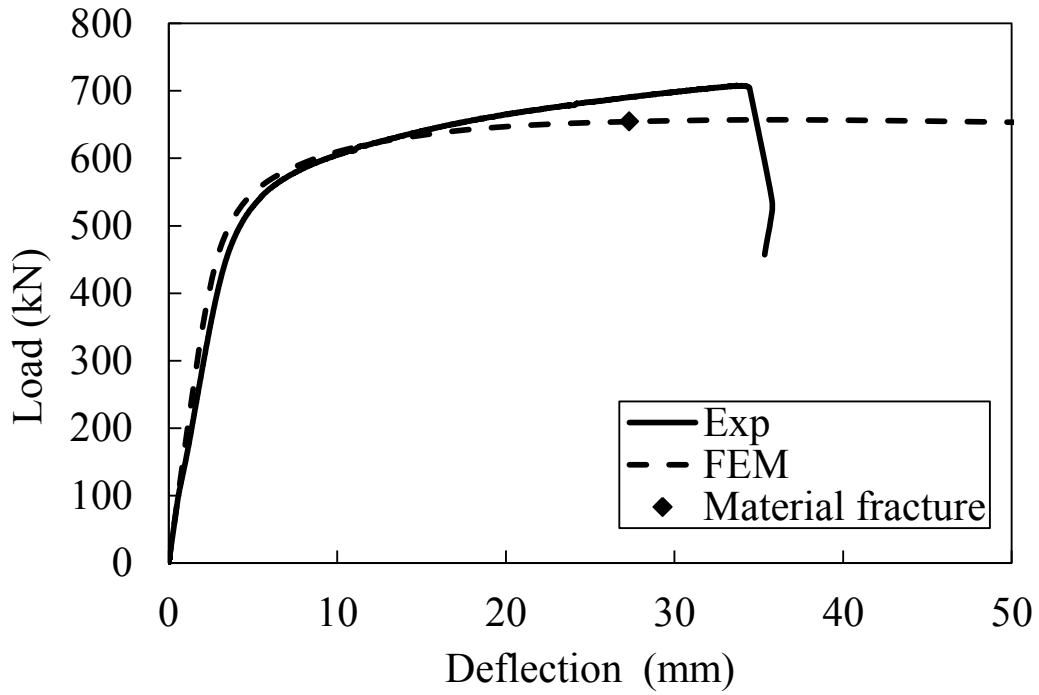
Fig. E.3.9 Load-deflection curves for +H70×120×10.5B5III
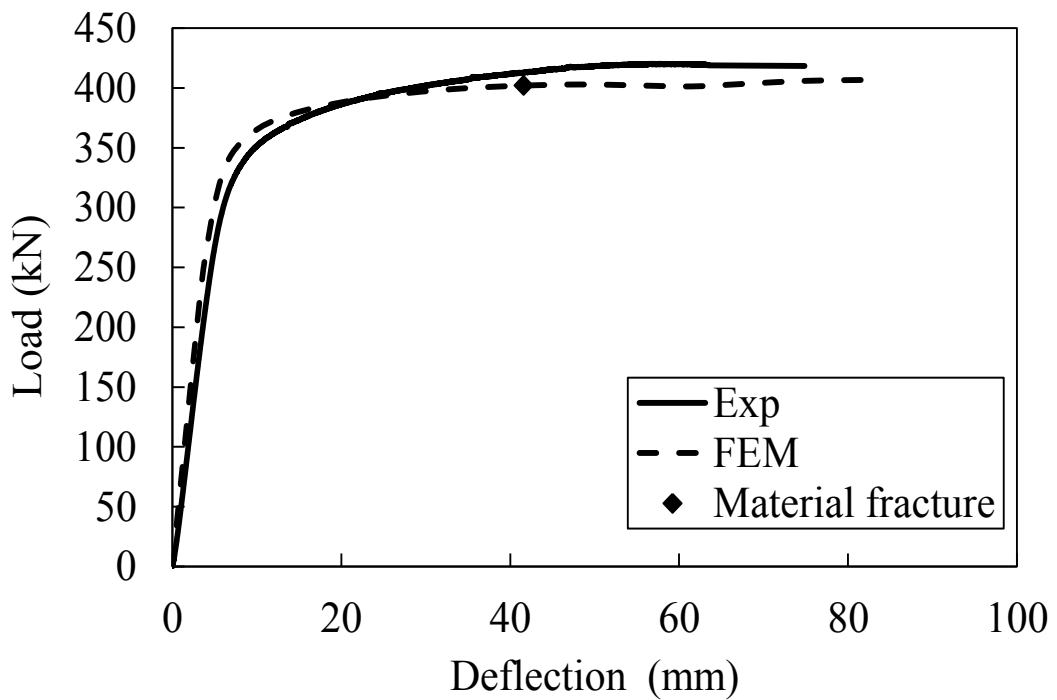
Fig. E.3.10 Load-deflection curves for +H120×70×10.5B5III

306
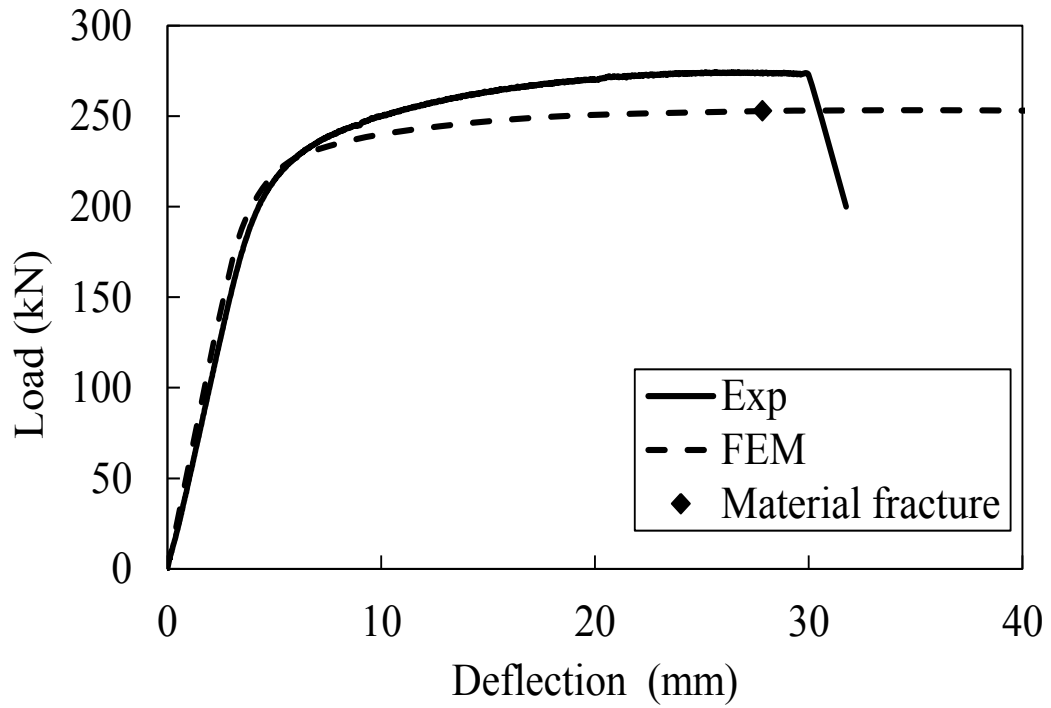
Fig. E.3.11 Load-deflection curves for +H95×95×4.3B5III
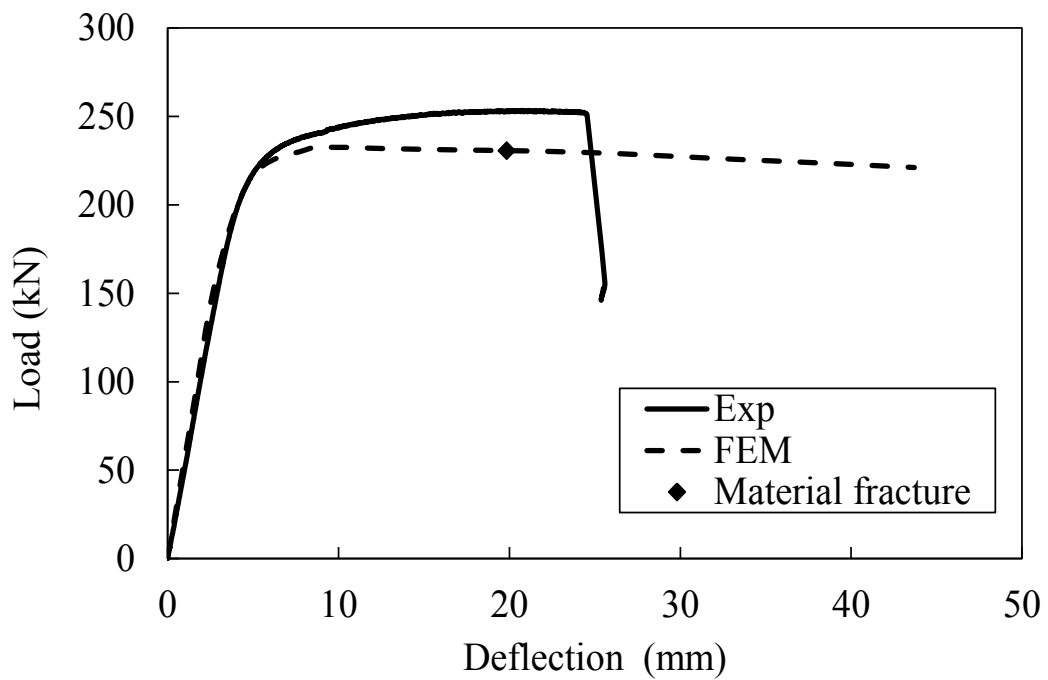
Fig. E.3.12 Load-deflection curves for +H95×95×4.3B5III-R
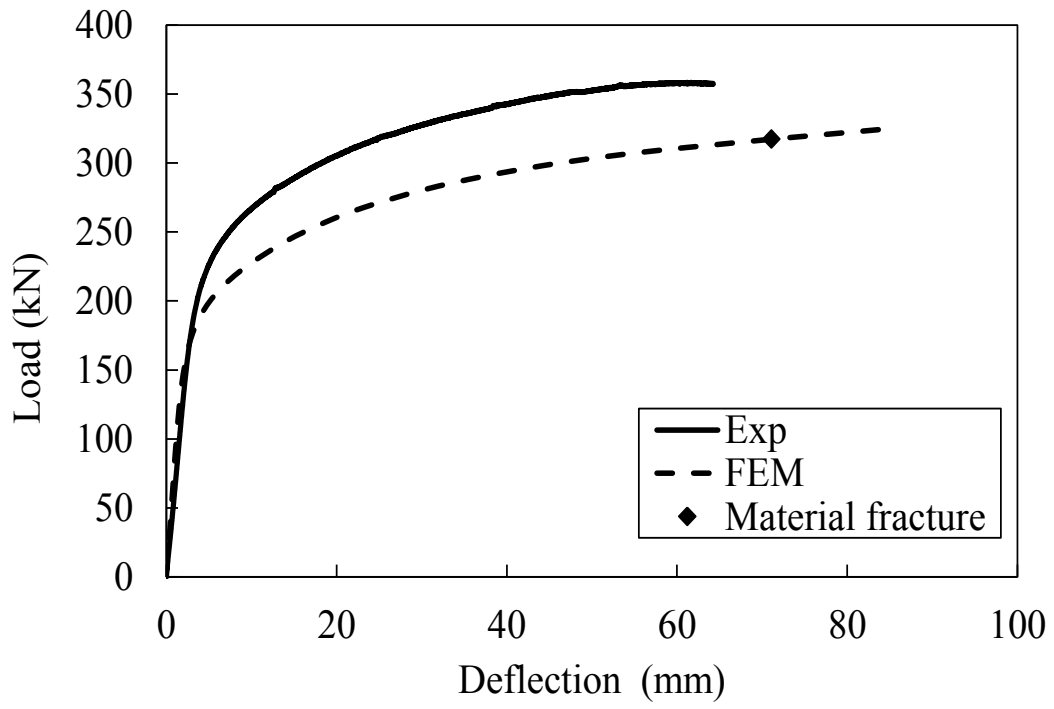
Fig. E.3.13 Load-deflection curves for +H50×95×10.5B5III

APPENDIX F.

NUMERICAL RESULTS FROM PARAMETRIC STUDIES

F.1   Three-point bending beams

Table F.1.1   Numerical results of three-point bending beams on SHS/RHS (high strength aluminium alloys)

Specimen	B (mm)	H (mm)	t (mm)	L (mm)	E (GPa)	f_y (MPa)	f_u (MPa)	M_{FE} (kNm)
H180×180×12.0 B3	180	180	12.00	1890	66	233	248	143.8
H180×180×9.0 B3	180	180	9.00	1890	66	233	248	107.9
H180×180×6.0 B3	180	180	6.00	1890	66	233	248	68.4
H180×180×3.5 B3	180	180	3.50	1890	66	233	248	31.1
H200×160×12.0 B3	200	160	12.00	1890	66	233	248	130.2
H200×160×9.0 B3	200	160	9.00	1890	66	233	248	95.0
H200×160×6.0 B3	200	160	6.00	1890	66	233	248	59.3
H200×160×3.5 B3	200	160	3.50	1890	66	233	248	27.5
H160×200×12.0 B3	160	200	12.00	1890	66	233	248	154.3
H160×200×9.0 B3	160	200	9.00	1890	66	233	248	113.7
H160×200×6.0 B3	160	200	6.00	1890	66	233	248	72.0
H160×200×3.5 B3	160	200	3.50	1890	66	233	248	33.1
H140×100×8.0 B3	140	100	8.00	1290	66	233	248	37.7
H140×100×6.5 B3	140	100	6.50	1290	66	233	248	27.2
H140×100×5.0 B3	140	100	5.00	1290	66	233	248	20.4
H140×100×3.5 B3	140	100	3.50	1290	66	233	248	13.1
H140×100×2.5 B3	140	100	2.50	1290	66	233	248	8.4
H100×140×8.0 B3	100	140	8.00	1290	66	233	248	47.3
H100×140×6.5 B3	100	140	6.50	1290	66	233	248	37.7
H100×140×5.0 B3	100	140	5.00	1290	66	233	248	28.0
H100×140×3.5 B3	100	140	3.50	1290	66	233	248	18.2
H100×140×2.5 B3	100	140	2.50	1290	66	233	248	11.6
H130×50×8.0 B3	130	50	8.00	890	66	233	248	13.4
H130×50×6.5 B3	130	50	6.50	890	66	233	248	11.2
H130×50×5.0 B3	130	50	5.00	890	66	233	248	8.6
H130×50×3.5 B3	130	50	3.50	890	66	233	248	5.7
H130×50×2.5 B3	130	50	2.50	890	66	233	248	3.3
H50×130×8.0 B3	50	130	8.00	890	66	233	248	32.5
H50×130×6.5 B3	50	130	6.50	890	66	233	248	25.9
H50×130×5.0 B3	50	130	5.00	890	66	233	248	18.9
H50×130×3.5 B3	50	130	3.50	890	66	233	248	12.2
H50×130×2.5 B3	50	130	2.50	890	66	233	248	8.0

Table F.1.2   Numerical results of three-point bending beams on SHS/RHS
(normal strength aluminium alloys)

Specimen	B (mm)	H (mm)	t (mm)	L (mm)	E (GPa)	f_y (MPa)	f_u (MPa)	M_{FE} (kNm)
N180×180×12.0 B3	180	180	12.00	1890	72	110	177	89.5
N180×180×9.0 B3	180	180	9.00	1890	72	110	177	67.6
N180×180×6.0 B3	180	180	6.00	1890	72	110	177	37.5
N180×180×3.5 B3	180	180	3.50	1890	72	110	177	17.2
N200×160×12.0 B3	200	160	12.00	1890	72	110	177	84.4
N200×160×9.0 B3	200	160	9.00	1890	72	110	177	58.3
N200×160×6.0 B3	200	160	6.00	1890	72	110	177	32.8
N200×160×3.5 B3	200	160	3.50	1890	72	110	177	15.3
N160×200×12.0 B3	160	200	12.00	1890	72	110	177	100.7
N160×200×9.0 B3	160	200	9.00	1890	72	110	177	71.3
N160×200×6.0 B3	160	200	6.00	1890	72	110	177	41.1
N160×200×3.5 B3	160	200	3.50	1890	72	110	177	18.9
N140×100×8.0 B3	140	100	8.00	1290	72	110	177	22.2
N140×100×6.5 B3	140	100	6.50	1290	72	110	177	17.1
N140×100×5.0 B3	140	100	5.00	1290	72	110	177	12.4
N140×100×3.5 B3	140	100	3.50	1290	72	110	177	7.7
N140×100×2.5 B3	140	100	2.50	1290	72	110	177	4.6
N100×140×8.0 B3	100	140	8.00	1290	72	110	177	29.3
N100×140×6.5 B3	100	140	6.50	1290	72	110	177	22.9
N100×140×5.0 B3	100	140	5.00	1290	72	110	177	16.1
N100×140×3.5 B3	100	140	3.50	1290	72	110	177	10.7
N100×140×2.5 B3	100	140	2.50	1290	72	110	177	6.5
N130×50×8.0 B3	130	50	8.00	890	72	110	177	7.6
N130×50×6.5 B3	130	50	6.50	890	72	110	177	6.0
N130×50×5.0 B3	130	50	5.00	890	72	110	177	4.5
N130×50×3.5 B3	130	50	3.50	890	72	110	177	2.9
N130×50×2.5 B3	130	50	2.50	890	72	110	177	1.9
N50×130×8.0 B3	50	130	8.00	890	72	110	177	21.5
N50×130×6.5 B3	50	130	6.50	890	72	110	177	16.8
N50×130×5.0 B3	50	130	5.00	890	72	110	177	11.7
N50×130×3.5 B3	50	130	3.50	890	72	110	177	7.7
N50×130×2.5 B3	50	130	2.50	890	72	110	177	4.6

Table F.1.3   Numerical results of three-point bending beams on SHS/RHS with internal cross stiffeners (high strength aluminium alloys)

Specimen	B (mm)	H (mm)	t (mm)	L (mm)	E (GPa)	f_y (MPa)	f_u (MPa)	M_{FE} (kNm)
+H180×180×9.0 B3	180	180	9.00	1890	66	233	248	120.3
+H180×180×6.0 B3	180	180	6.00	1890	66	233	248	78.4
+H180×180×3.5 B3	180	180	3.50	1890	66	233	248	42.2
+H160×200×9.0 B3	160	200	9.00	1890	66	233	248	131.6
+H160×200×6.0 B3	160	200	6.00	1890	66	233	248	90.6
+H160×200×3.5 B3	160	200	3.50	1890	66	233	248	50.3
+H140×100×6.5 B3	140	100	6.50	1290	66	233	248	35.9
+H140×100×5.0 B3	140	100	5.00	1290	66	233	248	28.0
+H140×100×2.5 B3	140	100	2.50	1290	66	233	248	13.5
+H130×50×6.5 B3	130	50	6.50	890	66	233	248	12.6
+H130×50×5.0 B3	130	50	5.00	890	66	233	248	10.4
+H130×50×2.5 B3	130	50	2.50	890	66	233	248	5.1
+H50×130×6.5 B3	50	130	6.50	890	66	233	248	31.8
+H50×130×5.0 B3	50	130	5.00	890	66	233	248	25.0
+H50×130×2.5 B3	50	130	2.50	890	66	233	248	11.9

Table F.1.4   Numerical results of three-point bending beams on SHS/RHS with internal cross stiffeners (normal strength aluminium alloys)

Specimen	B (mm)	H (mm)	t (mm)	L (mm)	E (GPa)	f_y (MPa)	f_u (MPa)	M_{FE} (kNm)
+N180×180×9.0 B3	180	180	9.00	1890	72	110	177	84.2
+N180×180×6.0 B3	180	180	6.00	1890	72	110	177	51.7
+N180×180×3.5 B3	180	180	3.50	1890	72	110	177	25.6
+N160×200×9.0 B3	160	200	9.00	1890	72	110	177	93.3
+N160×200×6.0 B3	160	200	6.00	1890	72	110	177	65.0
+N160×200×3.5 B3	160	200	3.50	1890	72	110	177	31.2
+N140×100×6.5 B3	140	100	6.50	1290	72	110	177	26.8
+N140×100×5.0 B3	140	100	5.00	1290	72	110	177	20.4
+N140×100×2.5 B3	140	100	2.50	1290	72	110	177	8.1
+N130×50×6.5 B3	130	50	6.50	890	72	110	177	8.5
+N130×50×5.0 B3	130	50	5.00	890	72	110	177	6.5
+N130×50×2.5 B3	130	50	2.50	890	72	110	177	3.3
+N50×130×6.5 B3	50	130	6.50	890	72	110	177	23.6
+N50×130×5.0 B3	50	130	5.00	890	72	110	177	18.3
+N50×130×2.5 B3	50	130	2.50	890	72	110	177	7.9

F.2   Four-point bending beams

Table F.2.1   Numerical results of four-point bending beams on SHS/RHS (high strength aluminium alloys)

Specimen	B (mm)	H (mm)	t (mm)	L (mm)	E (GPa)	f_y (MPa)	f_u (MPa)	M_{FE} (kNm)
H180×180×12.0 B4	180	180	12.00	2790	66	233	248	132.3
H180×180×9.0 B4	180	180	9.00	2790	66	233	248	97.4
H180×180×6.0 B4	180	180	6.00	2790	66	233	248	59.4
H180×180×3.5 B4	180	180	3.50	2790	66	233	248	27.7
H200×160×12.0 B4	200	160	12.00	2790	66	233	248	119.7
H200×160×9.0 B4	200	160	9.00	2790	66	233	248	88.3
H200×160×6.0 B4	200	160	6.00	2790	66	233	248	52.6
H200×160×3.5 B4	200	160	3.50	2790	66	233	248	24.6
H160×200×12.0 B4	160	200	12.00	2790	66	233	248	142.1
H160×200×9.0 B4	160	200	9.00	2790	66	233	248	105.6
H160×200×6.0 B4	160	200	6.00	2790	66	233	248	66.1
H160×200×3.5 B4	160	200	3.50	2790	66	233	248	30.7
H140×100×8.0 B4	140	100	8.00	1890	66	233	248	33.8
H140×100×6.5 B4	140	100	6.50	1890	66	233	248	26.7
H140×100×5.0 B4	140	100	5.00	1890	66	233	248	19.4
H140×100×3.5 B4	140	100	3.50	1890	66	233	248	12.2
H140×100×2.5 B4	140	100	2.50	1890	66	233	248	7.6
H100×140×8.0 B4	100	140	8.00	1890	66	233	248	44.1
H100×140×6.5 B4	100	140	6.50	1890	66	233	248	35.9
H100×140×5.0 B34	100	140	5.00	1890	66	233	248	26.8
H100×140×3.5 B4	100	140	3.50	1890	66	233	248	17.2
H100×140×2.5 B4	100	140	2.50	1890	66	233	248	10.6
H130×50×8.0 B4	130	50	8.00	1290	66	233	248	12.3
H130×50×6.5 B4	130	50	6.50	1290	66	233	248	10.1
H130×50×5.0 B4	130	50	5.00	1290	66	233	248	7.7
H130×50×3.5 B4	130	50	3.50	1290	66	233	248	4.8
H130×50×2.5 B4	130	50	2.50	1290	66	233	248	3.0
H50×130×8.0 B4	50	130	8.00	1290	66	233	248	28.2
H50×130×6.5 B4	50	130	6.50	1290	66	233	248	22.9
H50×130×5.0 B4	50	130	5.00	1290	66	233	248	17.6
H50×130×3.5 B4	50	130	3.50	1290	66	233	248	12.0
H50×130×2.5 B4	50	130	2.50	1290	66	233	248	8.0

Table F.2.2   Numerical results of four-point bending beams on SHS/RHS
(normal strength aluminium alloys)

Specimen	B (mm)	H (mm)	t (mm)	L (mm)	E (GPa)	f_y (MPa)	f_u (MPa)	M_{FE} (kNm)
N180×180×12.0 B4	180	180	12.00	2790	72	110	177	83.2
N180×180×9.0 B4	180	180	9.00	2790	72	110	177	60.5
N180×180×6.0 B4	180	180	6.00	2790	72	110	177	35.9
N180×180×3.5 B4	180	180	3.50	2790	72	110	177	15.2
N200×160×12.0 B4	200	160	12.00	2790	72	110	177	75.4
N200×160×9.0 B4	200	160	9.00	2790	72	110	177	50.4
N200×160×6.0 B4	200	160	6.00	2790	72	110	177	28.6
N200×160×3.5 B4	200	160	3.50	2790	72	110	177	13.5
N160×200×12.0 B4	160	200	12.00	2790	72	110	177	95.2
N160×200×9.0 B4	160	200	9.00	2790	72	110	177	68.4
N160×200×6.0 B4	160	200	6.00	2790	72	110	177	36.9
N160×200×3.5 B4	160	200	3.50	2790	72	110	177	16.8
N140×100×8.0 B4	140	100	8.00	1890	72	110	177	20.7
N140×100×6.5 B4	140	100	6.50	1890	72	110	177	16.0
N140×100×5.0 B4	140	100	5.00	1890	72	110	177	11.0
N140×100×3.5 B4	140	100	3.50	1890	72	110	177	6.6
N140×100×2.5 B4	140	100	2.50	1890	72	110	177	4.2
N100×140×8.0 B4	100	140	8.00	1890	72	110	177	29.3
N100×140×6.5 B4	100	140	6.50	1890	72	110	177	23.7
N100×140×5.0 B4	100	140	5.00	1890	72	110	177	16.1
N100×140×3.5 B4	100	140	3.50	1890	72	110	177	9.4
N100×140×2.5 B4	100	140	2.50	1890	72	110	177	5.9
N130×50×8.0 B4	130	50	8.00	1290	72	110	177	7.1
N130×50×6.5 B4	130	50	6.50	1290	72	110	177	5.6
N130×50×5.0 B3	130	50	5.00	1290	72	110	177	4.0
N130×50×3.5 B4	130	50	3.50	1290	72	110	177	2.6
N130×50×2.5 B4	130	50	2.50	1290	72	110	177	1.6
N50×130×8.0 B4	50	130	8.00	1290	72	110	177	18.8
N50×130×6.5 B4	50	130	6.50	1290	72	110	177	15.0
N50×130×5.0 B4	50	130	5.00	1290	72	110	177	11.1
N50×130×3.5 B4	50	130	3.50	1290	72	110	177	7.1
N50×130×2.5 B4	50	130	2.50	1290	72	110	177	4.4

Table F.2.3   Numerical results of four-point bending beams on SHS/RHS with internal cross stiffeners (high strength aluminium alloys)

Specimen	B (mm)	H (mm)	t (mm)	L (mm)	E (GPa)	f_y (MPa)	f_u (MPa)	M_{FE} (kNm)
+H180×180×9.0 B4	180	180	9.00	2790	66	233	248	116.6
+H180×180×6.0 B4	180	180	6.00	2790	66	233	248	75.7
+H180×180×3.5 B4	180	180	3.50	2790	66	233	248	40.6
+H160×200×9.0 B4	160	200	9.00	2790	66	233	248	123.2
+H160×200×6.0 B4	160	200	6.00	2790	66	233	248	84.4
+H160×200×3.5 B4	160	200	3.50	2790	66	233	248	46.4
+H140×100×6.5 B4	140	100	6.50	1890	66	233	248	30.4
+H140×100×5.0 B4	140	100	5.00	1890	66	233	248	23.2
+H140×100×2.5 B4	140	100	2.50	1890	66	233	248	12.0
+H130×50×6.5 B4	130	50	6.50	1290	66	233	248	11.0
+H130×50×5.0 B4	130	50	5.00	1290	66	233	248	8.6
+H130×50×2.5 B4	130	50	2.50	1290	66	233	248	4.5
+H50×130×6.5 B4	50	130	6.50	1290	66	233	248	27.5
+H50×130×5.0 B4	50	130	5.00	1290	66	233	248	21.5
+H50×130×2.5 B4	50	130	2.50	1290	66	233	248	10.7

Table F.2.4   Numerical results of four-point bending beams on SHS/RHS with internal cross stiffeners (normal strength aluminium alloys)

Specimen	B (mm)	H (mm)	t (mm)	L (mm)	E (GPa)	f_y (MPa)	f_u (MPa)	M_{FE} (kNm)
+N180×180×9.0 B4	180	180	9.00	2790	72	110	177	80.1
+N180×180×6.0 B4	180	180	6.00	2790	72	110	177	49.0
+N180×180×3.5 B4	180	180	3.50	2790	72	110	177	22.9
+N160×200×9.0 B4	160	200	9.00	2790	72	110	177	78.9
+N160×200×6.0 B4	160	200	6.00	2790	72	110	177	55.0
+N160×200×3.5 B4	160	200	3.50	2790	72	110	177	28.4
+N140×100×6.5 B4	140	100	6.50	1890	72	110	177	19.2
+N140×100×5.0 B4	140	100	5.00	1890	72	110	177	14.5
+N140×100×2.5 B4	140	100	2.50	1890	72	110	177	6.9
+N130×50×6.5 B4	130	50	6.50	1290	72	110	177	6.5
+N130×50×5.0 B4	130	50	5.00	1290	72	110	177	5.1
+N130×50×2.5 B4	130	50	2.50	1290	72	110	177	2.7
+N50×130×6.5 B4	50	130	6.50	1290	72	110	177	18.5
+N50×130×5.0 B4	50	130	5.00	1290	72	110	177	14.6
+N50×130×2.5 B3	50	130	2.50	1290	72	110	177	7.2

F.3 Five-point bending beams

Table F.3.1   Numerical results of five-point bending beams (configuration I) on SHS/RHS (high strength aluminium alloys)

Specimen	B (mm)	H (mm)	t (mm)	L (mm)	E (GPa)	f_y (MPa)	f_u (MPa)	F_{FE} (kN)
H180×180×12.0 B5I	180	180	12.00	3690	66	233	248	946.4
H180×180×9.0 B5I	180	180	9.00	3690	66	233	248	689.7
H180×180×6.0 B5I	180	180	6.00	3690	66	233	248	427.7
H180×180×3.5 B5I	180	180	3.50	3690	66	233	248	182.4
H160×200×12.0 B5I	160	200	12.00	3690	66	233	248	1006.2
H160×200×9.0 B5I	160	200	9.00	3690	66	233	248	717.5
H160×200×6.0 B5I	160	200	6.00	3690	66	233	248	431.8
H160×200×3.5 B5I	160	200	3.50	3690	66	233	248	183.4
H140×100×8.0 B5I	140	100	8.00	2490	66	233	248	378.1
H140×100×6.5 B5I	140	100	6.50	2490	66	233	248	306.4
H140×100×5.0 B5I	140	100	5.00	2490	66	233	248	231.6
H140×100×3.5 B5I	140	100	3.50	2490	66	233	248	150.8
H130×50×8.0 B5I	130	50	8.00	1690	66	233	248	220.8
H130×50×6.5 B5I	130	50	6.50	1690	66	233	248	183.4
H130×50×5.0 B5I	130	50	5.00	1690	66	233	248	142.7
H130×50×3.5 B5I	130	50	3.50	1690	66	233	248	99.3
H50×130×8.0 B5I	50	130	8.00	1690	66	233	248	521.2
H50×130×6.5 B5I	50	130	6.50	1690	66	233	248	419.8
H50×130×5.0 B5I	50	130	5.00	1690	66	233	248	316.8
H50×130×3.5 B5I	50	130	3.50	1690	66	233	248	207.9

Table F.3.2   Numerical results of five-point bending beams (configuration I) on
SHS/RHS (normal strength aluminium alloys)

Specimen	B (mm)	H (mm)	t (mm)	L (mm)	E (GPa)	f_y (MPa)	f_u (MPa)	F_{FE} (kN)
N180×180×12.0 B5I	180	180	12.00	3690	72	110	177	561.3
N180×180×9.0 B5I	180	180	9.00	3690	72	110	177	381.2
N180×180×6.0 B5I	180	180	6.00	3690	72	110	177	222.4
N180×180×3.5 B5I	180	180	3.50	3690	72	110	177	104.9
N160×200×12.0 B5I	160	200	12.00	3690	72	110	177	595.6
N160×200×9.0 B5I	160	200	9.00	3690	72	110	177	391.7
N160×200×6.0 B5I	160	200	6.00	3690	72	110	177	220.6
N160×200×3.5 B5I	160	200	3.50	3690	72	110	177	99.5
N140×100×8.0 B5I	140	100	8.00	2490	72	110	177	252.4
N140×100×6.5 B5I	140	100	6.50	2490	72	110	177	198.6
N140×100×5.0 B5I	140	100	5.00	2490	72	110	177	141.8
N140×100×3.5 B5I	140	100	3.50	2490	72	110	177	86.3
N130×50×8.0 B5I	130	50	8.00	1690	72	110	177	137.8
N130×50×6.5 B5I	130	50	6.50	1690	72	110	177	111.2
N130×50×5.0 B5I	130	50	5.00	1690	72	110	177	83.4
N130×50×3.5 B5I	130	50	3.50	1690	72	110	177	54.8
N50×130×8.0 B5I	50	130	8.00	1690	72	110	177	327.3
N50×130×6.5 B5I	50	130	6.50	1690	72	110	177	244.4
N50×130×5.0 B5I	50	130	5.00	1690	72	110	177	165.9
N50×130×3.5 B5I	50	130	3.50	1690	72	110	177	97.0

Table F.3.3   Numerical results of five-point bending beams (configuration I) on
SHS/RHS with internal cross stiffeners (high strength aluminium alloys)

Specimen	B (mm)	H (mm)	t (mm)	L (mm)	E (GPa)	f_y (MPa)	f_u (MPa)	F_{FE} (kN)
+H180×180×9.0 B5I	180	180	9.00	3690	66	233	248	860.0
+H180×180×6.0 B5I	180	180	6.00	3690	66	233	248	561.1
+H180×180×3.5 B5I	180	180	3.50	3690	66	233	248	307.0
+H160×200×9.0 B5I	160	200	9.00	3690	66	233	248	930.1
+H160×200×6.0 B5I	160	200	6.00	3690	66	233	248	604.9
+H160×200×3.5 B5I	160	200	3.50	3690	66	233	248	309.7
+H140×100×6.5 B5I	140	100	6.50	2490	66	233	248	340.5
+H140×100×5.0 B5I	140	100	5.00	2490	66	233	248	260.0
+H140×100×2.5 B5I	140	100	2.50	2490	66	233	248	119.9
+H130×50×6.5 B5I	130	50	6.50	1690	66	233	248	201.7
+H130×50×5.0 B5I	130	50	5.00	1690	66	233	248	157.1
+H130×50×2.5 B5I	130	50	2.50	1690	66	233	248	77.4
+H50×130×6.5 B5I	50	130	6.50	1690	66	233	248	463.5
+H50×130×5.0 B5I	50	130	5.00	1690	66	233	248	344.2
+H50×130×2.5 B5I	50	130	2.50	1690	66	233	248	159.8

Table F.3.4   Numerical results of five-point bending beams (configuration I) on
SHS/RHS with internal cross stiffeners (normal strength aluminium alloys)

Specimen	B (mm)	H (mm)	t (mm)	L (mm)	E (GPa)	f_y (MPa)	f_u (MPa)	F_{FE} (kN)
+N180×180×9.0 B5I	180	180	9.00	3690	72	110	177	529.8
+N180×180×6.0 B5I	180	180	6.00	3690	72	110	177	325.3
+N180×180×3.5 B5I	180	180	3.50	3690	72	110	177	154.1
+N160×200×9.0 B5I	160	200	9.00	3690	72	110	177	564.1
+N160×200×6.0 B5I	160	200	6.00	3690	72	110	177	347.4
+N160×200×3.5 B5I	160	200	3.50	3690	72	110	177	144.6
+N140×100×6.5 B5I	140	100	6.50	2490	72	110	177	238.3
+N140×100×5.0 B5I	140	100	5.00	2490	72	110	177	177.3
+N140×100×2.5 B5I	140	100	2.50	2490	72	110	177	76.9
+N130×50×6.5 B5I	130	50	6.50	1690	72	110	177	141.1
+N130×50×5.0 B5I	130	50	5.00	1690	72	110	177	108.0
+N130×50×2.5 B5I	130	50	2.50	1690	72	110	177	50.9
+N50×130×6.5 B5I	50	130	6.50	1690	72	110	177	340.1
+N50×130×5.0 B5I	50	130	5.00	1690	72	110	177	233.1
+N50×130×2.5 B5I	50	130	2.50	1690	72	110	177	104.2

Table F.3.5   Numerical results of five-point bending beams (configuration II) on SHS/RHS (high strength aluminium alloys)

Specimen	B (mm)	H (mm)	t (mm)	L (mm)	E (GPa)	f_y (MPa)	f_u (MPa)	F_{FE} (kN)
H180×180×12.0 B5II	180	180	12.00	3690	66	233	248	1069.5
H180×180×9.0 B5II	180	180	9.00	3690	66	233	248	721.7
H180×180×6.0 B5II	180	180	6.00	3690	66	233	248	375.2
H180×180×3.5 B5II	180	180	3.50	3690	66	233	248	149.0
H160×200×12.0 B5II	160	200	12.00	3690	66	233	248	1084.1
H160×200×9.0 B5II	160	200	9.00	3690	66	233	248	727.7
H160×200×6.0 B5II	160	200	6.00	3690	66	233	248	408.3
H160×200×3.5 B5II	160	200	3.50	3690	66	233	248	177.4
H140×100×8.0 B5II	140	100	8.00	2490	66	233	248	453.8
H140×100×6.5 B5II	140	100	6.50	2490	66	233	248	362.8
H140×100×5.0 B5II	140	100	5.00	2490	66	233	248	266.0
H140×100×3.5 B5II	140	100	3.50	2490	66	233	248	167.3
H130×50×8.0 B5II	130	50	8.00	1690	66	233	248	257.8
H130×50×6.5 B5II	130	50	6.50	1690	66	233	248	212.0
H130×50×5.0 B5II	130	50	5.00	1690	66	233	248	163.8
H130×50×3.5 B5II	130	50	3.50	1690	66	233	248	113.8
H50×130×8.0 B5II	50	130	8.00	1690	66	233	248	591.1
H50×130×6.5 B5II	50	130	6.50	1690	66	233	248	457.8
H50×130×5.0 B5II	50	130	5.00	1690	66	233	248	328.4
H50×130×3.5 B5II	50	130	3.50	1690	66	233	248	217.4

Table F.3.6   Numerical results of five-point bending beams (configuration II) on SHS/RHS (normal strength aluminium alloys)

Specimen	B (mm)	H (mm)	t (mm)	L (mm)	E (GPa)	f_y (MPa)	f_u (MPa)	F_{FE} (kN)
N180×180×12.0 B5II	180	180	12.00	3690	72	110	177	671.2
N180×180×9.0 B5II	180	180	9.00	3690	72	110	177	451.4
N180×180×6.0 B5II	180	180	6.00	3690	72	110	177	255.7
N180×180×3.5 B5II	180	180	3.50	3690	72	110	177	101.5
N160×200×12.0 B5II	160	200	12.00	3690	72	110	177	697.0
N160×200×9.0 B5II	160	200	9.00	3690	72	110	177	474.1
N160×200×6.0 B5II	160	200	6.00	3690	72	110	177	256.6
N160×200×3.5 B5II	160	200	3.50	3690	72	110	177	112.4
N140×100×8.0 B5II	140	100	8.00	2490	72	110	177	301.2
N140×100×6.5 B5II	140	100	6.50	2490	72	110	177	235.3
N140×100×5.0 B5II	140	100	5.00	2490	72	110	177	168.2
N140×100×3.5 B5II	140	100	3.50	2490	72	110	177	101.0
N130×50×8.0 B5II	130	50	8.00	1690	72	110	177	166.8
N130×50×6.5 B5II	130	50	6.50	1690	72	110	177	133.5
N130×50×5.0 B5II	130	50	5.00	1690	72	110	177	100.3
N130×50×3.5 B5II	130	50	3.50	1690	72	110	177	66.5
N50×130×8.0 B5II	50	130	8.00	1690	72	110	177	351.8
N50×130×6.5 B5II	50	130	6.50	1690	72	110	177	258.4
N50×130×5.0 B5II	50	130	5.00	1690	72	110	177	174.3
N50×130×3.5 B5II	50	130	3.50	1690	72	110	177	116.7

Specimen	B (mm)	H (mm)	t (mm)	L (mm)	E (GPa)	f_y (MPa)	f_u (MPa)	F_{FE} (kN)
+H180×180×9.0 B5II	180	180	9.00	3690	66	233	248	1030.0
+H180×180×6.0 B5II	180	180	6.00	3690	66	233	248	634.5
+H180×180×3.5 B5II	180	180	3.50	3690	66	233	248	318.1
+H160×200×9.0 B5II	160	200	9.00	3690	66	233	248	1061.0
+H160×200×6.0 B5II	160	200	6.00	3690	66	233	248	641.3
+H160×200×3.5 B5II	160	200	3.50	3690	66	233	248	307.8
+H140×100×6.5 B5II	140	100	6.50	2490	66	233	248	451.4
+H140×100×5.0 B5II	140	100	5.00	2490	66	233	248	331.1
+H140×100×2.5 B5II	140	100	2.50	2490	66	233	248	158.9
+H130×50×6.5 B5II	130	50	6.50	1690	66	233	248	265.5
+H130×50×5.0 B5II	130	50	5.00	1690	66	233	248	206.7
+H130×50×2.5 B5II	130	50	2.50	1690	66	233	248	100.3
+H50×130×6.5 B5II	50	130	6.50	1690	66	233	248	627.2
+H50×130×5.0 B5II	50	130	5.00	1690	66	233	248	452.8
+H50×130×2.5 B5II	50	130	2.50	1690	66	233	248	197.0

Table F.3.8   Numerical results of five-point bending beams (configuration II) on SHS/RHS with internal cross stiffeners (normal strength aluminium alloys)

Specimen	B (mm)	H (mm)	t (mm)	L (mm)	E (GPa)	f_y (MPa)	f_u (MPa)	F_{FE} (kN)
+N180×180×9.0 B5II	180	180	9.00	3690	72	110	177	644.4
+N180×180×6.0 B5II	180	180	6.00	3690	72	110	177	373.1
+N180×180×3.5 B5II	180	180	3.50	3690	72	110	177	177.4
+N160×200×9.0 B5II	160	200	9.00	3690	72	110	177	669.2
+N160×200×6.0 B5II	160	200	6.00	3690	72	110	177	394.4
+N160×200×3.5 B5II	160	200	3.50	3690	72	110	177	174.6
+N140×100×6.5 B5II	140	100	6.50	2490	72	110	177	312.6
+N140×100×5.0 B5II	140	100	5.00	2490	72	110	177	222.8
+N140×100×2.5 B5II	140	100	2.50	2490	72	110	177	102.8
+N130×50×6.5 B5II	130	50	6.50	1690	72	110	177	175.9
+N130×50×5.0 B5II	130	50	5.00	1690	72	110	177	138.0
+N130×50×2.5 B5II	130	50	2.50	1690	72	110	177	65.8
+N50×130×6.5 B5II	50	130	6.50	1690	72	110	177	450.4
+N50×130×5.0 B5II	50	130	5.00	1690	72	110	177	327.2
+N50×130×2.5 B5II	50	130	2.50	1690	72	110	177	120.9

Table F.3.9   Numerical results of five-point bending beams (configuration III) on SHS/RHS (high strength aluminium alloys)

Specimen	B (mm)	H (mm)	t (mm)	L (mm)	E (GPa)	f_y (MPa)	f_u (MPa)	F_{FE} (kN)
H180×180×12.0 B5III	180	180	12.00	3690	66	233	248	940.0
H180×180×9.0 B5III	180	180	9.00	3690	66	233	248	678.2
H180×180×6.0 B5III	180	180	6.00	3690	66	233	248	420.2
H180×180×3.5 B5III	180	180	3.50	3690	66	233	248	203.0
H160×200×12.0 B5III	160	200	12.00	3690	66	233	248	987.6
H160×200×9.0 B5III	160	200	9.00	3690	66	233	248	699.9
H160×200×6.0 B5III	160	200	6.00	3690	66	233	248	390.3
H160×200×3.5 B5III	160	200	3.50	3690	66	233	248	192.7
H140×100×8.0 B5III	140	100	8.00	2490	66	233	248	373.1
H140×100×6.5 B5III	140	100	6.50	2490	66	233	248	302.1
H140×100×5.0 B5III	140	100	5.00	2490	66	233	248	224.1
H140×100×3.5 B5III	140	100	3.50	2490	66	233	248	142.3
H130×50×8.0 B5III	130	50	8.00	1690	66	233	248	205.6
H130×50×6.5 B5III	130	50	6.50	1690	66	233	248	168.0
H130×50×5.0 B5III	130	50	5.00	1690	66	233	248	141.6
H130×50×3.5 B5III	130	50	3.50	1690	66	233	248	96.9
H50×130×8.0 B5III	50	130	8.00	1690	66	233	248	447.8
H50×130×6.5 B5III	50	130	6.50	1690	66	233	248	344.6
H50×130×5.0 B5III	50	130	5.00	1690	66	233	248	285.4
H50×130×3.5 B5III	50	130	3.50	1690	66	233	248	180.0

Table F.3.10   Numerical results of five-point bending beams (configuration III)
on SHS/RHS (normal strength aluminium alloys)

Specimen	B (mm)	H (mm)	t (mm)	L (mm)	E (GPa)	f_y (MPa)	f_u (MPa)	F_{FE} (kN)
N180×180×12.0 B5III	180	180	12.00	3690	72	110	177	638.8
N180×180×9.0 B5III	180	180	9.00	3690	72	110	177	438.4
N180×180×6.0 B5III	180	180	6.00	3690	72	110	177	256.0
N180×180×3.5 B5III	180	180	3.50	3690	72	110	177	121.7
N160×200×12.0 B5III	160	200	12.00	3690	72	110	177	669.8
N160×200×9.0 B5III	160	200	9.00	3690	72	110	177	446.8
N160×200×6.0 B5III	160	200	6.00	3690	72	110	177	262.2
N160×200×3.5 B5III	160	200	3.50	3690	72	110	177	123.5
N140×100×8.0 B5III	140	100	8.00	2490	72	110	177	247.6
N140×100×6.5 B5III	140	100	6.50	2490	72	110	177	194.4
N140×100×5.0 B5III	140	100	5.00	2490	72	110	177	140.2
N140×100×3.5 B5III	140	100	3.50	2490	72	110	177	86.3
N130×50×8.0 B5III	130	50	8.00	1690	72	110	177	134.2
N130×50×6.5 B5III	130	50	6.50	1690	72	110	177	105.4
N130×50×5.0 B5III	130	50	5.00	1690	72	110	177	80.8
N130×50×3.5 B5III	130	50	3.50	1690	72	110	177	54.5
N50×130×8.0 B5III	50	130	8.00	1690	72	110	177	311.2
N50×130×6.5 B5III	50	130	6.50	1690	72	110	177	231.5
N50×130×5.0 B5III	50	130	5.00	1690	72	110	177	160.0
N50×130×3.5 B5III	50	130	3.50	1690	72	110	177	111.4

Table F.3.11 Numerical results of five-point bending beams (configuration III)
on SHS/RHS with internal cross stiffeners (high strength aluminium alloys)

Specimen	B (mm)	H (mm)	t (mm)	L (mm)	E (GPa)	f_y (MPa)	f_u (MPa)	F_{FE} (kN)
+H180×180×9.0 B5III	180	180	9.00	3690	66	233	248	797.4
+H180×180×6.0 B5III	180	180	6.00	3690	66	233	248	512.7
+H180×180×3.5 B5III	180	180	3.50	3690	66	233	248	262.2
+H160×200×9.0 B5III	160	200	9.00	3690	66	233	248	863.5
+H160×200×6.0 B5III	160	200	6.00	3690	66	233	248	556.0
+H160×200×3.5 B5III	160	200	3.50	3690	66	233	248	262.7
+H140×100×6.5 B5III	140	100	6.50	2490	66	233	248	344.2
+H140×100×5.0 B5III	140	100	5.00	2490	66	233	248	251.0
+H140×100×2.5 B5III	140	100	2.50	2490	66	233	248	120.7
+H130×50×6.5 B5III	130	50	6.50	1690	66	233	248	192.1
+H130×50×5.0 B5III	130	50	5.00	1690	66	233	248	149.7
+H130×50×2.5 B5III	130	50	2.50	1690	66	233	248	72.5
+H50×130×6.5 B5III	50	130	6.50	1690	66	233	248	485.0
+H50×130×5.0 B5III	50	130	5.00	1690	66	233	248	364.8
+H50×130×2.5 B5III	50	130	2.50	1690	66	233	248	156.6

Table F.3.12 Numerical results of five-point bending beams (configuration III)
on SHS/RHS with internal cross stiffeners (normal strength aluminium alloys)

Specimen	B (mm)	H (mm)	t (mm)	L (mm)	E (GPa)	f_y (MPa)	f_u (MPa)	F_{FE} (kN)
+N180×180×9.0 B5III	180	180	9.00	3690	72	110	177	499.2
+N180×180×6.0 B5III	180	180	6.00	3690	72	110	177	295.0
+N180×180×3.5 B5III	180	180	3.50	3690	72	110	177	164.7
+N160×200×9.0 B5III	160	200	9.00	3690	72	110	177	524.9
+N160×200×6.0 B5III	160	200	6.00	3690	72	110	177	342.0
+N160×200×3.5 B5III	160	200	3.50	3690	72	110	177	170.5
+N140×100×6.5 B5III	140	100	6.50	2490	72	110	177	245.6
+N140×100×5.0 B5III	140	100	5.00	2490	72	110	177	170.2
+N140×100×2.5 B5III	140	100	2.50	2490	72	110	177	80.8
+N130×50×6.5 B5III	130	50	6.50	1690	72	110	177	132.4
+N130×50×5.0 B5III	130	50	5.00	1690	72	110	177	103.1
+N130×50×2.5 B5III	130	50	2.50	1690	72	110	177	51.3
+N50×130×6.5 B5III	50	130	6.50	1690	72	110	177	358.6
+N50×130×5.0 B5III	50	130	5.00	1690	72	110	177	269.4
+N50×130×2.5 B5III	50	130	2.50	1690	72	110	177	104.7

APPENDIX G.

EXPERIMENTAL DATA FROM LITERATURE

G.1   Stub columns

Table G.1.1   Experimental results of stub columns on SHS/RHS

Specimen	B (mm)	H (mm)	t (mm)	L (mm)	E (GPa)	f_y (MPa)	f_u (MPa)	F_{Exp} (kN)	References
N-S1-NW-L300	45	45	1.16	330	70	189	210	34.1	Zhu and
N-R1-NW-L300	44	100	1.31	301	69	196	219	42.3	Young
N-R2-NW-L300	44	100	2.92	300	68	189	213	147.9	(2006)
H-R2-NW-L300	44	100	2.92	299	69	275	283	209.2	
SHS1-A	44	100	1.33	301	70	260	276	53.3	Faella et al.
SHS1-B	15	15	1.90	45	68	214	241	30.6	(2000)
SHS2-A	15	15	1.90	46	68	214	241	29.7	
SHS2-B	40	40	4.10	116	72	224	244	158.4	
SHS3-A	40	40	4.10	120	72	224	244	160.8	
SHS3-B	51	50	3.06	149	65	223	245	132.4	
SHS4-A	51	50	3.06	149	65	223	245	131.3	
SHS4-B	50	50	4.27	149	64	203	225	186.6	
SHS5-A	50	50	4.27	149	64	203	225	180.9	
SHS5-B	70	70	4.12	210	70	176	203	213.8	
SHS6-A	70	70	4.12	210	70	176	203	208.7	
SHS6-B	80	80	4.25	239	72	194	220	264.4	
SHS7-A	80	80	4.25	239	72	194	220	263.8	
SHS7-B	100	100	3.93	296	71	210	228	300.2	
SHS8-A	100	100	3.93	299	71	210	228	304.8	
SHS8-B	60	60	2.26	179	72	158	187	82.7	
SHS9-A	60	60	2.26	179	72	158	187	83.3	
SHS9-B	80	80	2.08	240	65	187	204	84.7	
SHS10-A	80	80	2.08	239	65	187	204	84.6	
SHS10-B	100	100	6.00	303	65	294	324	728.5	
SHS11-A	100	100	6.00	303	65	294	324	731.5	
SHS11-B	150	150	5.00	437	75	209	252	605.5	
SHS12-A	150	150	5.00	451	75	209	252	592.5	
SHS12-B	150	150	5.11	451	68	258	300	626.5	
RHS1-A	150	150	5.11	452	68	258	300	643.5	
RHS1-B	34	20	3.00	47	63	219	251	78.7	

Specimen	B (mm)	H (mm)	t (mm)	L (mm)	E (GPa)	f_y (MPa)	f_u (MPa)	F_{Exp} (kN)	References
RHS2-A	34	20	3.00	47	63	219	251	77.5	Faella et al.
RHS2-B	40	30	4.00	74	70	202	214	124.3	(2000)
RHS3-A	40	30	4.00	120	70	202	214	122.4	
RHS3-B	50	20	4.08	52	68	211	233	134.8	
RHS4-A	50	20	4.08	52	68	211	233	136.8	
RHS4-B	50	30	3.05	81	71	217	243	109.8	
RHS5-A	50	30	3.05	149	71	217	243	109.2	
RHS5-B	50	40	2.70	105	70	222	245	108.5	
RHS6-A	50	40	2.70	211	70	222	245	109.1	
RHS6-B	60	34	3.00	89	78	213	235	122.4	
RHS7-A	60	34	3.00	179	78	213	235	122.9	
RHS7-B	60	40	2.55	180	63	235	259	120.6	
RHS8-A	60	40	2.55	176	63	235	259	118.7	
RHS8-B	80	40	3.95	235	64	222	259	212.0	
RHS9-A	80	40	3.95	234	64	222	259	212.0	
RHS9-B	100	40	3.98	236	70	217	242	222.6	
RHS10-A	100	40	3.98	236	70	217	242	224.9	
RHS10-B	120	51	4.18	361	69	216	227	271.2	
RHS11-A	120	51	4.18	361	69	216	227	255.6	
RHS11-B	151	41	4.09	225	69	225	256	290.8	
RHS12-A	151	41	4.09	225	69	225	256	261.2	
RHS12-B	181	41	4.18	242	75	212	247	313.2	
RHS13-A	181	41	4.18	237	75	212	247	315.6	
RHS13-B	100	50	3.95	299	69	216	237	248.1	
RHS14-A	100	50	3.95	298	69	216	237	248.2	
RHS14-B	60	40	2.10	181	62	220	243	85.1	
RHS14-C	60	40	2.10	178	62	220	243	79.1	
RHS15-A	60	40	2.10	176	62	220	243	79.7	
RHS15-B	80	40	3.94	235	69	189	212	185.7	
RHS15-C	80	40	3.94	236	69	189	212	190.7	
RHS16-A	80	40	3.94	234	69	189	212	185.2	
RHS16-B	80	40	2.08	239	60	225	261	92.5	
RHS17-A	80	40	2.08	238	60	225	261	92.8	
RHS17-B	60	40	1.99	180	69	234	253	89.4	
RHS18-A	60	40	1.99	178	69	234	253	88.6	
RHS18-B	100	26	2.30	125	68	265	285	92.7	
RHS19-A	100	26	2.30	127	68	265	285	89.4	
RHS19-B	120	61	2.65	359	69	210	229	137.7	
RHS20-A	120	61	2.65	355	69	210	229	139.6	
RHS20-B	200	100	4.87	601	65	235	283	513.5	

Table G.1.1 (cont'd)

Specimen	B (mm)	H (mm)	t (mm)	L (mm)	E (GPa)	f_y (MPa)	f_u (MPa)	F_{exp} (kN)	References
RHS21-A	200	100	4.87	601	65	235	283	506.5	Faella et al.
RHS21-B	47	40	2.90	140	68	251	277	115.3	(2000)
RHS22-A	47	40	2.90	141	68	251	277	116.5	
RHS22-B	180	70	4.59	540	72	320	353	493.0	
AA6060-T4-1.8	180	70	4.59	540	72	320	353	497.0	Langseth
AA6060-T4-2.0	80	80	1.80	310	68	77	167	38.0	and
AA6060-T4-2.5	80	80	2.00	310	68	77	167	45.0	Hopperstad
AA6060-T6-1.8	80	80	2.50	310	68	77	167	65.0	(1997)
AA6060-T6-2.0	80	80	1.80	310	68	188	214	81.0	
AA6060-T6-2.5	80	80	2.00	310	68	188	214	100.5	
AA6060-T4*-2.5	80	80	2.50	310	68	188	214	140.0	
RHS01	80	80	2.50	310	68	115	196	85.0	Mennick
RHS02	50	50	2.97	50	70	230	258	130.1	(2002)
RHS04	50	50	2.96	100	69	230	258	129.7	
RHS05	50	50	3.13	150	67	230	258	125.1	
RHS06	50	50	3.13	200	68	199	218	128.5	
RHS17	80	40	1.95	240	71	230	258	83.8	
RHS19	80	40	3.94	239	69	199	226	218.7	
RHS200	100	40	3.86	300	68	230	255	223.9	Hassinen
RHS240	20	20	0.91	100	65	178	215	12.7	(2000)
B-SS1-2×2×0.062	20	20	0.91	140	65	178	215	12.3	Bijlaard
B-SS2-2×2×0.062	51	51	1.57	300	70	303	−	79.2	and Fisher
B-ES1-2×2×0.062	51	51	1.54	302	70	303	−	78.8	(1953)
B-ES2-2×2×0.062	51	51	1.55	387	70	303	−	79.6	

Table G.1.2   Experimental results of stub columns on angles

Specimen	B (mm)	H (mm)	T_{flange} (mm)	t_{web} (mm)	L (mm)	E (GPa)	f_y (MPa)	f_u (MPa)	P_{exp} (kN)	Reference
L2A	34	51	2.90	2.90	153	63	235	259	42.7	Mazzolani
L2B	34	51	2.95	3.00	149	63	235	259	45.4	et al.
L3A	32	33	3.95	3.90	98	70	176	203	40.5	(2011)
L3B	33	33	3.90	3.90	96	70	176	203	41.3	
L5A	33	43	4.00	4.00	130	70	176	203	51.2	
L5B	33	43	3.90	3.90	130	70	176	203	49.3	
L6A	42	42	4.15	4.30	153	64	202	225	65.3	
L6B	41	41	4.10	4.00	153	64	202	225	58.7	
L8A	44	45	2.95	2.95	134	65	223	245	38.2	
L8B	44	45	3.00	3.00	135	65	223	245	43.4	
L11A	37	37	3.90	4.00	120	69	189	212	54.8	
L11B	37	37	4.00	3.90	118	69	189	212	53.8	
L12A	61	70	4.20	4.10	198	70	176	203	67.5	
L12B	62	70	3.90	3.90	199	70	176	203	56.0	
L14A	38	39	1.95	1.90	108	65	187	204	15.0	
L14B	38	39	1.90	2.00	110	65	187	204	15.9	
L15A	26	39	2.00	1.90	121	65	187	204	16.6	
L18B	40	53	2.45	2.45	146	63	235	259	30.7	
L21A	34	48	5.85	5.85	143	65	294	324	142.2	
L21B	34	46	5.85	5.85	137	65	294	324	140.2	
L23A	49	56	2.10	2.10	158	72	158	187	15.2	
L23B	52	56	2.10	2.10	160	72	158	187	16.7	
L24A	73	78	2.00	2.00	239	65	187	204	21.5	
L24B	72	77	2.00	2.00	238	65	187	204	20.2	
L25B	40	52	1.85	1.90	168	65	187	204	17.7	
L27A	86	88	5.80	5.95	309	65	294	324	207.7	
L27B	87	87	5.80	6.05	309	65	294	324	196.5	
L30A	71	80	4.10	4.00	242	72	194	220	81.2	
L30B	70	80	4.00	4.10	242	72	194	220	83.1	
L32A	47	60	5.75	5.85	176	65	294	324	176.2	
L32B	46	59	5.80	5.85	179	65	294	324	180.2	
L33A	47	48	5.00	5.10	139	68	258	300	100.8	
L33B	48	48	5.00	5.10	140	68	258	300	104.4	

Table G.1.3   Experimental results of stub columns on channels

Specimen	B (mm)	H (mm)	t_{flange} (mm)	t_{web} (mm)	L (mm)	E (GPa)	f_y (MPa)	f_u (MPa)	P_{exp} (kN)	Reference
US02	59	40	2.02	2.01	300	69	206	229	40.6	Mennick
US04	59	40	2.02	2.00	300	69	206	229	40.8	(2002)
US06	49	40	2.01	2.01	300	69	206	229	39.0	
US08	49	40	1.95	1.94	300	69	206	229	38.8	
US14	59	40	3.85	3.95	300	67	195	217	110.6	
US18	49	40	3.96	3.94	300	67	195	217	99.2	
US20	49	40	3.94	3.90	300	67	195	217	98.5	
US26	69	50	2.85	2.94	300	66	195	226	74.1	
US30	59	50	2.85	2.91	300	66	195	226	71.5	
C1A	48	40	3.90	4.10	97	70	217	242	106.7	Mazzolani
C1B	48	40	3.90	3.90	97	70	217	242	109.8	et al.
C3A	49	50	3.90	3.90	98	69	216	237	124.1	(2001)
C3B	47	50	3.95	4.00	98	69	216	237	123.2	
C4A	28	40	2.55	2.50	97	63	235	259	59.7	
C4B	28	40	2.50	2.50	97	63	235	259	59.0	
C5A	17	60	2.50	2.60	97	63	235	259	58.0	
C5B	19	60	2.55	2.50	97	63	235	259	59.3	
C6A	38	40	3.90	3.90	73	64	222	259	97.0	
C6B	39	40	3.90	3.90	73	64	222	259	99.1	
C7A	32	70	4.10	4.00	68	70	176	203	91.6	
C7B	34	70	4.00	3.90	68	70	176	203	89.5	
C8A	23	50	2.95	3.00	72	65	223	245	61.5	
C8B	23	50	3.00	3.00	72	65	223	245	60.8	
C9A	29	34	3.00	2.90	68	78	213	235	62.9	
C9B	28	34	3.00	3.00	68	78	213	235	61.9	
C10A	28	40	2.00	2.00	72	69	234	253	43.2	
C10B	28	40	2.00	2.00	72	69	234	253	41.7	
C11A	19	80	3.90	3.90	73	64	222	259	105.8	
C11B	17	80	3.90	3.80	73	64	222	259	100.5	
C12A	21	40	2.45	2.40	72	68	251	277	54.1	
C12B	21	40	2.45	2.50	72	68	251	277	55.9	
C13A	18	40	3.95	4.10	69	72	224	244	79.0	
C13B	18	40	3.95	4.10	69	72	224	244	77.3	
C14A	38	80	4.10	4.20	78	72	194	220	131.1	
C14B	38	80	4.10	4.00	78	72	194	220	130.7	
C15A	38	80	1.95	1.90	78	65	187	204	50.3	
C15B	38	80	1.95	1.90	78	65	187	204	49.4	
C16A	58	100	4.50	6.60	147	69	323	343	333.4	
C16B	59	100	4.50	6.60	147	69	323	343	333.0	

Specimen	B (mm)	H (mm)	t_{flange} (mm)	t_{web} (mm)	L (mm)	E (GPa)	f_y (MPa)	f_u (MPa)	P_{exp} (kN)	Reference
C17A	48	120	6.50	4.50	146	69	323	343	338.0	Mazzolani
C17B	48	120	6.50	4.50	146	69	323	343	319.8	et al.
C18A	29	50	4.05	4.10	100	69	216	237	95.0	(2001)
C18B	29	50	4.05	4.10	95	69	216	237	93.8	
C19A	64	25	2.05	2.05	99	68	265	285	44.0	
C19B	64	25	2.05	2.10	99	68	265	285	41.5	
C20A	32	25	2.10	2.10	99	68	265	285	37.1	
C20B	32	25	2.10	2.10	99	68	265	285	37.0	
C21A	47	25	2.10	2.10	98	68	265	285	40.5	
C21B	49	25	2.20	2.10	98	68	265	285	40.7	
C22A	48	100	6.10	6.00	98	65	294	324	356.2	
C23A	30	100	6.00	6.00	97	65	294	324	283.2	
C23B	30	100	5.95	5.90	97	65	294	324	284.4	
C24A	48	100	4.00	4.00	98	71	210	228	153.8	
C24B	48	100	4.00	4.00	98	71	210	228	153.9	
C25A	30	100	4.00	4.00	99	71	210	228	124.6	
C25B	30	100	4.00	4.00	95	71	210	228	125.6	
C26A	62	100	3.90	3.90	99	71	210	228	174.7	
C26B	62	100	3.95	3.90	95	71	210	228	173.5	
C27A	32	40	4.05	4.10	95	70	217	242	84.4	
C27B	32	40	4.05	4.10	94	70	217	242	84.9	
C28A	65	40	4.05	4.10	95	70	217	242	127.2	
C28B	65	40	4.05	4.10	94	70	217	242	125.9	
C29A	46	41	4.30	4.30	95	69	225	256	109.8	
C29B	47	41	4.30	4.30	96	69	225	256	109.3	
C30A	96	41	4.30	4.30	96	69	225	256	177.5	
C31A	67	50	4.05	4.10	95	69	216	237	144.4	
C31B	67	50	4.05	4.10	100	69	216	237	143.2	
C32A	62	100	6.00	6.00	97	65	294	324	405.2	
C32B	62	100	6.10	6.00	97	65	294	324	402.4	
C33A	27	121	2.60	2.80	115	69	210	229	60.9	
C33B	29	121	2.55	2.80	115	69	210	229	66.9	
C34A	38	60	2.65	2.50	114	69	210	229	56.2	
C34B	38	61	2.65	2.50	115	69	210	229	52.6	
C35A	78	60	2.65	2.50	114	69	210	229	71.7	
C35B	78	60	2.65	2.50	116	69	210	229	73.1	
C36A	59	61	2.85	2.60	116	69	210	229	67.4	
C36B	57	61	2.75	2.50	116	69	210	229	63.2	
C37A	37	120	2.60	2.60	114	69	210	229	73.5	

Specimen	B (mm)	H (mm)	t_{flange} (mm)	t_{web} (mm)	L (mm)	E (GPa)	f_y (MPa)	f_u (MPa)	P_{exp} (kN)	Reference
C37B	39	120	2.60	2.60	113	69	210	229	64.3	Mazzolani
C38A	44	154	6.60	4.20	156	72	309	330	307.2	et al.
C38B	44	154	6.55	5.10	155	72	309	330	344.8	(2001)
C39A	98	71	4.60	6.50	135	72	309	330	320.4	
C39B	98	71	4.60	6.60	135	72	309	330	301.6	
C40A	47	71	4.60	6.60	137	72	309	330	241.5	
C40B	49	71	4.60	6.60	136	72	309	330	250.6	
C41A	40	100	4.65	6.50	147	69	323	343	289.4	
C41B	40	101	4.65	6.50	147	69	323	343	288.0	
C42A	76	101	4.60	6.50	146	69	323	343	348.8	
C42B	76	101	4.60	6.50	146	69	323	343	367.8	
C43A	34	121	6.60	4.70	148	69	323	343	277.0	
C43B	34	121	6.60	4.50	147	69	323	343	265.8	
C44A	62	120	6.60	4.50	148	69	323	343	373.2	
C44B	62	121	6.60	4.70	147	69	323	343	388.2	
C45A	117	41	4.35	4.60	177	75	212	247	159.3	
C45B	117	41	4.35	4.00	174	75	212	247	154.1	
C46A	57	70	4.45	4.40	170	72	320	353	230.2	
C46B	57	70	4.45	4.40	173	72	320	353	217.1	
C47A	115	70	4.50	4.50	173	72	320	353	263.6	
C48B	47	71	4.75	6.60	157	72	309	330	234.3	
C49A	56	41	4.30	4.00	177	75	212	247	111.7	
C49B	56	41	4.25	4.40	174	75	212	247	121.7	
C51A	48	80	1.95	2.00	76	65	187	204	54.7	
C52A	51	40	2.20	2.40	76	60	225	261	52.4	
C52B	51	40	2.20	2.30	75	60	225	261	51.4	
C53A	19	40	2.65	2.60	95	63	235	259	50.8	
C53B	19	40	2.55	2.60	95	63	235	259	50.9	
C54A	38	40	2.65	2.60	95	63	235	259	66.4	
C54B	38	40	2.55	2.50	95	63	235	259	63.5	
C56A	27	60	2.65	2.70	96	63	235	259	67.0	
C56B	26	60	2.65	2.60	94	63	235	259	69.2	
C57A	26	40	4.00	4.00	74	64	222	259	87.9	
C57B	26	40	4.00	4.00	75	64	222	259	89.4	
C58A	50	40	4.00	4.10	74	64	222	259	121.5	
C58B	51	40	4.00	4.10	75	64	222	259	119.4	
C59A	50	40	4.00	4.00	74	69	189	212	109.9	
C59B	50	40	4.00	4.00	76	69	189	212	107.1	
C60A	38	40	2.10	2.10	70	69	234	253	44.2	

Specimen	B (mm)	H (mm)	t_{flange} (mm)	t_{web} (mm)	L (mm)	E (GPa)	f_y (MPa)	f_u (MPa)	P_{exp} (kN)	Reference
C60B	38	40	2.10	2.10	70	69	234	253	43.2	Mazzolani
C61A	21	40	4.05	4.00	70	72	224	244	83.7	et al.
C61B	23	40	4.05	4.00	70	72	224	244	86.5	(2001)
C62A	19	50	3.05	3.00	70	65	223	245	54.8	
C62B	18	50	3.05	3.00	70	65	223	245	53.2	
C63A	42	70	4.00	3.90	67	70	176	203	106.0	
C63B	42	70	4.00	3.90	68	70	176	203	101.5	
C64A	25	80	4.15	4.10	77	72	194	220	142.7	
C64B	47	80	4.15	4.20	77	72	194	220	139.8	
C65A	25	80	1.95	2.00	72	65	187	204	39.0	
C65B	25	80	1.90	2.00	76	65	187	204	43.1	
C66A	19	34	3.10	3.10	69	78	213	235	51.1	
C66B	19	34	3.15	3.10	67	78	213	235	51.4	
C67A	37	34	3.10	3.10	69	78	213	235	71.0	
C68A	26	40	4.00	4.00	74	69	189	212	80.5	
C68B	26	40	4.00	4.00	76	69	189	212	81.5	
C69A	19	80	2.20	2.00	55	60	225	261	40.3	
C69B	19	80	2.20	2.50	55	60	225	261	50.8	
C70A	25	40	2.15	2.10	76	60	225	261	38.7	
C70B	25	40	2.20	2.10	75	60	225	261	39.6	
C71A	19	40	2.10	2.10	70	69	234	253	33.0	
C71B	19	40	2.10	2.10	70	69	234	253	33.8	
C72A	20	40	2.50	2.60	70	67	251	277	45.5	
C72B	20	40	2.55	2.60	72	67	251	277	44.5	
C73A	28	40	2.50	2.40	72	67	251	277	60.0	
C73B	28	40	2.50	2.40	70	67	251	277	59.0	
C74B	28	50	3.05	3.00	70	65	223	245	69.8	
C75A	20	70	4.05	4.10	67	70	176	203	79.5	
C75B	20	70	4.00	4.10	68	70	176	203	77.8	
C76A	24	80	4.10	4.10	77	72	194	220	105.8	
C76B	47	80	4.10	4.20	78	72	194	220	106.7	
C77A	36	60	2.25	2.10	57	72	158	187	41.8	
C77B	36	60	2.20	2.20	57	72	158	187	44.4	
C78A	16	60	2.25	2.20	57	72	158	187	31.5	
C78B	16	60	2.15	2.20	56	72	158	187	31.5	
C80A	23	20	4.15	4.70	50	68	211	233	64.8	
C80B	22	20	4.20	4.00	50	68	211	233	61.1	
C81A	31	30	3.20	3.40	48	71	217	243	65.4	
C82A	19	30	3.85	3.90	48	70	202	214	70.1	

Specimen	B (mm)	H (mm)	t_{flange} (mm)	t_{web} (mm)	L (mm)	E (GPa)	f_y (MPa)	f_u (MPa)	P_{exp} (kN)	Reference
C82B	26	30	3.85	3.90	50	70	202	214	71.3	Mazzolani
C83A	39	40	4.10	4.10	60	69	189	212	96.0	et al.
C83B	37	40	4.10	4.10	60	69	189	212	90.1	(2001)
C84A	39	40	2.20	2.30	54	60	225	261	52.9	
C84B	37	40	2.15	2.10	53	60	225	261	41.9	
C85A	23	50	4.30	4.40	48	64	203	225	94.6	
C85B	23	50	4.30	4.30	48	64	203	225	92.6	
C86A	14	50	4.20	4.00	47	64	203	225	70.6	
C86B	15	50	4.15	4.30	47	64	203	225	74.0	
C87A	27	50	4.25	4.40	47	64	203	225	101.0	
C87B	28	50	4.20	4.10	47	64	203	225	98.3	
C88A	96	150	4.90	5.20	211	75	209	252	305.8	
C88B	96	150	4.90	4.80	201	75	209	252	247.7	
C89A	10	20	2.95	3.50	34	63	219	251	31.6	
C89B	10	20	3.05	3.10	34	63	219	251	30.2	
C90A	20	20	3.00	3.10	34	63	219	251	42.2	
C90B	20	20	3.00	3.10	34	63	219	251	42.0	
C91A	13	40	4.00	3.90	48	70	202	214	55.7	
C91B	13	40	4.05	4.20	49	70	202	214	56.2	
C92A	18	30	4.05	4.00	49	70	202	214	60.7	
C92B	18	30	4.00	4.10	49	70	202	214	61.2	
C93A	12	30	3.95	4.00	49	70	202	214	45.7	
C93B	10	30	4.00	4.00	50	70	202	214	40.5	
C94A	14	20	4.20	4.00	48	68	211	233	48.5	
C94B	14	20	4.15	4.00	49	68	211	233	48.1	
C95A	32	20	4.10	4.40	49	68	211	233	78.7	
C96A	25	30	3.10	3.00	49	71	217	243	52.5	
C96B	21	30	3.30	3.50	49	71	217	243	52.6	
C97A	15	30	3.10	3.00	48	71	217	243	44.1	
C97B	15	30	3.10	3.00	49	71	217	243	43.7	
C98A	87	41	4.40	4.00	215	75	212	247	135.7	
C98B	88	41	4.35	4.60	215	75	212	247	144.0	
C99A	18	80	4.05	4.10	61	69	189	212	90.6	
C99B	19	80	4.05	4.10	61	69	189	212	94.6	
C101A	61	100	5.05	5.00	284	65	235	283	229.6	
C101B	63	100	5.00	5.00	284	65	235	283	221.0	
C102A	129	100	4.90	4.90	288	65	235	283	248.6	
C102B	131	100	5.00	4.90	288	65	235	283	249.8	
C103A	99	71	4.55	6.80	158	72	309	330	292.2	

Specimen	B (mm)	H (mm)	t_{flange} (mm)	t_{web} (mm)	L (mm)	E (GPa)	f_y (MPa)	f_u (MPa)	P_{exp} (kN)	Reference
C103B	98	71	4.55	6.60	157	72	309	330	302.8	Mazzolani
C104A	75	150	5.10	5.30	198	68	214	241	303.6	et al.
C104B	73	150	5.25	4.90	194	68	214	241	275.0	(2001)
C105A	27	60	2.30	2.30	54	72	158	187	40.4	
C106A	46	150	5.00	4.80	209	75	209	252	231.8	
C106B	46	150	5.05	5.10	200	75	209	252	251.4	
C108A	96	152	5.10	4.90	286	75	212	247	272.8	
C108B	96	152	5.10	4.90	286	75	212	247	274.6	

G.2   Three-point bending beams

Table G.2.1   Experimental results of three-point bending beams on SHS/RHS

Specimen	B (mm)	H (mm)	t (mm)	L (mm)	E (GPa)	f_y (MPa)	f_u (MPa)	M_{exp} (kNm)	Reference
Q1-1m-1	100	100	5.91	1000	69	316	324	24.1	Moen et
Q1-1m-2	100	100	5.91	1000	69	316	324	24.1	al.
Q1-2m-1	100	100	5.91	2000	69	316	324	23.5	(1999)
Q1-2m-3	100	100	5.91	2000	69	316	324	23.7	
Q2-1m-1	100	100	5.91	1000	67	177	283	15.9	
Q2-1m-2	100	100	5.91	1000	67	177	283	15.8	
Q2-2m-1	100	100	5.91	2000	67	177	283	15.4	
Q2-2m-2	100	100	5.91	2000	67	177	283	15.8	
Q3-1m-1	100	100	2.87	1000	67	120	221	4.5	
Q3-1m-2	100	100	2.87	1000	67	120	221	4.4	
Q3-2m-1	100	100	2.87	2000	67	120	221	4.3	
Q3-2m-3	100	100	2.87	2000	67	120	221	4.5	
Q4-2m-1	100	100	5.97	2000	67	314	333	25.1	
Q4-2m-2	100	100	5.97	2000	67	314	333	24.2	
R1-1m-1	60	119	2.45	1000	67	289	302	7.8	
R1-2m-1	60	119	2.45	2000	67	289	302	7.8	
R1-2m-2	60	119	2.45	2000	67	289	302	7.8	
R1-3m-1	60	119	2.45	3000	67	289	302	7.4	
R1-3m-2	60	119	2.45	3000	67	289	302	7.3	
R2-1m-1	60	100	2.93	1000	66	281	290	8.0	
R2-1m-2	60	100	2.93	1000	66	281	290	8.0	
R2-2m-1	60	100	2.93	2000	66	281	290	7.9	
R2-2m-2	60	100	2.93	2000	66	281	290	8.1	
R2-3m-1	60	100	2.93	3000	66	281	290	8.4	
R2-3m-2	60	100	2.93	3000	66	281	290	8.3	

Table G.2.2   Experimental results of three-point bending beams on I-sections

Specimen	B (mm)	H (mm)	t_{flange} (mm)	t_{web} (mm)	L (mm)	E (GPa)	f_y (MPa)	f_u (MPa)	M_{exp} (kNm)	Reference
I1-2m-1	120	120	7.96	5.09	1000	67	312	324	34.5	Moen et
I2-1m-1	70	80	4.94	4.97	1000	67	279	301	9.5	al.
I2-1m-2	70	80	4.94	4.97	1000	67	279	301	9.2	(1999)
I2-1m-3	70	80	4.94	4.97	1000	67	279	301	9.2	
I2-2m-1	70	80	4.94	4.97	2000	67	279	301	9.1	
I2-2m-2	70	80	4.94	4.97	2000	67	279	301	9.2	
I2-2m-3	70	80	4.94	4.97	2000	67	279	301	9.3	
I2-3m-1	70	80	4.94	4.97	3000	67	279	301	8.9	

G.3 Four-point bending beams

Table G.3.1   Experimental results of four-point bending beams on SHS/RHS

Specimen	B (mm)	H (mm)	t_{flange} (mm)	t_{web} (mm)	L (mm)	E (GPa)	f_y (MPa)	f_u (MPa)	M_{exp} (kNm)	Reference
S1-PB	45	45	1.14	1.14	–	68	296	300	0.8	Zhu and
R1-PB	100	44	1.32	1.32	–	70	260	276	1.0	Young
R2-PB	100	44	2.90	2.90	–	69	275	283	3.5	(2006)
R2-PB#	100	44	2.91	2.91	–	69	275	283	3.5	
H32×32×2	32	32	1.94	1.94	1240	66	243	261	0.7	Zhu and
H40×40×5	40	40	4.85	4.85	1440	70	226	246	2.2	Young
H50×50×2	51	51	1.95	1.95	1640	67	264	271	1.7	(2009)
H50×50×3	51	51	3.09	3.09	1640	64	268	273	2.8	
H65×65×3	64	64	2.99	2.99	1840	68	222	236	3.9	
H76×76×3	76	76	3.10	3.10	1840	68	246	264	5.7	
H90×90×2	88	88	1.75	1.75	2040	67	246	263	3.1	
H100×100×2	102	102	2.31	2.31	2240	68	234	258	6.2	
H110×110×3	112	112	3.13	3.13	2640	66	290	291	12.9	
H153×153×3	154	154	3.36	3.36	3000	72	244	267	18.7	
N-1000-P-2	51	102	4.50	5.20	1000	71	373	430	20.5	Lai and
N-1000-P-3	51	102	4.50	5.20	1000	71	373	430	20.9	Nethercot
N-2000-P-1	51	102	4.50	5.20	2000	71	373	430	18.4	(1992)
N-2000-P-2	51	102	4.50	5.20	2000	71	373	430	18.9	